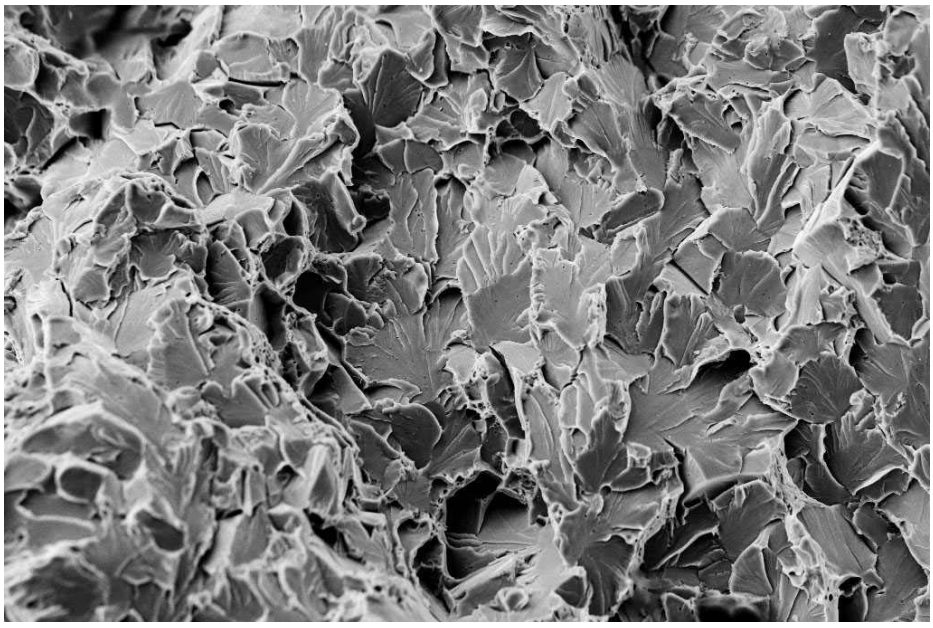
JRC Scientific and Technical Reports

COMMENTARY AND WORKED EXAMPLES
to EN 1993-1-10 “Material toughness and through thickness properties“
and other toughness oriented rules in EN 1993

G. Sedlacek, M. Feldmann, B. Kühn, D. Tschickardt, S. Höhler, C. Müller, W. Hensen, N. Stranghöner
W. Dahl, P. Langenberg, S. Münstermann, J. Brozetti, J. Raoul, R. Pope, F. Bijlaard

Background documents in support to the implementation, harmonization and further development of the Eurocodes



Joint Report
Prepared under the JRC – ECCS cooperation agreement for the evolution of Eurocode 3 (programme of CEN / TC 250)

Editors: M. Géradin, A. Pinto and S. Dimova

First Edition, September 2008

EUR 23510 EN - 2008

JRC EUROPEAN COMMISSION

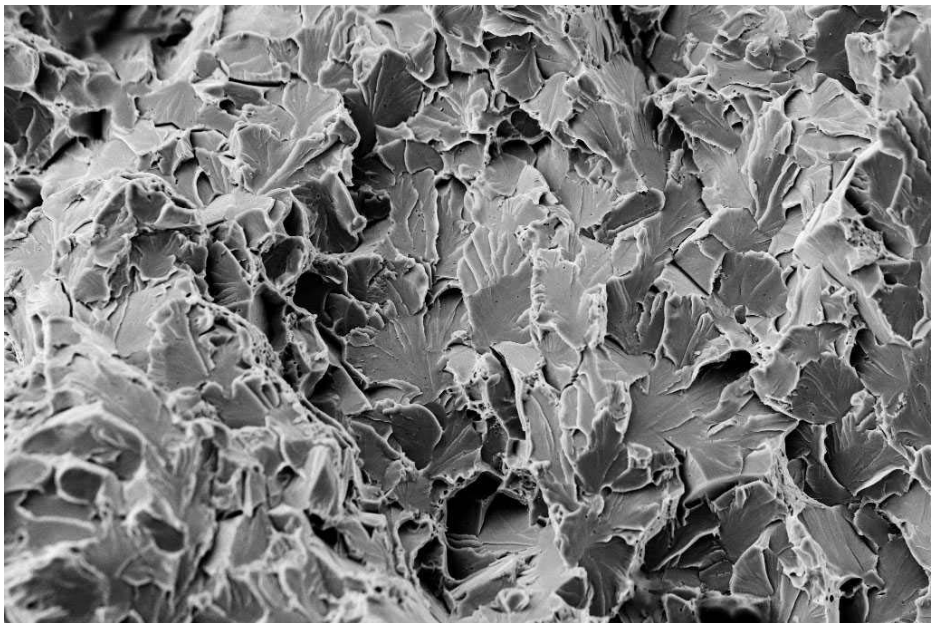
ECCS CECM E K S

JRC Scientific and Technical Reports

COMMENTARY AND WORKED EXAMPLES
to EN 1993-1-10 “Material toughness and through thickness properties“
and other toughness oriented rules in EN 1993

G. Sedlacek, M. Feldmann, B. Kühn, D. Tschickardt, S. Höhler, C. Müller, W. Hensen, N. Stranghöner
W. Dahl, P. Langenberg, S. Münstermann, J. Brozetti, J. Raoul, R. Pope, F. Bijlaard

Background documents in support to the implementation, harmonization and further development of the Eurocodes



Joint Report
Prepared under the JRC – ECCS cooperation agreement for the evolution of Eurocode 3 (programme of CEN / TC 250)

Editors: M. Géradin, A. Pinto and S. Dimova

First Edition, September 2008

EUR 23510 EN - 2008

JRC
EUROPEAN COMMISSION

ECCS
CECM
E K S

The mission of the JRC is to provide customer-driven scientific and technical support for the conception, development, implementation and monitoring of EU policies. As a service of the European Commission, the JRC functions as a reference centre of science and technology for the Union. Close to the policy-making process, it serves the common interest of the Member States, while being independent of special interests, whether private or national.

European Commission
Joint Research Centre

The European Convention for Constructional Steelwork (ECCS) is the federation of the National Associations of Steelwork industries and covers a worldwide network of Industrial Companies, Universities and Research Institutes.

http://www.steelconstruct.com/

Contact information
Address: Mies-van-der-Rohe-Straße 1, D-52074 Aachen
E-mail: sed@stb.rwth-aachen.de
Tel.: +49 241 80 25177
Fax: +49 241 80 22140
http://www.stb.rwth-aachen.de

Legal Notice
Neither the European Commission nor any person acting on behalf of the Commission is responsible for the use which might be made of this publication.

A great deal of additional information on the European Union is available on the Internet.
It can be accessed through the Europa server
http://europa.eu/

JRC 47278

EUR 23510 EN
ISSN 1018-5593

Luxembourg: Office for Official Publications of the European Communities

© European Communities, 2008
Reproduction is authorised provided the source is acknowledged

Printed in Italy

Acknowledgements

This report with a commentary and worked examples to the design rules in EN 1993-1-10 and other toughness oriented-rules in EN 1993 has been prepared on the basis of numerous sources:

- working papers worked out for the project teams for the preparation of the ENV-version and EN-version of Eurocode 3 with funding by the ECCS,

- reports from research projects funded by the European Community for Steel and Coal (ECSC) and the Research Fund for Coal and Steel (RFCS),

- reports from research projects funded by the Deutsche Forschungsgemeinschaft (DFG), and Arbeitsgemeinschaft industrieller Forschung (AIF),

- various doctoral thesis' and a habilitation thesis mentioned in the bibliography that were prepared in particular at the Institute of Steel Construction and the Institute of Ferrous Metallurgy at RWTH Aachen,

- results of expertises for practical applications of the methods mentioned in the bibliography,

- numerous discussions in particular with Mr. Sanz, Mr. Wallin, Prof. Dahl, Prof. Burdekin and with members of the project teams, in particular J. Brozzetti, J. Raoul, J.B. Schleich and R. Pope, who helped in this interdisciplinary field to develop rules of good practice.

All these valuable contributions from pre-normative and co-normative research aiming at laying the basis of the toughness ortiented rules in Eurocode 3 are gratefully acknowledged.

The preparation of the manuscript of this report was in the hands of D. Tschickardt, B. Kühn and C. Müller. Prof. M. Feldmann, Prof. W. Dahl, P. Langenberg and Prof. N. Stranghöner gave useful contributions. Prof. F. Bijlaard helped in the proof-reading of the text. Thanks to all of them for the valuable works and contributions.

Aachen, September 2008

Gerhard Sedlacek

Foreword

The EN Eurocodes are a series of European standards which provide a common series of methods for calculating the mechanical strength of elements playing a structural role in construction works, i.e. the structural construction products. They make it possible to design construction works, to check their stability and to give the necessary dimensions of the structural construction products.

They are the result of a long procedure of bringing together and harmonizing the different design traditions in the Member States. In the same time, the Member States keep exclusive competence and responsibility for the levels of safety of works.

According to the Commission Recommendation of 11 December 2003 on the implementation and use of Eurocodes for construction works and structural construction products, the Member States should take all necessary measures to ensure that structural construction products calculated in accordance with the Eurocodes may be used, and therefore they should refer to the Eurocodes in their national regulations on design.

The Member States may need using specific parameters in order to take into account specific geographical, geological or climatic conditions as well as specific levels of protection applicable on their territory. The Eurocodes contain thus 'nationally determined parameters', the so-called NDPs, and provide for each of them a recommended value. However, the Member States may give different values to the NDPs if they consider it necessary to ensure that building and civil engineering works are designed and executed in a way that fulfils the national requirements.

The so-called background documents on Eurocodes are established and collected to provide technical insight on the way the NDPs have been selected and may possibly be modified at the national level. In particular, they intend to justify:

- The theoretical origin of the technical rules,
- The code provisions through appropriate test evaluations whenever needed (e.g. EN 1990, Annex D),
- The recommendations for the NDPs,
- The country decisions on the choice of the NDPs.

Collecting and providing access to the background documents is essential to the Eurocodes implementation process since they are the main source of support to:

- The Member States, when choosing their NDPs,
- To the users of the Eurocodes where questions are expected,
- To provide information for the European Technical Approvals and Unique Verifications,
- To help reducing the NDPs in the Eurocodes when they result from different design cultures and procedures in structural analysis,
- To allow for a strict application of the Commission Recommendation of 11 December 2003,
- To gradually align the safety levels across Member States,
- To further harmonize the design rules across different materials,
- To further develop the Eurocodes.

This joint ECCS-JRC report is part of a series of background-documents in support to the implementation of Eurocode 3. It provides background information on the specific issue of design rules affected by the toughness of steel.

In its various parts, EN 1993 – Eurocode 3 currently addresses steel properties essentially with regard to strength. The toughness properties are also dealt with in Part 1-10 and Part 1-12.

The interrelation between toughness properties and the safety of steel structures is not commonly known, and therefore EN 1993-1-10 does not explicitly address this issue. The background material to EN 1993-1-10 presented in this report provides the necessary explanations on the underlying principles and their application rules. It also opens the door to the application of these principles to situations not yet fully covered by EN 1993.

Due to its rather innovative character, some of the contents of this joint ECCS-JRC still needs to be complemented through additional research likely to be carried out in the context of the further development of Eurocode 3.

The European Convention for Constructional Steelwork (ECCS) has initiated the development of this commentary in the frame of the cooperation between the Commission (JRC) and the ECCS for works on the further evolution of the Eurocodes. It is therefore published as a Joint Commission (JRC)-ECCS-report.

Aachen, Delft and Ispra, September 2008

Gerhard Sedlacek
Director of ECCS-research

Frans Bijlaard
Chairman of CEN/TC 250/SC3

Michel Géradin, Artur Pinto and Silvia Dimova
European Laboratory for Structural Assessment, IPSC, JRC

TABLE OF CONTENTS

SECTION 1 1

1. GENERAL GUIDANCE THROUGH THE COMMENTARY AND SUMMARY 1

1.1 Section 1: Objective of the guidance 1

1.2 Section 2: Commentary and background of EN 1993-1-10, section 2: Selection of materials for fracture toughness 1

1.2.1 Designation of steels and selection to performance requirements *1*

1.2.2 The use of strength-values f_y and f_u from coupon tests and of toughness values T_{27J} of the material in EN 1993 *3*

1.2.3 Conclusions *5*

1.3. Section 3: Commentary and background of EN 1993-1-10, section 3: Selection of materials for through-thickness properties 6

1.4 Section 4: Complementary rules for the design to avoid brittle fracture on the basis of the background to EN 1993-1-10 6

1.4.1 Scope *6*

1.4.2 Assessment of residual safety and service life of old riveted structures *7*

1.4.3 Choice of material for welded connections in buildings *7*

1.5 Section 5: Other toughness-related rules in EN 1993 8

1.6 Section 6: Finite element methods for determining fracture resistances in the upper shelf area of toughness 8

1.6.1 The use of porous metal plasticity models *8*

1.6.2 Damage curves *11*

1.7 Section 7: Liquid metal embrittlement in hot dip zinc coating 11

1.8 Bibliography 12

SECTION 2 13

2 SELECTION OF MATERIALS TO AVOID BRITTLE FRACTURE (TOUGHNESS REQUIREMENTS) 13

2.1 General 13

2.1.1 Basis of the selection method *13*

2.1.2 Applicability of the selection method *13*

2.2 Procedure 15

2.2.1 Fracture-behaviour of steel and temperature *15*

2.2.2 Principals of Fracture-Mechanics used for the brittle fracture concept *17*

2.2.3 Design situation for fracture assessment *22*

2.2.4 Basis of the fracture mechanic assessment *26*

2.2.5 Transformation to the temperature format *30*

2.2.6 Explanation of temperature shifts ΔT_i *32*

2.2.7 Application of the fracture mechanic method to develop table 2.1 of EN 1993-1-10 *60*

2.3 Maximum permitted thickness values - Examples **80**

2.3.1 Use of table 2.1 of EN 1990-1-10 *80*

2.3.2 Examples for the use of table 2.1 of EN 1993-1-10 *82*

2.4 Specific cases for using fracture mechanics **90**

2.4.1 General *90*

2.4.2 Example for the calculative determination of material quality *93*

2.4.3 Example for the use of fracture mechanics calculations assisted by testing *97*

2.4.4 Some other typical examples *102*

2.5 Bibliography **106**

SECTION 3 **110**

3 SELECTION OF MATERIALS FOR THROUGH-THICKNESS PROPERTIES **110**

3.1 General **110**

3.2 Procedure **113**

3.2.2 Allocation of influence to the requirement Z_{Ed} *113*

3.2.3 Minimum requirement Z_{Ed} *121*

3.2.4 Allocation of Z_{Ed} to Z-classes in EN 10164 *121*

3.3 Examples of application **122**

3.3.1 Connection of the hangers of a tied-arch-bridge to the arch *122*

3.3.2 Welded connection of the arch of a tied arch bridge to the main girder *122*

3.3.3 Connection of troughs to cross-beams in an orthotropic steel deck of a road bridge *123*

3.3.4 More general examples *125*

3.4 Bibliography **126**

SECTION 4 **128**

4. COMPLEMENTARY RULES FOR THE DESIGN TO AVOID BRITTLE FACTURE ON THE BASIS OF THE BACKGROUND TO EN 1993-1-10 **128**

4.1 Assessment of the residual safety and service life of old riveted structures **128**

4.1.1 General *128*

4.1.2 Hazards from stress situation and stress ranges *132*

4.1.3 Material check and evaluation *139*

4.1.4 Assessment of the "safe service period" *141*

4.1.5 Design tables *149*

4.1.6 Example for the fracture mechanics based safety assessment *167*
4.1.7 Bibliography *168*
4.2 Choice of material for welded connections in buildings **170**
4.2.1 Objective *170*
4.2.2 Basis of fracture mechanical assessment *171*
4.2.3 Tables for the choice of material to avoid brittle fracture *175*
4.2.4 Example *178*
4.2.5 Bibliography *180*
SECTION 5 **181**
5. OTHER TOUGHNESS-RELATED RULES IN EN 1993 **181**
5.1 The role of upper-shelf toughness **181**
5.1.1 Resistance rules in Eurocode 3 and upper-shelf toughness *181*
5.1.2 Appropriate models for calculation of upper shelf toughness requirements *182*
5.1.3 Transfer of upper shelf toughness models into practice *187*
5.2 Empirical rules for minimum upper-shelf toughness **187**
5.2.1 General *187*
5.2.2 AUBI-quality and correlations *188*
5.3 Explanations of net-section resistances in EN 1993-1-1 **193**
5.3.1 General *193*
5.3.1 Influence of upper-shelf toughness on net-section resistance to tension *193*
5.4 Choice of material for capacity design **199**
5.4.1 General requirement *199*
5.4.2 Conclusions for „capacity design“ *199*
5.4.3 Behaviour of components subject to capacity design in the temperature-transition area *200*
5.5 Bibliography **202**
SECTION 6 **203**
6. DAMAGE MECHANICS – CALCULATION OF LIMIT STATE CONDITION OF FRACTURE IN THE UPPER SHELF WITH LOCAL MODELS **203**
6.1 Introduction **203**
6.2 Model for determining crack initiation **204**
6.3 The GTN – Damage model **205**
6.3.1 General *205*
6.3.2 Examples for the determination of micro structures parameters *207*
6.3.3 Mesh sizes for FEM calculations *208*

6.3.4 Calculation of J-integral values J_i *209*
6.3.5 Conclusions for practical FEM-calculations *210*
6.3.6 Example of practical application *212*
6.4 The use of damage curves for crack initiation for cyclic straining **214**
6.4.1 General *214*
6.4.2 The combined isotropic-kinematic hardening model *214*
6.4.3 Accumulation of effective equivalent strains $\bar{\varepsilon}_{p,eff}$ *215*
6.5 Numerical simulation of crack growth **216**
6.6 Bibliography **218**
SECTION 7 **219**
7. LIQUID METAL EMBRITTLEMENT IN HOT DIP ZINC-COATING **219**
7.1 Introduction **219**
7.2 Equivalent plastic strain resistances of steels in the zinc bath **221**
7.2.1 General *221*
7.2.2 LNT-test specimen and test set up *222*
7.2.3 Test results *223*
7.3 Equivalent plastic strain requirements from the steel components **227**
7.3.1 General *227*
7.3.2 Assessment for the limit state case a) *230*
7.3.3 Assessment for the limit state case b) *239*
7.3.4 Conclusions for standardisation *244*
7.4 Testing of structural elements that are zinc coated for cracks **245**
7.5 Bibliography **246**

Section 1

1. General guidance through the commentary and summary

1.1 Section 1: Objective of the guidance

(1) This commentary gives explanations and worked examples to the design rules in Eurocode 3 that are influenced by toughness properties of the structural steels used.

(2) It is therefore a commentary and background document to EN 1993-1-10 “Material toughness and through thickness properties” and its extension in EN 1993-1-12 “Design rules for high-strength steels”, where toughness properties are expressively addressed. It is however also a background to other parts of EN 1993, e.g. to EN 1993-1-1 “Design of steel structures – Basic rules and rules for buildings”, where the design rules are related only to strength properties as the yield strength f_y and the tensile strength f_u without explicitly mentioning the role of toughness that is hidden behind the resistance formulae.

(3) Finally it gives some comments to chapter 6 of EN 1998-1: “Design of structures for earthquake resistance – Part 1: General rules, seismic actions and rules for buildings”.

1.2 Section 2: Commentary and background of EN 1993-1-10, section 2: Selection of materials for fracture toughness

1.2.1 Designation of steels and selection to performance requirements

(1) The term „steel“ comprises a group of about 2500 materials with iron (ferrum) being the main component which are tailor-made to meet the performance requirements of various applications.

(2) Structural steels are designated according to their application, mechanical properties, physical properties, particular performances and the type of coating according to fig. 1-1.

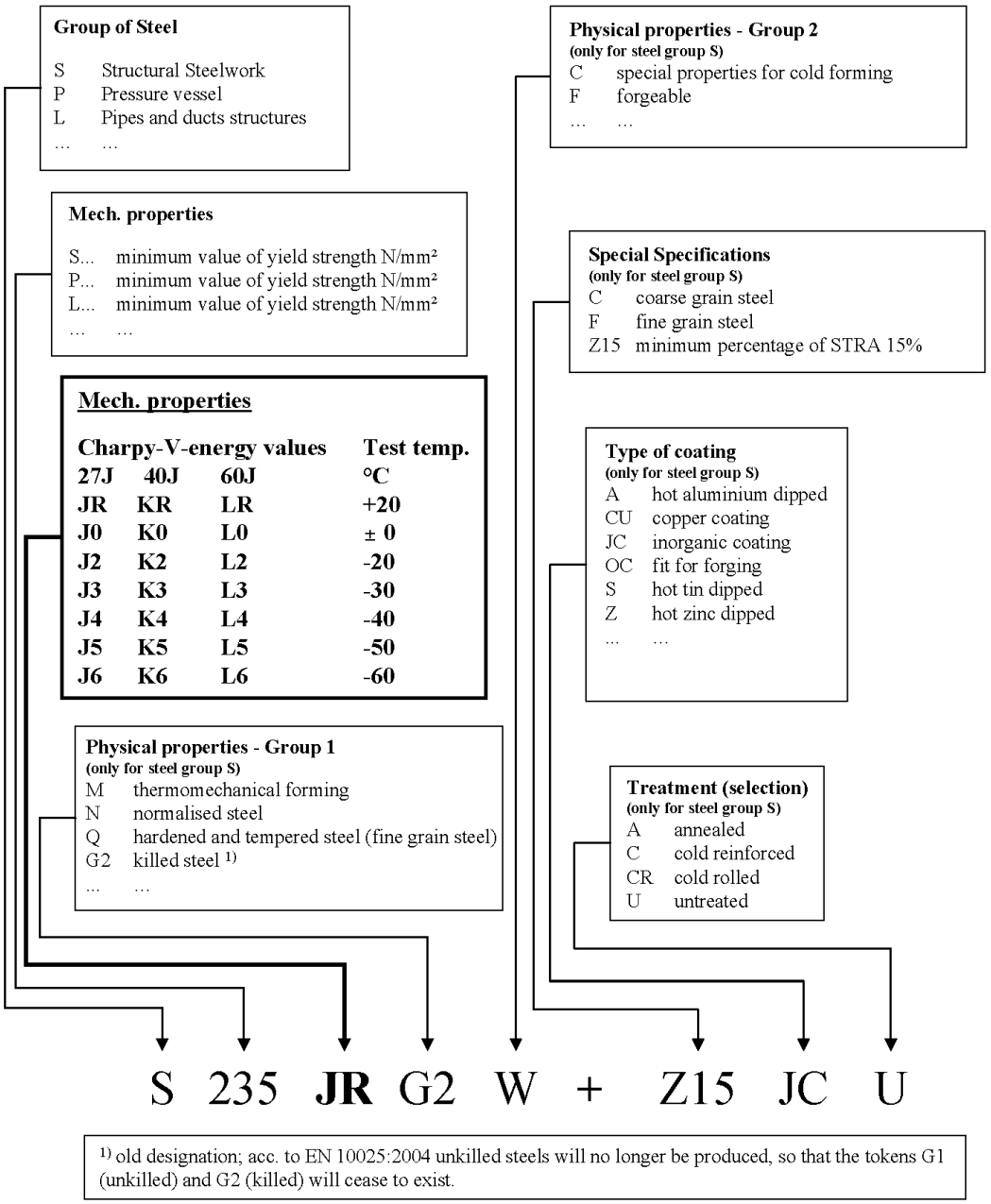


Fig. 1-1: Distinction of structural steels

(3) The selection of steels normally is related to the following performance requirements:

1. Strength requirements, e.g. related to the characteristic values of the yield strength f_y and tensile strength f_u (mostly in relation to the maximum strain ε_u at fracture).

2. Applicability to fabrication, e.g. weldability (controlled by the chemical analysis and heat-treatment), applicability for cold forming (also depending in the contents of nitrogen) and applicability for zinc-coating (for sufficient resistance to cracking in the zinc-bath and also for sufficient quality of the coating depending on the silicon-content).

3. Applicability for different temperatures, e.g. with regard to strength- and creeping behaviour (at elevated service temperatures), strength

behaviour in the case of fire and fracture behaviour at low temperatures (brittle fracture).

4. Resistance to corrosion, e.g. steels with normal corrosion resistance without or with corrosion protection by painting or coating, weathering steels, stainless steels.

5. Special properties, as e.g. wearing resistance or magnetic properties.

(4) EN 1993-1-10 section 2 addresses the steel selection of ferritic structural steels with different strength that are exposed transiently or pertinently to low temperatures to avoid brittle fracture.

1.2.2 The use of strength-values f_y and f_u from coupon tests and of toughness values T_{27J} of the material in EN 1993

(1) The design rules for ultimate limit states in the various parts of EN 1993 are based on a "technical stress strain curve" as given in fig. 1-2, where f_y is the yield strength and f_u is the tensile ultimate strength, determined from steel coupons tests at room temperature.

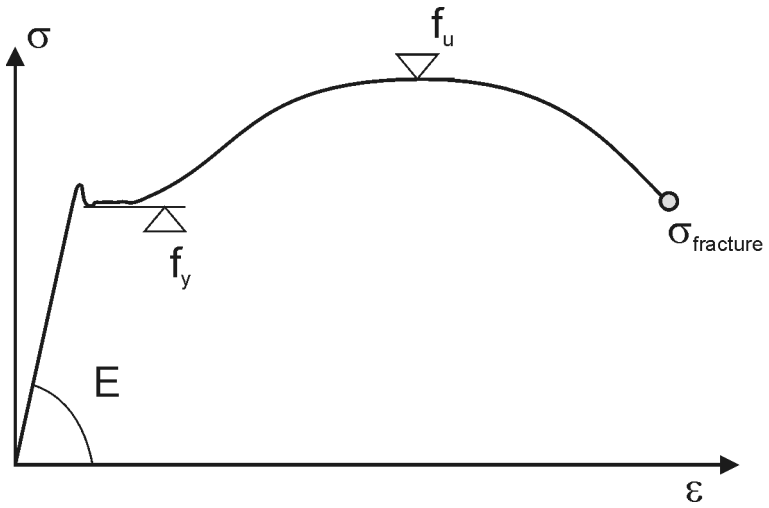


Fig. 1-2: "Technical stress-strain-curve" from steel coupon tests for room temperature as used for design

(2) The yield strength f_y varies with the temperature T, see also section 2, fig. 2.1 and fig. 2.5, and with the strain rate $\dot{\varepsilon}$ that can be considered together with the temperature T according to table 1.1.

Steel grade	$f_y(\dot{\varepsilon},T)$	m
S235	$f_{y,RT}+960\cdot\left[1-1.0767\cdot10^{-4}\cdot T\cdot\ln\left(\frac{10^8}{\dot{\varepsilon}}\right)\right]^m$	2.8
S275		
S355		3.27
S460		
S690	$f_{y,RT}+960\cdot\left[1-7.2993\cdot10^{-5}\cdot T\cdot\ln\left(\frac{10^{10}}{\dot{\varepsilon}}\right)\right]^m$	3.74
S890		

Table 1-1: Yield strength f_y depending on T and $\dot{\varepsilon}$ [1]

(3) Such variations from the conditions of the steel coupon tests are normally neglected for structures exposed to climatic actions in Europe.

(4) The fracture strength $\sigma_{fracture}$ results from the "notch situation" of the test piece considered (e.g. effected by initial cracks) and from the toughness of the material, that depends on the temperature as well, see also fig. 2.1, fig. 2.2 and fig. 2.5.

(5) The resistance functions for "cold design" in all parts of EN 1993 are based on experimental tests of prefabricated components also carried out at room temperature and hence apply to the upper shelf region of the toughness-temperature curve, see also fig. 2.2.

(6) The behaviour at the ultimate limit state is therefore ductile, and the design models used for the resistances are only related to the material strength f_y and f_u as given in fig. 1-2, see fig. 1.3.

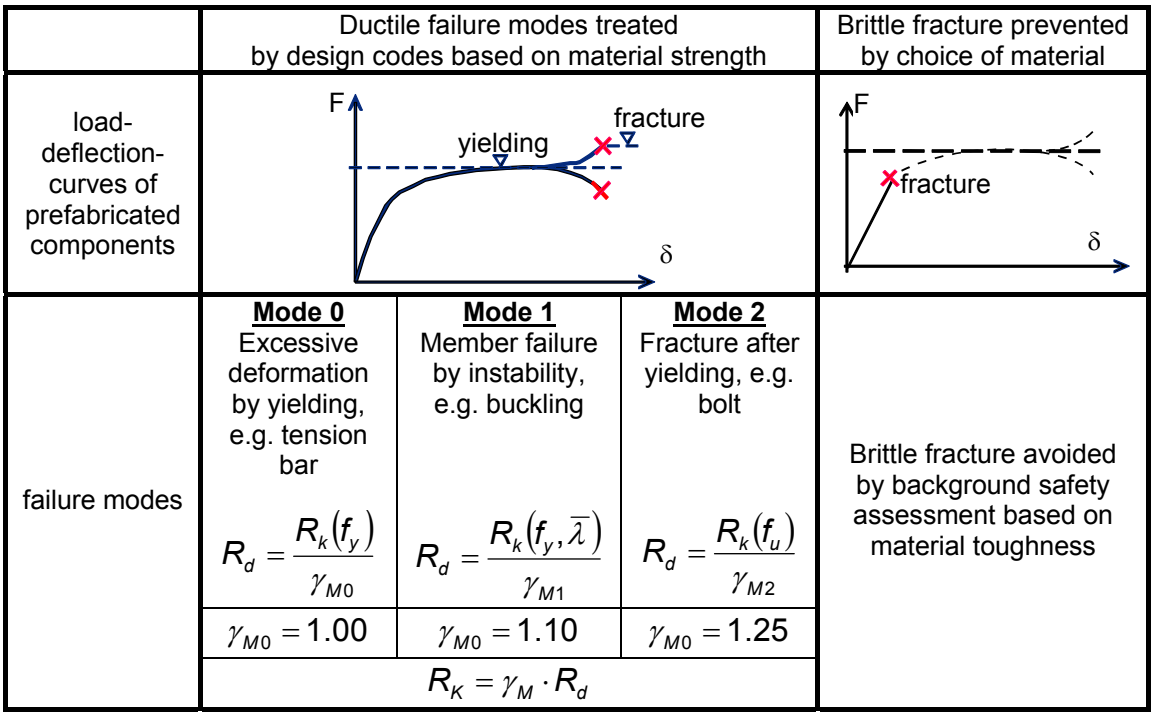


Fig. 1.3: Load-deflection curves of prefabricated components in tests at room temperature and associated resistance functions based on f_y an f_u only

(7) The influence of toughness on the resistance functions in the upper shelf region is taken into account only indirectly by factors applied to the tensile strength f_u, see section 5.

(8) An explicit toughness-oriented verification has been carried out as a background study to justify the quantitative elements of the rules for the choice of materials in EN 1993-1-10 that are related to the lower part of the transition area of the toughness-temperature curve. The principles of the fracture-mechanics assessment method used are stated in section 2 of EN 1993-1-10; details however and guidance how to use it for other cases are only given in section 2 of this commentary.

1.2.3 Conclusions

(1) The two-way safety assessments for steel-structures, i.e.:

- the strength related checks for ultimate limit states in the various parts of EN 1993, which as far as tension resistance is concerned indirectly take toughness properties in the upper shelf region into account, and
- the toughness related checks hidden behind the rules for the choice of material to avoid brittle fracture

ensure appropriate safety of steel structures in the full temperature range of application.

(2) The safety assessment in the upper shelf region is based on ductile behaviour, the consequences of which are

- nominal stresses can be used and stress concentrations and residual stresses can be neglected,
- plastic design assumptions can be applied for members and connections, e.g. secondary moments can be ignored,
- energy dissipation is possible by hysteretical behaviour that produces beneficial behaviour-factors q for seismic design.

(3) The toughness assessment behind section 2 of EN 1993-1-10 is based on an accidental design situation with extremely low temperatures and consequently low toughness values on one side and a crack-scenario to determine onerous toughness requirements on the other side. It is performed in the elastic range of material properties where no significant influence of plastification can be expected. Such an explicit toughness assessment needs not be made any more in design if the rules for the selection of material in EN 1993-1-10, section 2 are used.

(4) A prerequisite of the strength-oriented and toughness-oriented design rules in EN 1993 is, that the fabrication of the structural component considered complies with EN 1090-Part 2.

1.3. Section 3: Commentary and background of EN 1993-1-10, section 3: Selection of materials for through-thickness properties

(1) Section 3 of this commentary relates to section 3 of EN 1993-1-10: Selection of materials for through-thickness properties according to Z-grades as specified in EN 10164.

(2) The commentary explains the phenomenon, gives different routes for the choice of through-thickness-quality and presents a numerical procedure based on a limit state for Z-values (percentage short transverse reduction of area (STRA) in a tensile test:

$$Z_{Ed} \leq Z_{Rd}.$$

(3) The Z-requirements are associated with various influences, mainly the weld configuration and weld size and the restraint to welding shrinkage.

(4) The efficiency and reliability of the procedure is proved by test results.

1.4 Section 4: Complementary rules for the design to avoid brittle fracture on the basis of the background to EN 1993-1-10

1.4.1 Scope

(1) Section 4 gives complementary non conflicting informations to section 2 of EN 1993-1-10 in that some additional application rules are given that comply with the principles, basic assumptions and methods given in EN 1993-1-10.

(2) These application rules apply to

- Assessment of residual safety and service life of old riveted structures (section 4.1)
- Choice of material for welded connections in buildings (section 4.2).

1.4.2 Assessment of residual safety and service life of old riveted structures

(1) The assessment of residual safety and service life of old riveted structures is an example for how any such assessment could be performed for any existing steel structure, that is subjected to fatigue loads.

(2) The procedure given complements the general procedure given in the JRC-Scientific Technical Report: “Assessment of Existing Steel Structures: Recommendations for Estimation of Remaining Fatigue Life (EUR 23252-EN-2008) by giving a fracture mechanics based method to prove “damage-tolerance” of existing structures.

(3) Whereas for the selection of material for new projects the “safe service periods” between inspections are specified such that the fatigue load for that “safe service periods” is equivalent to 1/4 of the full fatigue damage accepted for the full nominal service life of the structures (e.g. a safe-service period of 30 years for a full nominal service life of 120 years). Subsequently the associated steel grade and toughness properties are the unknowns; the assessment of existing structures however works with known values of the steel grade and toughness properties of the existing steel and asks for the associated value of “safe service period”

(4) The “safe service period” should be sufficiently large, so that the formation of cracks can be detected in usual inspections by NDT-methods before they get critical (sufficient prewarning).

(5) If the “safe service periods” are too small, the inspection intervals or the fatigue loading can be reduced or appropriate retrofitting measures can be applied.

(6) The assessment method presented is based on the conservative assumption of through cracks and gives design aids to perform the assessment with tables and graphs.

1.4.3 Choice of material for welded connections in buildings

(1) As EN 1993-1-10, section 2 has been developed for structures subjected to fatigue as bridges, crane runways or masts subjected to vortex induced vibrations, its use for buildings where fatigue plays a minor role would be extremely safe-sided.

(2) Section 4.2 gives for the particular case of welded connections of tension elements with slots in gusset plates (as e.g. for bracings or tension rods) alternative rules based on assumptions more appropriate for buildings with predominant static loading.

(3) These assumptions are:

- a structural detailing not classified in EN 1993-1-9
- initial cracks as through cracks with a larger size than in EN 1993-1-10

- crack growth by fatigue with a smaller fatigue load than in EN 1993-1-10: This fatigue load is equivalent to the damage $D = \Delta\sigma^3 \cdot n = 26^3 \cdot 10^5$
- certain limits for the dimensions following good practice.

(4) As a result tables for the selection of materials are given that are similar to table 2.1 given in EN 1993-1-10.

1.5 Section 5: Other toughness-related rules in EN 1993

(1) Section 5 of this commentary refers to the influence of toughness on the resistance rules in EN 1993 and EN 1998 which nominally relate to the strength properties of material only. The influence of toughness, which is in the upper shelf region of the toughness-temperature diagram, is normally hidden in factors to the strength or in other descriptive rules.

(2) The first part 5.1 of this section explains the relationship between experimental results for fracture loads from large wide plate tests and various fracture mechanics approaches in the upper shelf region.

(3) Part 5.2 explains the background of a recommendation for the choice of material for bridges given in table 3-1 of EN 1993-2 – Design of steel bridges – that is based on a traditional empirical approach to secure a certain toughness level at room temperature for plate thicknesses above 30 mm. It is not performance oriented but may still be used as a requirement in addition to the minimum requirement in EN 1993-1-10 by some bridge authorities.

(4) Part 5.3 explains the background of the ultimate resistance formula for net sections in Part 1-1 and Part 1-12 of EN 1993 also addressing the assumption of geometrical imperfections in the form of crack-like flaws by which toughness aspects enter into the formula.

Also the effects of strength on the maximum strains for ductile behaviour are highlighted.

(5) Part 5.4 finally deals with the conclusions from “capacity design” for the material properties. The requirements for material toughness, structural detailing and fabrication are the higher, the higher the material strengths are.

1.6 Section 6: Finite element methods for determining fracture resistances in the upper shelf area of toughness

1.6.1 The use of porous metal plasticity models

(1) Sections 2 to 5 of this commentary are related to the dual approach for safety assessments to avoid failure:

1. the strength-controlled approach represented by the resistance formulae in EN 1993
2. the toughness-controlled approach usually carried out by fracture mechanics, where the method used depends on the temperature and its impact on the toughness properties in the toughness-temperature-diagram as follows:
   a) in the lower shelf region: relevant material properties: K_{IC} or J_c leading to the fracture stress $\sigma_{fracture}$.

b) in the transition area between the lower shelf region and the upper shelf region: relevant material properties:

A_v-T-curve or J-T-curve

c) upper shelf region: relevant material properties: J_R-curve (J-Δa) from large plate tests.

(2) Section 6 tackles with an alternative to this dual approach that is based on damage theory. With this theory it is possible to determine material properties from the microstructure of the steel and to simulate numerically with FE-methods

a) the performance of steel coupon tests,
b) the performance of fracture mechanics tests,
c) the performance of any structural member, the failure of which may have been modelled using the results of steel coupon tests or fracture mechanics tests.

Thus the damage theory has the potential to cover both the application fields of the strength controlled and of the fracture mechanics controlled methods in the future.

(3) Table 1-2 gives a survey on consequences of damage theory on the constitutive law to be applied to a single cell (of grain size) of a FE-mesh, to simulate the behaviour of a structural member.

The parameters of the GTN-model are determined for the material in consideration from tests (fitted parameters), so that effects of damages can be calculated for members of different shape made of this material.

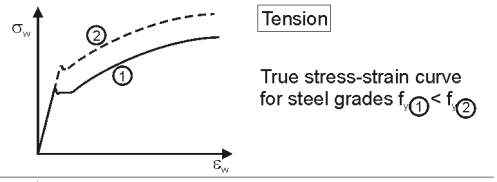
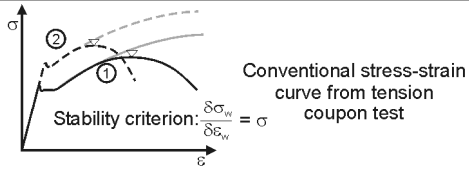
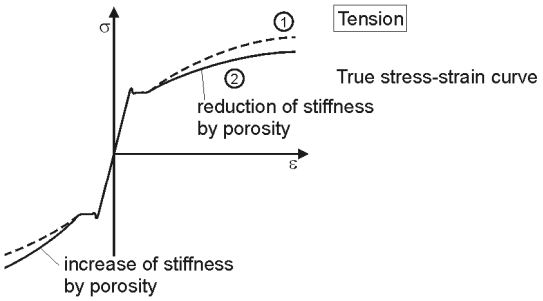
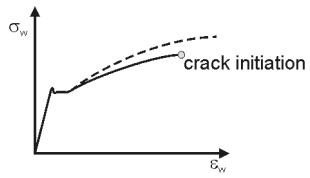
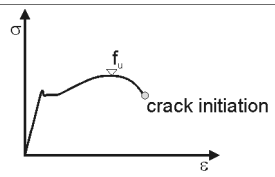
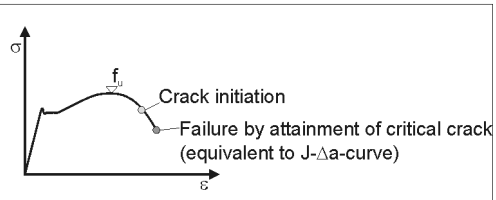
Ductile models without cracks	Constitutive law for a single cell without damage effect	Derivation of tensile strength from “true” stress-strain curve	
		Effect on tension coupon test: stability strength f_u ε_u dependent on f_u	
	Constitutive law with damage effect	Effect of voids in a single cell of material, e.g. by GTN-model: Decrease or increase of stiffness of true stress-strain curve	
	Crack initiation with damage effect	Attainment of a final void volume fraction f_f at microscopic failure at which the stress transfer through a cell is interrupted	
		Effect on tension coupon test: Attainment of strain equivalent to the attainment of J_i	
Models with cracks	Stable crack growth to failure load	Introduction of cohesive models between finite elements to model stable crack growth Cohesive models calibrated to J-Δa-curves	

Table 1-2: Features of GTN-model to simulate damage effects of a single cell of material

(4) A typical example giving the the consequences of effects of different constitutive laws (true stress-strain curves) is the plastic resistance of cold-formed profiles, see fig. 1.4.

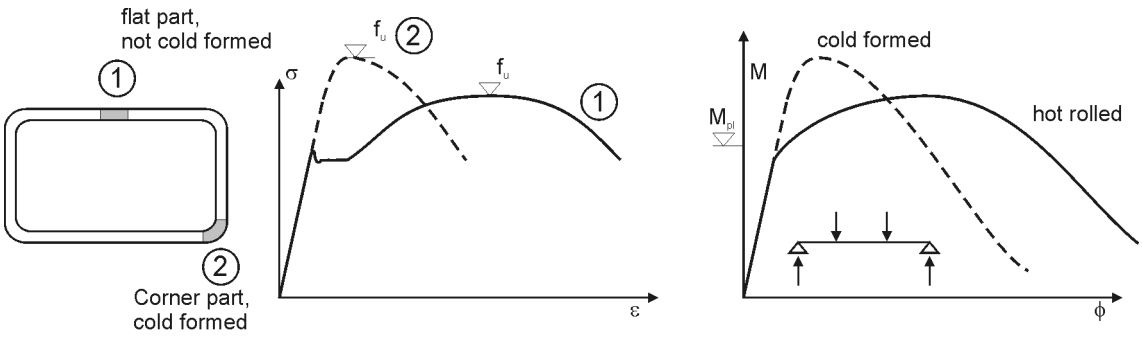


Fig. 1.4: Effects of increase of strength by cold forming on constitutive laws for cold-formed and not cold-formed regions of sections.

(5) Part 6.4 of section 6 also deals with the use of the damage theory for cyclic straining as experienced in the response to seismic actions. It includes a model for strain accumulation.

1.6.2 Damage curves

(1) With using a constitutive law for ductile material behaviour the results of tests or of calculations with the damage theory may be plotted in damage-curves, that give local ultimate equivalent plastic strains limited by the formation of micro cracks (equivalent to J_i) in finite elements versus the relevant parameter "stress triaxiality" $h = \frac{\sigma_1 + \sigma_2 + \sigma_3}{3\sigma_v}$, see 6.3.5 and 6.4.3

(2) Whereas the "stability strength" allows to determine failure loads for load-controlled design situations (e.g. tension rods), the use of the damage curve is appropriate, where in deformation-controlled design situations the ultimate strains, to avoid cracking, are looked for (e.g. for pressure vessels).

(3) For cases of failure controlled by "stability strength" it is sufficient that the ultimate strain of material causing cracking is greater that the maximum strain ε_u associated with f_u.

1.7 Section 7: Liquid metal embrittlement in hot dip zinc coating

(1) In the years 2000-2005 an increased number of cracks in galvanised steel components have been observed that formed in the zinc bath during the dipping process.

(2) Research has been reactivated to find out the causes for these cracks and to initiate measures to avoid them.

(3) The research revealed that cracking occurred where a limit state defined by the balance between the crack driving plastic equivalent strains $\varepsilon_{pl,E}$ and the strain-capacity $\varepsilon_{pl,R}$ of the steel influenced by dipping speed and by more or less corrosive compositions of the liquid zinc-alloy was exceeded.

(4) Both the actions $\varepsilon_{pl,E}$ and the resistances $\varepsilon_{pl,R}$ follow the concept of the damage curves in section 5; they also are time-dependant, so that the rules for strain-accumulation for cyclic loading in section 5 apply.

(5) Section 7 gives the background of the limit state assessment for avoiding cracking of steel components in the hot zinc bath as far as needed to understand the process and the basis for more descriptive rules for design, fabrication and zinc-coating that could be part of a future amendment of Eurocode 3 and of EN 1090.

1.8 Bibliography

[1] Kühn, B., Beitrag zur Vereinheitlichung der europäischen Regelungen zur Vermeidung von Sprödbruch, Dissertation am Lehrstuhl für Stahlbau, RWTH Aachen, Shaker-Verlag, ISBN 3-8322-3901-4.

Section 2

2 Selection of materials to avoid brittle fracture (toughness requirements)

2.1 General

2.1.1 Basis of the selection method

(1) The basis of the selection of materials for fracture toughness is an Ultimate Limit State verification based on fracture mechanics for an accidental design situation for structural members in tension or bending.

(2) This verification includes the following influences:

- structural detailing of the steel member considered
- effects from external actions and residual stresses on the member
- assumption of crack-like flaws at spots with strain concentrations
- material toughness dependent on the temperature

For particular applications also the influences of cold forming and large strain-rates are included.

(3) As the material toughness for the steel-grade to be chosen is specified in the product standards, e.g. EN 10025, as the test-temperature T_{KV} [°C] of Charpy impact energy tests, for which a certain minimum value KV of impact energy shall be achieved, (e.g. for steel S355 J2: T_{27J} = -20°C, or $KV_{min} \geq 27$ Joule for the testing temperature T_{27J} = - 20°C) the fracture mechanics verification has to be carried out in such a way that it refers to this specification of product property.

(4) According to EN 10025-1 KV_{min} is the lower limit to the mean value of 3 tests carried out in a qualification procedure for steel as given in the Harmonised European materials standards as EN 10025, where the minimum value measured must exceed 70% of KV_{min}. There are also cases where another 3 tests are required to fulfil requirements for KV_{min}.

2.1.2 Applicability of the selection method

(1) The selection method for fracture toughness has been developed on the basis of safety assumptions which include the presence of initial cracks (e.g. from fabrication) that may have been undetected during inspections and may grow in service from fatigue.

(2) Therefore the verification has been performed for rather large design values of crack sizes. It is applicable to unwelded and welded structures subjected to fatigue loading, such as bridges or crane runways.

(3) The method covers all structural details for which fatigue classes are given in EN 1993-1-9.

(4) The method may also be used for building structures, where fatigue is less pronounced. In this case the use of the large design values of crack sizes may be justified by the fact that, due to less refined welding controls, the initial

cracks may be larger, so that they compensate the smaller crack growth from fatigue.

(5) The selection method in EN 1993-1-10 presumes that the selection of material shall be made in the design stage to specify the steel grade for material delivery. It is therefore related to the numerical values of T_{KV} specified in the product standards (e.g. in EN 10025) and takes into account that actual values are probably much higher than those specified.

(6) If the method is to be used to confirm or justify the suitability of existing material by a "fitness for purpose" study (e.g. for existing structures or material already available, from which measured data can be taken), the method may not be used without a modification of the safety elements.

(7) The core of the method is table 2.1 of EN 1993-1-10 which is based on the following:

1. Standard curve of design value of crack size versus plate thickness t, that envelopes all design values of crack size resulting from initial cracks and crack growths for the fatigue classes in EN 1993-1-9
2. Safety elements covering the use of T_{KV}-values specified in the Harmonised European material standards for steel
3. Definition of yield strength as specified in the Harmonised European material standards for steel
4. Nominal stresses from external loading for an accidental design situation
5. Static loading without dynamic impact effect limited by a strain rate $\dot{\varepsilon} = \frac{\partial \varepsilon}{\partial t} \leq 4 \cdot 10^{-4}$/sec.
6. Welding in conformity with EN 1090-Part 2
7. Residual stress, both local from welding and global from remote restraints to shrinkage of welded components
8. No modification of material toughness by cold forming: $\varepsilon_{cf} \leq 2\%$.

(8) Table 2.1 of EN 1993-1-10 may also be used where the assumptions for $\dot{\varepsilon}$ and ε_{cf} are not met by modifying the reference temperature T_{Ed} by $\Delta T_{\dot{\varepsilon}}$ according to (2.2.6.4) or $\Delta T_{\varepsilon,cf}$ according to (2.2.6.5).

(9) For other cases, there is no full guidance in EN 1993-1-10, but the principles are given in sections 2.2 and 2.3 and the door opener for more refined methods is established is section 2.4.

(10) The commentary and background document gives explanations to the standard procedure in EN 1993-1-10 and also gives supplementary non contradicting information on how the principles and the door opener for more refined methods in EN 1993-1-10 may be used.

2.2 Procedure

2.2.1 Fracture-behaviour of steel and temperature

(1) For ferritic steels, the fracture behaviour of tensile loaded components, in particular the extent, to which they exhibit a non-linear load-deformation curve by yielding, depends strongly on the temperature.

(2) Fig. 2-1 shows in a schematic way the fracture behaviour of tensile loaded components wich bear a crack-like flaw. The figure contains different informations which are related to the fracture behaviour. Characteristic temperatures are also defined which enable the distinction of fracture behaviour into brittle and ductile:

1. The fracture mechanism (on a microscopic scale) being cleavage at low temperatures and becoming shear or ductile above a temperature T_i.

2. The fracture stress depending on temperature and increasing from low temperatures to a temperature T_{gy}, where net section yielding is observed before fracture and going further up to a temperature T_m where the full plastic behaviour in the gross section and the ultimate load is reached.

3. The macroscopic description of the fracture behaviour is defined as brittle if fracture occurs before net section yielding and where the global behaviour is linear elastic or as ductile behind this point, where plasticity can be observed in the cross section and the load displacement deviates from linearity.

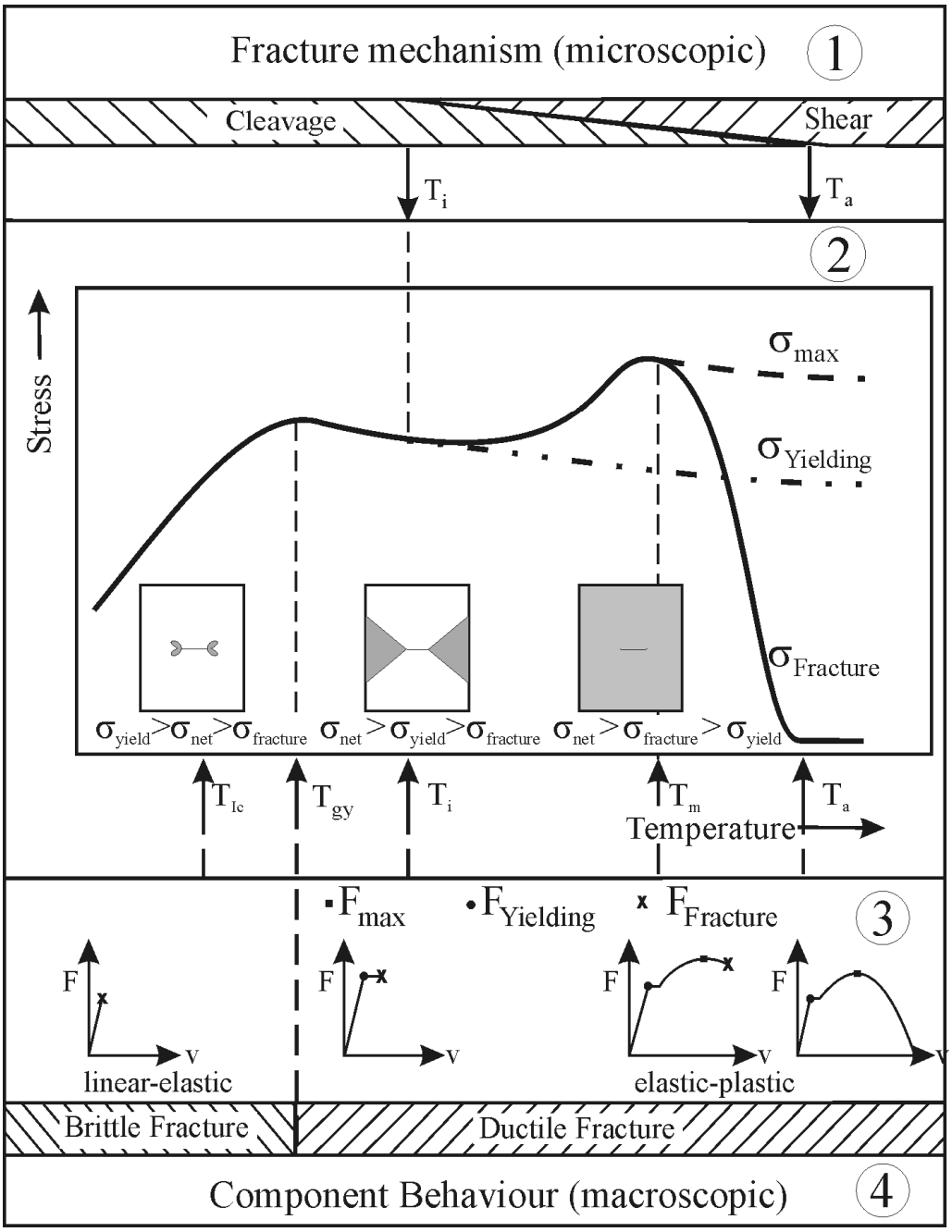


Fig. 2-1: Fracture behaviour of components depending on temperature (schematic view)

(3) The temperature region above T_m signifies the region with large plastic strains which enable plastic redistribution of stress concentrations in the cross-section and the formation of plastic hinges for plastic mechanisms. In the upper shelf region above T_a the ultimate tension strength results from the stability criterion

$$A \cdot \partial\sigma = \partial A \cdot \sigma \qquad (2\text{-}1)$$

and is not controlled by toughness.

(4) In the range $T \geq T_m$ (room temperature) all member tests have been carried out, from which the resistance functions and design rules for steel structures in Eurocode 3 have been derived, see fig. 2-2.

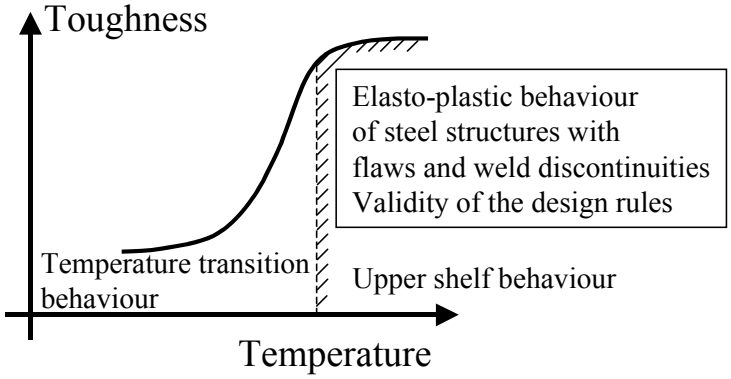


Fig. 2-2: Temperature range for validity of design rules in Eurocode 3

(5) Below T_m is the temperature transition range that leads to the lower shelf behaviour, where the material toughness decreases with temperature and the failure modes change from ductile to brittle.

Below T_m the macroscopic plastic deformations are smaller than those above T_m. They suffice to reduce stress concentrations in the cross-sections so that the nominal stress concept can be applied. They are, however, no longer sufficient for plastic hinge rotations, so that global analysis should be made on an elastic basis.

A limit that separates this macroscopic ductile failure mode from the brittle failure mode is the temperature T_{gy}, at which net section yielding is reached before failure. The brittle fracture avoidance concept presented here is related to this area.

Below T_{gy} the plastic deformations are restricted to local crack tip zones, which can be quantified with fracture mechanics parameters like K, CTOD or J-Integral.

2.2.2 Principals of Fracture-Mechanics used for the brittle fracture concept

(1) The principals of fracture mechanics are based on the perception that the local stress concentration in the vicinity of a crack in any component can be quantified by a single parameter. This single parameter can be calculated analytically or by use of Finite Element Simulation as crack driving force depending on the outer stress and (if necessary) of secondary stresses.

(2) The parameters which have been developed are:

- Stress Intensity Factor K (Unit: $MPam^{0,5}$), which is limited to linear elastic behaviour and in most cases cannot be applied for structural steels due to there good local and global yielding behaviour.

- J-Integral (Unit: N/mm), which is presenting a path independent line Integral around the crack tip and provides the crack driving force as an energy parameter which allows the optimal quantitative description of effects of local plasticity.

- CTOD (Crack Tip Opening Displacement, Unit: mm) which also suites for elastic-plastic behaviour and represents the opening of the crack tip as a measure of local plasticity ahead of the crack tip.

(3) To allow for the calculation of the critical limit condition where fracture may occur in a structure with possible defects it is necessary to obtain the resistance of the material against crack initiation with the same fracture mechanics parameters, see fig. 2-3.

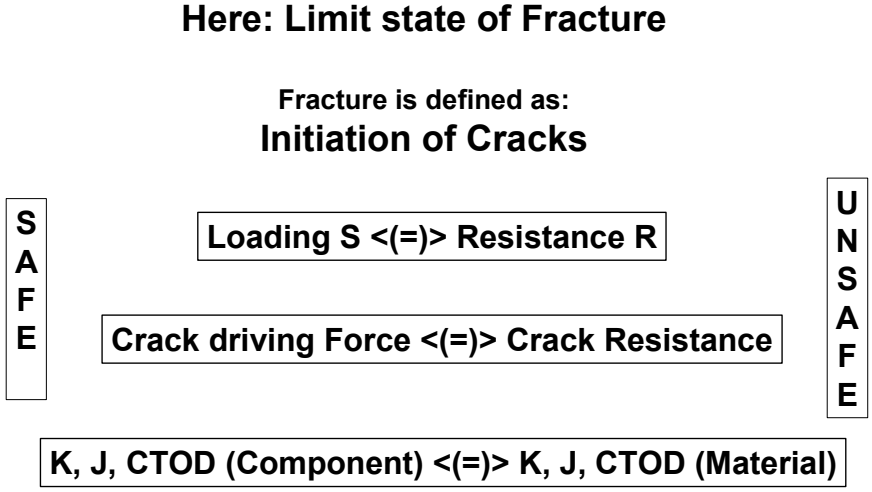


Fig. 2.3: Limit state design for fracture problems

(4) Special small scale laboratory test specimens have been developed from which the most widely used are the CT- (Compact Tension) and the SENB- (Single Edge Notch Bending) specimen (fig. 2-4).

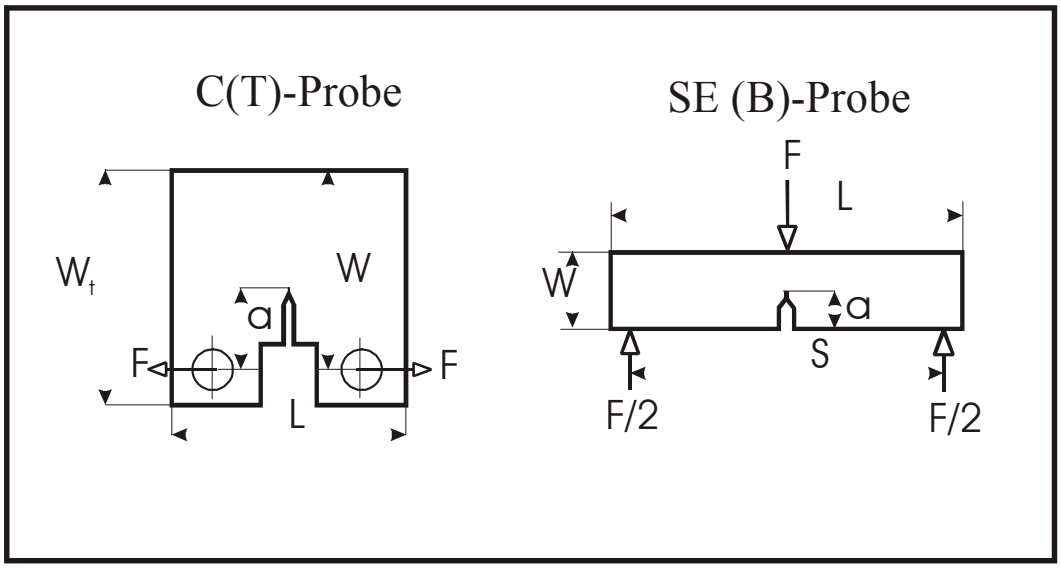


Fig. 2-4: Fracture Mechanics specimen

(5) The transitional behaviour of ferritic steels is also observed from the fracture mechanics test as shown schematically in fig. 2-5.

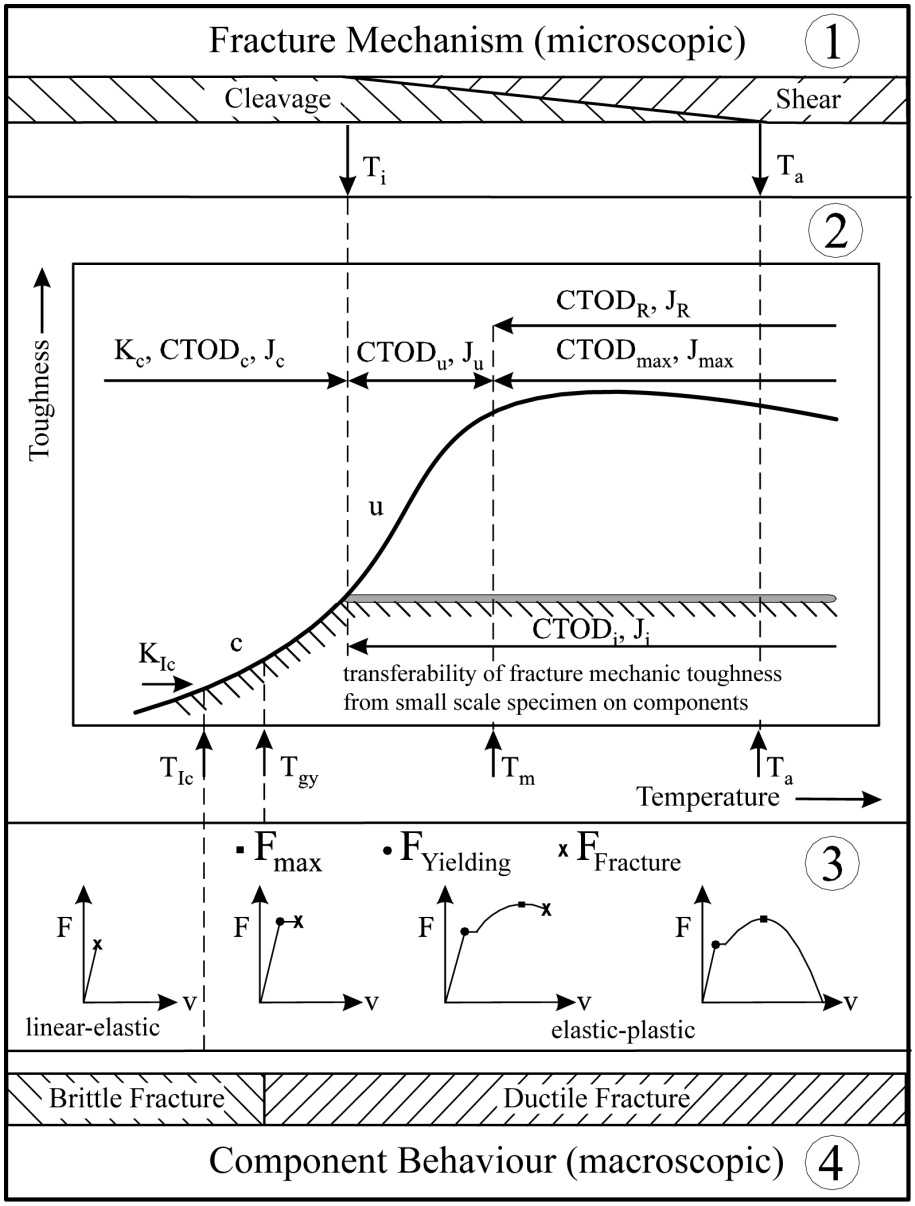


Fig. 2-5: Transitional fracture behaviour of fracture mechanics specimen

The fig. 2-5 is similar to that shown in fig. 2-1. The major difference is the definition of the indices related to fracture mechanics tests. The indices can be interpreted as follows:

c: the fracture mechanism at crack initiation is cleavage. Further crack growth is spontaneous without energy consumption. The crack behaviour is also named unstable crack growth.

i: the mechanism at crack initiation is ductile. Further increase of load is necessary to drive the crack further. Hence, the crack grows under energy assumption. The crack behaviour is also named stable crack growth.

u: in the transition region the fracture mode changes from ductile to cleavage after initiation of stable crack growth (index i)

m: the load displacement curve reaches a maximum value.

In view of this background it is important to know that only the fracture mechanics values obtained for crack initiation (index i or c) are transferable geometry independent material values.

(6) The fracture mechanics analysis can now be performed in the following way:

1. Derive a fracture mechanics model of the structure concerned with a representative flaw assumption.

2. Derive the crack driving force with analytical solutions like stress intensity factor solutions from handbooks corrected by plastic correction factor as given by the failure assessment diagram FAD (fig. 2-6).

3. Derive material resistance as fracture toughness value from tests at adequate temperature or from correlation. Correlations which have specifically been developed for structural steels and weldments are provided from the master curve concept, see fig. 2-7 and fig. 2-8.

4. Calculate in the limit condition for fracture from three parameters free to choose (crack geometry, toughness, stress) one when the other two are known. This means that you can calculate critical crack length for fitness for purpose or critical toughness for material selection or critical stress fracture for component dimension and strength, fig. 2-3.

5. Verify results from either experience or larges scale tests and select appropriate safety factors to cover scatter from input parameters and model uncertainty.

(7) Another important feature is that material toughness values obtained with elastic plastic fracture mechanics test procedure like J-Integral or CTOD can be transferred into units of stress intensity factor K, thus not being the same value as a valid K_{Ic} value, but a representative of the elastic plastic fracture toughness and for use in conjunction with FAD analysis. The formula to be used is:

$$K_J = [J^*E/(1-\upsilon^2))^{0,5} \qquad (2\text{-}2)$$

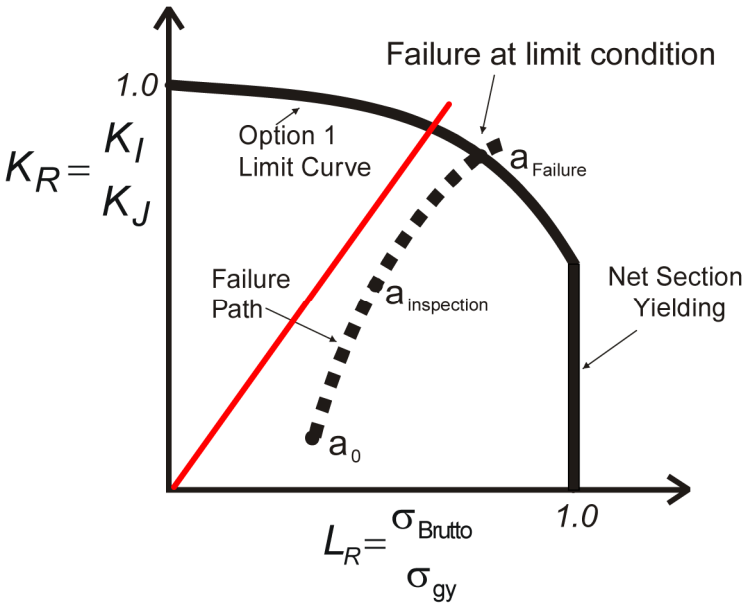


Fig. 2-6: Schematic view of the failure assessment diagram (FAD)

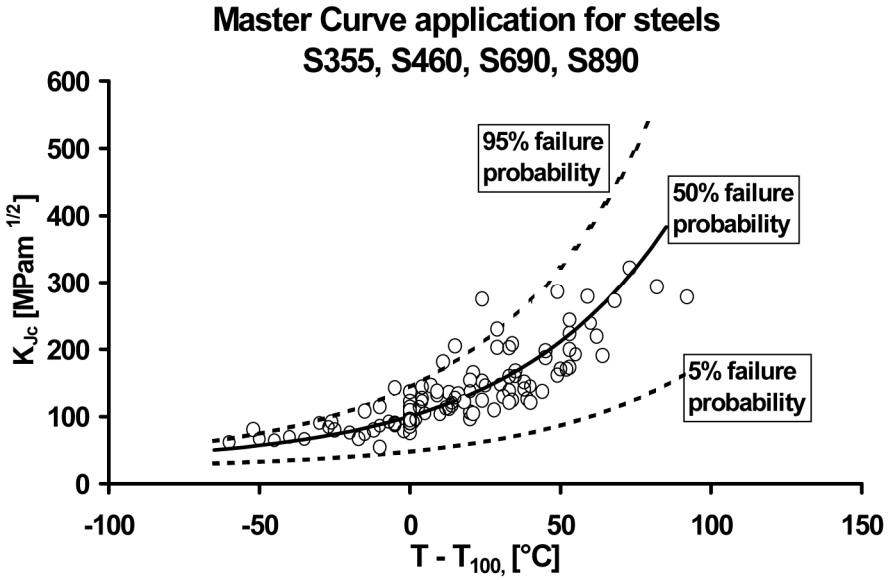


Fig. 2-7: Fracture mechanics master curve for ferritic steels

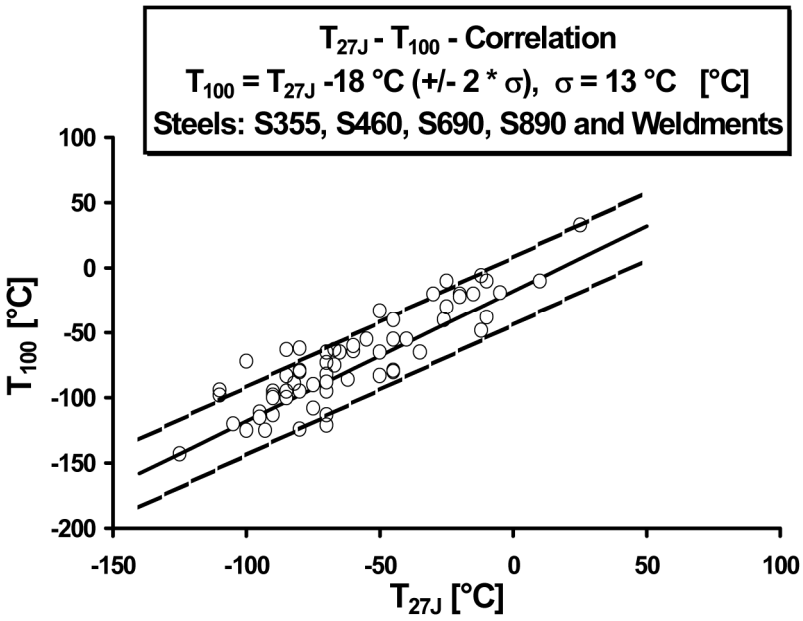


Fig. 2-8: Transition temperature correlation between fracture mechanics transition temperature T_{100} and charpy transition temperature T_{27J}

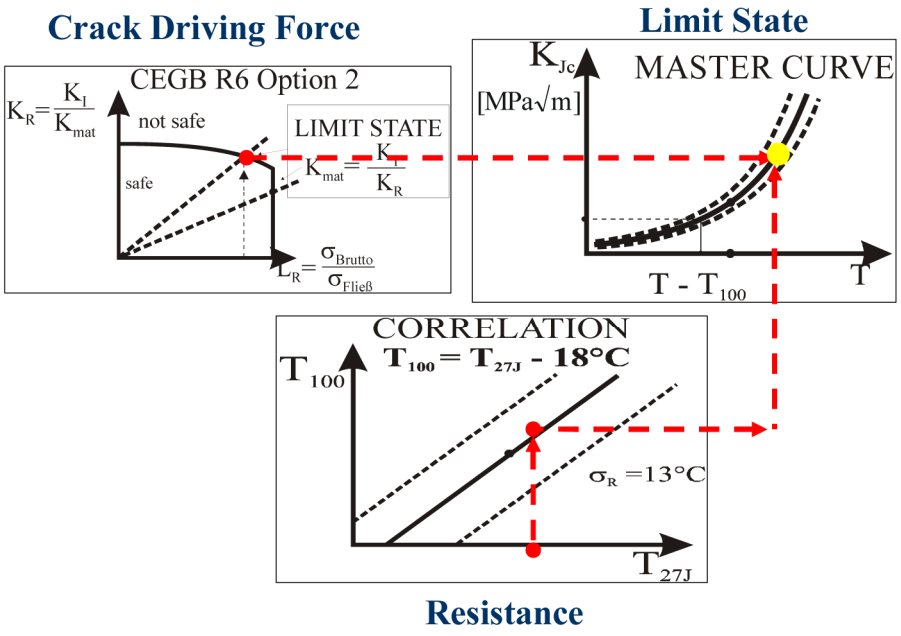


Fig. 2-9: Principal of fracture mechanics analysis as being used for brittle fracture concept in EN1993-1-10

2.2.3 Design situation for fracture assessment

2.2.3.1 Requirements for ultimate limit state verification with ductile behaviour

(1) In general, ultimate limit state verifications are carried out by balancing design values of action effects E_d and resistances R_d:

$$E_d \leq R_d \qquad (2\text{-}3)$$

(2) The design values of resistance R_d in Eurocode 3 have been determined from:

$$R_d = \frac{R_k}{\gamma_M} \tag{2-4}$$

where

R_k = characteristic values of resistance determined from the statistical evaluation of large scale tests carried out in test laboratories at room temperature (in general defined as 5% fractiles of a large representative population).

γ_M = partial factor to obtain design values (also determined by test evaluations for α_R = 0.8 and β = 3.80. However, for practical reason classified into γ_{M0}, γ_{M1} and γ_{M2})

These resistance values reflect ductile failure modes as encountered in the upper shelf region of the toughness-temperature curve.

(3) Fig. 2-10 gives a schematic view on how member tests to determine R-values for Eurocode 3 have been carried out:

1. Members made of semi-finished products according to EN-product standards and fabricated according to execution standards as EN 1090-2 are considered to be representative for the statistical distribution of properties (e.g. geometries, mechanical properties, imperfections) controlled by these standards).

2. Such members have been subjected to tests with boundary conditions, load applications and load paths that mirror real loading conditions. The results are experimental resistances $R_{exp,i}$, for which an appropriate calculative design model R_{calc} is proposed.

3. From a comparison of the experimental values $R_{exp,i}$ with the calculative values $R_{calc,i}$ the model uncertainty is determined (mean value-correction and error term), from which the statistical properties and hence the characteristic values R_k and the design values R_d are determined and after classification of γ_M the R_k-value can be corrected.

4. The statistical characteristics, obtained from the test evaluation (e.g. the mean values and standard deviations for geometrical and mechanical properties) can then be used to check the results of the quality control of the manufacturers.

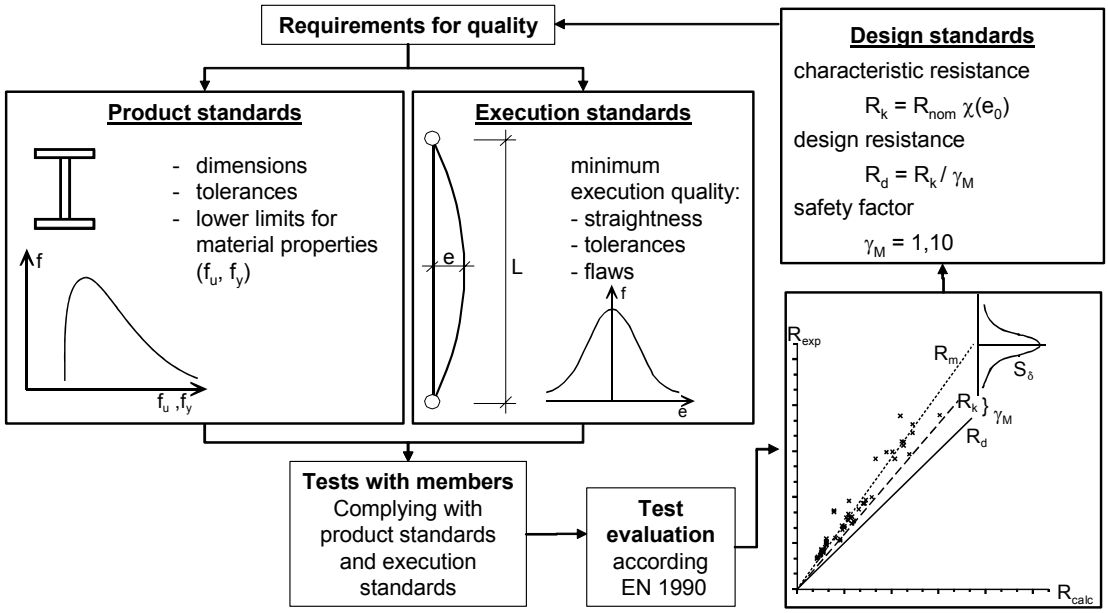


Fig. 2-10: Consistency of product standards, execution standards and design standards

(4) This procedure, providing consistency between the properties specified in product standards and the design rules in Eurocode 3, is only valid for ductile behaviour excluding any brittle fracture.

(5) To secure ductile behaviour for all design situations covered by Eurocode 3, two conditions must be met:

1. Sufficient ductility by specifying the material properties in the upper-shelf region of the temperature-toughness diagram as in section 3 of EN 1993-1-1.

2. Avoidance of brittle fracture by performing additional safety verification in the temperature transition range of the temperature-toughness diagram with toughness properties of the material, which leads to a selection of material.

2.2.3.2 Requirements for ultimate limit state verifications to avoid brittle behaviour

(1) Fig. 2-11 gives an overview on the design situations for the ultimate limit state verifications for ductile behaviour and the ultimate limit state verification to avoid brittle behaviour together with the temperature-toughness diagram.

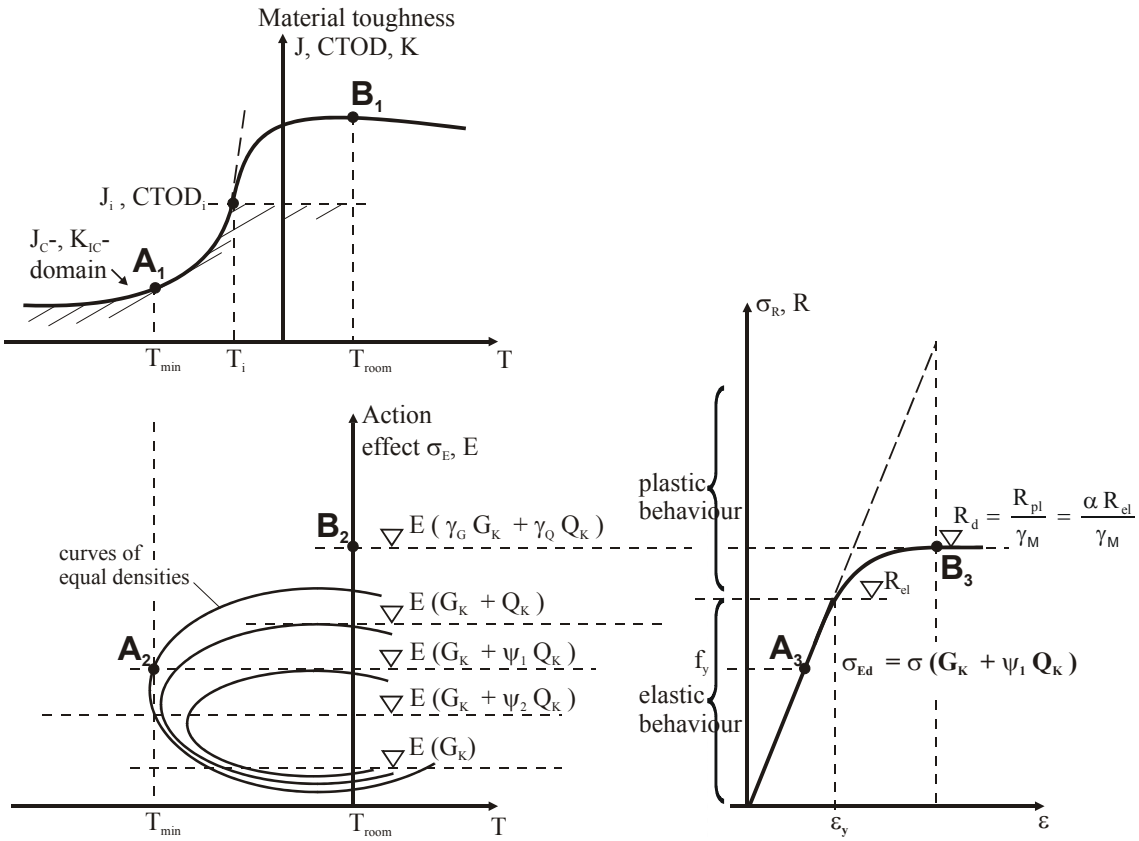


Fig. 2-11: Design situations in the upper-shelf region B and the transition region A of the toughness-temperature diagram.

(2) The design point B_1 (for ductile behaviour) in the upper shelf region corresponds to the load level B_2 of the load-temperature-diagram, which results in the design values of action effects

$$E_d = E (\gamma_g \cdot G_k + \gamma_Q \cdot Q_k + ...) \qquad (2\text{-}5)$$

that are compared with the design values of resistances R_d at point B_3 on the elasto-plastic part of the load deformation curve R-ε from the member tests.

(3) Supplementary requirements for the material to achieve ductile behaviour in the region B have been related to the following:

- requirements for the strain behaviour of the material at fracture, e.g. $\varepsilon_u > 15\ \varepsilon_y$ or $A_5 \geq 1{,}5\%$ aiming at sufficient plastic deformation capacity (to neglect stress concentrations and residual stresses) and at sufficient rotation capacity for redistribution of stresses in cross-sections or of moments by plastic mechanisms

- toughness requirements depending on the plate thickness, e.g. in view of sufficient resistance to instable crack growth initiated by welding defects, as given in section 3 of EN 1993-Part 2.

(4) The design point A_1 designates the verification to avoid brittle fracture in the lower part of the temperature transition of the toughness temperature diagram. This verification is necessary for structures that are not protected against low temperatures, e.g. by facades. The verification therefore is carried out for the

lowest possible temperature of the member T_{md}, for which the material toughness takes the minimum value.

(5) In general, for structures exposed to climate actions, the temperature and other actions are correlated in such a way, that the load-level A_2 in the load temperature diagram is relevant, which because of probability of occurrence is below the load level B_2. The design point A_2 is also below the design point B_2 because the verification in the temperature transition area is carried out with accidental assumptions for the location and size of crack-like defects, so that an accidental design situation may be applied. For such an accidental design situation the design value of action effect is

$$E_d = E\ (G_k + \psi_1\ Q_{k1} + ...) \qquad (2\text{-}6)$$

instead of equation (2-5).

For the load level A_2 according to (2-6) the relevant loading point on the load deformation curve is A_3, which is on its linear elastic part. This means that plastic deformations are very small (restricted to a limited local reduction of stress concentrations in the cross-section), and the analysis is performed with an elastic global behaviour without plastic redistribution of action effects.

(6) This explains why, depending on the design case, the loading level for the fracture mechanical verification (EN 1993-1-10 equation (2.1)) is below the loading level for the other ultimate limit state verifications in other parts of EN 1993.

The accidental design situation applied for the fracture mechanical verification takes the minimum temperature T_{Ed} as the leading action A (T_{Ed}) and the other actions as accompanying actions, so that the combination rule (EN 1993-1-10, Equation 2.1) reads according to EN 1990, section 6:

$$E_d = E\ \{A\ (T_{Ed})\ \text{“+“}\ \Sigma G_k\ \text{“+“}\ \psi_1\ Q_{k1}\ \text{“+“}\ \Sigma\ \psi_{2i}\ Q_{ki}\} \qquad (2\text{-}7)$$

The use of this load-combination results in a stress σ_{Ed}, taken as a nominal stress, which is then expressed as a portion of $f_y(t)$, see EN 1993-1-10, 2.3.2(1) equation (2.6), between the limits

$$0.25\ f_y(t) \le \sigma_{Ed} \le 0.75\ f_y(t) \qquad (2\text{-}8)$$

for which table 2.1 of EN 1993-1-10 applies.

2.2.4 Basis of the fracture mechanic assessment

(1) Fracture assessments in the brittle area below the temperature T_i below which no stable crack growth may occur could be performed with fracture mechanical parameters as J-integrals or CTOD-values that take both the elastic and the plastic strains into account.

However for practical reasons, the stress intensity functions, initially valid for the fully elastic range $T < T_{IC}$ only, can be used in a more practical way because of their availability from handbooks where solutions can be found for most relevant cases.

The stress intensity factor K is taken for mode I actions, see fig. 2-12 and has been derived from a stress field around the crack tip according to fig. 2-13. Its validity is limited to elastic behaviour where plasticity even in the vicinity of the crack tip is limited.

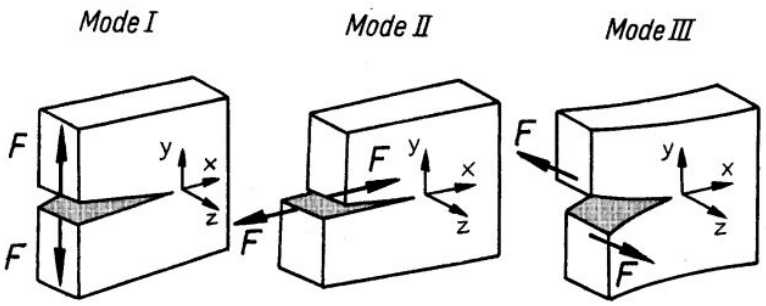
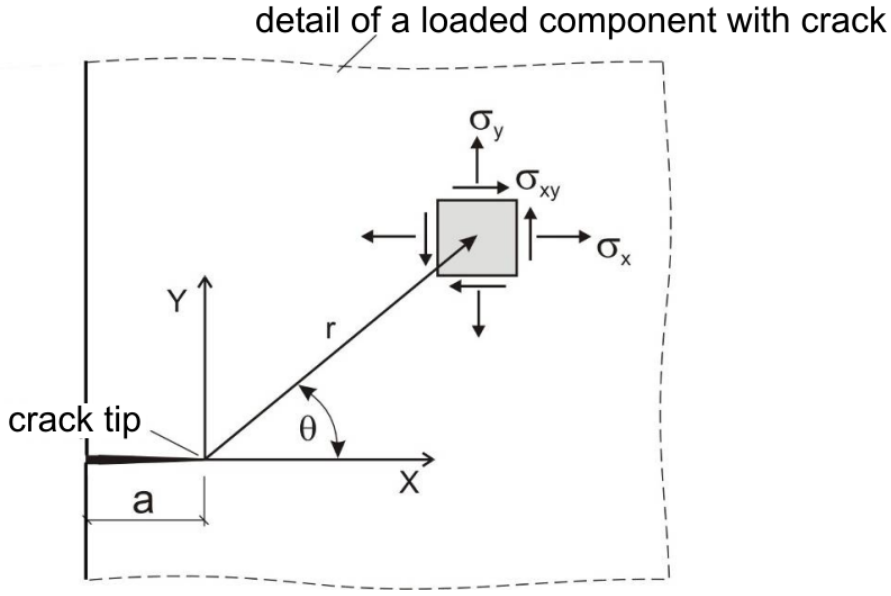


Fig. 2-12: Action modes for cracks



$$\sigma_x = \sigma\sqrt{\frac{a}{2r}}\cdot\cos\frac{\theta}{2}\left[1-\left(\sin\frac{\theta}{2}\cdot\sin\frac{3\theta}{2}\right)\right] = \frac{K}{\sqrt{2\pi\, r}}\cdot f_x(\theta)$$

$$\sigma_y = \sigma\sqrt{\frac{a}{2r}}\cdot\cos\frac{\theta}{2}\left[1+\left(\sin\frac{\theta}{2}\cdot\sin\frac{3\theta}{2}\right)\right] = \frac{K}{\sqrt{2\pi\, r}}\cdot f_y(\theta)$$

$$\sigma_{xy} = \sigma\sqrt{\frac{a}{2r}}\cdot\cos\frac{\theta}{2}\cdot\sin\frac{\theta}{2}\cdot\cos\frac{3\theta}{2} \qquad = \frac{K}{\sqrt{2\pi\, r}}\cdot f_{xy}(\theta)$$

Fig. 2-13: Definition of the stress intensity factor K

(2) The error resulting from neglecting the local plasticity at the crack tip is considered by a correction factor k_{R6} from the CEB6-R6-Failure Assessment Diagram (FAD) [9] applied to the elastic value of the action effect K_{appld}, which results in

$$K_{appld,correct} = \frac{K_{appld}}{k_{R6}-\rho} = \frac{\sigma_{Ed}\sqrt{\pi a_d}\cdot Y\cdot M_K}{k_{R6}-\rho}\left[MPa\sqrt{m}\right] \tag{2-9}$$

where

σ_{Ed} is the design value of the stress applied to the member from external loads [MPa ≙ N/mm²]

a_d is the design size of the crack [m]

Y is the correction function for various crack positions and shapes (see table 2-3) taken from Raju-Newman) [-]

M_K is the correction function for various attachments with semi-elliptical crack shapes (see table2-4) [-]

k_{R6} is the plasticity correction factor from the R6-Failure Assessment Diagram (FAD) (see table 2-5) [-]

ρ is a correction factor for local residual stresses (see table 2-6), that may be taken ρ = 0 for non welded details [-].

(3) The corresponding resistance is $K_{Mat,d}$ depending on T_{Ed}, which may be determined from J-Integral, CTOD or valid K_{IC}-values from CT-tests.

(4) The basic verification format with these values reads:

$$E_d\,(K) \le R_d\,(K) \quad \text{or}$$

$$K_{appld} \le K_{Matd} \tag{2-10}$$

Which, however, needs further processing to achieve two goals:

1. Correlation between the resistance K_{Ic} and the standard values T_{KV},

2. Transformation to a format for verifying with temperatures T_{Ed} and T_{KV}.

(5) The first goal is reached in two steps:

1. by expressing $K_{Mat,d}$ as a function of T_{Ed} by the standardized K-(T_{K100} - T_{Ed})-Master curve from Wallin [3], which refers to the temperature T_{K100}, for which K_{Mat} takes the value 100 MPa$\sqrt{m}$:

$$K_{Mat} = 20 + \left(77 \cdot e^{\frac{T_{min} - T_{K100} - T_K}{52}} + 11\right)\left(\frac{25}{b_{eff}}\right)^{0,25} \cdot \left(\ell n \frac{1}{1-p_f}\right)^{0,25} \tag{2-11}$$

where

$$T_K = 13\,(0.5 - p_f) \tag{2-12}$$

represents the effect of the standard deviation in the correlation between K_{Mat} and T_{K100} for a required probability level p_f.

For the use of EN 1993-1-10 p_f is taken 50% (mean value), as corrections for sufficient reliability are not performed for the individual elements of the procedure, but for the procedure as a whole, as explained in fig. 2-10.

2. by correlating the temperature T_{100} for the fracture mechanical parameter K = 100 MPa $\sqrt{m}$ with the temperature T_{27J} for the Charpy-impact energy K_v = 27J (modified Sanz-correlation [43],[44]), which reads in the mean:

$$T_{K100} = T_{27J} - 18\ °C \qquad (2\text{-}13)$$

This correlation of the K-(T_{K100} – T_{Ed})-Master curve with the Charpy-energy curve K_V-T_{Ed} is supplemented by an additional safety element ΔT_R, which controls the overall reliability of the total formula in a modified way according to the procedure illustrated in fig. 2-10.

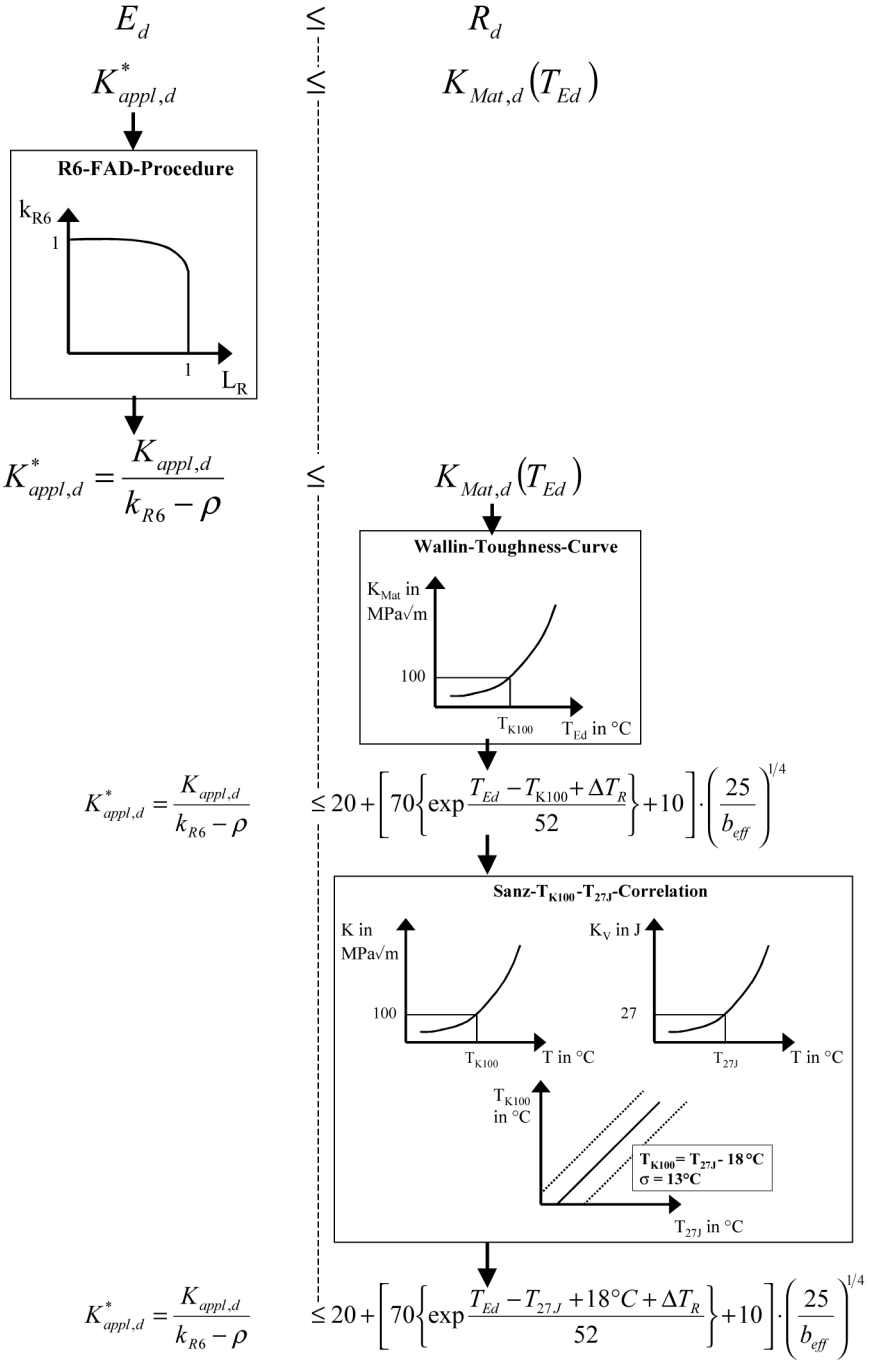


Fig. 2-14: Fracture mechanical assessment using stress intensity functions K

(6) Fig. 2-14 gives the total process and the final expression for the verification in terms of K-values.

(7) The expression $\left(\frac{25}{b_{eff}}\right)^{\frac{1}{4}}$ addresses the effect of the crack front on the failure probability and has been derived from a weakest link model with b_{eff} representing the length of the critical crack front.

b_{eff} takes the values given in table 2-7 depending on the crack shape. E.g. for through thickness cracks the total front length is b_{eff} = 2t.

ΔT_R is the safety term that effects a temperature shift according to the reliability required.

2.2.5 Transformation to the temperature format

(1) The verification formula based on K-values as presented in fig. 2-14 may be transferred to a formula based on temperature values T by applying logarithms, see fig. 2-15, so that the final assessment scheme reads:

$$T_{Ed} \geq T_{Rd} \tag{2-14}$$

where

$$T_{Ed} = T_{md} + \Delta T_r + \Delta T_\sigma + \Delta T_R \left[+ \Delta T_{\dot{\varepsilon}} + \Delta T_{cf}\right] \quad [°C] \tag{2-15}$$

$$T_{Rd} = T_{K100} + \Delta T_t - 18 \quad [°C] \tag{2-16}$$

and

T_{md} = lowest air temperature (e.g. – 25°C)

ΔT_r = radiation loss for member considered (e.g. - 5K) [45]

$$\Delta T_\sigma = -52\, \ell n \left[\frac{\left(\frac{K_{appl,d}}{k_{R6} - \rho} - 20\right)\left(\frac{b_{eff}}{25}\right)^{\frac{1}{4}} - 10}{70} \right] [K] \tag{2-17}$$

= temperature shift according to stress situation limited to 120 [K].

ΔT_t = term to consider the variation of material toughness in the thickness direction of the product (inhomogeneity of material properties)

ΔT_R= additive safety element, determined from large scale test evaluations according to EN 1990 Annex D (e.g. ΔT_R = +7 [K] for T_{27J} values taken from EN 10025)

$$\Delta T_{\dot{\varepsilon}} = -\frac{1440 - f_y(t)}{550} \left(\ell n \, \frac{\dot{\varepsilon}}{\dot{\varepsilon}_0} \right)^{1,5} [K] \tag{2-18}$$

= influence of the strain rate with $\dot{\varepsilon}_0$ = 0,0001 [s^{-1}].

$\dot{\varepsilon}_0 = 4 \cdot 10^{-4}$ [s^{-1}] is the limit for static loading where $\Delta T_{\dot{\varepsilon}}$ is ignored

ΔT_{cf} = - 3 DCF [K] (2-19)

with DCF = degree of cold forming [%]

$K^*_{appl,d} \leq K_{mat,d}$ → **Transformation** → $T_{Ed} \geq T_{Rd}$

Assessment scheme

$T_{Ed} \geq T_{Rd}$

Action side

$$T_{Ed} = T_{md} + \Delta T_r + \Delta T_\sigma + \Delta T_R \left[+ \Delta T_{\dot{\varepsilon}} + \Delta T_{epl} \right]$$

- Lowest air temperature with a suitable return period in combination with σ_{Ed}, e.g.,
  $T_{md,Germany} = -25°\,C$
- Radiation loss
  $\Delta T_r = -5K$
- Influence of stress, crack imperfection and member shape and dimension

$$\Delta T_\sigma = -52 \cdot \ln \left[\frac{\left(\frac{K_{appl}}{k_{R6} - \rho} - 20 \right) \cdot \left(\frac{b_{eff}}{25} \right)^{1/4} - 10}{70} \right] \; [K]$$

with $\Delta T_\sigma \leq +120$ K

- Additive safety element
  e.g. $\Delta T_R = +7K \;\; (\text{with } \beta = 3{,}8)$
  for the case that T_{27J}-values are used from standards EN 10025, ...

---

may be supplemented by

- Influence of the strain rate

$$\Delta T_{\dot{\varepsilon}} = -\frac{1440 - f_y(t)}{550} \cdot \left(\ln \frac{\dot{\varepsilon}}{\dot{\varepsilon}_0} \right)^{1,5} \; [K]$$

with $\dot{\varepsilon}_0 = 0{,}0001\; s^{-1}$

- Influence from cold forming
  $\Delta T_{cf} = -3 \cdot DCF \; [K]$
  with *DCF* = Degree of Cold Forming [%]

Resistance

$$T_{Rd} = T_{K100} + \Delta T_t$$

- Influence of material toughness
  $T_{100} = T_{27J} - 18 \; [°\,C]$
- Variation of material toughness in through thickness direction
  $\Delta T_t = 12{,}9 \cdot \tanh(1{,}9 \cdot \ln(t) - 7{,}6) + 12{,}8 \; [K]$

Fig. 2-15: Transformation into a verification formula based on temperature values and final assessment scheme

(2) Though the temperature shifts ΔT_i affect the resistance side of the material, they are listed on the action side for achieving an easy-to-use format for the application of table 2.1.

(3) In the following, the temperature shifts ΔT_i in fig. 2-15, that may be supplemented by further shifts from other effects, are explained in detail.

2.2.6 Explanation of temperature shifts ΔT_i

2.2.6.1 Shift from stresses ΔT_σ

(1) ΔT_σ in (2-15) represents the temperature shift due to the actual stresses in the member and may be calculated from the fracture mechanical action effect in (2-9) using the correction factor k_{R6} from

$$k_{R6} = \frac{1}{\sqrt{1+0{,}5L_r^2}} \quad \text{for} \quad L_r = \frac{\sigma_p}{\sigma_{gy}} \le 1 \tag{2-20}$$

$$k_{R6} = 0{,}816 \quad \text{for} \quad L_r = 1 \tag{2-21}$$

where

σ_p is the stress from external loads applied to the gross-section

σ_{gy} is the stress applied to the gross-section to obtain yielding in the net section

2.2.6.2 Shift from inhomogeneity of material ΔT_t

(1) The inhomogeneity of the material is characterized by a decrease in toughness from the surface to the middle of thick plates, as identified by Nießen [37], Haesler [38] and Brecht [39] for steels S 355, S 460, und S 690. As sampling for Charpy energy tests is made close to the surface of plates (≤ 2 mm), the reduction of toughness in the middle of the plate is not taken into account by using the T_{27J}-values. The formula to take the difference between the position of the samples and the middle of the plate into account in the mean, is according to Kühn [34]

$$\Delta T_t = 12{,}9 \tanh\left(2{,}1 \cdot \ln(t) - 7{,}6\right) + 12{,}8 \tag{2-22}$$

see fig. 2-16,

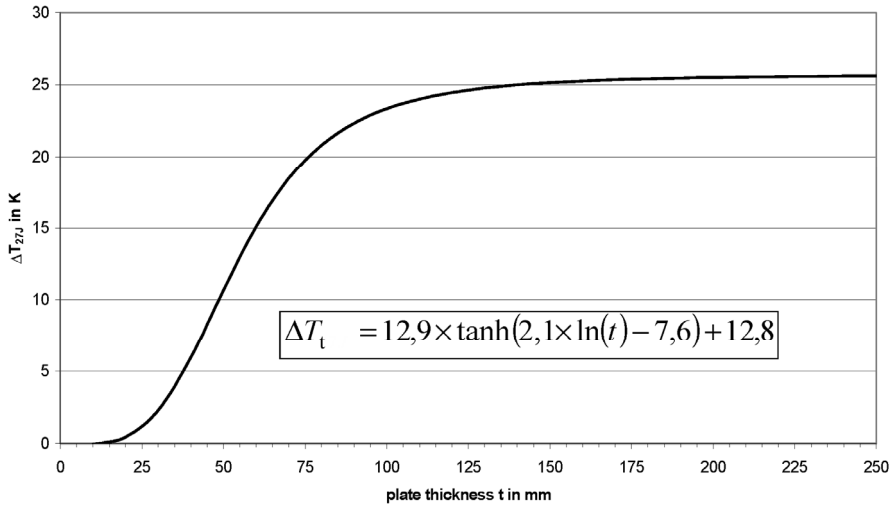


Fig. 2-16: Temperature shift ΔT_t for accounting for the inhomogeneity of thick plates

(2) The procedure for applying expression (2-22) is as follows:

1. Consider the core of the plate according to fig. 2-17

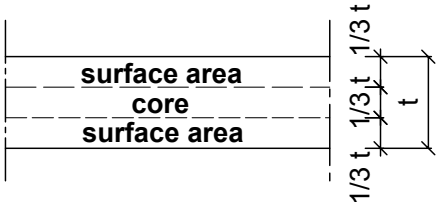


Fig. 2-17: Definition of surface area and core area of plate

2. If the design crack depth a_d of the critical surface crack reaches the core of the plate, formula (2-22) applies.

(3) In fig. 2-18 a comparison is given between temperature shifts as measured and temperature shifts according to formula (2-22) for various plate thicknesses.

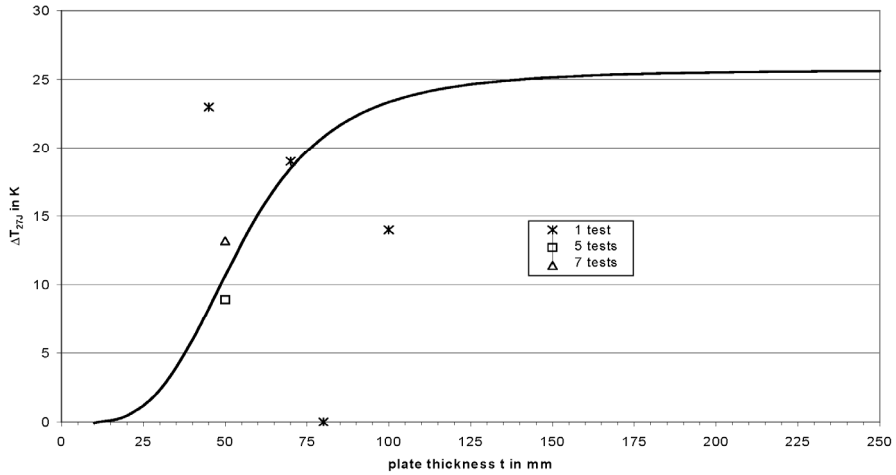


Fig. 2-18: Formula for Temperature shift ΔT_t in comparison with test results

2.2.6.3 Additional safety element ΔT_R

2.2.6.3.1 General

(1) The strength functions T_{Rd} and ΔT_i in the formulae (2-15) and (2-16) have been chosen such that they give about the expected values for failure (~ 50 %-fractiles). The additional safety element ΔT_R shall produce the reliability of assessment required.

(2) As required in EN 1990-Annex D, ΔT_R shall be determined from large scale tests that are performed in such a way that they are representative for actual structures.

(3) The application rules in EN 1990, however, apply to resistances R, for which the relationship between R_d and R_K is expressed in a multiplicative way, see (2-4), whereas the verification format for the assessment to avoid brittle fracture combines the variables in an additive way. Therefore the principle presented in Annex D had to be transferred from multiplicative safety elements to additive safety elements as presented in fig. 2-19.

(4) The design values are given by

$$R_d = m_R + \alpha_R \beta \sigma_R \qquad (2\text{-}22)$$

with

$\alpha_R = 0.8$

$\beta = 3.8$

where m_R and σ_R statistical parameters of the distribution of R

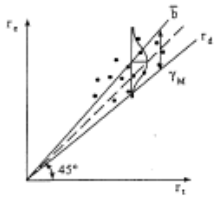
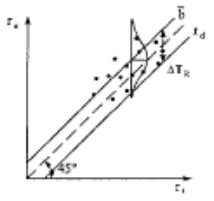
Multiplicative Form	Additive Form
1. Strength function $g_R(x) = x_1 \cdot x_2 \cdot x_3 \ldots$ 	1. Strength function $g_R(x) = x_1 + x_2 + x_3 + \ldots$ 
2. Correction term $b_i = \frac{r_{ei}}{r_{ti}}$	2. Correction term $b_i = r_{ei} - r_{ti}$
3. Mean value $\bar{b} = \frac{1}{n} \sum b_i$	3. Mean value $\bar{b} = \frac{1}{n} \cdot \sum_{i=1}^{n} b_i$
4. Error term $\delta_i = \frac{r_{ei}}{\bar{b} \cdot r_{ti}} = \frac{b_i}{\bar{b}}$	4. Error term $\delta_i = b_i - \bar{b}$
5 $\overline{\delta'} = \frac{1}{n} \sum \delta_i' \Rightarrow 0$	5 $\bar{\delta} = \frac{1}{n} \cdot \sum_{i=1}^{n} \delta_i \Rightarrow 0$
6 $S_{\delta'} = \sqrt{\frac{1}{n-1} \sum_{i=1}^{n} (\delta_i' - \bar{\delta})^2}$	6 $\sigma_\delta = \sqrt{\frac{1}{n-1} \sum_{i=1}^{n} (\delta_i - \bar{\delta})^2}$
If the test population is representative, it follows $S_D' = S_{\delta'}$ else $S_D' = \sqrt{(S_{\delta'})^2 + \sum \left(\frac{\partial g(X_M)}{\partial X_{M,i}} \cdot \sigma_{X,i} \right)^2}$	If the test population is representative, it follows $\sigma_D = \sigma_\delta$ else $\sigma_D = \sqrt{(\sigma_\delta)^2 + \sum \left(\frac{\partial g(X_M)}{\partial X_{M,i}} \cdot \sigma_{X,i} \right)^2}$
7. Design function $r_d = g_R(X_M) \cdot \bar{b} \cdot e^{-\alpha_R \cdot \beta \cdot S_D' - 0{,}5 \cdot (S_D')^2}$	7. Design function $r_d = \underbrace{g_R(X_M) + \bar{b}}_{m_R} + \alpha_R \cdot \beta \cdot \sigma_D$
8. Partial safety element $\gamma_M^* = \frac{g_R(X_N)}{r_d}$ where X_N are nominal values	8. Partial safety element $\Delta T_R = g_R(X_N) - r_d$ where X_N are nominal values

Fig. 2-19: Statistical evaluation of the safety element ΔT_R by the procedure in EN 1990, Annex D (additive form) [4, 41, 42]

2.2.6.3.2 Tests for calibration

(1) Two test series with large scale fracture tests at low temperatures T_{exp} have been used to determine the model uncertainty of the design model developed and to determine the safety element ΔT_R for achieving the required reliability of resistance:

1. test series with Double Edge Cracked Tension (DECT) elements according to fig. 2-20,

2. test series with welded details according to fig. 2-21, that had semi-elliptical surface cracks with the dimension ($a_d/2c_d$) at the hot spots for fatigue.

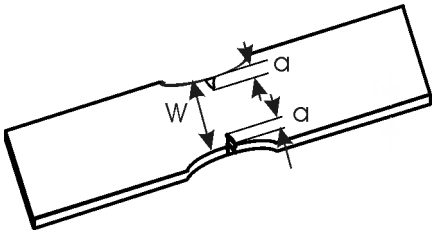


Fig. 2-20: DECT-test elements

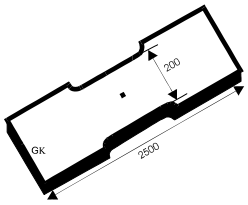
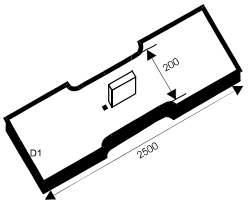
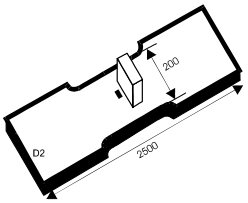
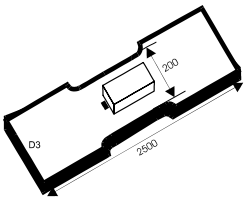
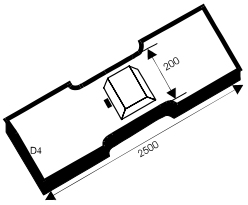
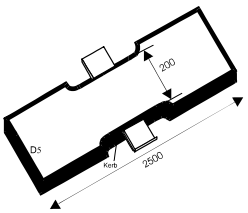
Detail Index	Large scale test specimen	$\Delta\sigma_c$ acc. EC 3-2	$\Delta\sigma$ used in tests
GK	Reference plate 	125	160
D1	Longitudinal attachment 	56	71
D2	Transverse attachment 	71	71
D3	Reinforcing plate 	56	56
D4	Reinforcing plate according to DS 804 	56	56
D5	Horizontal attachments 	71	71

Fig. 2-21: Test elements with welded details

DECT-Test Specimens									
No	Steel Grade	t [mm]	2a [mm]	2W [mm]	a/W [-]	$f_{y,measured}^{*}$ [N/mm²]	$\sigma_{fracture}$ [N/mm²]	T_{27J} [K]	T_{exp} [K]
1	S355J2G3	30	60	300	0,2	418	350	248	238
2	S355J2G3	30	60	300	0,2	405	349	248	253
3	S355N	30	60	300	0,2	400	377	213	254
4	S690Q	30	60	300	0,2	780	503	186	232
5	S690Q	30	60	300	0,2	805	494	203	223
6	S690Q	30	60	300	0,2	800	477	203	233
7	S890Q	30	60	300	0,2	1023	784	203	243
8	S890Q	30	60	300	0,2	1011	824	203	258
9	S890Q	30	60	300	0,2	1008	822	203	263
10	S890Q	30	60	300	0,2	1010	760	205	251
11	S355J0	30	37,36	300	0,125	398	362,3	263	232
12	S355M	30	39	300	0,13	557,6	332,9	173	163
13	S690Q	30	36,36	300	0,121	769,9	354,9	233	232
14	S690Q	30	36	300	0,12	754,1	521	233	248
15	S690Q	30	37,2	300	0,124	875,4	395,2	203	204
16	S890Q	30	38	300	0,127	984,5	703,2	233	273
17	S890Q	30	38,4	300	0,128	980,3	651,4	233	278
18	S890Q	30	40,9	300	0,136	958,5	662,9	198	232
19	S890Q	30	39,9	300	0,133	946,3	606,9	198	245

* Yield strengths at testing temperature

Table 2-1: Properties of DECT-test specimens and test results [42]

(2) The test results for the DECT-tests are given in table 2-1.

(3) For the test specimens 1 to 10 in table 2-1, the yield strengths f_y (t, T) had been measured, whereas for specimens 11 to 19 the yield strengths had to be calculated using the formula according to TWI and Wallin [3, 42].

$$f_y(t, T) = f_{y,T=293K} + \frac{55555}{T} - 189 - 0{,}25\frac{t}{t_0} \qquad (2\text{-}24)$$

where

$f_{y,T = 293\ K}$ = yield strength [N/mm²] related to T = 293 K ≙ 20°C

T = testing temperature [K]

t = plate thickness [mm]

t_0 = reference plate thickness 1 mm

(4) A comparison between the results of equation (2-24) and the yield strength values f_y (t,T) as measured is given in fig. 2-22 [42].

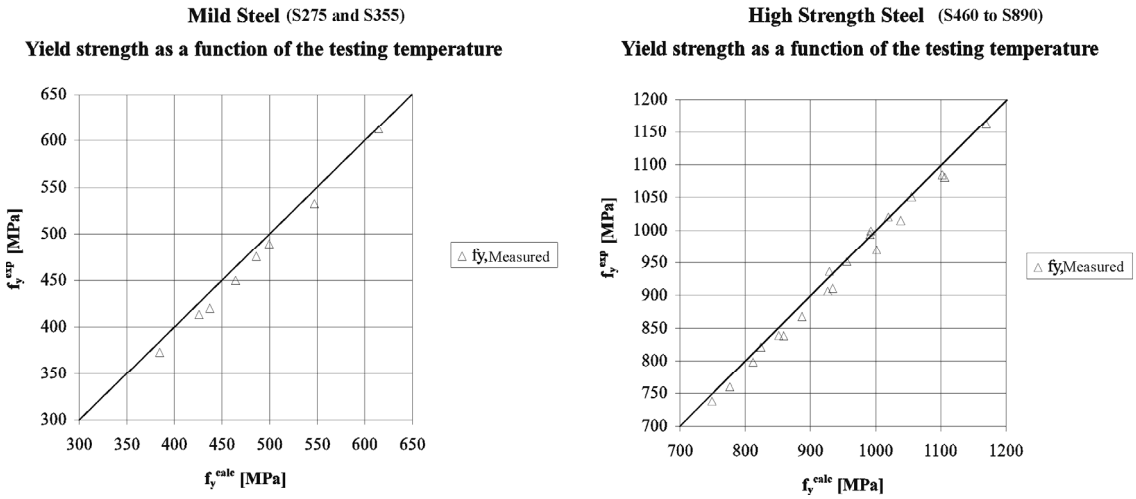


Fig. 2-22: Comparison between the results of equation (2-23) and yield strength values as measured [42]

(5) As the DECT-tests, according to fig. 2-20, see table 2-1, did not contain any welded attachments and hence not any residual stresses from welds, a further test series, see fig. 2-21 and table 2-2, has been used to include these effects in the evaluation for ΔT_R.

(6) In total 48 large scale tension tests were carried out with specimens that had various welded attachments according to the fatigue classes in EN 1993-1-9.

(7) These test pieces had initial semi-elliptical surface cracks with a depth of a_0 ~ 2.2 mm and a width of 2 c_0 ~ 11 mm, artificially cut in by electro-erosion at the hot spots for fatigue at the weld toes, so that the a_0/c_0-ratio was about 0.40.

(8) These artificial initial cracks were subjected to a first high fatigue loading $\Delta\sigma_1$ to initiate a realistic sharp crack front and then to a fatigue load with stress ranges $\Delta\sigma_2 = \Delta\sigma_c$ according to fig. 2-21, with a mean stress of about 0.5 f_y

1. to obtain sufficiently large crack sizes ($a_d/2c_d = a_{end}/2c_{end}$), the subsequent fracture tests were carried out (anders loopt de zin niet, denk ik) at low temperatures of about T = - 100°C to -120°C, so that brittle fracture could be achieved.

2. to check, as a side effect, the predictability of crack growth from initial crack sizes via the Paris equation by comparing $a_0/2c_0$ with $a_{end}/2c_{end}$.

test	detail	crack					specimen dimensions				statical tensile test				
		a_0 [mm]	$2c_0$ [mm]	a/c [-]	a_{end} [mm]	$2c_{end}$ [mm]	width [mm]	thickness [mm]	A_{brut} [mm²]	A_{net} [mm²]	temp [°C]	$\sigma_{brut,\ fracture}$ [MPa]	$\sigma_{net,\ fracture}$ [MPa]	$\sigma_{brut,yield}$ [MPa]	$\sigma_{net,yield}$ [MPa]
S35GK 2	reference plate	2,19	10,96	0,4	7,3	28,15 (c_{end})	198,0	81,9	16216	15934	-130	500	509	525	534
S35D11	longitudinal stiffener	2,08	10,85	0,38	46,13	113,4	198,0	81,4	16117	12113	-120	351	467	314	419
S35D12	longitudinal stiffener	2,17	10,58	0,41	50,55	125,0	198,0	81,5	16137	11136	-106	321	465	306	443
S35D13	longitudinal stiffener	2,2	10,76	0,41	48,8	125,7	198,5	81,4	16150	11454	-121	334	471	319	450
S35D14	longitudinal stiffener	2,01	10,63	0,38	50,38	130,5	198,5	81,41	16160	11015	-120	286	420	-	-
S35D21	transverse stiffener	2,18	10,8	0,4	14,93	64,9	198,0	81,46	16129	15485	-120	397	413	-	-
S35D23	transverse stiffener	2,31	10,68	0,4	21,1	56,75	198,5	81,42	16162	15288	-110	454	480	364	386
S35D24	transverse stiffener	2,18	10,87	0,4	30,73	99,55	198,0	81,5	16137	14052	-120	327	376	-	-
S35D31	cover plate	2,20	10,93	0,4	17,06	152	198,0	81,3	16097	14585	-120	247	272	-	-
S35D32	cover plate	1,88	10,89	0,35	16,85	143,7	198,0	81,56	16149	14180	-110	266	303	-	-
S35D33	cover plate	2,74	10,95	0,5	38,41	145,4	198,0	81,38	16113	12277	-118	211	277	-	-
S35D34	cover plate	2,13	10,96	0,39	25,88	91,71	198,5	81,42	16162	14411	-119	287	322	-	-
S35D41	cover plate DS 804	1,66	10,47	0,4	42,38	142	198,5	81,45	16168	11466	-120	285	401	-	-
S35D42	cover plate DS 804	2,17	10,86	0,4	20,51	93,18	199	81,5	16219	14903	-110	256	279	-	-
S35D43	cover plate DS 804	1,92	10,87	0,35	25,15	97,12	198,0	81,38	16113	14471	-121	250	278	-	-
S35D44	cover plate DS 804	2,2	10,93	0,4	25,42	103,5	198,0	81,44	16125	14377	-127	268	268	-	-
S35D51	lateral stiffeners	2,13	10,7	0,4	38,61	81,4	199,5	81,4	16239	13507	-118	313	376	-	-
S35D52	lateral stiffeners	2,19	10,83	0,4	37,74	81,4	199	81,43	16205	13680	-112	332	393	324	384
S35D53	lateral stiffeners	2,11	10,89	0,39	30,69	75,6	199,5	81,43	16245	14544	-119	449	501	not detectable	not detectable
S35D54	lateral stiffeners	1,8	10,68	0,34	38,6	81,6	199	81,6	16238	13804	-119	408	494	331	400
S46GK 1	reference plate	1,97	10,63	0,37	65,4	157,7	198,0	81,46	16129	7848	-100	223	459	213	437
S46GK 2	reference plate	1,97	10,88	0,36	43,8	97,1	198,5	81,28	16134	12758	-120	331	418	-	-
S46GK 3	reference plate	2,01	10,84	0,37	46,22	100,8	198,0	81,45	16127	12446	-110	420	544	406	526
S46GK 4	reference plate	2,22	10,9	0,41	47,59	10,08	198,5	81,0	16079	12270	-122	452	593	427	560
S46D11	longitudinal stiffener	2,44	10,7	0,46	38,03	94,52	198,0	81,46	16129	13013	-120	353	437	-	-
S46D12	longitudinal stiffener	2,1	10,89	0,39	37,4	98,15	198,5	81,35	16146	13296	-109	410	410	396	396
S46D13	longitudinal stiffener	2,2	10,75	0,41	39,85	98,53	198,0	81,42	16121	13130	-111	439	538	428	526

Table 2-2: Properties of welded test specimens and test results

test	detail	crack					specimen dimensions				statical tensile test				
		a_0 [mm]	$2c_0$ [mm]	a/c [-]	a_{end} [mm]	$2c_{end}$ [mm]	width [mm]	thickness [mm]	A_{brut} [mm²]	A_{net} [mm²]	temp [°C]	$\sigma_{brut,fracture}$ [MPa]	$\sigma_{net,fracture}$ [MPa]	$\sigma_{brut,yield}$ [MPa]	$\sigma_{net,yield}$ [MPa]
S46D14	longitudinal stiffener	2,22	10,91	0,41	37,78	94,1	198,0	81,46	16129	13257	-119	284	347	-	-
S46D21	transverse stiffener	2,02	10,79	0,37	44,3	124	196,5	81,43	16001	12142	-120	263	347	-	-
S46D22	transverse stiffener	2,2	10,85	0,41	24,4	81	198,0	81,5	16137	14752	-111	283	311	-	-
S46D23	transverse stiffener	2,17	10,89	0,4	21	73,8	198,0	81,2	16086	14983	-109	373	401	-	-
S46D24	transverse stiffener	2,18	10,84	0,4	26,38	88,47	198,2	81,6	16173	14813	-121	341	373	-	-
S46D31	cover plate	2,16	10,9	0,4	28,56	167,4	198,0	81,42	16121	12369	-120	296	386	-	-
S46D32	cover plate	2,29	10,58	0,43	32,91	171	195,5	81,4	16178	12100	-109	375	502	318	426
S46D33	cover plate	2,08	10,89	0,38	36,9	182,6	198,0	81,36	16109	10874	-111	267	385	-	-
S46D34	cover plate	2,25	10,88	0,41	31,4	103,8	198,2	81,46	16145	13795	-120	268	313	-	-
S46D41	cover plate DS 804	2,13	10,86	0,39	18,81	101,3	198,5	81,5	16177	14783	-120	240	262	-	-
S46D42	cover plate DS 804	2,08	10,8	0,39	22,3	93,8	198,0	81,4	16117	14731	-100	294	321	-	-
S46D43	cover plate DS 804	1,97	10,7	0,37	31,87	119	198,0	81,43	16123	13337	-103	314	314	-	-
S46D44	cover plate DS 804	2,16	10,93	0,4	20,88	72,47	198,5	81,5	16178	15139	-119	291	311	-	-
S46D51	lateral stiffeners	2,24	10,43	0,43	35,9	81,46	199,0	81,46	16211	13966	-106	361	418	-	-
S46D52	lateral stiffeners	2,05	10,87	0,38	37,46	81,44	200,5	81,44	16329	13865	-118	226	226	-	-
S46D53	lateral stiffeners	2,18	10,94	0,4	35,17	81,22	199,5	81,22	16203	13947	-112	358	416	-	-
S46D54	lateral stiffeners	2,11	10,89	0,39	37,32	81,45	199,0	81,54	16227	14238	-121	311	354	-	-

in test S35... steel grade S 355 made in quality ML (acc. to EN 10113, Part 3) is used
in test S46... steel grade S 460 made in quality ML (acc. to EN 10113, Part 3) is used

Table 2-2: Properties of welded test specimens and test results (continued)

2.2.6.3.3 Calculation models

(1) For obtaining $\Delta T_{R,}$ the experimental test results T_{exp} from section 2.2.6.3.2 had to be compared with calculative results T_{calc}, which are determined for the geometrical and mechanical data as measured for the test specimens, e.g. the crack sizes a_d and c_d and the values T_{27J} and f_y.

(2) For calculating ΔT_σ according to equation (2-17), the values $K_{appl,d}$, k_{R6}, ρ and b_{eff} needed to be determined.

(3) For the determination of $K_{appl,d}$, see equation (2-9), table 2-3 gives the correction functions Y for various crack positions and shapes and table 2-4 gives the correction functions M_K for various attachments with semi-elliptical crack shapes.

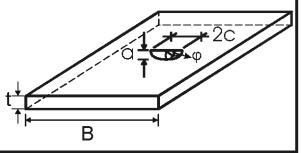
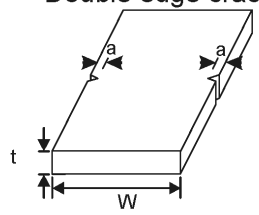
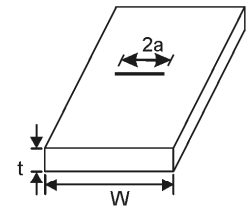
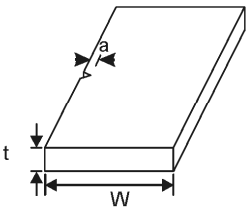
Case	Function Y	Source
Surface crack  range of validity $0 \le \frac{a}{c} \le 1$ $\frac{2c}{B} \le 0.5$ $0 \le \varphi \le \pi$ $0 \le \frac{a}{t} \le 1$	$Y = \frac{F_s}{\sqrt{Q}}$ $\quad Q = 1 + 1.464\left(\frac{a}{c}\right)^{1.65}$ $F_s = \left[M_1 + M_2 \cdot \left(\frac{a}{t}\right)^2 + M_3 \cdot \left(\frac{a}{t}\right)^4\right] \cdot g \cdot f_\varphi \cdot f_w$ $M_1 = 1.13 - 0.09 \cdot \left(\frac{a}{c}\right)$ $\quad M_2 = -0.54 + \frac{0.89}{0.2 + \frac{a}{c}}$ $M_3 = 0.5 - \frac{1}{0.65 + \frac{a}{c}} + 14 \cdot \left(1 - \frac{a}{c}\right)^{24}$ $\quad g = 1 + \left[0.1 + 0.35\left(\frac{a}{t}\right)^2\right] \cdot (1 - \sin\varphi)^2$ $f_\varphi = \left[\left(\frac{a}{c}\right)^2 \cdot \cos^2\varphi + \sin^2\varphi\right]^{\frac{1}{4}}$ $\quad f_w = \left[\frac{1}{\cos\left(\frac{\pi \cdot c}{B}\sqrt{\frac{a}{t}}\right)}\right]^{1/2}$	Raju - Newman
Double edge crack  	$Y = 1.122 - 0.154 \cdot (\alpha) + 0.807 \cdot (\alpha)^2 - 1.894 \cdot (\alpha)^3 + 2.494 \cdot (\alpha)^4$ where $\alpha = \frac{2 \cdot a}{W}$	Murakami
Through-thickness central crack  	$Y = 1 - 0.025 \cdot (\alpha)^2 + 0.06 \cdot (\alpha)^4 \cdot \sqrt{\frac{1}{\cos\left(\frac{\alpha \cdot \pi}{2}\right)}}$ where $\alpha = \frac{2 \cdot a}{W}$	Murakami
Single edge crack  	$Y = 1.12 - 0.231 \cdot (\alpha) + 10.55 \cdot (\alpha)^2 - 21.72 \cdot (\alpha)^3 + 30.39 \cdot (\alpha)^4$ where $\alpha = \frac{a}{W}$	Murakami

Table 2-3: Stress intensity correction factors Y for various crack configurations [15], [21]

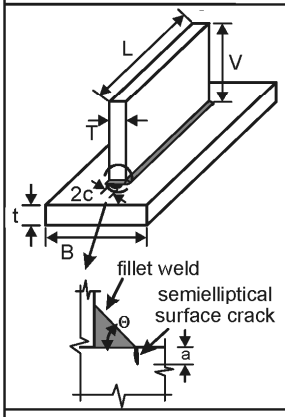
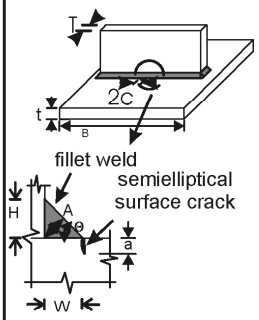
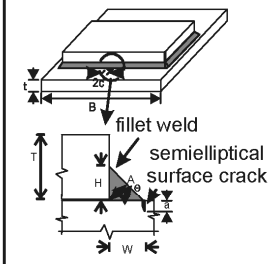
Case	Function	Source
	$M_k = C \cdot \left(\frac{a}{t}\right)^k$ and $M_k \geq 1$	Hobbacher
range of validity $0.5 \leq \frac{L}{t} \leq 40$ $\quad 0.15 \leq \frac{T}{t} \leq 2$ $2.5 \leq \frac{B}{t} \leq 40$ $\quad 30° \leq \Theta \leq 60°$	$C = 0.9089 - 0.2357 \cdot \frac{T}{t} + 0.0249 \cdot \left(\frac{L}{t}\right) - 0.00038 \cdot \left(\frac{L}{t}\right)^2 + 0.0186 \cdot \frac{B}{t} - 0.1414 \cdot \frac{\Theta}{45°}$ $k = -0.02285 + 0.0167 \cdot \frac{T}{t} - 0.3863 \cdot \frac{\Theta}{45°} + 0.1230 \cdot \left(\frac{\Theta}{45°}\right)^2$	
	$M_k = C \cdot \left(\frac{a}{t}\right)^k$ and $M_k \geq 1.0$	Hobbacher
range of validity $0.2 \leq \frac{H}{t} \leq 1.0$ $\quad 0.125 \leq \frac{T}{t} \leq 4.0$ $0.2 \leq \frac{W}{t} \leq 1.0$ $\quad 0.175 \leq \frac{A}{t} \leq 0.72$ $15° \leq \Theta \leq 60°$	$C = 0.8068 - 0.1554 \cdot \frac{H}{t} + 0.0429 \cdot \left(\frac{H}{t}\right)^2 + 0.0794 \cdot \frac{W}{t}$ $k = -0.1993 - 0.1839 \cdot \frac{H}{t} + 0.0495 \left(\frac{H}{t}\right)^2 + 0.0815 \cdot \frac{W}{t}$	
	$M_k = \frac{SCF}{1 + \frac{1}{0.1473} \cdot \left(\frac{a}{t}\right)^{0.4348}}$ and $M_k \geq 1.0$	Fischer and Zettelmoyer
range of validity $0.32 \leq \frac{H}{t} \leq 0.96$ $\quad 0.64 \leq \frac{T}{t} \leq 2.0$	$SCF = -3.539 \cdot \log\left(\frac{H}{t}\right) + 1.981 \cdot \log\left(\frac{T}{t}\right) + 5.798$	

Table 2-4: Stress intensity correction factors M_K for welded attachments and semi-elliptical surface cracks at the weld toe [16], [17]

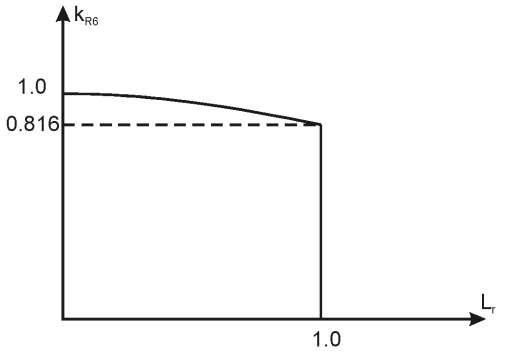
(4) The input parameters of the failure assessment diagram (FAD), see fig. 2-14, are given in table 2-5 and the correction factor ρ may be taken from table 2-6.

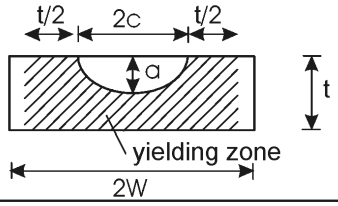
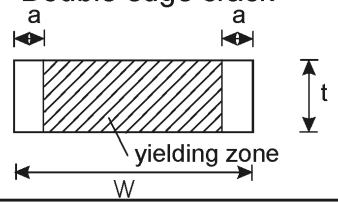
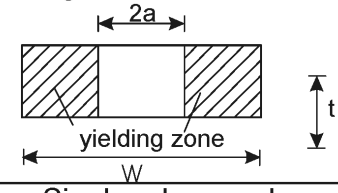
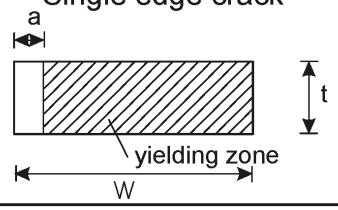
$$k_{R6} = \frac{1}{\sqrt{1 + 0.5 \cdot L_r^2}}$$

where

$$L_r = \frac{\sigma_{Ed}}{\sigma_{gy}},$$

$$\sigma_{Ed} = \sigma_G + \psi_1 \cdot \sigma_Q + 100\ N/mm^2$$



Case	Function Y	Source
Surface crack 	$\sigma_{gy}(t) = f_y(t)\left(1 - \frac{\pi \cdot 2.5 \cdot a_d^2}{2 \cdot t \cdot (5 \cdot a_d + t)}\right)$	Harrison
Double edge crack 	$\sigma_{gy}(t) = f_y(t)\left(1 - \frac{2a}{W}\right) \cdot \left(1 + 0.3 \cdot \frac{2a}{W}\right)$	Beltrami
Through-thickness central crack 	$\sigma_{gy}(t) = f_y(t)\left(1 - \frac{2a}{W}\right)$	Silcher
Single edge crack 	$\sigma_{gy}(t) = f_y(t)\left(1 - \frac{a}{W}\right)$	Silcher

$$f_y(t) = f_y - 0.25\,\frac{t}{t_0}$$

where

$t_0 = 1.0$ mm

Table 2-5: Determination of k_{R6} [9], [22], [46]

Definition of ρ	
$L_r \leq 0{,}8$	$\rho = \rho_1$
$0{,}8 \leq L_r \leq 1{,}05$	$\rho = 4\,\rho_1\,(1{,}05 - L_r)$
$1{,}05 \leq L_r$	$\rho = 0$
Definition of ρ_1	
$\psi = \frac{\sigma_S\, L_r}{\sigma_P} \leq 0$	$\rho_1 = 0$
$\psi = \frac{\sigma_S\, L_r}{\sigma_P} \leq 5{,}2$	$\rho_1 = 0{,}1\,\psi^{0{,}714} - 0{,}007\,\psi^2 + 0{,}00003\,\psi^5$
$\psi = \frac{\sigma_S\, L_r}{\sigma_P} > 5{,}2$	$\rho_1 = 0{,}25$

Table 2-6: Definition of ρ

(5) The value b_{eff} is given in table 2-7.

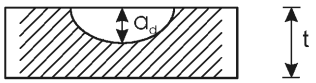
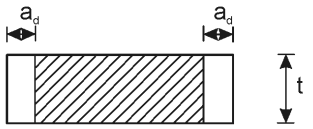
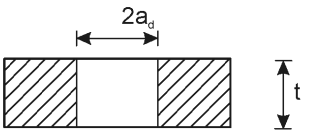
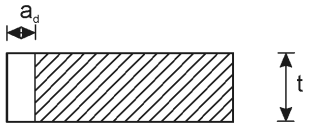
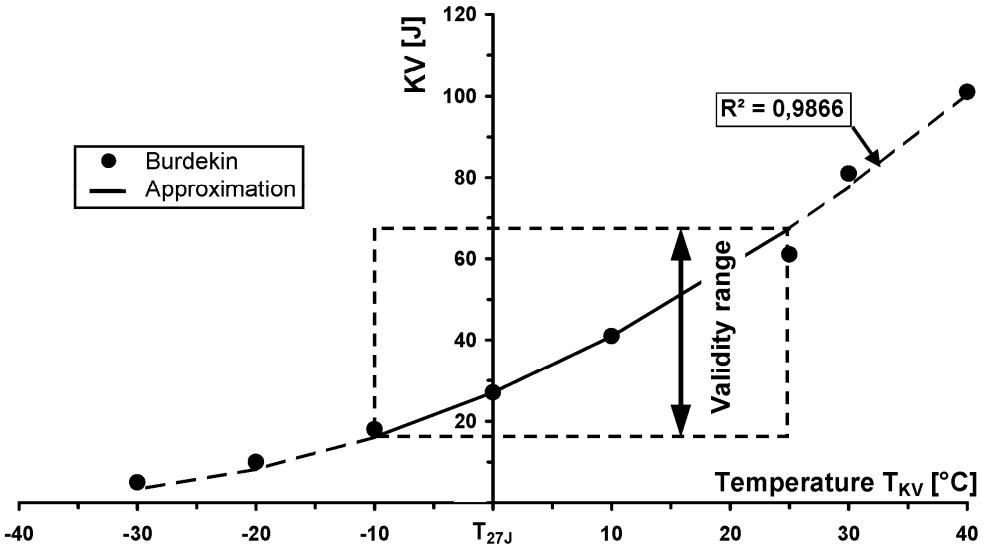
Case	b_{eff} [mm]
Surface crack 	5 a_d
Double edge crack 	2 t
Through-thickness central crack 	2 t
Single edge crack 	t

Table 2-7: Definition of b_{eff}

(6) Where T_{27J} has to be determined from other values T_{KV}, fig. 2-23 gives a suitable relationship.

KV [J]	T [°C]
101	T + 40
81	T + 30
61	T + 20
41	T + 10
27	T
18	T - 10



$$T_{27J} = T_{KV} + 41{,}33 - 8{,}16 \cdot \sqrt{KV - 1{,}373}$$

for $16J \le KV \le 67J$

resp. $-10°C \le T_{KV}-T_{27J} \le 25°C$

Fig. 2-23 Relationship between T_{27J} and T_{KV}

2.2.6.3.4 Evaluation of fracture tests for DECT-elements

(1) For the DECT-tests table 2-8 gives a comparison of the values T_{calc} and T_{exp} together with the values for the mean value corrections b_i and the error terms δ_I according to fig. 2-19.

DECT-Test Specimens										
No	$f_y(T,t)_{exp}$ [MPa]	$\sigma_{gy}(T,t)_{exp}$ [MPa]	L_r [-]	k_{R6} [-]	K_{mat} [N/mm$^{3/2}$]	ΔT [K]	$r_{t,i} = T_{calc}$ $=T_{27J}-18+\Delta T$ [K]	$r_{e,i} = T_{exp}$ [K]	$b_i = r_{e,i}-r_{t,i}$ [K]	$\delta_i = b_i - \bar{b}$ [K]
1	418	354,5	0,99	0,82	4610	38	268	238	-30,46	-21,45
2	405	343,4	1,0	0,816	4616	39	269	253	-15,55	-6,54
3	400	339,2	1,0	0,816	4986	43	238	254	15,53	24,54
4	780	661,4	0,76	0,881	6167	57	225	232	7,36	16,38
5	805	682,6	0,72	0,89	5992	55	240	223	-16,88	-7,87
6	800	678,4	0,70	0,895	5752	52	237	233	-4,38	4,63
7	1023	867,5	0,90	0,843	10047	85	270	243	-27,28	-18,27
8	1011	857,3	0,96	0,827	10758	89	274	258	-16,17	-7,15
9	1008	854,8	0,96	0,827	10734	89	274	263	-11,04	-2,03
10	1010	856,5	0,89	0,847	9689	83	270	251	-19,20	-10,19
11	398	361,0	1,0	0,816	3801	26	271	232	-38,73	-29,72
12	557,6	504,0	0,66	0,906	3198	14	169	163	-5,69	3,32
13	769,9	701,2	0,51	0,942	3169	13	228	232	3,98	12,99
14	754,1	687,5	0,76	0,881	4944	43	258	248	-9,94	-0,93
15	875,4	795,4	0,50	0,943	3562	21	206	204	-2,28	6,73
16	984,5	892,5	0,79	0,874	6917	64	279	273	-5,54	3,47
17	980,3	887,6	0,73	0,888	6339	58	273	278	4,70	13,71
18	958,5	861,7	0,77	0,878	6727	62	242	232	-9,87	-0,86
19	946,3	853,2	0,71	0,893	5981	55	244	245	10,23	19,24

Table 2-8: Comparison of calculative results T_{calc} and experimental test results T_{exp} [42]

(2) In fig. 2-24 the values T_{exp}/T_{calc} are plotted; they are arrayed about the mean line (diagonal: $T_{exp} = T_{calc}$), which needs the temperature shift ΔT_R to obtain design values related to measured input values.

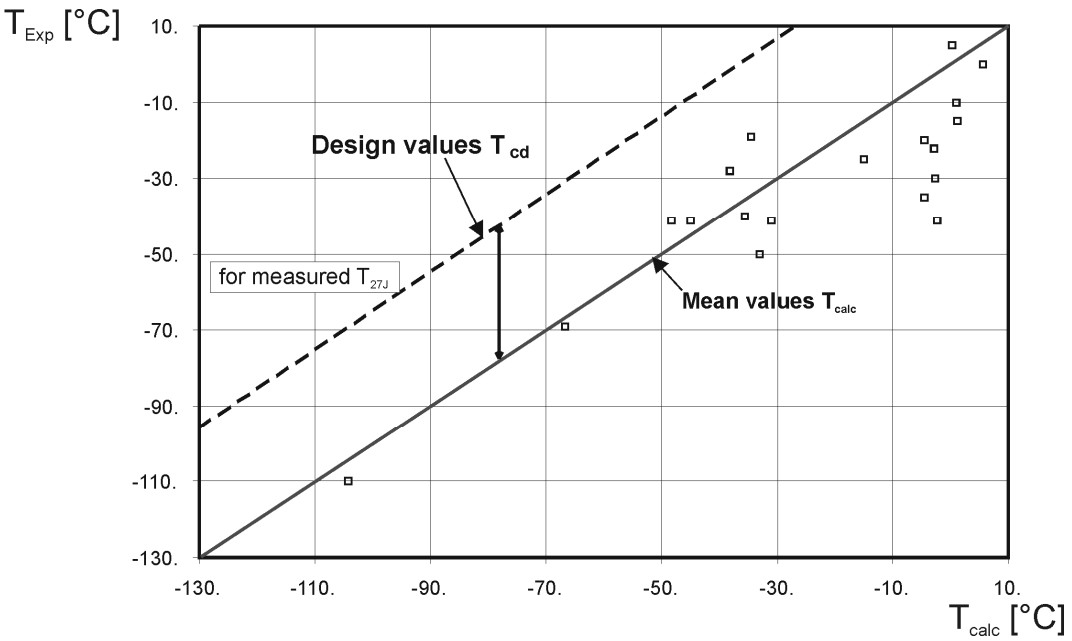


Fig. 2-24: Comparison of experimental T_{exp}-values and calculative T_{calc}-values for DECT-elements

(3) In fig. 2-25, the differences $b_i = T_{exp} - T_{calc}$ are arrayed in descending order and plotted on Gaussian paper. According to this plot, the formula (2-17) fits to the test results in the mean, so that for predicting expected values the safety element $\Delta T_R = 0$ K may be used.

This corresponds fully with the prior assumption that for the various functions in the fracture mechanics assessment, see fig. 2-14, mean value functions should be applied.

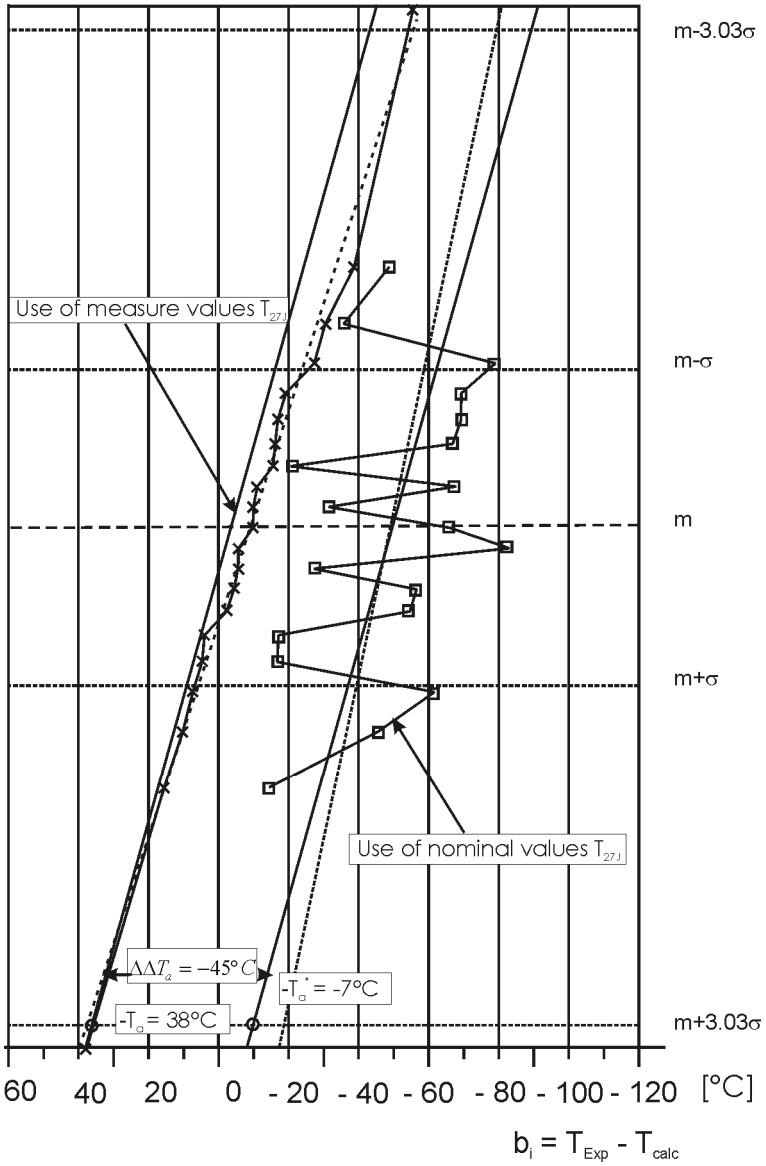


Fig. 2-25: Determination of the safety element ΔT_R for DECT-elements

(4) In applying the definition of design values according to equation (2-23), the safety element ΔT_R for ULS-verifications related to the use of measured values T_{27J} and f_y is obtained on the level

$$R_d = m_R + 3.03\ \sigma_R \tag{2-25}$$

which, according to fig. 2-25, gives a safety element

$$\Delta T_{R,measured} = +\ 38\ K \tag{2-26}$$

(5) When the mean value correction values b_i are referred to nominal values T_{27J} and f_y instead of measured ones, the mean line of distribution is shifted in parallel by

$$\Delta\Delta T_R = -\ 45K \tag{2-27}$$

(6) This value $\Delta\Delta T_R$ represents the positive effect of the difference between actual values of T_{27J} and f_y as measured and the nominal values T_{27J} and f_y as

specified in product standards; hence it mirrors the over-quality of the material as delivered.

(7) The safety element ΔT_R related to the use of nominal values T_{27J} and f_y is therefore

$$\Delta T_{R,nom} = -7K \tag{2-28}$$

This value has been justified also by the evaluation of test results with welded details, see chapter 2.2.6.3.5, and therefore has been adopted for any fracture mechanical assessment related to nominal material properties including the determination of the allowable plate thicknesses in table 2.1 of EN 1993-1-10.

2.2.6.3.5 Evaluation of tests with welded details

(1) The evaluation of tests with welded details included two steps:

1. Evaluation on the basis of the actual geometry and material properties as measured.
2. Evaluation of the fatigue tests to derive suitable standard assumptions for design values of crack sizes.

(2) For the evaluation of the first step, T_{calc} was determined by the hand formulae for Y and M_K-functions given in table 2-3 and table 2-4 and by FEM calculations.

(3) The results T_{exp} and T_{calc} are given in fig. 2-26 together with the results of the evaluation of the DECT-tests.

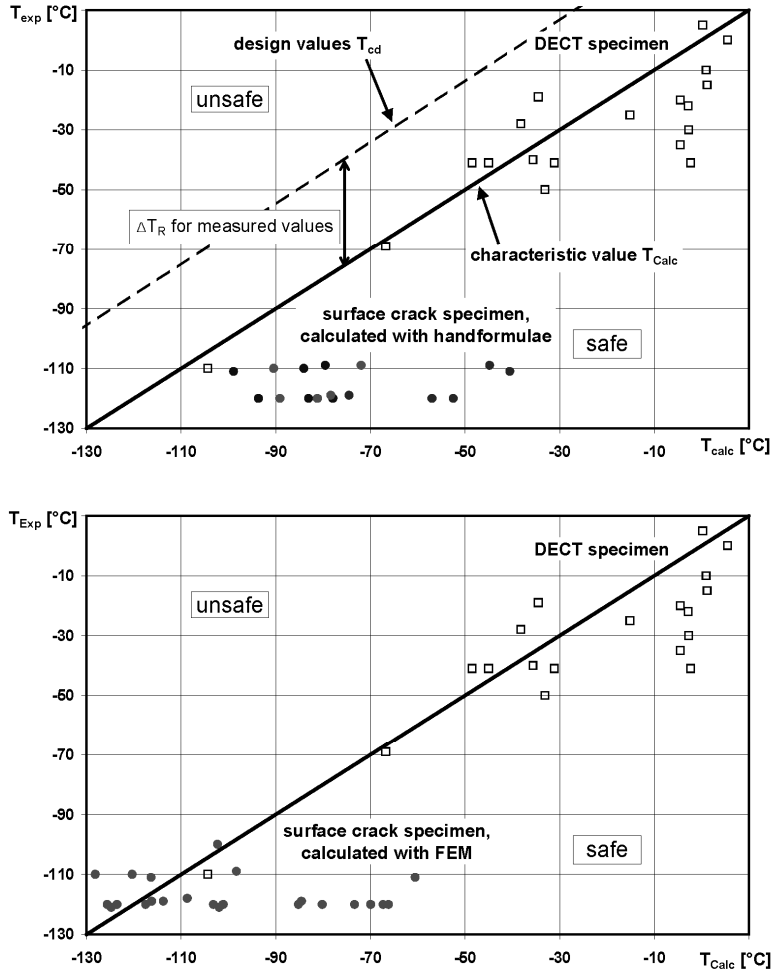


Fig. 2-26: Evaluation of tests with welded details

(4) The comparison shows that the Y- and M_K-functions from handbooks, see fig. 2-26a) are safe-sided with regard to FEM -calculations, see fig. 2-26 b), so that only those values have been used for the further evaluations of safety factors.

(5) The plot of the results $b_i = T_{exp} – T_{calc}$ for the test group with non-welded details and longitudinal attachments is given in fig. 2-27 and for the test group with details with transverse welds in fig. 2-28.

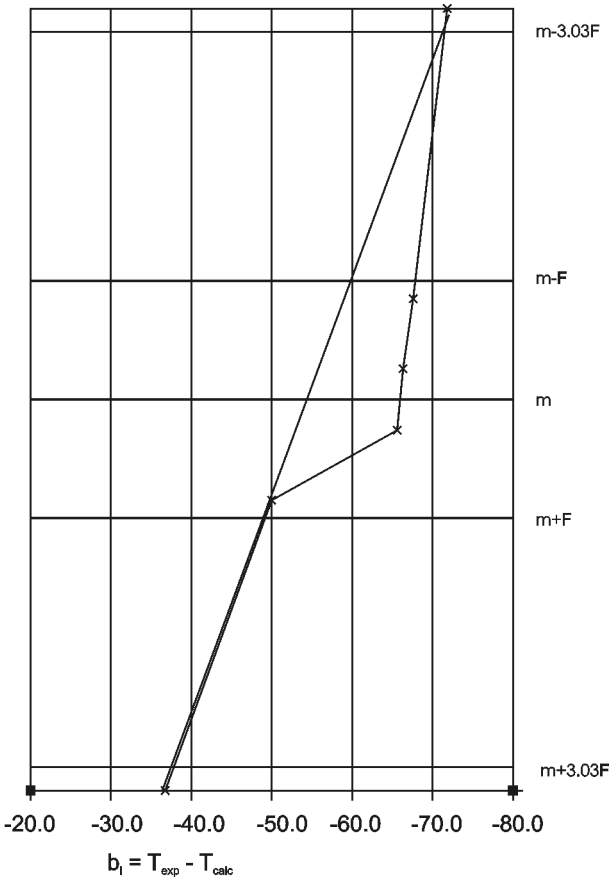


Fig. 2-27: Determination of the safety element $\Delta T_{R,\ meas}$ for the test group with non-welded details and details with longitudinal attachments

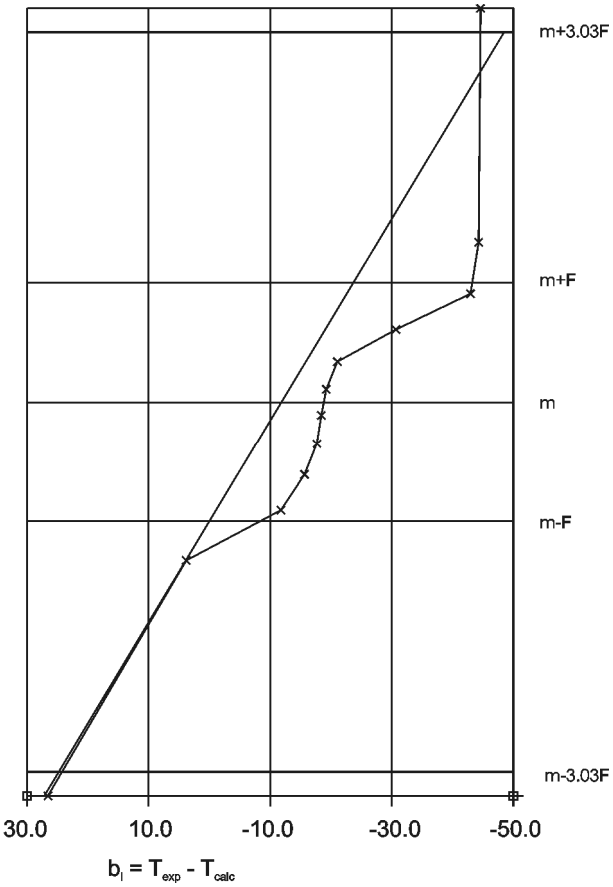


Fig. 2-28: Determination of the safety element $\Delta T_{R,\ meas}$ for the test group with details with transversal attachments

(6) The results show that the safety elements $\Delta T_{R,\ meas}$ for measured values T_{27J} and f_y and the safety elements $\Delta T_{R,\ nom}$ for nominal values T_{27J} and f_y are all safe-sided with respect to the ΔT_R-values derived from the DECT-tests.

(7) The results also show that the effects of local residual stresses σ_S from welding of the attachments can be neglected in the calculation model for the sake of ease of use. They have not been included in the determination of the toughness requirement $K_{appl,d}$ (no ρ-value considered) and therefore they are covered by the mean value corrections b_i and error terms δ_i and subsequently by the model-uncertainty expressed by the ΔT_R-values, can be neglected in the calculation model for the sake of ease of use.

(8) The evaluation of the second step, the evaluation of the fatigue tests to derive suitable standard assumptions for the design values of crack sizes, was carried out in the following way:

1. On one side the crack growth was calculated using the Paris equation

$$\frac{\Delta a}{\Delta N} = C \cdot \Delta K^m \qquad (2\text{-}29)$$

where

$$\Delta K = \Delta\sigma_c \sqrt{\pi a_i}\, Y \cdot M_K \qquad (2\text{-}30)$$

with a/c ratios varying from cycle step to cycle step and C and m taken from measurements for each test specimen, see fig. 2-29,

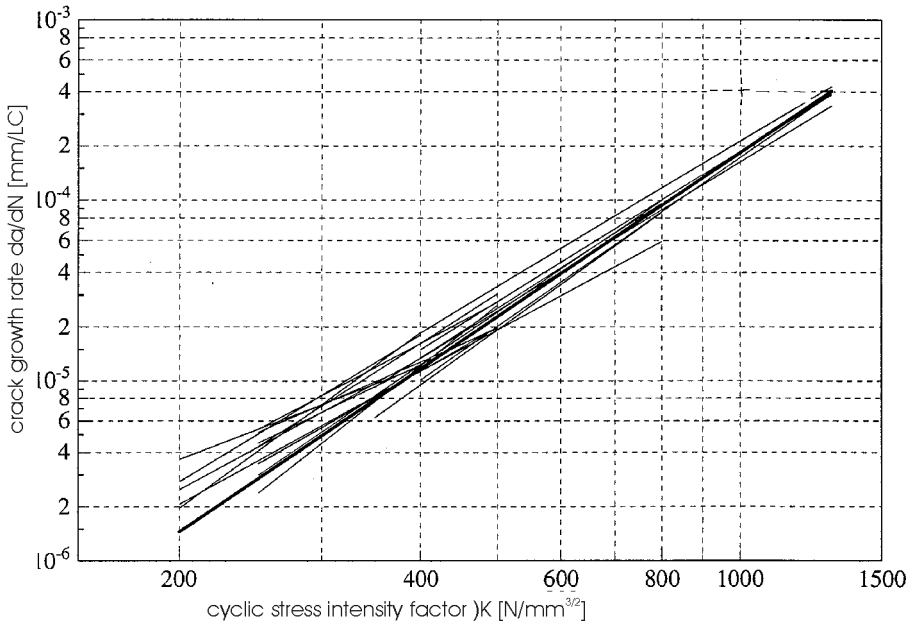


Fig. 2-29: Crack growth curves calculated with values C and m in the Paris-equation, determined from large scale tests

On the other hand the crack growth was calculated with a boundary element programme (BEASY), also with C- and m-values from material tests that fitted well to the Gurney-correlation, see fig. 2-30.

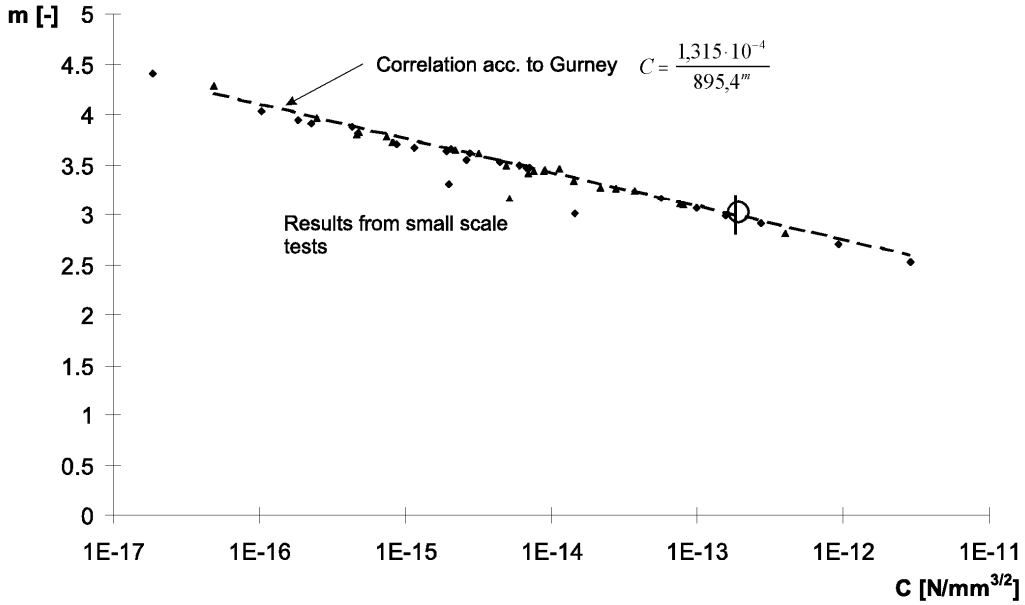


Fig. 2-30: Correlation of C-and m-values according to Gurney

2. In fig. 2-31 and fig. 2-32 some comparisons are given for typical crack growth histories from experiments and calculations are given, revealing:

   - the good accuracy of BEM-calculations,
   - the safe-sidedness of calculations with hand formulae, in particular with constant a/c ratios.

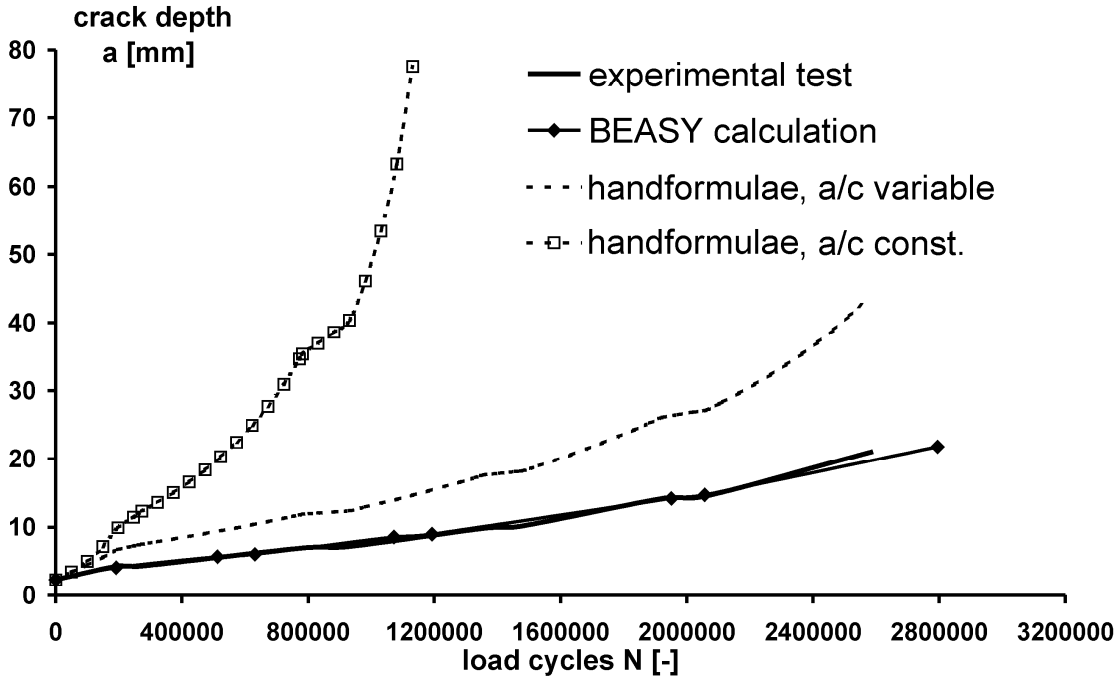


Fig. 2-31: Comparison of typical crack growth histories from experiments and calculations

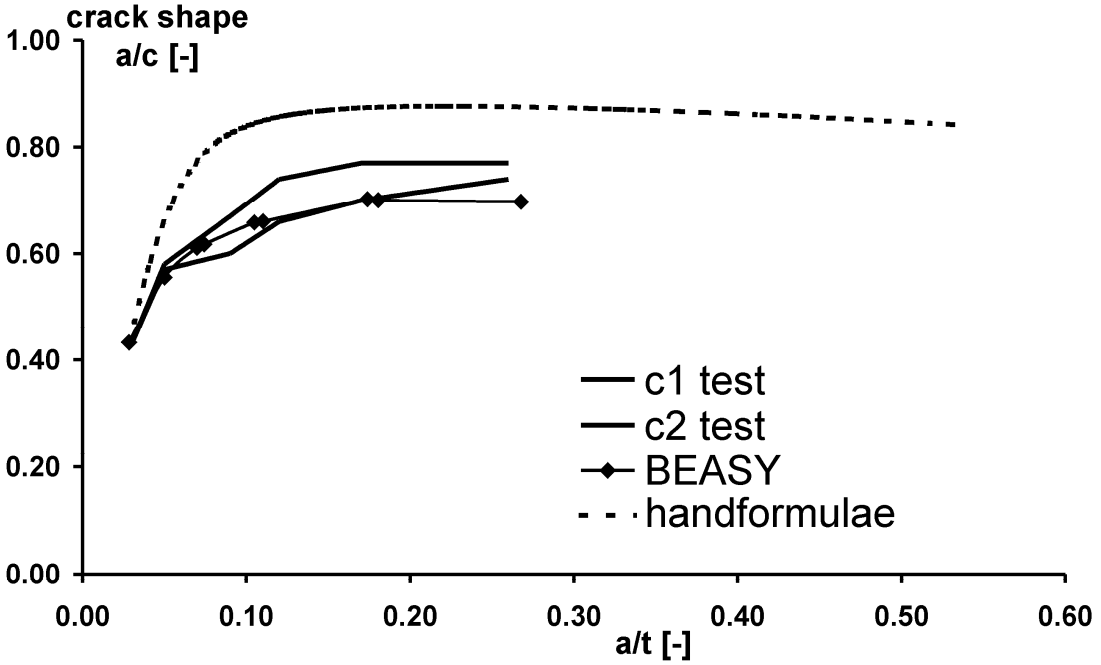


Fig. 2-32: Comparison of typical crack growth histories from experiments and calculations

3. The conclusions drawn are the following:

a) In principle, two types of crack growth can be distinguished:

- those for non welded details and details with longitudinal attachments where the initial crack developed to the final crack size and
- those for details with transverse welds where in parallel to the growth of the artificial initial crack other initial cracks developed along the welded toe that first grew independently from each other and finally grew together to a single crack only, see fig. 2-33.

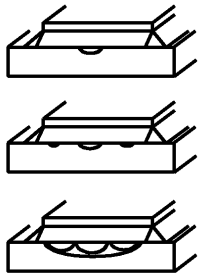


Fig. 2-33: Stages of crack growth for cracks at transverse weld toes

In order to compensate these effects, the following assumptions should be made for initial ratios a_0/c_0:

- for non welded details and longitudinal attachments

$$a_0/c_0 = 0.40$$

- for details with transverse welds (2-31)

$$a_0/c_0 = 0.15$$

b) The C- and m-values should be taken for tests to obtain best coincidence. If such values do not exist, they can be chosen as:

$m = 3$ and $C = 1.80 \cdot 10^{-13}$

to fit the Gurney-correlation, see fig. 2-30.

2.2.6.3.6 Conclusions for the safety element ΔT_R

(1) For the test-evaluations to determine ΔT_R in 2.2.6.3, the following conclusions can be made:

1. - ΔT_R values have been determined from test evaluations for a design fractile level $\alpha_R\beta$ = 3,03 corresponding with the reliability requirement in EN 1990.

- For these evaluations only tests that exhibited brittle fracture and not ductile failure have been considered and treated, as if only

brittle fracture would always happen in the cases of the testing conditions (100%).

- In fact only a portion (~ 70 %) of the total number of test specimen has shown brittle fracture and this portion depends on the temperature, see fig. 2-34.

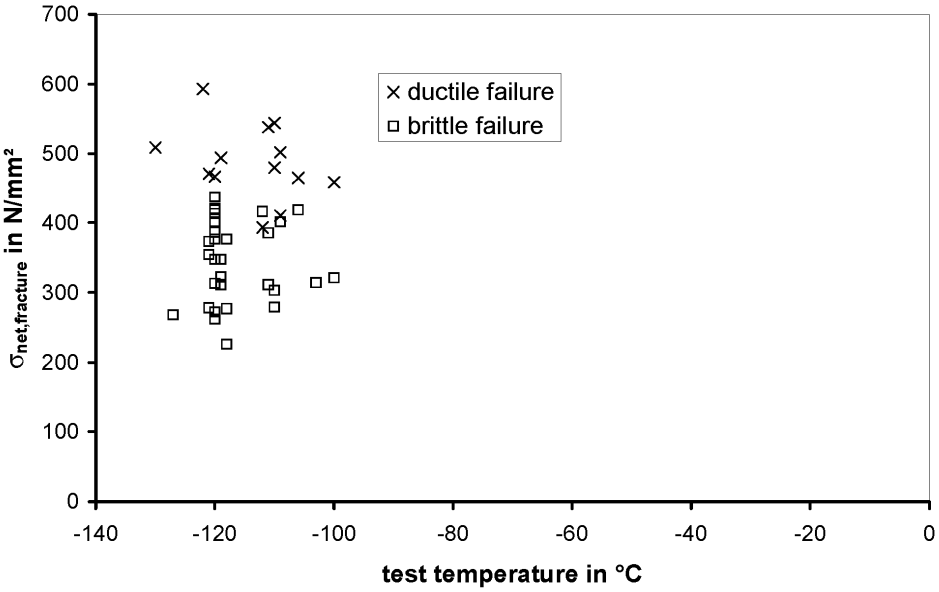


Fig. 2-34: Portion of the test specimens showing brittle fracture (~ 70 %)

Therefore, for efficiency reasons, the expensive tests were carried out at very low temperatures.

- Hence $\alpha_R\beta$ = 3,03 may be considered as an upper bound, and the lower the real design fractile, the higher the temperature.

2. Of all test evaluations, the DECT-tests give the most onerous conditions for the safety elements ΔT_R.

- There may be doubts whether the large scale tests with welded attachments actually cover all practical cases and also the crack sizes a_d/c_d used for the fracture tests may have been too large to give the extreme values of the relative toughness requirements, see fig. 5-16. Therefore, the ΔT_R-values from DECT-tests have been further used for all other details, also including welded ones.

3. - The ΔT_R-values cover local residual stresses from weld attachments on large scale specimens. Therefore such residual stresses need not be further considered in determining $K^*_{appl,d}$.

- However, global residual stresses resulting from remote restraints that were not included in the tests, see fig. 2-35, shall be additionally considered in $K^*_{appl,d}$ as an applied external stress σ_S in addition to the working stress σ_p from external loads.

- Finally, global residual stresses have been assumed in the preparation of table 2.1 of EN 1993-1-10 to be σ_S = 100 N/mm^2 as a lump value for all cases considered.

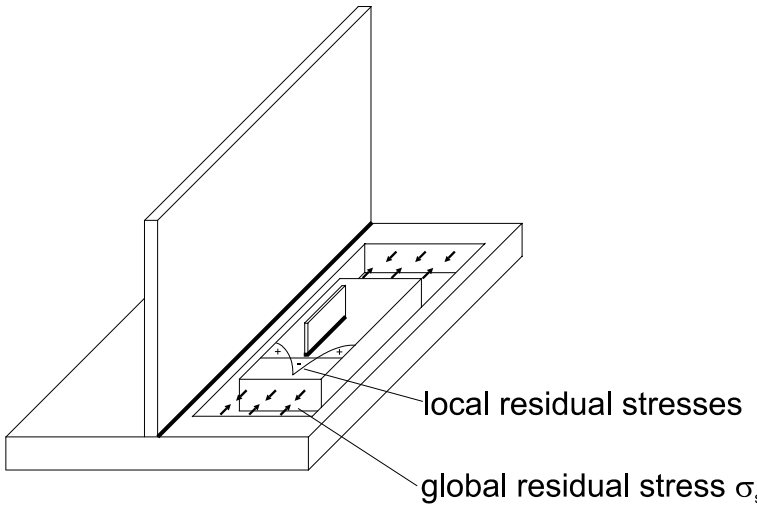


Fig. 2-35: Local and global residual stresses for a fracture mechanics model with weld attachment

4. There are various ΔT_R-values for different purposes:

   a) - For the case of mean value predictions on the basis of measured input values (e.g. for expected values in tests) ΔT_R = 0 K should be used.

   b) - For unique verifications of a project, where measured input values exist for T_{27J} and f_y, the value ΔT_R = -38 K is required to cover model uncertainty of the verification procedure.

      - In this case expert advice is recommended.

   c) - For normal design, where T_{27J} and f_y-values are used from standards (EN 10025), which represent a lower bound value that is rarely reached, the safety element ΔT_R = + 7K may be used that takes account of the usual over-quality of steels delivered.

      - This value ΔT_R = + 7 K is close to the value ΔT_R = 0 K for mean value-prediction for measured input values, so that the extreme accidental case, that the steel delivered only attains the nominal standard value T_{27J}, is sufficiently covered.

5. The maximum allowable values of element thickness in table 2.1 of EN 19931-10 were calculated for the case, that T_{27J}-values are used from appropriate EN-standards, which requires a safety element ΔT_R = + 7 K. Hence the values in table 2.1 do include this safety element already and ΔT_R = 0 K is recommended in using the tabulated values.

6. To consider special national safety aspects or other reliability requirements the safety element ΔT_R and possibly a shift of σ_{Ed} may be given in the National Annex to EN 1993-1-10.

7. For any calculative approaches, the shape of the initial crack imperfection should depend on the notch case when fatigue can control crack growth. The a_0/c_0-ratio should be

   - for non-welded details and longitudinal attachments

     $a_0/c_0 = 0.40$

   - for details with transverse welds

     $a_0/c_0 = 0.15$.

8. Models for crack growth calculations based on BEM give reliable results. Solutions with correction functions Y and M_K from handbooks are safe-sided when calculations with varying a/c-ratios are performed.

   For calculations with constant a_0/c_0-ratios the results are even more conservative.

2.2.6.4 Temperature shift from strain rate $\Delta T_{\dot{\varepsilon}}$

(1) The term $\Delta T_{\dot{\varepsilon}}$ according to equation (2-17)

$$\Delta T_{\dot{\varepsilon}} = \frac{1440 - f_y(t)}{550}\left(\ln\frac{\dot{\varepsilon}}{\dot{\varepsilon}_0}\right)^{1,5} \quad \text{with } \dot{\varepsilon}_0 = 10^{-4}\,s^{-1}$$

takes the strain-rate effect for $4\cdot10^{-4} < \dot{\varepsilon} < 5\cdot10^{3}/s$ into account. The upper limit of $5\cdot10^{3}/\mathrm{s}$ is given by the boundary for validity without “dynamic stress concentration factors”.

(2) This term originates form test-evaluations of [1] and [20], see fig. 2-36 and shows that the lower the strain-rate effects, the higher the yield strength of the material.

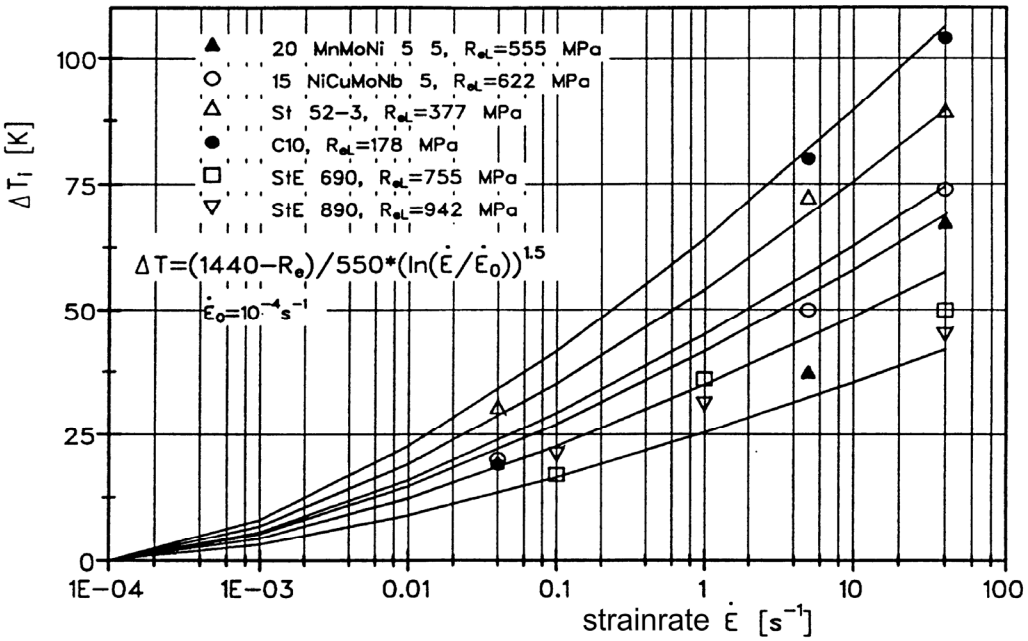


Fig. 2-36: Influence of strain-rate on the toughness-temperature shift, $\dot{\varepsilon}_0 = 0{,}0001/\mathrm{s}$

(3) For developing table 2.1 of EN 1993-1-10, the term $\Delta T_{\dot{\varepsilon}}$ has been taken as $\Delta T_{\dot{\varepsilon}}=0$, so that any strain rate exceeding the limit $4 \cdot 10^{-4}$ should be taken into account.

(4) Studies made on behalf on the stress fluctuations in bridges under moving traffic show that for that type of loading the limit is not exceeded. The limit of $4 \cdot 10^{-4}$ is also the magnitude of strain rate used in tension coupon tests.

2.2.6.5 Temperature shift from cold forming ΔT_{cf}

(1) Cold forming produces a reduction of toughness mainly from the enhancement of yield-strength by cold-straining, see fig. 2-37.

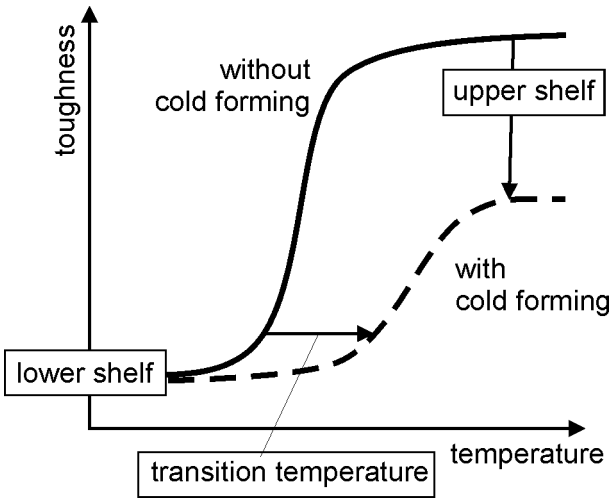


Fig. 2-37: Influence of cold forming on the toughness-temperature diagram

(2) Though fig. 2-37 refers to cold forming with straining in the direction of tension stresses σ_{Ed}, it may also be applied for cold-forming in the direction transverse to the direction of tension stresses.

(3) The term

$\Delta T_{cf} = - 3\ DCF$

where

DCF is the degree of cold forming in [%]

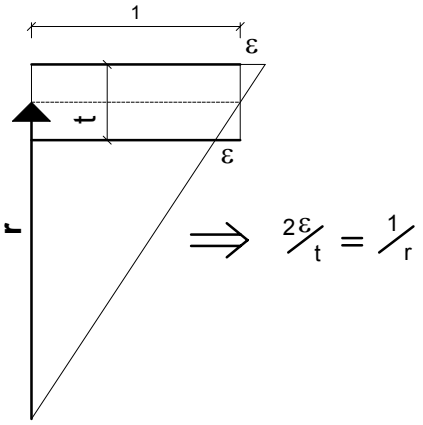
applies only for

$DCF \geq 2\ \%$

and is constant for

$DCF \geq 15\ \%$

(4) Here the degree of cold forming DCF, e.g. for bending is defined as given in fig. 2-38.



$$\Rightarrow \quad {}^{2\varepsilon}/_{t} = {}^{1}/_{r}$$

$$DCF = \varepsilon_{max} - \varepsilon_d = \left(\frac{t}{2r} \cdot 100 - 2 \right) [\%]$$

Fig. 2-38: Geometrical definition of DCF for a yield point elongation of 2%

(5) In EN 1993-1-8 conditions for welding in cold-formed zones and adjacent material are given, that make it plausible that cold-forming has negative influences on material properties. In using the situation for T_{Ed} = -5°C (without ΔT_{CF}), T_{Ed}-values including ΔT_{CF} according to fig. 2-39 are calculated that according to table 2.1 of EN 1993-10 result in allowable plate thicknesses as given in fig. 2-40.

Ratio between bending radius r in mm and material thickness t in mm	Maximum applied plastic strain DCF in %	ΔT^*_{DCF} in K	T_{Ed} (without ΔT_{DCF}) in ° C	T_{Ed} in ° C
≥ 25	≤ 2	0	-5	-5
10 ≤ r/t < 25	≤ 5	-8	-5	-13
3,0 ≤ r/t 10	≤ 14	-21	-5	-26
2,0 ≤ r/t < 3,0	≤ 20	-30	-5	-35

Fig. 2-39: Calculation of ΔT_{Cf} for cold forming for $\sigma_{Ed} = 0{,}75\ f_y$

Ratio between bending radius r in mm and material thickness t in mm	Maximum applied plastic strain DCF in %	T_{Ed} in ° C	Maximum allowable plate thickness t in mm	
			EN 1993-1-10	EN 1993-1-8
≥ 25	≤ 2	-5	30	all
10 ≤ r/t < 25	≤ 5	-13	23	16
3,0 ≤ r/t 10	≤ 14	-26	17	12
2,0 ≤ r/t < 3,0	≤ 20	-35	15	10

Fig. 2-40: Comparison of permissible plate thickness for cold forming products according to EN 1993-1-10 and EN 1993-1-8

2.2.7 Application of the fracture mechanic method to develop table 2.1 of EN 1993-1-10

2.2.7.1 Assumptions for application

(1) The assumptions for the application of table 2.1 of EN 1993-1-10 were the following:

1. The table should be developed for the most onerous case of structures susceptible to fatigue, where the design crack $a_d/2c_d$ should not only cover the crack sizes overlooked in inspections after fabrication (denoted as initial cracks $a_0/2c_0$), but also the crack growth that results from fatigue from putting the structure into use until the moment the cracks grown are detected.

2. As the crack growth does not only depend on the size of the initial crack, but also on the fatigue class and the fatigue loading, the fatigue resistance and the fatigue load applied for crack growth should cover all relevant fatigue classes in EN 1993-1-9 and be defined such, that it takes reference to the maximum possible load in fatigue assessments.

3. The basis of the table should be defined in a mathematical way, so that it can be easily reproduced by computers.

(2) In conclusion, the following assumptions had to be made:

1. Description of size of initial cracks
2. Definition of fatigue loading for determining the crack growth to obtain design cracks
3. Choice of a fracture mechanics model and of a simplified way of calculation to determine the design values of crack size a_d and subsequently $K^*_{appl,d}$ as input to ΔT_σ
4. Justification of the safe-sidedness of the results by a refined analysis for a large series of details
5. Presentation of the results in table 2.1 of EN 1993-1-10 versus suitably scaled input-parameters

2.2.7.2 Description of the size of initial cracks

(1) For a structural detail, e.g. as given in fig. 2-41, the initial crack in the form of a semi-elliptical crack is assumed to be located at the hot spot for fatigue.

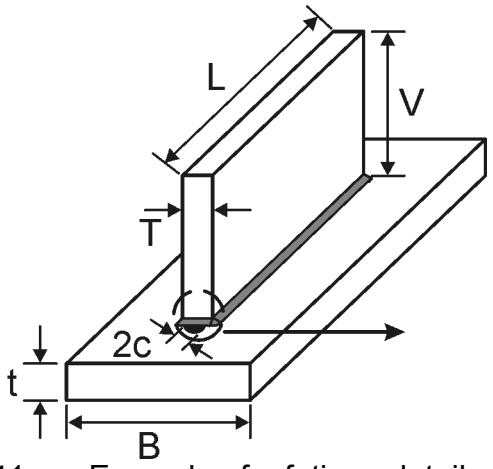


Fig. 2-41: Example of a fatigue detail with the hot spot for fatigue

It has a crack depth of

$$a_0 = 0.5 \ln\left(1 + \frac{t}{t_0}\right) \qquad \text{for } t < 15 \text{ mm} \tag{2-32}$$

where t_0 = 1 mm

and

$$a_0 = 0.5 \ln a_0 = 0{,}5 \ln\left(\frac{t}{t_0}\right) \quad \text{for } t \geq 15 \text{ mm} \tag{2-33}$$

see fig. 2-42.

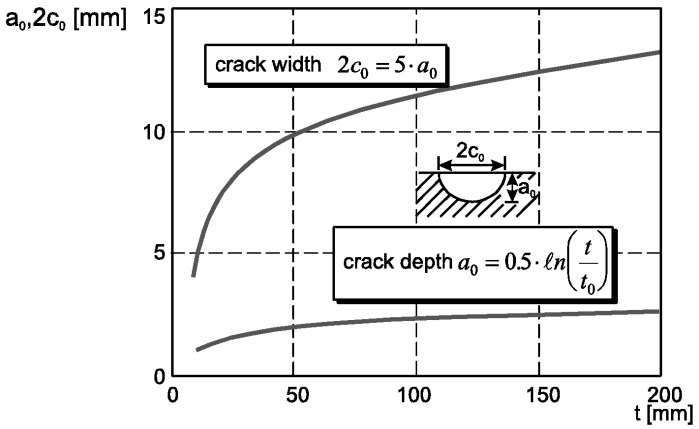


Fig. 2-42: Size of the initial surface crack depending on the plate thickness

(2) The a_0/c_0-ratio, that gives the width $2c_0$ of the initial crack, if the crack depth a_0 is known, is chosen as

$$a_0/c_0 = 0.4 \qquad (2\text{-}34)$$

taking into account rest-line evaluations from fatigue tests as given in fig. 2-43.

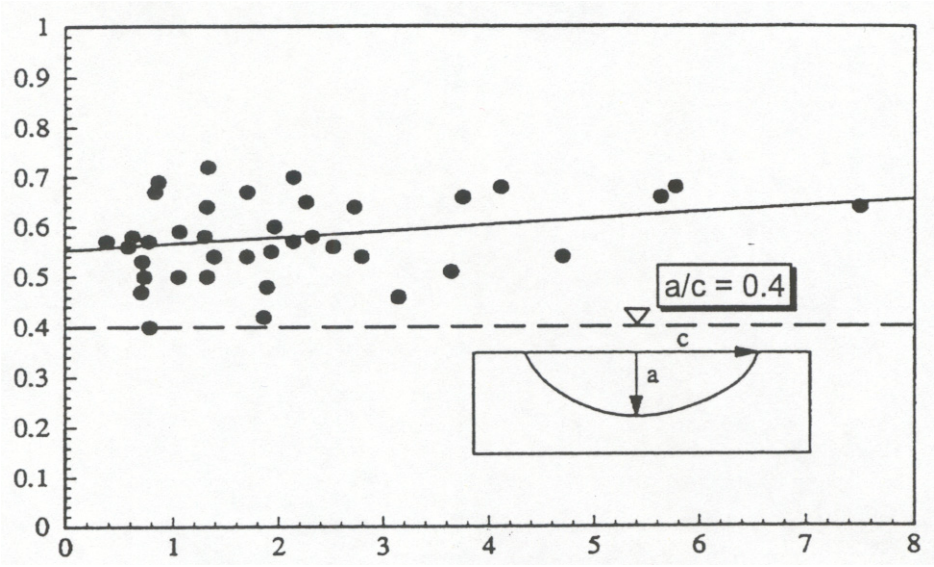


Fig. 2-43: a/c-ratios from evaluations of rest-lines from fatigue tests

(3) With the crack width, a comparison was made with the detectability of cracks with non-destructive testing (NDT) methods, demonstrating that such initial cracks are most probably detectable with Magnetic Testing (MP) and even with Ultra-Sonic Testing (US), see fig. 2-44.

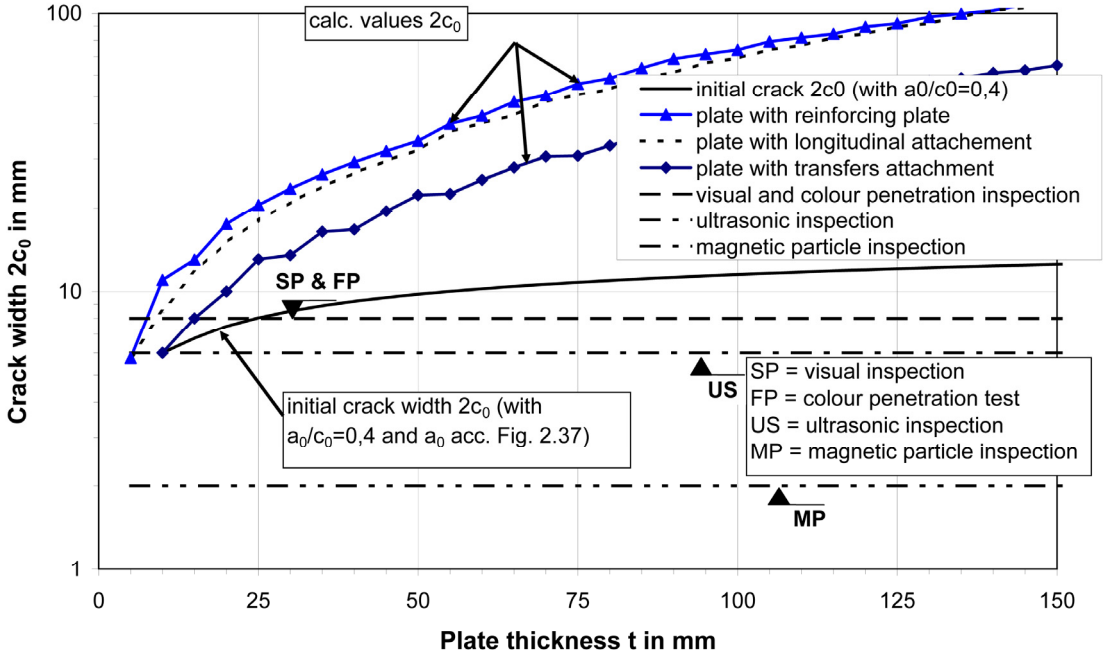


Fig. 2-44: Minimum crack width $2c_0$ detectable by inspection methods after fabrication

2.2.7.3 Definition of fatigue loading for determining design cracks

2.2.7.3.1 General

(1) The maximum fatigue load a structure can bear with a survival probability of 95% is defined for the fatigue detail class $\Delta\sigma_c$ by the damage equation applied for the full service life:

$$D_{5\%} = 1 = \frac{\Sigma\left(\Delta\sigma_{Ei}^3 \cdot n_i\right)}{\Delta\sigma_c^3 \cdot 2 \cdot 10^6} \tag{2-35}$$

(2) This fatigue load represents the characteristic value of the fatigue strength according to EN 1993-1-9, see fig. 2-45, and includes any damage equivalent loading spectrum $\{\Delta\sigma_i, n_i\}$ during the service life that fulfils the equation (2-35).

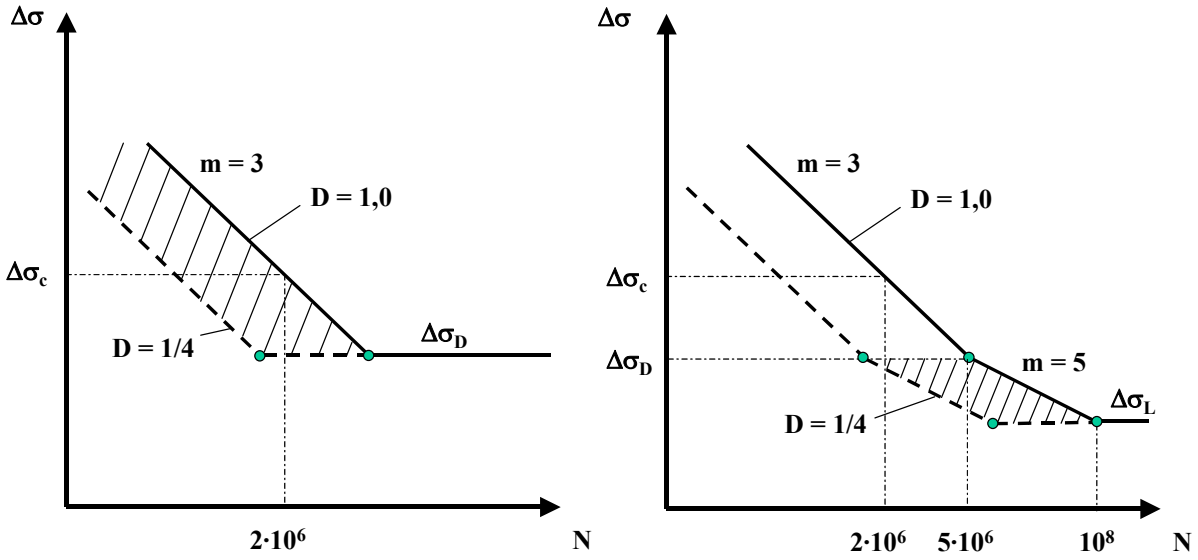


Fig. 2-45: S-N-curves for fatigue and damage curves D = 1 and D = 1/4

(3) The fatigue load for the growth of the initial crack to its design value has been chosen as

$$D_{5\%} = \frac{1}{4} \tag{2-36}$$

(4) In the case of $\Delta\sigma_{Ei} = \Delta\sigma_C$ this means that the fatigue load for crack growth reads:

$$\Delta\sigma_c^3 \cdot 500.000 \tag{2-37}$$

(5) The lapse of time in which this fatigue load makes undetected initial cracks grow to their design values, is called hereafter “safe service period”.

2.2.7.3.2 Consequences for damage tolerance

(1) The fatigue assessment in EN 1993-1-9 includes partial factors to obtain the target reliability and is expressed by

$$D_d = \sum \frac{n_{di}}{N_{Rdi}} = \underbrace{\frac{\sum \left(\gamma_{Ff} \Delta\sigma_{Ei}\right)^3 \cdot n_{Ei}}{\left(\frac{\Delta\sigma_c}{\gamma_{Mf}}\right)^3 \cdot 2 \cdot 10^6}}_{\text{for } \gamma_{Ff}\Delta\sigma_i > \frac{\Delta\sigma_D}{\gamma_{Mf}}} + \underbrace{\frac{\sum \left(\gamma_{Ff} \Delta\sigma_{Ej}\right)^5 \cdot n_{Ej}}{\left(\frac{\Delta\sigma_D}{\gamma_{Mf}}\right)^5 \cdot 5 \cdot 10^6}}_{\text{for } \frac{\Delta\sigma_D}{\gamma_{Mf}} > \gamma_{Ff}\Delta\sigma_j > \frac{\Delta\sigma_L}{\gamma_{Mf}}} = k \le 1 \qquad (2\text{-}38)$$

(2) The stress ranges from the use of long life structures as bridges are mainly in the range

$$\frac{\Delta\sigma_D}{\gamma_{Mf}} > \gamma_{Ff}\Delta\sigma_j > \frac{\Delta\sigma_L}{\gamma_{Mf}}$$

so that on the safe side for the service life of bridges

$$D_d = \frac{\sum \left(\gamma_{Ff} \Delta\sigma_j\right)^5 \cdot n_j}{\left(\frac{\Delta\sigma_D}{\gamma_{Mf}}\right)^5 \cdot 5 \cdot 10^6} = k \le 1 \qquad (2\text{-}39)$$

can be applied.

(3) From equation (2-39) and the load for crack growth the following conclusions ´ may be drawn:

1. For γ_{Ff} = 1,0 and γ_{Mf} = 1,0 the fatigue load for crack growth leads to a “safe service period” of only ¼ of the total fatigue life (e.g. ¼ of 120 years = 30 years for bridges).

2. If after this “safe service period” an inspection of the structure is carried out similar to the one after fabrication, the starting position after this inspection is the same as after fabrication:

   - if no damages are detected, the presence of undetected initial cracks may be assumed and a new “safe service period” may start,
   - if damages are detected, relevant measures for repair or retrofitting can be taken before a new “safe service period” may start, see fig. 2-46.

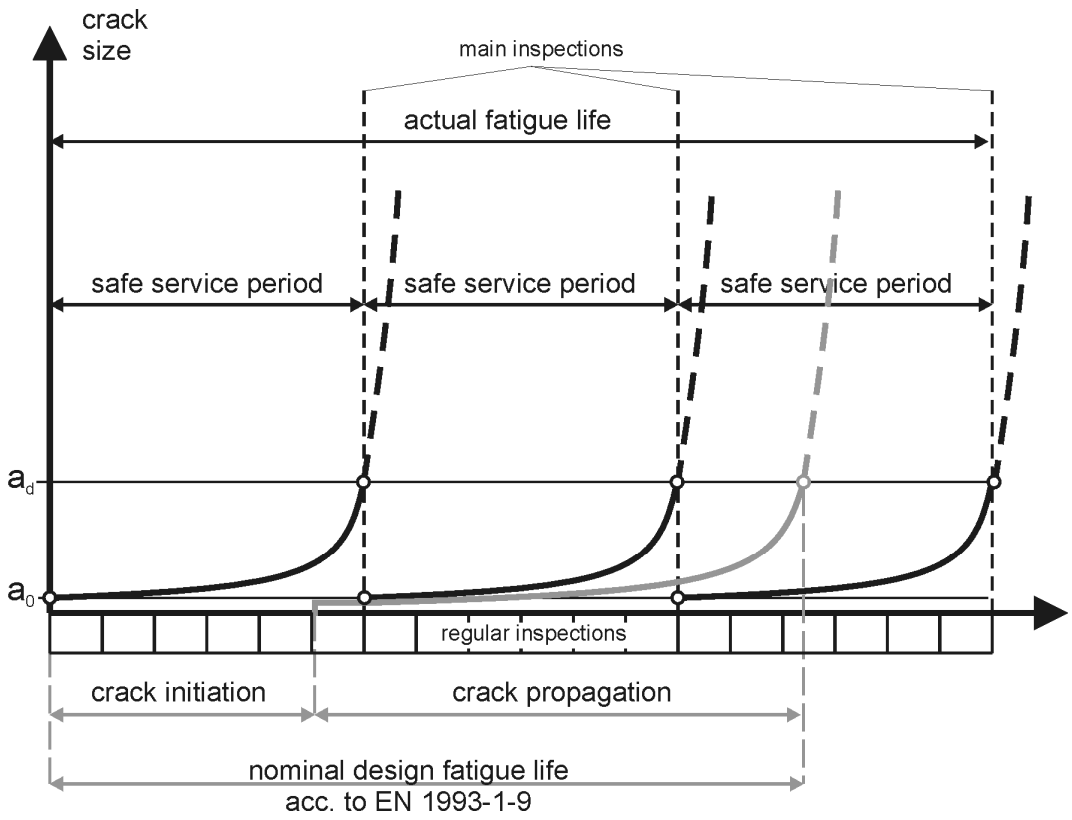


Fig. 2-46: Nominal design fatigue life of a structure and sequence of "safe service periods" with regular inspections and main inspections

So the "safe service period" takes the role of a period between main inspections, the number n of which is during the total fatigue life:

$$n = \frac{T_{Life}}{T_{period}} - 1 = 4 - 1 = 3 \tag{2-40}$$

3. The target reliability of 5% for the resistance as applied for the case with γ_{Ff} = 1.0 and γ_{Mf} = 1.0, is sufficient for the determination of "safe service periods". Hence γ_{Ff}-factors and γ_{Mf} = factors greater than 1.0 applied in the normal fatigue design according to EN 1993-1-9 can be used to extend the "safe service period" by

$$r = \left(\gamma_{Ff} \cdot \gamma_{Mf}\right)^5 \tag{2-41}$$

This results in an expression for the necessary number of inspections, which is

$$n = \frac{4}{\left(\gamma_{Ff} \cdot \gamma_{Mf}\right)^5} - 1 \tag{2-42}$$

This equation gives a link between the number of inspections and the recommended partial factors in EN 1993-1-9, see table 2-9, and allows to choose $\gamma_{Ff} \cdot \gamma_{Mf} = 1.0$ without loosing safety, as this is ensured by

inspections. The choice of $\gamma_{Ff} \cdot \gamma_{Mf} = 1.35$ would mean that the "safe service period" is identical with the nominal fatigue life and an inspection would only be necessary when the end of the nominal fatigue life is reached.

Partial factors $\gamma_{Ff} \cdot \gamma_{Mf}$	Number n of inspections during design fatigue life
1,0	3
1,15	1
1,35	0

Table 2-9: Number of inspections between "safe service periods" during service life

(4) This link between the reliability of the fatigue assessment and the choice of the toughness of the material by the inherent concept of "safe service periods" between inspections controlled by crack growth from a quarter of the full fatigue load during the full design life makes structures "damage tolerant".

(5) The concept of "damage tolerance" is a feature of structural robustness as it ensures that not failure can occur without pre-warning by very large and visible cracks. It also justifies the efficiency of inspections in that it ensures that the occurrence of such large and visible cracks is possible and that those cracks are detectable before a failure will happen.

(6) A side effect of "damage tolerance" of structures is that their use is not limited to the nominal fatigue life, see fig. 2-47. Damage tolerance also makes structures robust against unforeseen developments of fatigue loads and errors in the choice of fatigue class.

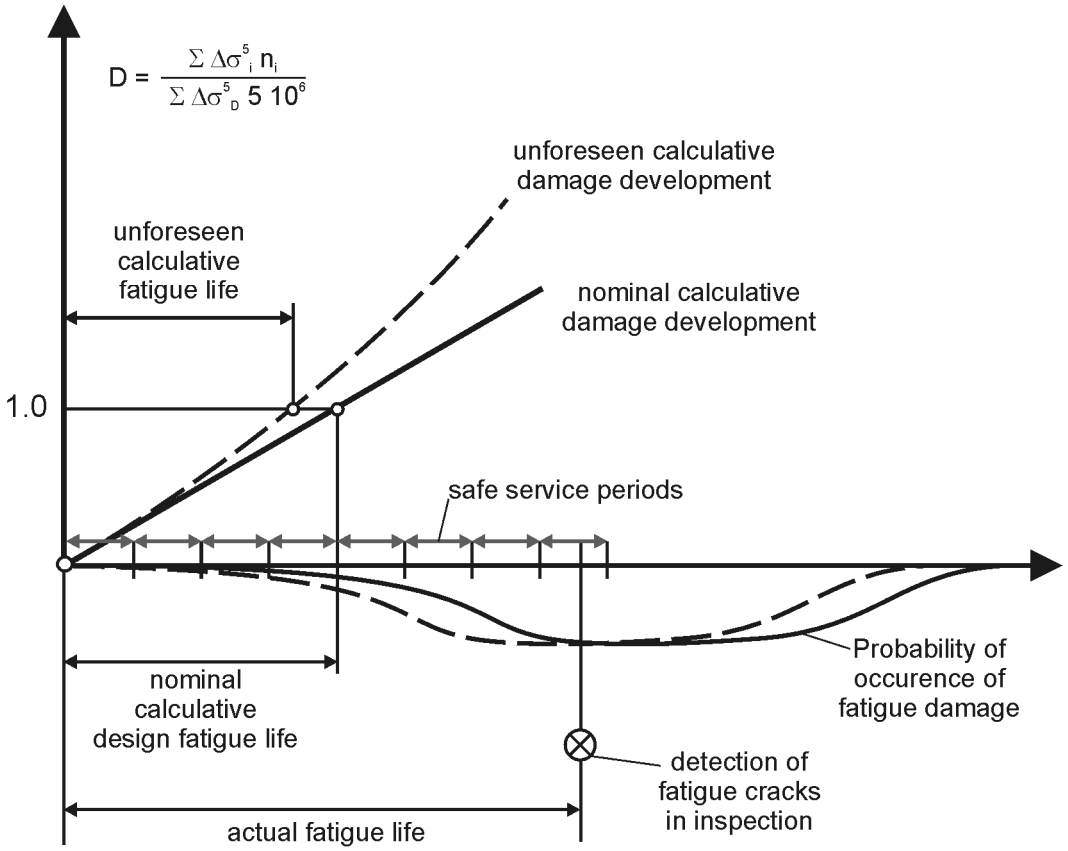


Fig. 2-47: Damage tolerance by “safe service periods” between inspections makes fatigue life independent of calculative design fatigue life

(7) Tension elements in old riveted bridges built up from many thin plates have been “damage tolerant”, because the poor toughness of the material then used has been compensated by the crack arresting effect of the joints between the lamellas and the redundancies of their number. Equivalence to such crack arresting effects and redundancies is obtained for thick plates without any crack arresting joint by high toughness of the material, which provides sufficiently long “safe service periods” between inspections similar to the ones for riveted components.

(8) The alternative to “damage tolerance” is the “safe life” concept that should only be adopted in exceptional cases where inspections are not possible. This concept works without any pre-warning mechanisms and requires that both the design values for fatigue loading and the design values for fatigue resistances are chosen such that they reliably cover the full nominal design life (e.g. for bridges ~ 100 years) and that at the end of the nominal fatigue life the structure still has a failure probability comparable with the one used for ultimate limit states. It therefore works with very large partial factors and possibly with monitoring the loads, see fig. 4-16. At the end of the nominal fatigue life the structure is no longer useable and has to be replaced by a new one.

2.2.7.4 Choice of fracture mechanics model to determine $K^*_{appl,d}$

2.2.7.4.1 Pilot studies

(1) To fulfil the requirements for a reference fracture mechanics model that gives the numerical values for allowable plate thicknesses in table 2.1 of EN 1993-1-10 in a reproducible way, the following pilot studies have been undertaken

1. Studies with alternatives to choose a reference detail and a model for that detail that can be considered as representative for common design practice.
2. Use of geometric parameters for that detail that cover actual design situations.
3. Use of a calculation method for the crack growth that is simple and conservative enough to give design values of crack sizes a_d and action effects $K_{appl,d}$ that do not only cover the detail considered, but also all other details in EN 1993-1-9.

2.2.7.4.2 Choice of fracture mechanics model

(1) From studies of many design situations the structural situation in fig. 2-48 has been chosen to be representative, which applies to the steel beam of a composite bridge with transverse web stiffeners, for which the allowable plate thickness of the bottom flange is questioned.

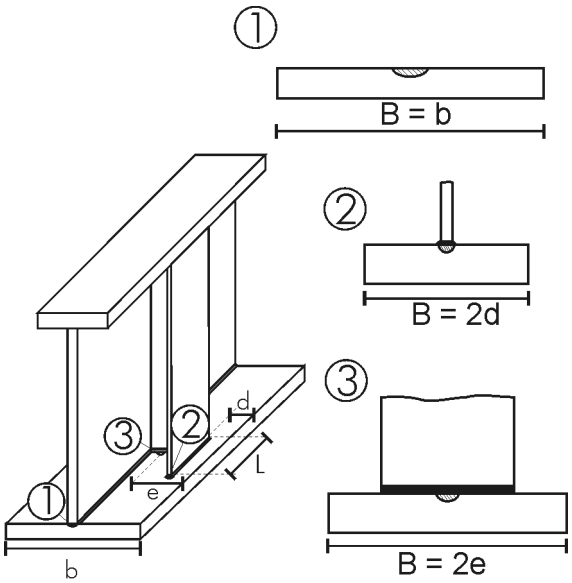


Fig. 2-48: Steel beam with fracture mechanics models ①, ②, ③ representing fatigue details

(2) The notch situation for this bottom flange may be associated with the fatigue classes of the following structural details:

① the welded connection between the web plate and the flange
② a longitudinal attachment to the flange
③ a transverse attachment to the flange

(3) The fracture mechanical model 2 with a longitudinal attachment and the fatigue class $\Delta\sigma_c$ = 56 N/mm^2 and a semi-elliptical surface crack at the weld

toe has been finally chosen to determine the allowable plate thickness t of flanges, see fig. 2-49.

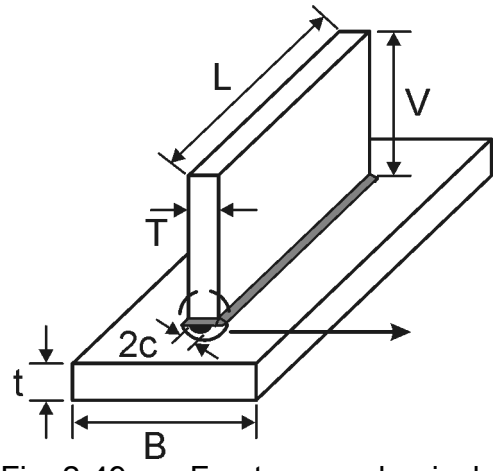


Fig. 2-49: Fracture mechanical model chosen for determining the allowable plate thickness

2.2.7.4.3 Choice of geometrical parameters

(1) For concretizing the standard detail according to fig. 2-49, the following geometrical parameters have been assumed:

a) for the dimensions:

L/t = 8.20
T/t = 0.15
B/t = 7.50
Θ = 45°

b) for the initial cracks

a_0 according to fig. 2-42.

a_0/c_0 = constant = 0.40.

(2) Fig. 2-50 shows that the assumptions for dimensions cover a range of parameters, and fig. 2-51 makes it clear that with respect to the values M_k (a_0) practical design situations are covered in the mean.

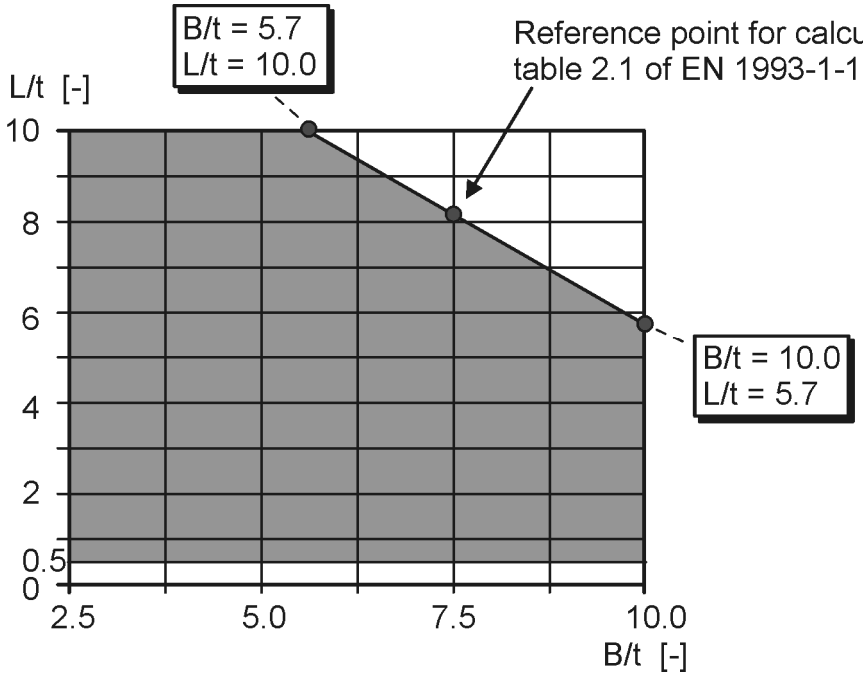


Fig. 2-50: Example for boundary conditions for the geometrical parameters for t = 80 mm

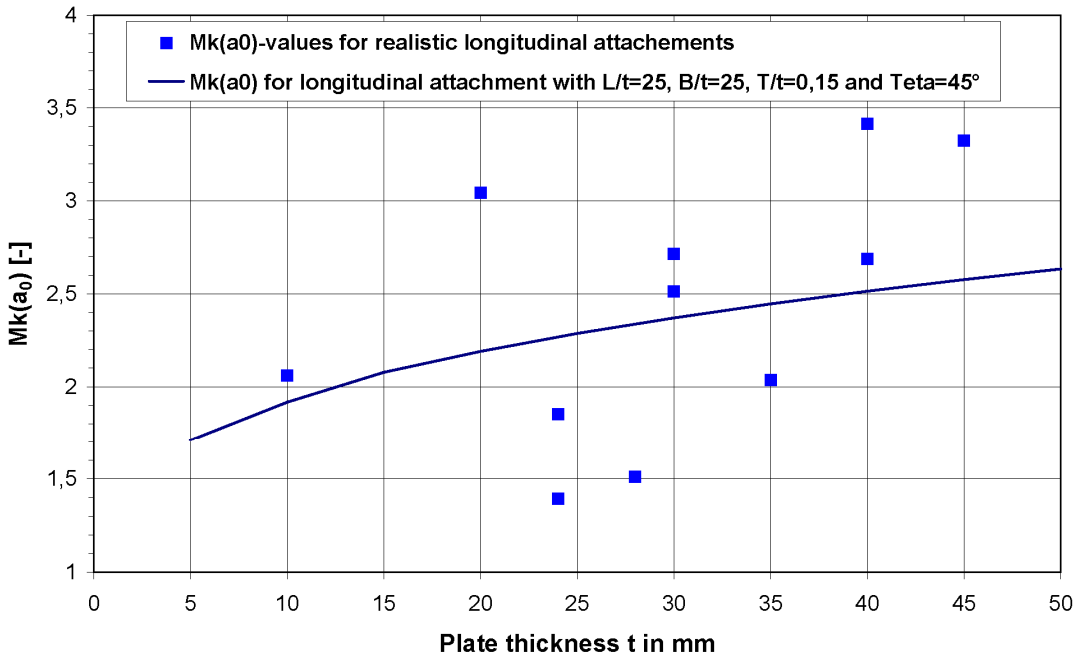


Fig. 2-51: Comparison of M_k (a_0) for the dimensions chosen and for practical cases

(3) These assumptions and the safe-sidedness of a_0/c_0 = constant is taken into account to obtain design values a_d and hence $K_{appl,d}$-values that also cover other structural details of EN 1993-1-9 and their variations in terms of dimensions.

2.2.7.4.4 Performance of calculation of a_d and $K_{appl,d}$

(1) The calculation of the design values of a_d and $K_{appl,d}$ follows the flow given in fig. 2-52.

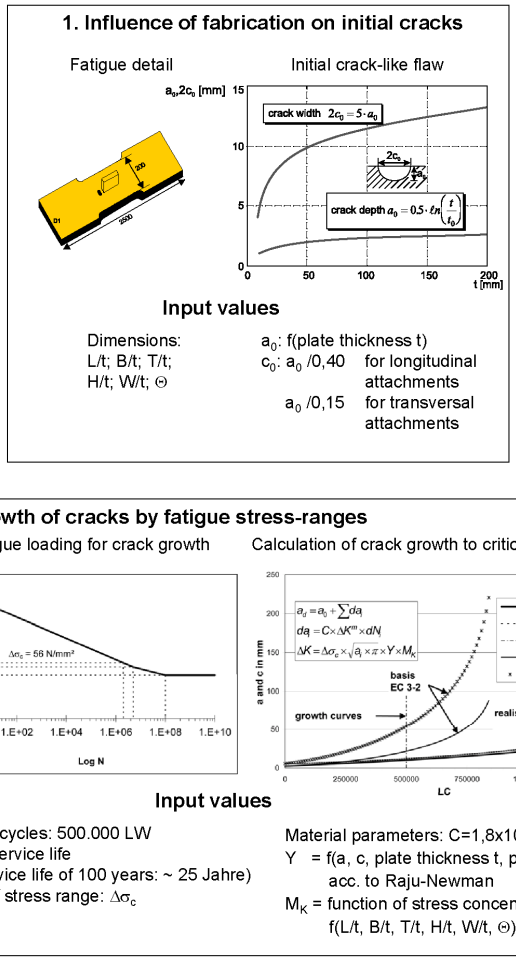


Fig. 2-52: Flow for the calculation of a_d and $K_{appl,d}$

(2) Fig. 2-53 shows the results a_d versus the plate thickness t, which can be expressed by a numerical function

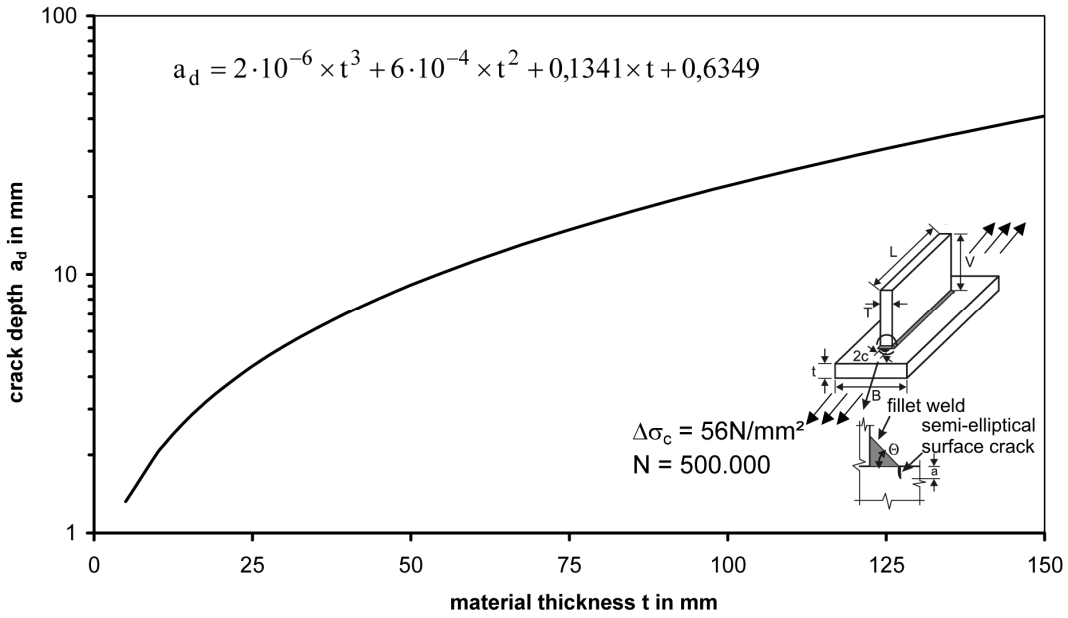


Fig. 2-53: Curve a_d for the standard detail

(3) Fig. 2-54 shows that the design values a_d and c_d (for a/c = 0,4) are actually detectable by various methods.

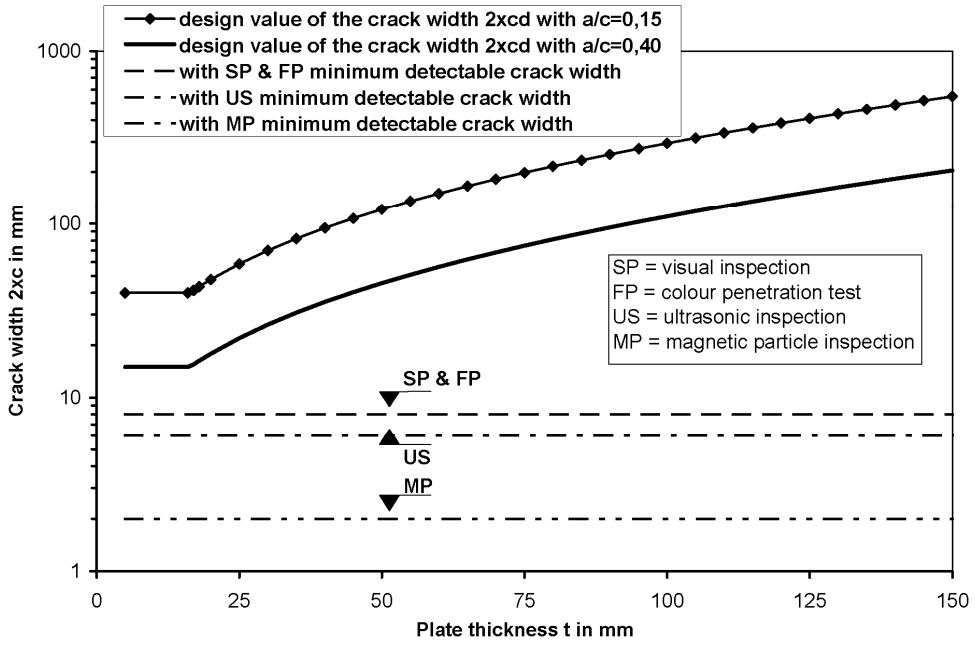


Fig. 2-54: Design values of crack width {$2c_d$} and detectability by NDT-methods

(4) Fig. 2-55 gives the $K_{appl,d}$-curve determined with a_d calculated for the stress level 100 MPa and its mathematical presentation.

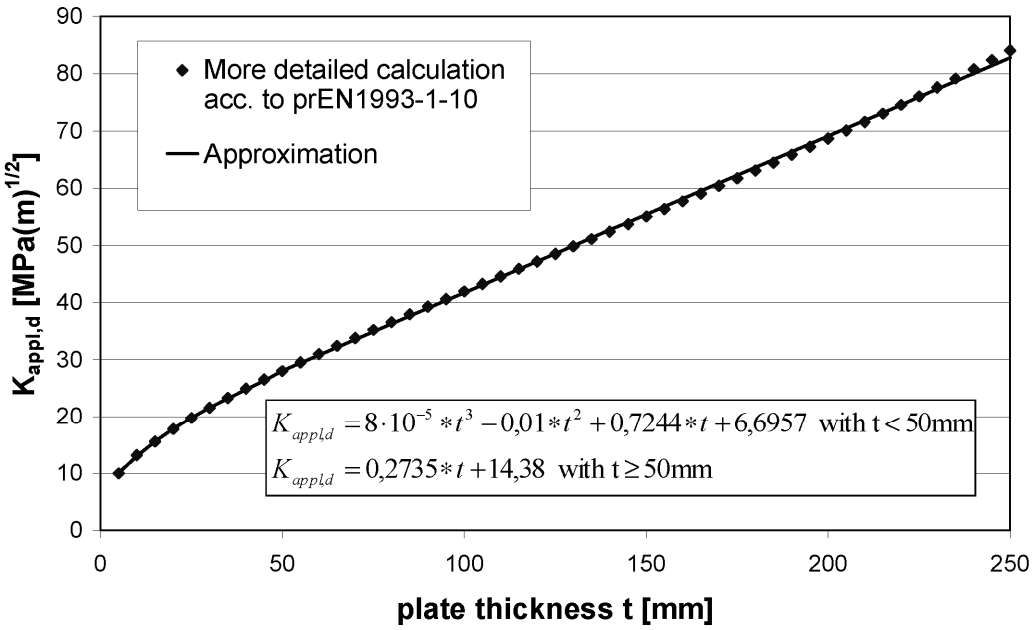


Fig. 2-55: $K_{appl,d}$-curve determined with a_d for a unique stress of 100 MPa

2.2.7.4.5 Justification of the simplified method chosen by more refined analysis

(1) Fig. 2-56 gives a series of results for $K_{appl,d}$ from more refined calculations of a_d and c_d with Boundary Element Methods (BEM) for various details that contain both initial cracks with a_0/c_0 = 0.4 and with a_0/c_0 = 0.15 and it demonstrates that the results obtained in fig. 2-55 are safe-sided.

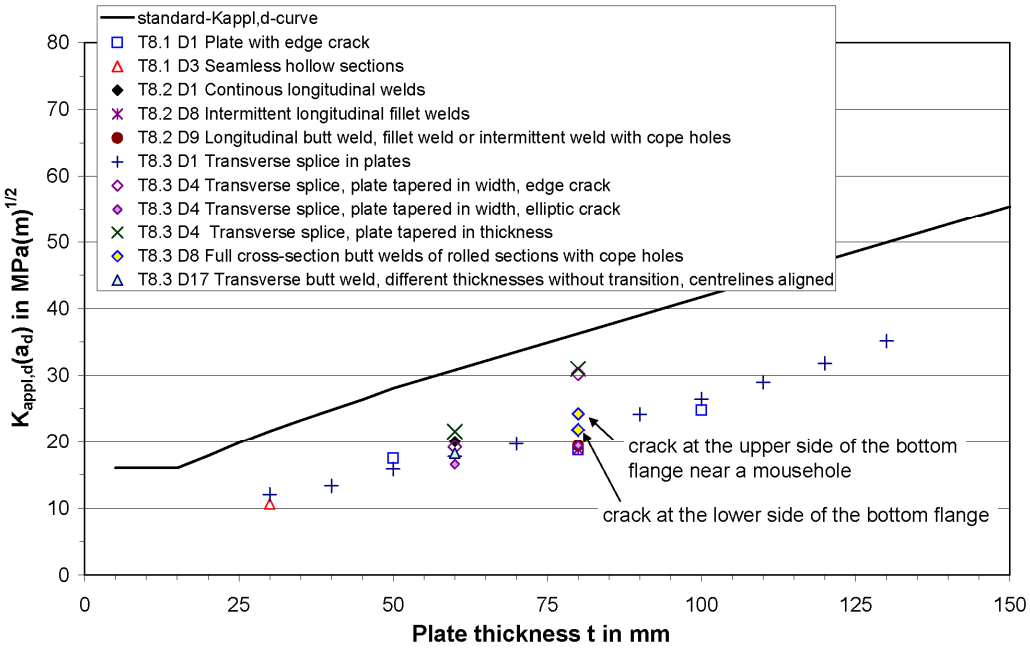


Fig. 2-56: Comparison of the standard $K_{appl,d}$-curve with more accurate calculations for practical cases

(2) The details calculated with more refined methods are given in table 2-10.

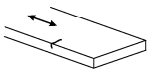
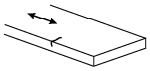
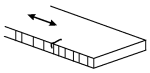
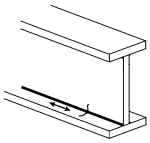
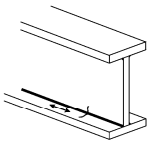
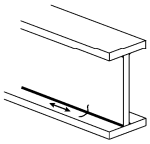
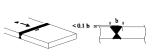
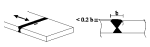
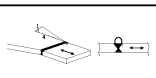
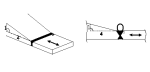
$\Delta\sigma_c$	Constructional details according to EN 1993-1-9	Description	Requirements	Investigated dimensions
160		Rolled and extruded products: Plates and flats.	Sharp edges, surface and rolling flaws to be improved by grinding.	plate thickness t = 30mm up to 130mm
140		Machine gas cut material with subsequent dressing.	All visible signs of edge discontinuities should be removed. The cut areas are to be machined or ground and all burrs are to be removed.	plate thickness t = 60mm
125		Material with machine gas cut edges having shallow and regular drag lines or manual gas cut material, subsequently dressed to remove all edge discontinuities.	Re-entrant corners to be improved by grinding (slope ≤ 1:4) or evaluated using the appropriate stress concentration factors.	plate thickness t = 60mm
125		Continuous longitudinal welds: Automatic butt welds carried out from both sides.	No stop/start position is permitted except when the repair is performed by a specialist and inspection is carried out to verify the proper execution of the repair.	plate thickness of the flange t = 60mm + 80mm
112		Automatic fillet or butt weld carried out from both sides but containing stop/start positions.		plate thickness t = 60mm
100		Manual fillet or butt weld.		plate thickness t = 60mm
112		Transverse splices in plates, flats and rolled sections.	All welds ground flush to plate surface parallel to direction of the arrow.	plate thickness t = 30mm up to 130mm
90		Transverse splices in plates, flats and rolled sections.	The height of the weld convexity not to be greater than 10% of the weld width, with smooth transition to the plate surface. Welds made in flat position.	plate thickness t = 60mm
80		Transverse splices in plates, flats and rolled sections.	The height of the weld convexity not to be greater than 20% of the weld width.	plate thickness t = 60mm
112		Transverse splices in plates or flats tapered in width with a slope ≤ 1:4.	All welds ground flush to plate surface parallel to direction of the arrow.	plate thickness t = 60mm + 80mm
112		Transverse splices in plates or flats tapered in thickness with a slope ≤ 1:4.	All welds ground flush to plate surface parallel to direction of the arrow.	plate thickness t = 60mm + 80mm

Table 2-10 Details from EN 1993-1-9 analysed with more refined calculation methods

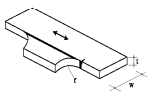
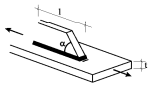
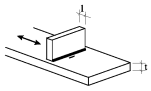
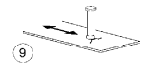
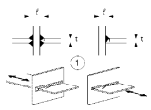
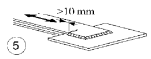
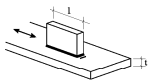
$\Delta\sigma_c$	Constructional details according to EN 1993-1-9	Description	Requirements	Investigated dimensions
90		Gusset plate, welded to the edge of a plate or beam flange.	r/w ≥ 1/3; r ≥ 150mm. Smooth transition radius r formed by initially machining or gas cutting the gusset plate before welding, then grinding sub-sequently the weld area parallel to the direction of the arrow so that the transverse weld toe is fully removed.	plate thickness t = 60mm + 80mm
71		Longitudinal attachments	$\alpha > 45°$	plate thickness t = 60mm + 80mm $\alpha = 50° + 60°$
80		Transverse attachments: Welds which terminate more than 10mm from the edge of the plate.	l ≤ 50 mm	plate thickness t = 30mm up to 130mm
71			50 < l ≤ 80 mm	t = 60mm
63			80 < l ≤ 100 mm	t = 60mm
56			100 < l ≤ 120 mm	t = 60mm
80		The effect of welded shear connectors on base material.		plate thickness t = 60mm
80		Cruciform and Tee joints: 1) Toe failure in full penetration butt welds and all partial penetration joints.	l<50mm and all t Inspected and found free from dis-continuities and misalignments outside the tolerances of EN 1090.	plate thickness t = 60mm
45*		Overlapped: 5) Fillet welded lap joint.	$\Delta\sigma$ to be calculated in the overlapping plates and the weld terminations more than 10 mm from plate edge.	plate thickness t = 60mm
80		Longitudinal attachment: The detail category varies according to the length of the attachment l.	l ≤ 50 mm	plate thickness t = 30mm up to 130mm
71			50 < l ≤ 80 mm	t = 60mm
63			80 < l ≤ 100 mm	t = 60mm
56			l > 100 mm	t = 30mm + 60mm and investigation of extreme values of the ratio l/t

Table 2-10 (continued) Details from EN 1993-1-9 analysed with more refined calculation methods

2.2.7.5 Determination of values in table 2.1

(1) The calculation of the values for allowable plate thicknesses in table 2.1 of EN 1993-1-10 was carried out according to the flow given in fig. 2-57.

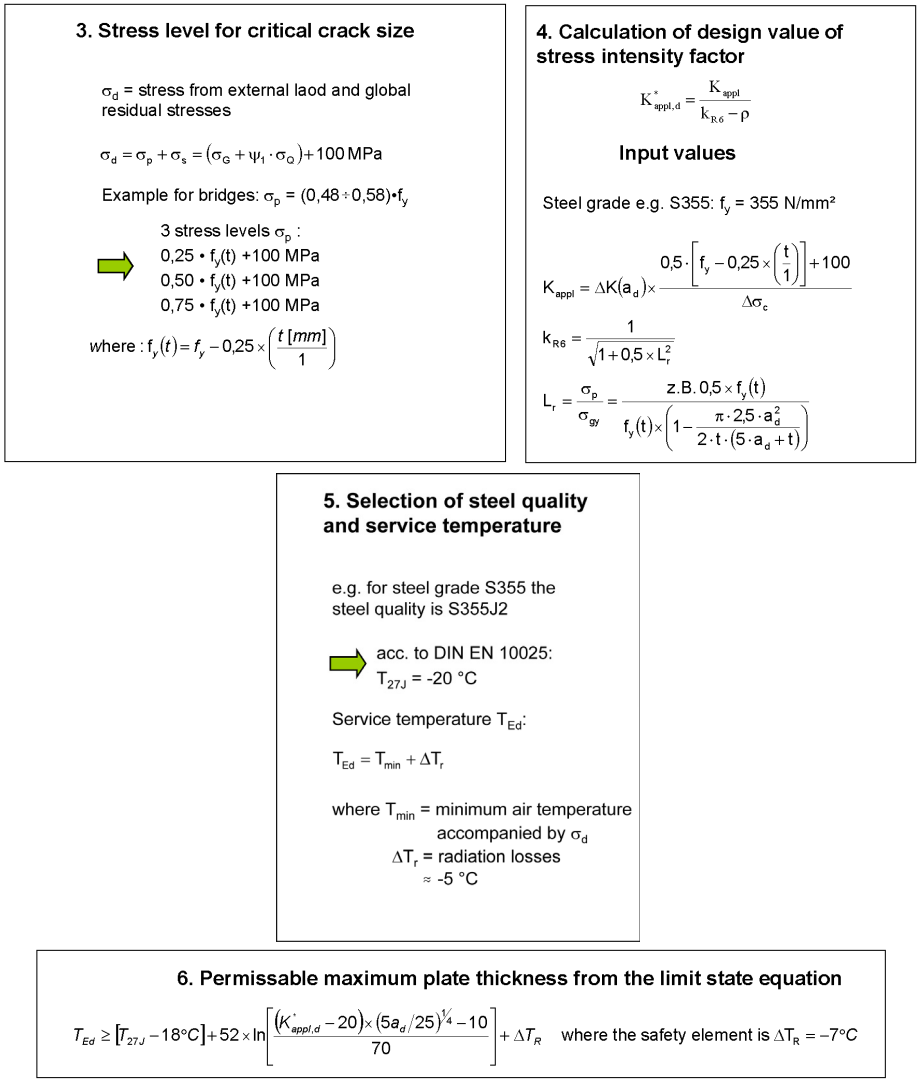


Fig. 2-57: Flow of calculation of the allowable plate thicknesses in table 2.1 of EN 1993-1-10

(2) Three levels of σ_{Ed} from "frequent loads" have been chosen, the maximum being σ_{Ed}= 0.75 f_y (t). This value corresponds to the maximum possible "frequent stress", where for the ultimate limit state verification yielding of the extreme fibre of the elastic cross-section has been assumed:

$$\sigma_{Ed} = \frac{f_y(t)}{1{,}35} = 0{,}75\, f_y \qquad (2\text{-}43)$$

(3) A basic assumption for the external loading on the fracture mechanics model is that it contains in addition to the "frequent" stress σ_p from actual external loads also residual stresses σ_S = 100 MPa from remote restraints.

(4) The presentation of table 2.1 of EN 1993-1-10, however, is related only to the stresses σ_p from actual external loads (the residual stress σ_S is silently included in the calculation).

(5) The choice of σ_S = 100 MPa is justified by the following:

1. stress measurements of residual stresses in components from remote restrains

2. assuming that σ_{Ed} = 0.75 f_y + 100 MPa gives the yield strength
3. assuming that σ_{Ed} = f_y + 100 MPa would give the mean value of f_y.

(6) For the yield strength referred to by the stress levels σ_p, that are expressed as portions of the yield strength, and for determining the FAD-correction factor k_{R6} the values specified in the product standards should be used that depend on the plate thickness t in the form of a step function.

To facilitate the situation, the step function for f_y (t) has been substituted by a continuous approximation

$$f_y(t) = f_{y,nom} - 0.25\left(\frac{t}{t_1}\right), \quad t_1 = 1mm \tag{2-44}$$

(7) Fig. 2-58 shows the values ΔT_σ calculated for table 2.1 of EN 1993-1-10 with $\sigma_p = 0.75 f_y(t)$ and various plate thicknesses for S355 and the results of studies with BEM for practical design situations to demonstrate the safe-sidedness.

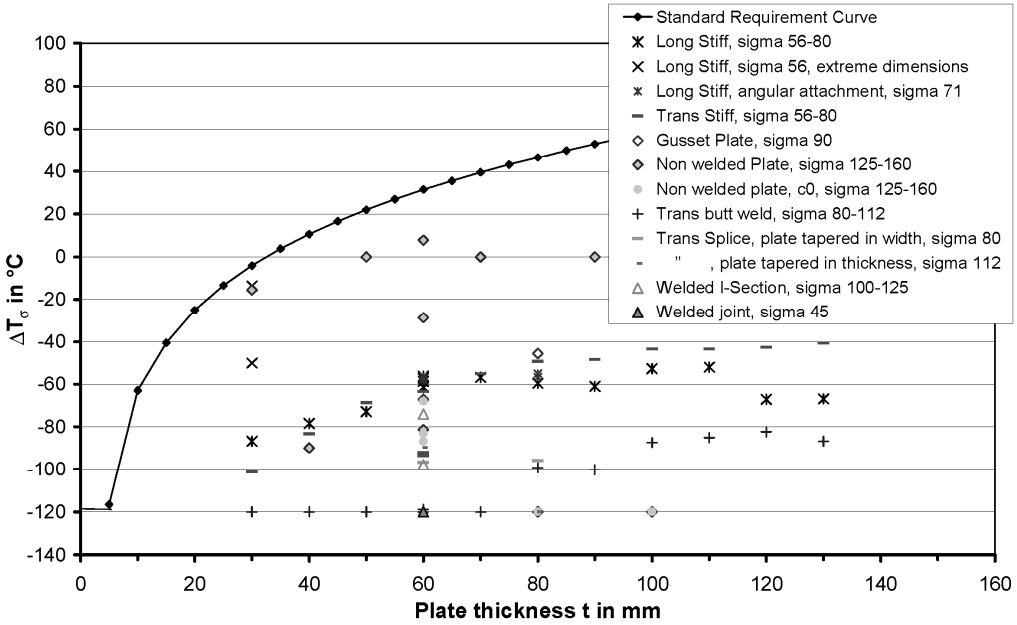


Fig. 2-58: ΔT_σ-values for S355, σ_p = 0.75 f_y compared with results from BEM-calculations with practical details

(8) Where T_{KV}-values in the standards were not expressed in terms of T_{27J} but in terms of T_{40J} or T_{30J}, the following correlations were used:

$T_{40J} = T_{27J} + 10$ [°C]
$T_{30J} = T_{27J} + 0$ [°C] (2-45)

(9) Table 2-11 includes the final results from table 2.1 of EN 1993-1-10.

Steel grade	Sub-grade	Charpy energy CVN		Reference temperature T_{Ed} [°C]																						
		at T [°C]	J_{min}	10	0	-10	-20	-30	-40	-50	10	0	-10	-20	-30	-40	-50	10	0	-10	-20	-30	-40	-50
				σ_{Ed} = 0,75 $f_y(t)$							σ_{Ed} = 0,50 $f_y(t)$							σ_{Ed} = 0,25 $f_y(t)$						
S235	JR	20	27	60	50	40	35	30	25	20	90	75	65	55	45	40	35	135	115	100	85	75	65	60
	J0	0	27	90	75	60	50	40	35	30	125	105	90	75	65	55	45	175	155	135	115	100	85	75
	J2	-20	27	125	105	90	75	60	50	40	170	145	125	105	90	75	65	200	200	175	155	135	115	100
S275	JR	20	27	55	45	35	30	25	20	15	80	70	55	50	40	35	30	125	110	95	80	70	60	55
	J0	0	27	75	65	55	45	35	30	25	115	95	80	70	55	50	40	165	145	125	110	95	80	70
	J2	-20	27	110	95	75	65	55	45	35	155	130	115	95	80	70	55	200	190	165	145	125	110	95
	M,N	-20	40	135	110	95	75	65	55	45	180	155	130	115	95	80	70	200	200	190	165	145	125	110
	ML,NL	-50	27	185	160	135	110	95	75	65	200	200	180	155	130	115	95	230	200	200	200	190	165	145
S355	JR	20	27	40	35	25	20	15	15	10	65	55	45	40	30	25	25	110	95	80	70	60	55	45
	J0	0	27	60	50	40	35	25	20	15	95	80	65	55	45	40	30	150	130	110	95	80	70	60
	J2	-20	27	90	75	60	50	40	35	25	135	110	95	80	65	55	45	200	175	150	130	110	95	80
	K2,M,N	-20	40	110	90	75	60	50	40	35	155	135	110	95	80	65	55	200	200	175	150	130	110	95
	ML,NL	-50	27	155	130	110	90	75	60	50	200	180	155	135	110	95	80	210	200	200	200	175	150	130
S420	M,N	-20	40	95	80	65	55	45	35	30	140	120	100	85	70	60	50	200	185	160	140	120	100	85
	ML,NL	-50	27	135	115	95	80	65	55	45	190	165	140	120	100	85	70	200	200	200	185	160	140	120
S460	Q	-20	30	70	60	50	40	30	25	20	110	95	75	65	55	45	35	175	155	130	115	95	80	70
	M,N	-20	40	90	70	60	50	40	30	25	130	110	95	75	65	55	45	200	175	155	130	115	95	80
	QL	-40	30	105	90	70	60	50	40	30	155	130	110	95	75	65	55	200	200	175	155	130	115	95
	ML,NL	-50	27	125	105	90	70	60	50	40	180	155	130	110	95	75	65	200	200	200	175	155	130	115
	QL1	-60	30	150	125	105	90	70	60	50	200	180	155	130	110	95	75	215	200	200	200	175	155	130
S690	Q	0	40	40	30	25	20	15	10	10	65	55	45	35	30	20	20	120	100	85	75	60	50	45
	Q	-20	30	50	40	30	25	20	15	10	80	65	55	45	35	30	20	140	120	100	85	75	60	50
	QL	-20	40	60	50	40	30	25	20	15	95	80	65	55	45	35	30	165	140	120	100	85	75	60
	QL	-40	30	75	60	50	40	30	25	20	115	95	80	65	55	45	35	190	165	140	120	100	85	75
	QL1	-40	40	90	75	60	50	40	30	25	135	115	95	80	65	55	45	200	190	165	140	120	100	85
	QL1	-60	30	110	90	75	60	50	40	30	160	135	115	95	80	65	55	200	200	190	165	140	120	100

steel grade	sub grade	charpy energy CVN		Reference temperature T_{Ed}[°C]																						
				10	0	-10	-20	-30	-40	-50	10	0	-10	-20	-30	-40	-50	10	0	-10	-20	-30	-40	-50
		T at °C	J_{min}	σ_{Ed} = 0,75 $f_y(t)$							σ_{Ed} = 0,50 $f_y(t)$							σ_{Ed} = 0,25 $f_y(t)$						
EN 10025-6																										
S500	Q	0	40	55	45	35	30	20	15	15	85	70	60	50	40	35	25	145	125	105	90	80	65	55
	Q	-20	30	65	55	45	35	30	20	15	105	85	70	60	50	40	35	170	145	125	105	90	80	65
	QL	-20	40	80	65	55	45	35	30	20	125	105	85	70	60	50	40	195	170	145	125	105	90	80
	QL	-40	30	100	80	65	55	45	35	30	145	125	105	85	70	60	50	200	195	170	145	125	105	90
	QL1	-40	40	120	100	80	65	55	45	35	170	145	125	105	85	70	60	200	200	195	170	145	125	105
	QL1	-60	30	140	120	100	80	65	55	45	200	170	145	125	105	85	70	205	200	200	195	170	145	125
S550	Q	0	40	50	40	30	25	20	15	10	80	65	55	45	35	30	25	140	120	100	85	75	60	50
	Q	-20	30	60	50	40	30	25	20	15	95	80	65	55	45	35	30	160	140	120	100	85	75	60
	QL	-20	40	75	60	50	40	30	25	20	115	95	80	65	55	45	35	185	160	140	120	100	85	75
	QL	-40	30	90	75	60	50	40	30	25	135	115	95	80	65	55	45	200	185	160	140	120	100	85
	QL1	-40	40	110	90	75	60	50	40	30	160	135	115	95	80	65	55	200	200	185	160	140	120	100
	QL1	-60	30	130	110	90	75	60	50	40	185	160	135	115	95	80	65	200	200	200	185	160	140	120
S620	Q	0	40	45	35	25	20	15	15	10	70	60	50	40	30	25	20	130	110	95	80	65	55	45
	Q	-20	30	55	45	35	25	20	15	15	85	70	60	50	40	30	25	150	130	110	95	80	65	55
	QL	-20	40	65	55	45	35	25	20	15	105	85	70	60	50	40	30	175	150	130	110	95	80	65
	QL	-40	30	80	65	55	45	35	25	20	125	105	85	70	60	50	40	200	175	150	130	110	95	80
	QL1	-40	40	100	80	65	55	45	35	25	145	125	105	85	70	60	50	200	200	175	150	130	110	95
	QL1	-60	30	120	100	80	65	55	45	35	170	145	125	105	85	70	60	200	200	200	175	150	130	110
S690	Q	0	40	40	30	25	20	15	10	10	65	55	45	35	30	20	20	120	100	85	75	60	50	45
	Q	-20	30	50	40	30	25	20	15	10	80	65	55	45	35	30	20	140	120	100	85	75	60	50
	QL	-20	40	60	50	40	30	25	20	15	95	80	65	55	45	35	30	165	140	120	100	85	75	60
	QL	-40	30	75	60	50	40	30	25	20	115	95	80	65	55	45	35	190	165	140	120	100	85	75
	QL1	-40	40	90	75	60	50	40	30	25	135	115	95	80	65	55	45	200	190	165	140	120	100	85
	QL1	-60	30	110	90	75	60	50	40	30	160	135	115	95	80	65	55	200	200	190	165	140	120	100
EN 10149-2																										
S500	MC	-20	40	80	65	55	45	35	30	20	125	105	85	70	60	50	40	195	170	145	125	105	90	80
S550	MC	-20	40	75	60	50	40	30	25	20	115	95	80	65	55	45	35	185	160	140	120	100	85	75
S600	MC	-20	40	70	55	45	35	30	20	15	105	90	75	60	50	40	35	180	155	130	110	95	80	70
S650	MC	-20	40	65	50	40	30	25	20	15	100	85	70	55	45	35	30	170	145	125	105	90	75	65
S700	MC	-20	40	60	45	35	30	25	20	15	95	80	65	50	45	35	30	165	140	120	100	85	70	60

Table 2-11: Tabulated values from table 2.1 of EN 1993-1-10 and table 4 of EN 1993-1-12 for the choice of material to avoid brittle fracture

(10) Table 2-11 also includes values from table 4 in EN 1993-1-12 that covers the choice of material for high strength steels not listed in EN 1993-1-10.

2.2.7.6 Summary

(1) Table 2-12 gives a summary of formulae used in the application of the fracture mechanic method to develop table 2.1 of EN 1993-1-10

Initial cracks (a_0)

Position: at hot spots for fatigue

Shape: semielliptical

Sizes: $a_0 = 0{,}5 \cdot \ln(t/t_0)$ with $t_0 = 1$mm

$2 \cdot c_0 = 5 \cdot a_0$ for longitudinal stiffener and pure plate

$3 \cdot c_0 = 20 \cdot a_0$ for transverse stiffener and reinforced plate

Loading of structural member

$\sigma_{Ed} = \sigma_p + \sigma_s$

$\sigma_p = \sigma\{G_k$ "+" $\psi_1 Q_k\}$

σ_s = 100 N/mm² from remote restraints of structural member, effects of residual stresses at hot spots from local welding are included in ΔT_R (test evaluation)

Fatigue load

Applied in terms of damage $D = \frac{\sum \Delta\sigma_i^m \cdot n_i}{\Delta\sigma_c^m \cdot 2 \cdot 10^6} = \frac{1}{4}$ with constant stress ranges $\Delta\sigma_i = \Delta\sigma_c$

Fatigue crack growth to critical crack size (a_d)

Use of C and m in $\Delta a/\Delta N = C \cdot \Delta K^m$ from material tests,
satisfying the Gurney-Correlation $C = 1{,}315 \cdot 10^{-4} \frac{1}{895{,}4^m}$

Determination of $K^*_{appl,d}$

For $K^*_{appl,d} = \frac{\sigma_{Ed} \cdot \sqrt{\pi \cdot a_d} \cdot Y \cdot M_k}{k_{R6} - \rho}$ $MPa\sqrt{m}$ (σ_{Ed} in N/mm² and a_d in m) where

Y = Correction function for various crack position and shapes,	see table 2-3
M_k = Correction function for various attachments,	see table 2-4
k_{R6} = plasticity correction factor from R6-FAD,	see table 2-5
ρ = correction factor for local residual stresses,	see table 2-6

Standardized $K^*_{appl,d}$-curve

$K^*_{appl,d}(t) = \frac{\sigma_{Ed}}{\sigma_0} \cdot \left(\frac{8 \cdot 10^{-5} \cdot t^3 - 0{,}01 \cdot t^2 + 0{,}7244 \cdot t + 6{,}6957}{k_{R6} - \rho} \right)$ for the case t < 50mm

$K^*_{appl,d}(t) = \frac{\sigma_{Ed}}{\sigma_0} \cdot \left(\frac{0{,}2735 \cdot t + 14{,}38}{k_{R6} - \rho} \right)$ for the case t ≥ 50mm

complying with

σ_0 = 100 MPa

$a_d = 2 \cdot 10^{-6} \cdot t^3 + 0{,}0006 \cdot t^2 + 0{,}1341 \cdot t + 0{,}6349$ (with t in mm)

$2 \cdot c_d = 5 \cdot a_d$

Effective crack front b_{eff}

b_{eff} see table 2-7

Table 2-12: Summary of assumptions and formulae to develop table 2.1 of EN 1993-1-10

(2) This table 2-12 may be referred to where table 2.1 of EN 1993-1-10 shall be bypassed by more refined methods, see section 2.4.

2.3 Maximum permitted thickness values - Examples

2.3.1 Use of table 2.1 of EN 1990-1-10

(1) The use of table 2.1 of EN 1990-1-10 follows the flow chart given in fig. 2-59.

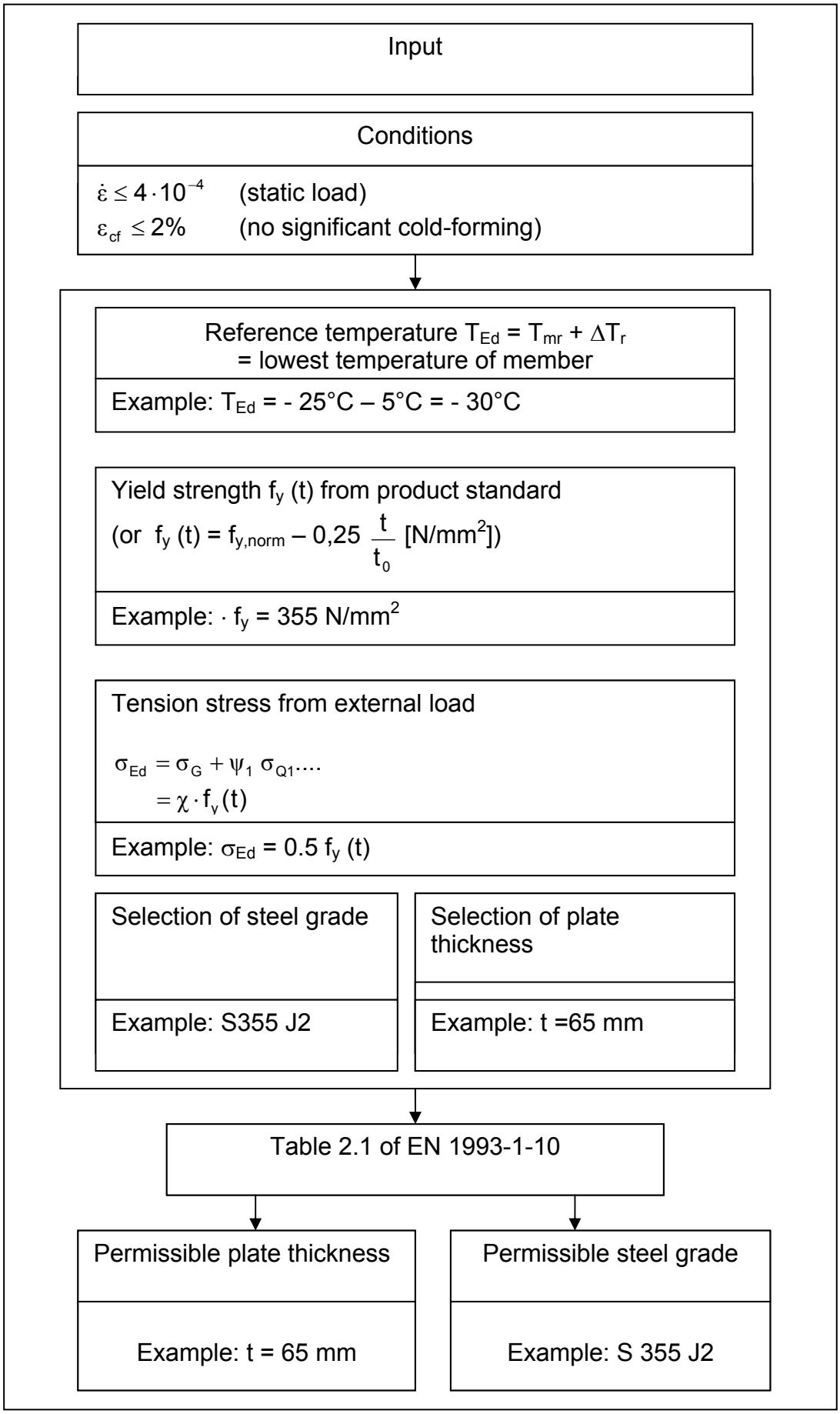


Fig. 2-59: Flow chart for using table 2.1 of EN 1993-1-10

(2) Where the conditions for $\dot{\varepsilon}$ and ε_{cf} for the use of table 2.1 of EN 1993-1-10 are not met, the reference temperature T_{Ed} should be adjusted by using the $\Delta T_{\dot{\varepsilon}}$- and $\Delta T_{\varepsilon,cf}$ -values that shift the requirements towards lower temperatures.

(3) For values T_{Ed} and σ_{Ed}, which are between the tabulated values, interpolations may be carried out.

(4) For central Europe (Germany) the values T_{Ed} may be used according to table 2-13.

No.	Member	Reference Temperature T_{Ed} [°C]
1	Steel bridges and Composite bridges	- 30° C
2	Buildings	
	Members exposed to external climate	- 30° C
	Members protected from external climate	0° C
3	Crane runways	
	Members exposed to external climate	- 30° C
	Members protected from external climate	0° C
4	Hydraulic structures	
	Members fully or almost fully emerged from water	- 30° C
	Members with one sided contact with water	- 15° C
	Members partially submerged in water	- 15° C
	Members fully submerged in water	- 5° C

Table 2-13: Reference temperatures for various applications in central Europe (Germany)

2.3.2 Examples for the use of table 2.1 of EN 1993-1-10

2.3.2.1 The use for steel bridges

(1) The development of table 2.1 of EN 1993-1-10 has been primarily oriented to the use for steel bridges with particular emphasis on fatigue.

(2) Particular choices of the material for bridges may be based on the following assumptions:

1. For road bridges the stresses from permanent and variable loads may be estimated as

$$\frac{\sigma(G_k)}{\sigma(Q_K)} \sim 1.0$$

The ULS-verification reads with the following assumptions:

γ_G = 1.35
γ_Q = 1.35
ψ_1 = 0.4
$\gamma_{M0} = \gamma_{M1}$ = 1.10

$$\sigma_{ult} = 1.35\ \sigma(G_k) + 1.35\ \sigma(Q_k) = \frac{f_y(t)}{1.10}$$

The tension stress is

$$\sigma_{Ed} = \sigma((G_K) + \psi_1 \cdot (Q_K))$$

$$= \frac{f_y(t)}{1.35 \cdot \frac{2}{1+0.4} \cdot 1.1} \approx \underline{0.50\ f_y(t)}$$

2. For railway bridges ψ_1 may be taken as 1.0, so that σ_{Ed} follows from

$$\sigma_{Ed} = \sigma(G_K) + \sigma(Q_K)$$

$$= \frac{f_y(t)}{1.35 \cdot 1.1} \approx 0.66\ f_y(t)$$

where γ_{M0} is taken as 1.0, it follows

$$\sigma_{Ed} = 0.75\ f_y(t)$$

(3) The allowable plate thicknesses for these stress levels are given in fig. 2-60 and fig. 2-61.

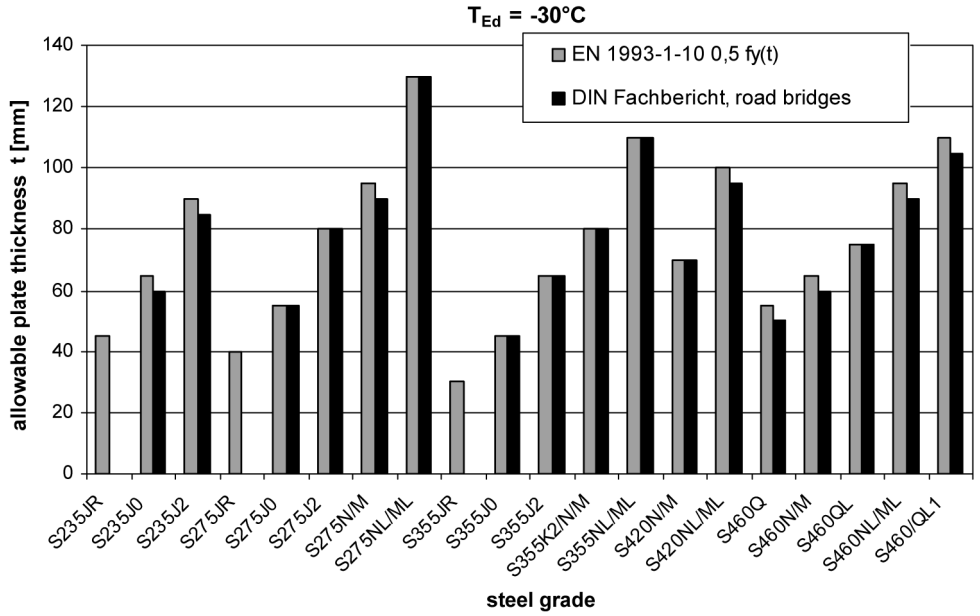


Fig. 2-60: Allowable plate thicknesses for road bridges

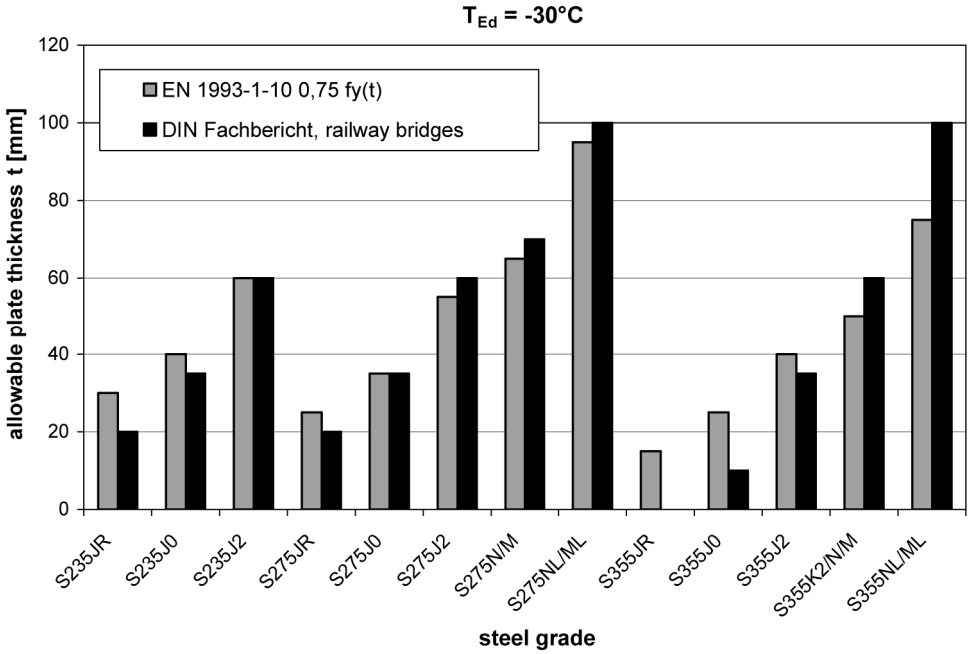


Fig. 2-61: Allowable plate thicknesses for railway bridges

2.3.2.2 Worked examples

2.3.2.2.1 Composite Bridge

(1) For a composite road bridge with the cross-section in fig. 2-62 the choice of material for the bottom flange of the steel girder is questioned.

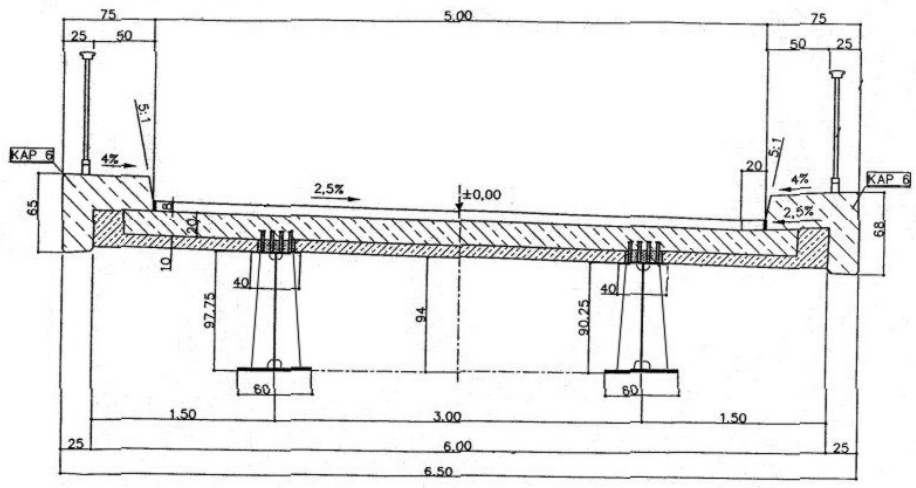


Fig. 2-62: Cross-section of composite bridge at mid-span (continuous over 2 spans; location Magdeburg-Germany)

(2) The dimensions of the steel girder are given in fig. 2-63

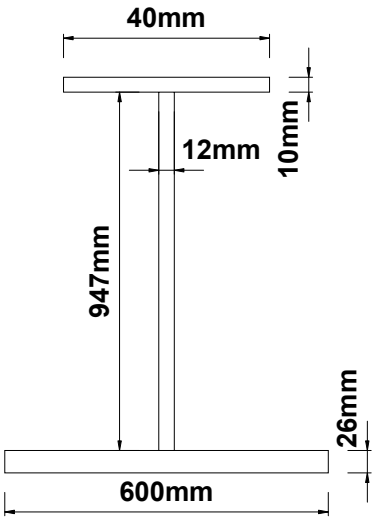


Fig. 2-63: Cross-section of the steel beam at mid-span; material S355

(3) The action effects are summarized in table 2-14.

No.	Load case	Reduction factor for concrete	M [kNm]	N [kN]	$\sigma_{steel,\ bottom\ flange}$ [kN/cm^2]
1	Self weight steel		130		1,024
2	Self weight prefabricated concrete slabs		384		3,024
3	Construction load		198		1,559
4	In situ concrete, t_0	n_0	780		4,333
5	In situ concrete, t_1 = 130 days	$n_{F,B1}$	772		4,568
6	In situ concrete, t_∞	$n_{F,B2}$	768		4,741
7	Construction load	n_0	213		1,183
8	Permanent finish, t_1 = 100 days	$n_{F,B1}$	720		3,600
9	Permanent finish, t_∞	$n_{F,B2}$	717		3,696
10	Creeping t_1 = 100 days	$n_{F,Bx1}$	- 55,4		- 0,274
11	Creeping $t_2 = \infty$	$n_{F,Bx2}$	- 81,1		- 0,410
12	Traffic load, max	n_0	2.230		10,773
13	Traffic load, min	n_0	- 690		- 3,333
14	Shrinkage t_1= 100 days	$n_{F,S1}$	84,2	639	-0,180
15	Shrinkage t_∞	$n_{F,S2}$	500	2989	-1,025
16	Settlement	n_0	80,9		0,391
17	Temperature ΔT_{top+}=10K	n_0	257		1,242
18	Temperature ΔT_{top-}= 7K	n_0	-180		-0,869
19	Wind, vertical	n_0	80,1		0,387
20	Braking load	n_0	96,3		0,465

Table 2-14: Load cases and stresses in bottom flange

(4) The reference temperature is determined in table 2-15

No	Effect	Value
1	Minimum air temperature T_{md}	- 25 °C
2	Radiation loss of member, ΔT_r	- 5 °K
3	ΔT_σ (detail: transverse stiffener welded to bottom flange covered by EN 1993-1-9)	0 °K
4	ΔT_R (National Annex)	0 °K
5	$\dot{\varepsilon} = 0.005\ s^{-1}$ (from project specification): $\Delta T\dot{\varepsilon}$	- 16 K*)
6	DCF = 0 (no cold-forming): ΔT_{DCF}	0 °K
7	T_{Ed}	- 46 °C

*) fy(t) = 355 – 0,25 · 26/1 = 349 N/mm²

$$\Delta T\dot{\varepsilon} = -\frac{1440-349}{550}\left(\ell n\,\frac{0.005}{0.0001}\right)^{1.5} = -15{,}3\,K \sim 16\,K$$

Table 2-15: Determination of reference temperature T_{Ed}

(5) The relevant stress σ_{Ed} is calculated with $\psi_1 = 0.7$ from the load combination: 1.0 {1 "+" 2 "+" 5 "+" 8 "+" 16} + 0.7 {12 "+" 17 "+" 19 "+" 20}:

σ_{Ed} = 1.0 { 1.024 + 3.024 + 4.568 + 3.6 + 0.391} +
0.7 { 10.773 + 1.242 + 0.387 + 0.465}
= 21.50 KN/cm² = 215 N/mm²

$$\sigma_{Ed} = \frac{215}{349}\cdot f_y(t) = \underline{0.62\, f_y(t)}$$

(6) The use of table 2.1 of EN 1993-1-10 gives the minimum toughness requirement T_{27J} = - 20C, or S355J2, see fig. 2-64, where

$$t_{permissable}\left(0{,}62\cdot f_y(t)\right) = 39\,mm > t_{available} = 26\,mm\,.$$

steel grade	sub grade	Charpy energy CVN at T °C	Charpy energy CVN $J_{min.}$	reference temperature T_{Ed} [°C] 10	0	-10	-20	-30	-40	-50	10	0	-10	-20	-30	-40	-50	10	0	-10	-20	-30	-40	-50
				σ_{Ed}=0,75 x $f_y(t)$							σ_{Ed}=0,50 x $f_y(t)$							σ_{Ed}=0,25 x $f_y(t)$						
S235	JR	20	27	60	50	40	35	30	25	20	90	75	65	55	45	40	35	135	115	100	85	75	65	60
	J0	0	27	90	75	60	50	40	35	30	125	105	90	75	65	55	45	175	155	135	115	100	85	75
	J2	-20	27	125	105	90	75	60	50	40	170	145	125	105	90	75	65	200	200	175	155	135	115	100
S275	JR	20	27	55	45	35	30	25	20	15	80	70	55	50	40	35	30	125	110	95	80	70	60	55
	J0	0	27	75	65	55	45	35	30	25	115	95	80	70	55	50	40	165	145	125	110	95	80	70
	J2	-20	27	110	95	75	65	55	45	35	155	130	115	95	80	70	55	200	190	165	145	125	110	95
	M, N	-20	40	135	110	95	75	65	55	45	180	155	130	115	95	80	70	200	200	190	165	145	125	110
	ML, NL	-50	27	185	160	135	110	95	75	65	200	200	180	155	130	115	95	230	200	200	200	190	165	145
S355	JR	20	27	40	35	25	20	15	15	0	65	55	45	40	30	25	25	110	95	80	70	60	55	45
	J0	0	27	60	50	40	35	25	20	15	95	80	65	55	45	40	30	150	130	110	95	80	70	60
	J2	-20	27	~~90~~	~~75~~	~~60~~	~~50~~	~~40~~	~~35~~	**25**	~~135~~	~~110~~	~~95~~	~~80~~	~~65~~	~~55~~	**45**	200	175	150	130	110	95	80
	K2, M, N	-20	40	110	90	75	60	50	40	35	155	135	110	95	80	65	55	200	200	175	150	130	110	95
	ML, NL	-50	27	155	130	110	90	75	60	50	200	180	155	135	110	95	80	210	200	200	200	175	150	130
S420	M, N	-20	40	95	80	65	55	45	35	30	140	120	100	85	70	60	50	200	185	160	140	120	100	85
	ML, NL	-50	27	135	115	95	80	65	55	45	190	165	140	120	100	85	70	200	200	200	185	160	140	120
S460	Q	-20	30	70	60	50	40	30	25	20	110	95	75	65	55	45	35	175	155	130	115	95	80	70
	M, N	-20	40	90	70	60	50	40	30	25	130	110	95	75	65	55	45	200	175	155	130	115	95	80
	QL	-40	30	105	90	70	60	50	40	30	155	130	110	95	75	65	55	200	200	175	155	130	115	95
	ML, NL	-50	27	125	105	90	70	60	50	40	180	155	130	110	95	75	65	200	200	200	175	155	130	115
	QL1	-60	30	150	125	105	90	70	60	50	200	180	155	130	110	95	75	215	200	200	200	175	155	130
S690	Q	0	40	40	30	25	20	0	0	0	65	55	45	35	30	20	20	120	100	85	75	60	50	45
	Q	-20	30	50	40	30	25	20	0	0	80	65	55	45	35	30	20	140	120	100	85	75	60	50
	QL	-20	40	60	50	40	30	25	20	0	95	80	65	55	45	35	30	165	140	120	100	85	75	60
	QL	-40	30	75	60	50	40	30	25	20	115	95	80	65	55	45	35	190	165	140	120	100	85	75
	QL1	-40	40	90	75	60	50	40	30	25	135	115	95	80	65	55	45	200	190	165	140	120	100	85
	QL1	-60	30	110	90	75	60	50	40	30	160	135	115	95	80	65	55	200	200	190	165	140	120	100

Fig. 2-64: Interpolation of steel grade from table 2-1 of EN 1993-1-10

2.3.2.2.2 Industrial building

(1) For a steel frame of a steel production plant, see fig. 2-65, the choice of material shall be made for the end plate of the beam at the bolted beam-column connection.

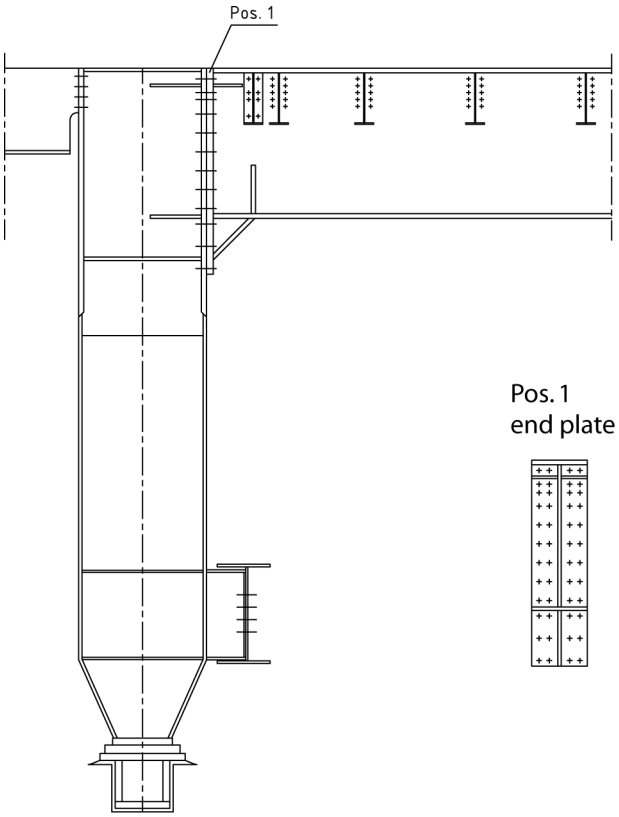


Fig. 2-65: End plate (pos. 1) of the bolted beam-column-connection of a steel frame made of S235, t = 80 mm

(2) The static analysis gives the following values for the ULS-verification:

a) Maximum stress in end plate: $\sigma_{Ed,ULS}$ = 18.2 kN/cm²
b) Permanent and variable loads with the same relevant load arrangement for calculating $\sigma_{Ed,ULS}$:

G_k = 8.6 kN/m²
Q_k = 20 kN/m²

c) $\gamma_G = \gamma_Q$ = 1.35
d) ψ_1 = 0.70

3) The relevant stress σ_{Ed} follows from

$$\sigma_{Ed} = \frac{1.0}{1.35}\,\sigma_G + \psi_1\,\frac{1.0}{1.35}\,\sigma_Q$$

(4) With

$$\frac{G_K}{G_K + Q_K} = \frac{8.6}{8.6 + 20} = 0.30$$

follows

$\sigma_G = 0.30\ \sigma_{Ed,ULS}$
$\sigma_Q = 0.70\ \sigma_{Ed,ULS}$

and

$\sigma_{Ed} = 0.74 \cdot 0.3\ \sigma_{Ed,ULS} + 0.7 \cdot 0.74 \cdot 0.7\ \sigma_{Ed,ULS}$
$= 0.58\ \sigma_{Ed,ULS}$
$= 0.58 \cdot 182 = 105.6\ N/mm^2$

(5) With

$$f_y(t) = 235 - 0.25\ \frac{80}{1.0} = 215\ N/mm^2$$

follows

$$\sigma_{Ed} = \frac{105.6}{215}\ f_y(t) = 0.49\ f_y(t)$$

(6) The reference temperature T_{Ed} is specified for the most severe action scenario with full service loading according to table 2-16:

$$t_{permissable}(-15°C) = 82{,}5\,mm \approx t_{available} = 80\,mm$$

No	Effect	Value
1	Minimum air temperature T_{md} (for the specific project)	- 10 °C
2	Radiation loss of member (as specified)	- 5 °K
3	ΔT_σ	0 °K
4	ΔT_R	0 °K
5	$\Delta T_{\dot{\varepsilon}}$	0 °K
6	ΔT_{DCF}	0 °K
7	T_{Ed}	- 15 °C

Table 2-16: Determination of reference temperature T_{Ed}

(7) The use of table 2.1 of EN 1993-1-10 gives the minimum toughness requirement T_{27J} = 0 °C or S235 J0, see fig. 2-66:

steel grade	sub grade	Charpy-V-values CVN at T °C	Charpy-V-values CVN $J_{min.}$	Reference temperature T_{Ed} [°C] 10	0	-10	-20	-30	-40	-50	10	0	-10	-20	-30	-40	-50	10	0	-10	-20	-30	-40	-50
				σ_{Ed}=0,75 x f_y(t)							σ_{Ed}=0,50 x f_y(t)							σ_{Ed}=0,25 x f_y(t)						
S235	JR	20	27	60	50	40	35	30	25	20	90	75	65	55	45	40	35	135	115	100	85	75	65	60
	J0	0	27	~~90~~	~~75~~	~~60~~	~~50~~	~~40~~	~~35~~	~~30~~	~~125~~	~~105~~	**90**	**75**	65	55	45	175	155	135	115	100	85	75
	J2	-20	27	125	105	90	75	60	50	40	170	145	125	105	90	75	65	200	200	175	155	135	115	100
S275	JR	20	27	55	45	35	30	25	20	15	80	70	55	50	40	35	30	125	110	95	80	70	60	55
	J0	0	27	75	65	55	45	35	30	25	115	95	80	70	55	50	40	165	145	125	110	95	80	70
	J2	-20	27	110	95	75	65	55	45	35	155	130	115	95	80	70	55	200	190	165	145	125	110	95
	M, N	-20	40	135	110	95	75	65	55	45	180	155	130	115	95	80	70	200	200	190	165	145	125	110
	ML, NL	-50	27	185	160	135	110	95	75	65	200	200	180	155	130	115	95	230	200	200	200	190	165	145
S355	JR	20	27	40	35	25	20	15	15	0	65	55	45	40	30	25	25	110	95	80	70	60	55	45
	J0	0	27	60	50	40	35	25	20	15	95	80	65	55	45	40	30	150	130	110	95	80	70	60
	J2	-20	27	90	75	60	50	40	35	25	135	110	95	80	65	55	45	200	175	150	130	110	95	80
	K2, M, N	-20	40	110	90	75	60	50	40	35	155	135	110	95	80	65	55	200	200	175	150	130	110	95
	ML, NL	-50	27	155	130	110	90	75	60	50	200	180	155	135	110	95	80	210	200	200	200	175	150	130
S420	M, N	-20	40	95	80	65	55	45	35	30	140	120	100	85	70	60	50	200	185	160	140	120	100	85
	ML, NL	-50	27	135	115	95	80	65	55	45	190	165	140	120	100	85	70	200	200	200	185	160	140	120
S460	Q	-20	30	70	60	50	40	30	25	20	110	95	75	65	55	45	35	175	155	130	115	95	80	70
	M, N	-20	40	90	70	60	50	40	30	25	130	110	95	75	65	55	45	200	175	155	130	115	95	80
	QL	-40	30	105	90	70	60	50	40	30	155	130	110	95	75	65	55	200	200	175	155	130	115	95
	ML, NL	-50	27	125	105	90	70	60	50	40	180	155	130	110	95	75	65	200	200	200	175	155	130	115
	QL1	-60	30	150	125	105	90	70	60	50	200	180	155	130	110	95	75	215	200	200	200	175	155	130
S690	Q	0	40	40	30	25	20	0	0	0	65	55	45	35	30	20	20	120	100	85	75	60	50	45
	Q	-20	30	50	40	30	25	20	0	0	80	65	55	45	35	30	20	140	120	100	85	75	60	50
	QL	-20	40	60	50	40	30	25	20	0	95	80	65	55	45	35	30	165	140	120	100	85	75	60
	QL	-40	30	75	60	50	40	30	25	20	115	95	80	65	55	45	35	190	165	140	120	100	85	75
	QL1	-40	40	90	75	60	50	40	30	25	135	115	95	80	65	55	45	200	190	165	140	120	100	85
	QL1	-60	30	110	90	75	60	50	40	30	160	135	115	95	80	65	55	200	200	190	165	140	120	100

Fig. 2-66: Interpolation of steel grade from table 2-1 of EN 1993-1-10

2.4 Specific cases for using fracture mechanics

2.4.1 General

(1) Section 2.4 of EN 1993-1-10 opens the door for using fracture mechanics methods for by-passing table 2-1 in section 2.3 by more refined assessments.

(2) Such more refined methods should be consistent with the way how table 2.1 of EN 1993-1-10 has been derived and hence be based on assumptions not contradictory to EN 1993-1-10.

(3) Fig. 2-67 summarizes the procedure for the determination of numerical values in table 2.1 of EN 1993-1-10 (left side of the chart).

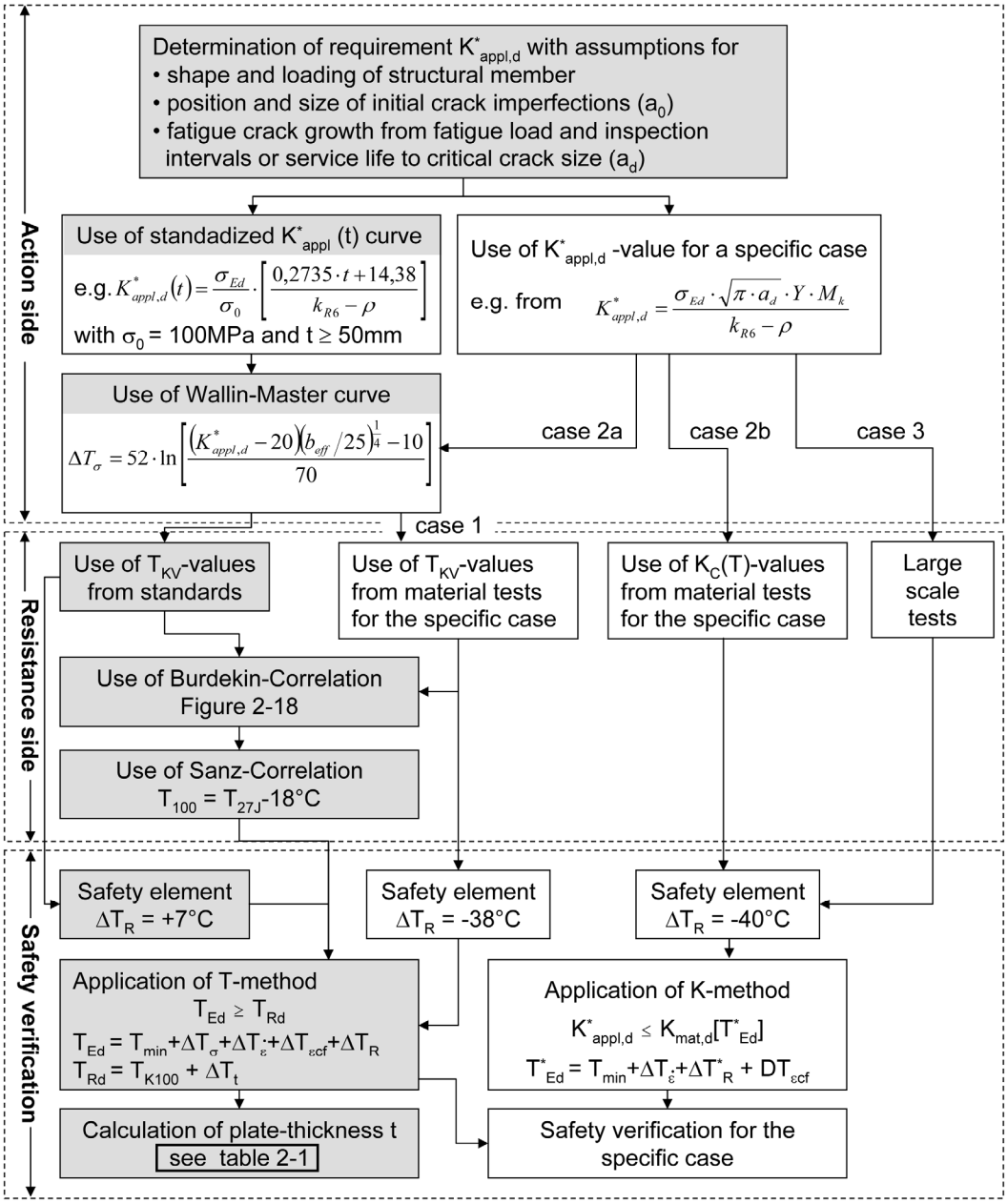


Fig. 2-67: Fracture mechanics procedure

(4) The possibilities for by-passing are expressed by the following cases (right side of the chart in fig. 2.67):

case 1: The conservative standardized $K^*_{appl,d}$-curve is used, however, T_{KV} values are not taken from the standards, but from material tests for the specific case.

case 2 a) The conservative standardized $K^*_{appl,d}$-curve is substituted by a more refined value $K^*_{appl,d}$ for the specific case of a design situation very close to the one used for developing table 2.1 of EN 1993-1-10, so that it can be assumed to be covered by the large scale tests described in section 2.2.6.3.2.

The assumptions for a_0/c_0 are as in table 2-1, however, crack growth is calculated with varying a/c-values.

Either T_{KV}-values from standards or from material tests can be used.

case 2 b) When a K-verification is used to eliminate uncertainties of the Wallin-Master-Curve and Sanz-correlation, the fracture mechanical resistance should be based on $K_c(T)$ values from small scale material tests for the specific case. The safety element ΔT_R = - 40 °C is based on the scatter of the K-T-transition curve experienced in general for steel material.

case 3: Where the design situation to be considered differs from the one assumed in the development of table 2.1 of EN 1993-1-10 and is not covered by the tests described in section 2.2.6.3.2, a combined calculative-experimental procedure should be used where calculations follow the procedure mentioned in case 2 and in addition large scale fracture tests are performed to be used to check the predictability of crack growth and fracture resistance by calculative means, see fig. 2-68.

In this case, the large scale test should follow a load temperature path that includes the safety elements to be adopted in the calculative design, see fig. 2-69.

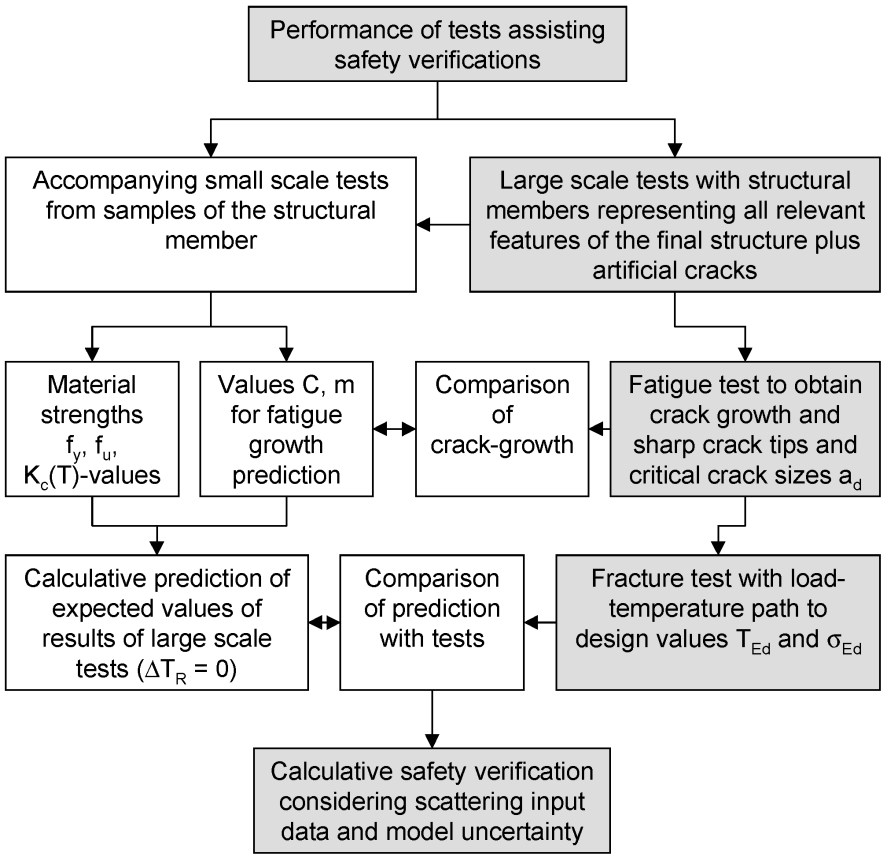


Fig. 2-68: Fracture mechanical safety evaluation assisted by large scale testing

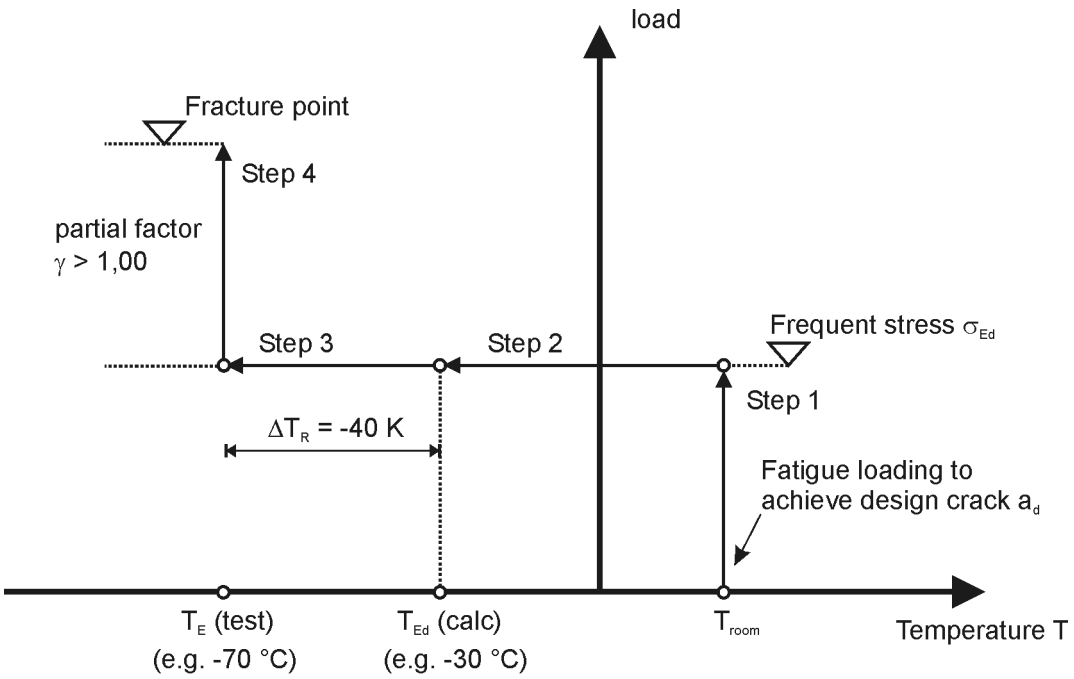


Fig. 2-69: Load temperature path for large scale fracture tests.

2.4.2 Example for the calculative determination of material quality

2.4.2.1 Design situation

(1) For a road bridge according to fig. 2-70 with a cross-section as given in fig. 2-71, a central arch has been provided with hangers made of solid steel bars connecting the bridge deck with the arch.

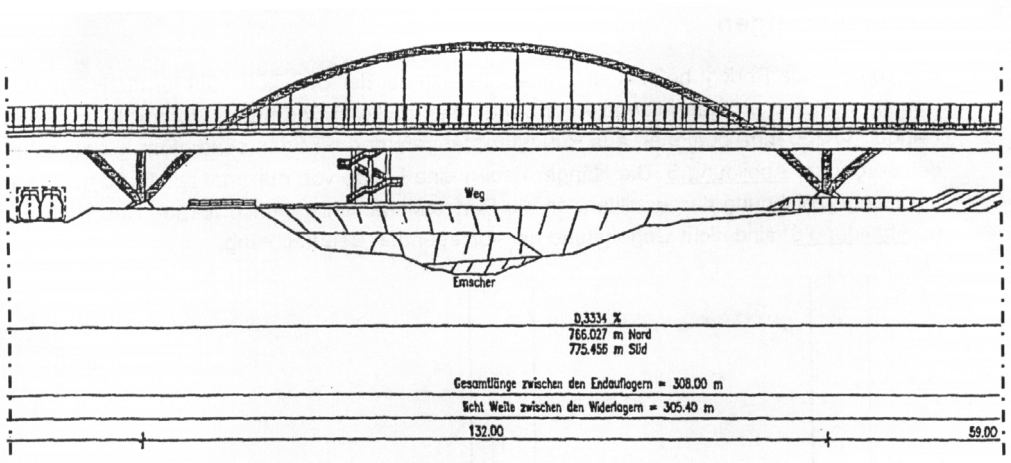


Fig. 2-70: Main bridge span with central arch

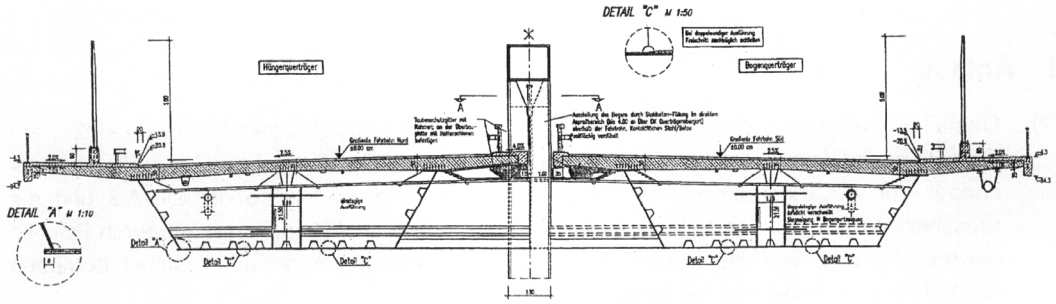


Fig. 2-71: Cross-section of the bridge with central arch

(2) The geometry of the hangers with a diameter of 220 mm and made of steel S420, is given in fig. 2-72. Because of the lengths of some hangers that exceeded the production length, welded splices were necessary, see fig. 2-73

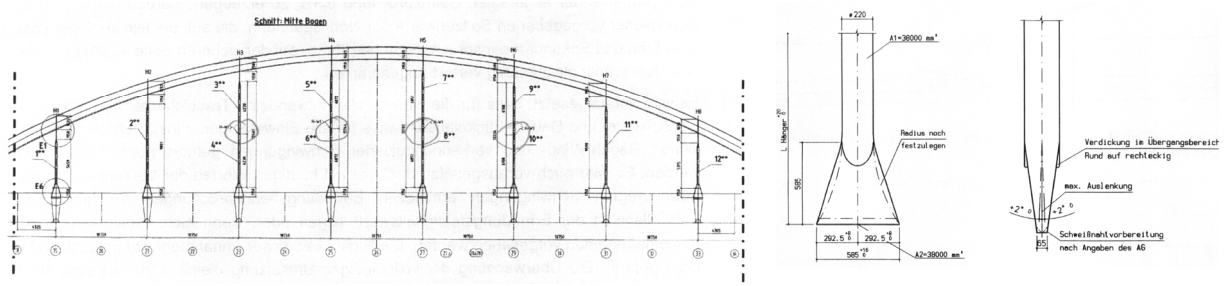


Fig. 2-72: Configuration of the hangers with position of welded splices and detailing of forged ends

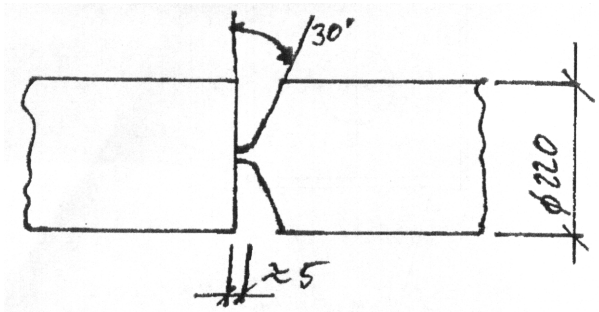


Fig. 2-73: Detail of welded splice

(3) The ends of the hangers were forged; details of the connections of the hanger ends to the arch and to the cross-beams of the deck may be taken from fig. 2-74 and fig. 2-75.

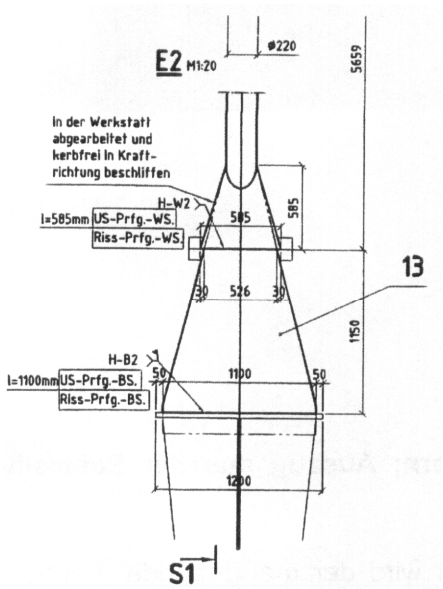


Fig. 2-74: Connection of hangers to the cross-beams of deck

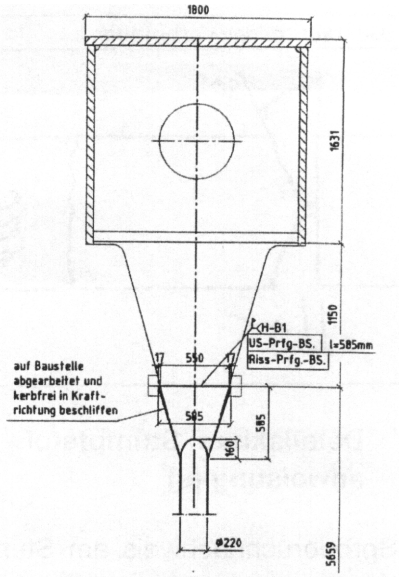
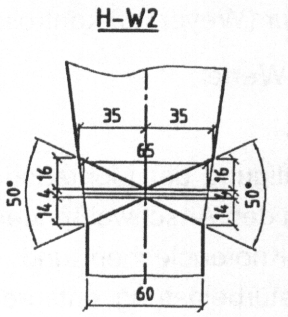
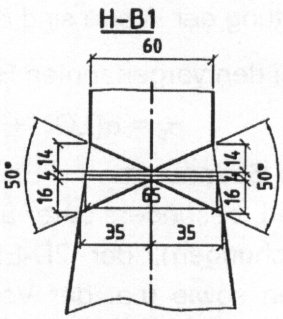


Fig. 2-75: Connection of hangers to the arch





(4) The purpose of the calculative assessment using section 2.4 of EN 1993-1-10 was to verify the choice of the material S420 for the hangers, which are not included in table 2.1 of EN 1993-1-10.

2.4.2.2 Critical cross-sections and choice of fracture mechanical models

(1) The critical cross-sections to be checked are:

1. at the welded splice in the middle of the hanger length
2. at the transition of the round section to the forged flat ends of the hangers
3. at the welded ends of the forged parts of hanger.

(2) The fracture mechanical models for the critical cross-section are the following:

a) at the welded splice, see fig. 2-76 a) with the assumption of a surface crack
b) at the welded splice, see fig. 2-76 b) with the assumption of a central crack
c) at the transition of the round section to the forged flat ends, see fig. 2-76 a) with the assumption of a surface crack
d) for the welded end connections, see fig. 2-76 c) with the assumption of a semi-elliptical surface crack

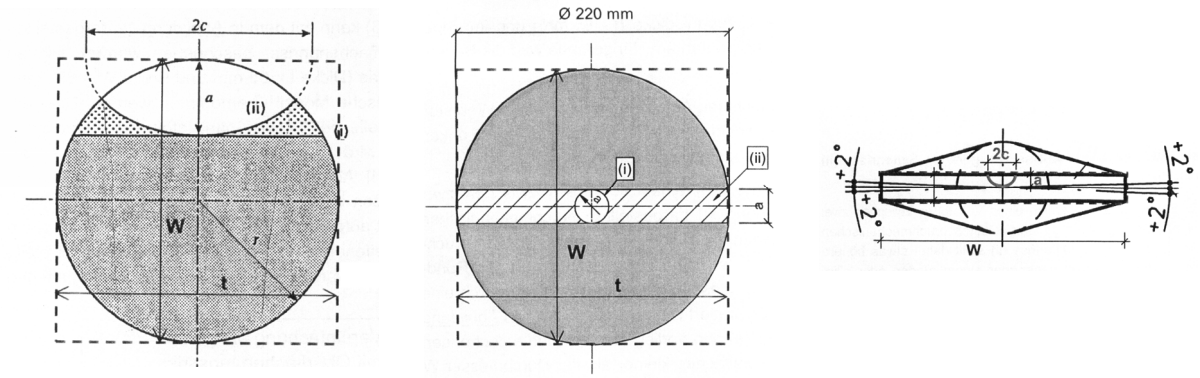


Fig. 2-76: Fracture mechanical models used for the choice of material

2.4.2.3 Determination of the fracture mechanical requirement $K^*_{appl,d}$ and ΔT_σ and safety verification

(1) The fracture mechanical requirements for the critical sections a), b), c) and d) are given in Table 2-17

	a) surface crack at hanger splice	b) central crack at hanger splice	c) surface crack at transition of round to forged section	d) surface crack at welded connection of hanger ends
Plate thickness t_{max}	220 mm	220 mm	220 mm	65 mm
yield strength f_{y0}	420 N/mm²	420 N/mm²	420 N/mm²	420 N/mm²
frequent stress σ_p	0,55 f_y (t)	0,55 f_y (t)	0,925 f_y (t)	0,73 f_y (t)
residual stress σ_s	100 Mpa	100 Mpa	100 Mpa	100 Mpa
initial crack depth a_0	6,00 mm	6,00 mm	6,00 mm	6,00 mm
inhomogeneity ΔT_{27J}	0 K	50 K (from tests)	0 K	0 K
$\Delta\sigma_p$	≤ 15 N/mm²	≤ 15 N/mm²	≤ 15 N/mm²	≤ 15 N/mm²
$\Delta K < \Delta K_{th}$	2,8 Mpa $\sqrt{m}$ < 5	2,5 Mpa $\sqrt{m}$ < 5	3,1 Mpa $\sqrt{m}$ < 5	4,2 Mpa $\sqrt{m}$ < 5
Crack growth Δa	0 mm	0 mm	0 mm	0 mm
Design crack depth a_d	6 mm	6 mm	6 mm	6 mm
a/w	0,027	0,055 (2a/w)	0,027	$\{ K_{appl,d}(\sigma = 100Mpa) = 22,3Mpa\sqrt{m}$
Y for crack (Murakami)	1,1211	1,0015	1,12111	
M_k for plate	1,0	1,00	1,00	
f_y (t)	320 N/mm²	320 N/mm²	320 N/mm²	320 N/mm²
σ_p	176 N/mm²	176 N/mm²	296 N/mm²	233,6 N/mm²
$\sigma_{Ed} = \sigma_p + \sigma_S$	276 N/mm²	276 N/mm²	396 N/mm²	344,0 N/mm²
$K_{appl,d}$ (a_i, σ_{Ed})	42 Mpa $\sqrt{m}$	37,96 Mpa $\sqrt{m}$	61 Mpa $\sqrt{m}$	74,5 Mpa $\sqrt{m}$
W	220 mm	220 mm	220 mm	526 mm
σ_{gy}	311,3 N/mm²	302,5 N/mm²	311,3 N/mm²	312,7 N/mm²
$L_r = \sigma_{Ed}/\sigma_{gy}$	0,89	0,91	1,27	1,07
K_{R6}	0,85	0,84	0,74	0,80
Residual stresses ψ	0,32	0,33	0,32	0,32
ρ_1	0,0437	0,0446	0,0437	0,0436
ρ	0,0286	0,0246	0,000	0,000
$K^*_{appl,d}$	51,89 Mpa $\sqrt{m}$	46,52 Mpa $\sqrt{m}$	81,99 Mpa $\sqrt{m}$	93,35 Mpa $\sqrt{m}$
b_{eff}	220 mm	440 mm	220 mm	30
ΔT_σ	+ 23,1 K	+ 23,8 K	- 16,8 K	+ 2,5 K

Table 2-17: Determination of $K^*_{appl,d}$ and ΔT_σ

(2) The verification is performed using the limit state equation:

$$T_{Ed} \geq T_{Rd}$$

where

$$T_{Ed} = T_{min} + \Delta T_r + \Delta T_\sigma + \Delta T_R + \left[\Delta T_{\dot{\varepsilon}} + \Delta T_{cf}\right]$$
$$T_{Rd} = \left(T_{27J} - 18\right) + \Delta T_t$$

(3) The input values are:

T_{min} = -25°C T_{27J} = -50°C (S420 NL)
ΔT_r = - 5° K ΔT_t see Table 2-17
ΔT_σ see Table 2-17
ΔT_R = +7 K

$\Delta T_{\dot{\varepsilon}}$ = 0 K

ΔT_{cf} = 0 K

(4) The verification is given in Table 2-18:

Critical section	a)	b)	c)	d)
T_{min}	-25	-25	-25	-25
ΔT_r	-5	-5	-5	-5
ΔT_σ	+23	+24	-17	+2
ΔT_R	+7	+7	+7	+7
T_{Ed}	0 °C	+1 °C	-40 °C	-21 °C
T_{27J}	-50 °C	-50 °C	-50 °C	-50 °C
ΔT_{27J}	0 K	+50 K	0 K	0 K
Sanz-Correlation	-18 K	-18 K	-18 K	-18 K
T_{Rd}	-68 °C	-18 °C	-68 °C	-68 °C

Table 2-18: Safety verification

(5) According to Table 2-18 the section relevant for the choice of material is section b) and the choice of S420 NL can be confirmed.

2.4.3 Example for the use of fracture mechanics calculations assisted by testing

2.4.3.1 Design situation for a unique verification

(1) For a building that had to be suspended to a bridge on top of two towers, see fig. 2-77, the choice of material for that bridge was subject to discussion. Details of the bridge structure are given in fig. 2-78.

Roof truss for the Sony Center, Berlin

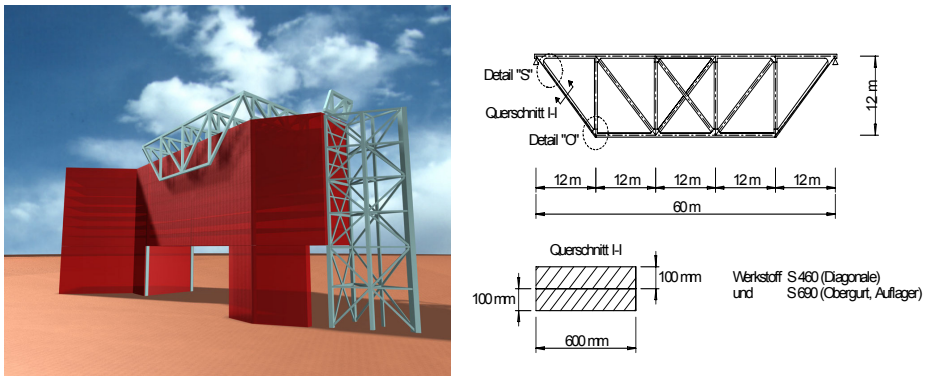


Fig. 2-77: Steel bridge on top of towers to bear suspended storeys of a building

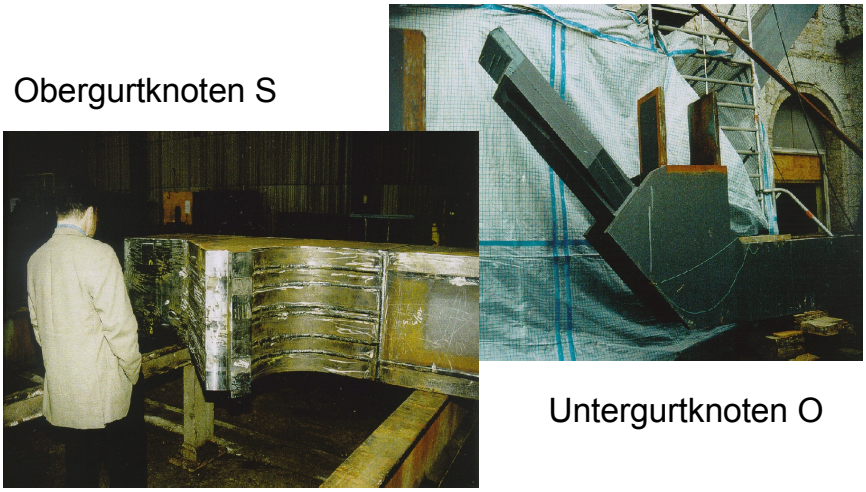


Fig. 2-78: Details of the bridge structure

(2) Materials were S460 and S690 with plate thicknesses up to 100 mm.

(3) The choice of material had to be justified by a unique verification that included the following tests:

1. Material tests for getting input values for the numerical assessment

2. Single large scale tests to confirm the results of the numerical assessment for two details.

(4) Whereas the number of material test was such that the scatter could be determined, the single large scale tests were only meant to serve for comparison with a numerical simulation of the behaviour of the test specimens in the context of prior knowledge. The amount of prior knowledge may be gauged by the extent to which the simulation is based, on direct previous experience, authoritative reference and reported results from comparable tests if available.

(5) It is not reasonable to rely on the results of a single test if there is very little applicable prior knowledge. In such cases, at least two results should be established so that it is easier to detect an anomalous result. In this example it was achieved by the safe-sided procedure of testing a symmetrical specimen and using the test results from one of the two possible failure positions that actually fails.

(6) If prediction from a simulation differs significantly from a single test result, even safe-sidedly, then the following steps should be taken:

1. Error bounds should be established for experimental accuracy and statistical reliability of the numerical simulation to assess whether the result is truly anomalous.

2. A search of additional prior knowledge should be undertaken to improve the simulation or reduce its unreliability.

3. If these steps do not resolve the difference, at least one further test should be performed.

(7) Below items of the example that are of general concern are addressed:

1. Design and fabrication of large scale specimens
2. Introduction of artificial flaws
3. Execution of tests
4. Safety evaluation

2.4.3.2 Design and fabrication of large scale test specimens

(1) Test specimens should include all features of the member as built that are relevant for the brittle fracture at low temperature.

(2) Fig. 2-79 gives above the actual details with the “critical spots” for the initiation of brittle fracture (upper line) and the design of the test specimens which are symmetrical and reduced in scale such that fracture may be achieved in the testing machine at lower level (lower line).

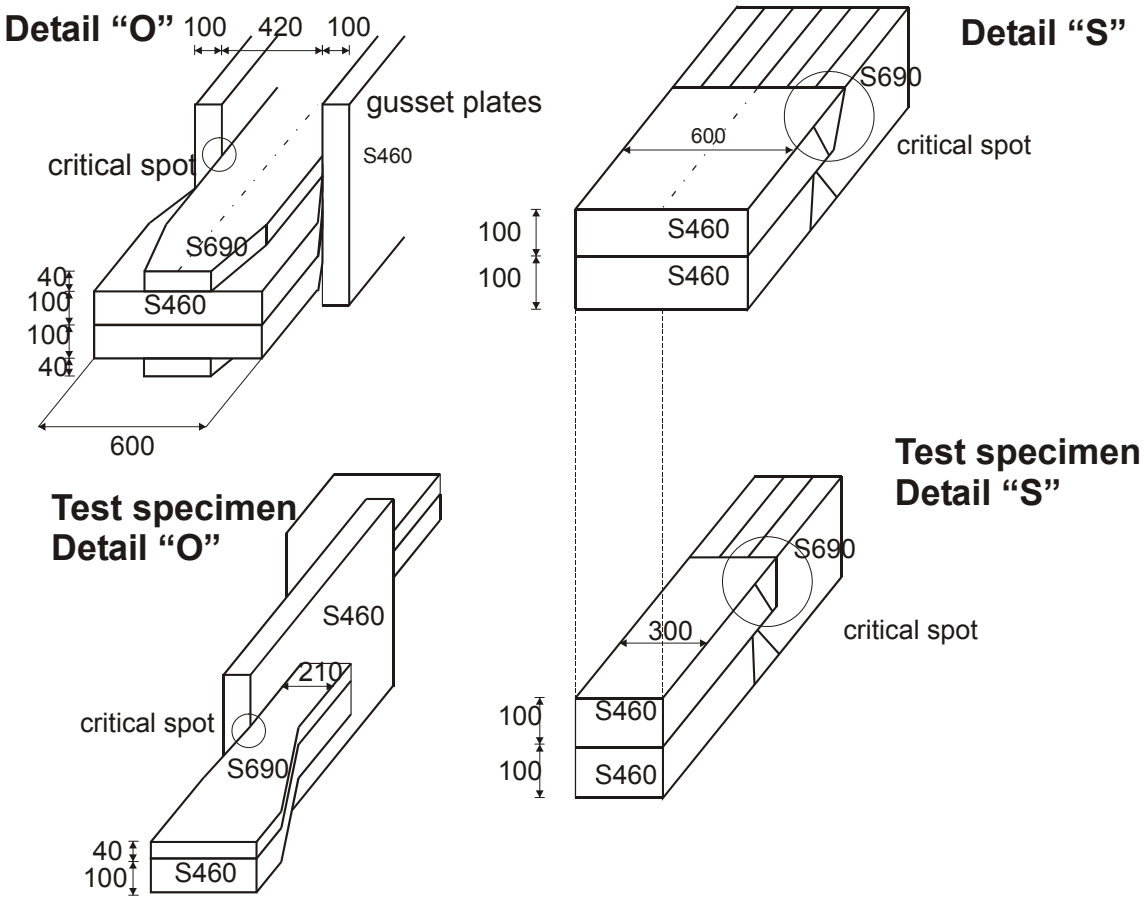


Fig. 2-79: Examples for structural details as built (above) and design of test specimens (below)

(3) The test specimens should be produced in the same way as the structural parts built in using the same material and fabrication and welding techniques as well as NDT-techniques for quality control.

(4) The equivalence of the stress-situation for the test specimen and the structural member built in should be proved by a comparison of SCF-factors or K-factors

at the critical locations where cracks have the most severe effects. Fig. 2-80 gives a comparison of numerical values.

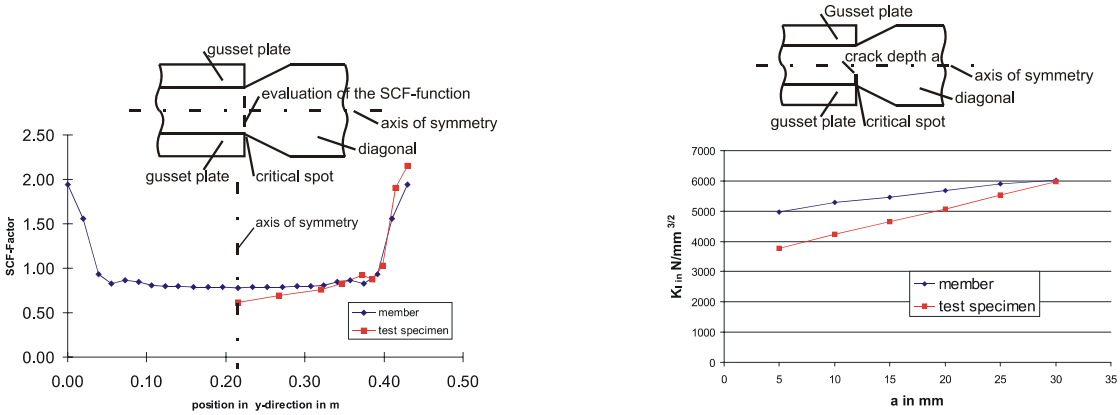


Fig. 2-80: Comparison of SCF-functions and K-values to check the stress-equivalence of the structural detail as built and the test specimen (below)

2.4.3.3 Introduction of flaws

(1) Flaws should be introduced either during fabrication (e.g. by including ceramic blades (e.g. 5 mm x 0.3 mm) in the welds) or after fabrication (e.g. by saw or electric erosion). The introduced flaw shall be subjected to sufficient cyclic loading to generate initial growth of the crack. This should be carried out at room temperature.

(2) If the member is subject to fatigue, the test specimen should be subjected to suitable fatigue loading, also at room temperature. If the member is subject to predominantly static loads an additional fatigue loading is not necessary.

(3) Flaws should achieve at least the size of the design values (see fig. 2-53 and fig. 2-54). They may be larger to reduce the fracture load for the testing machine.

(4) Samples should be taken from the test specimens that permit the determination of all material data necessary for the numerical simulations.

2.4.3.4 Execution of tests

(1) Each test specimen should be loaded with the actions from fig. 2-69 in the following order:

1. The nominal load from permanent load (G_k) should be applied at a temperature representative for the erection phase (e.g. room temperature). This loading may effect a possible favourable redistribution of residual stresses before the action of low temperature is applied.
2. The temperature is reduced to T_{Ed} and then the additional nominal stresses from variable loads $(\psi_1 \cdot Q_k)$ are applied to reach the design situation the structure must (be able to) sustain.

3. After this, the temperature is further reduced by T_{test} to investigate the influence of the scatter of the toughness properties in the temperature transition range. A scatter of 40°C may be assumed.
4. In the last phase, the loading is increased until fracture is reached.

2.4.3.5 Numerical simulations

(1) In parallel to the large scale test numerical calculations should be performed to check the yielding resistance and the brittle fracture resistance of the test specimen using the material data determined from the large scale test specimens.

(2) The calculations aim at mean values and may be performed with the K-method or the T-method. In order to obtain expected values, the safety element ΔT_R in the T-method should be taken as $\Delta T_R = 0°C$.

(3) By comparing the test results with the numerical model, the simulation model should be checked and subsequently improved if necessary. The following should be checked:

(i) whether yielding occurs before brittle fracture, because if not, residual stress effects may require reconsideration.
(ii) that brittle fracture starts where expected.
(iii) that the resistance as tested corresponds to the resistance as calculated, subject to an estimated allowance for experimental and statistical errors.

2.4.3.6 Safety evaluation

(1) If the simulation is close to that experienced in the test, the numerical model may be used for the safety evaluation.

(2) If the K-method is used, the $K_{Mat,d}(T_{Ed})$ value may be determined by using prior knowledge from former material tests from comparable material together with the specific material tests from the test specimen at a temperature ($T_{Ed} - \Delta T$).

(3) If the T-method is used, the T_{27J}-value may be determined for the temperature T_{Ed} and the safety requirement be met by using the safety element ΔT_R =
- 38°C for measured T_{27J}-values.

2.4.4 Some other typical examples

(1) Some other typical examples for the use of section 2.4 of EN 1993-1-10 are given in the following:

1. Plate thickness of the top flange and bottom flange of a composite bridge, see fig. 2-81 and fig. 2-82.

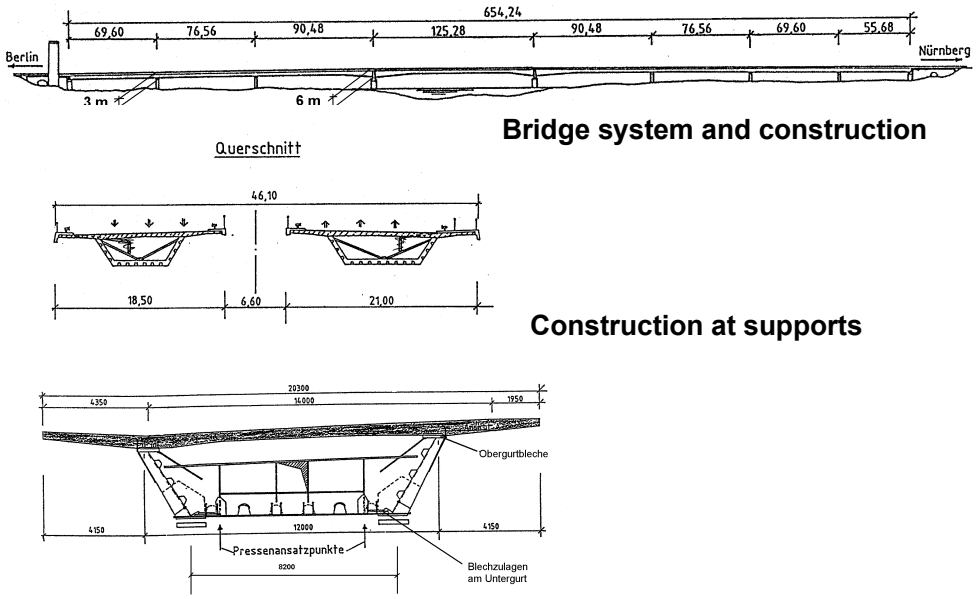


Fig. 2-81: Composite road bridge-cross-sections.

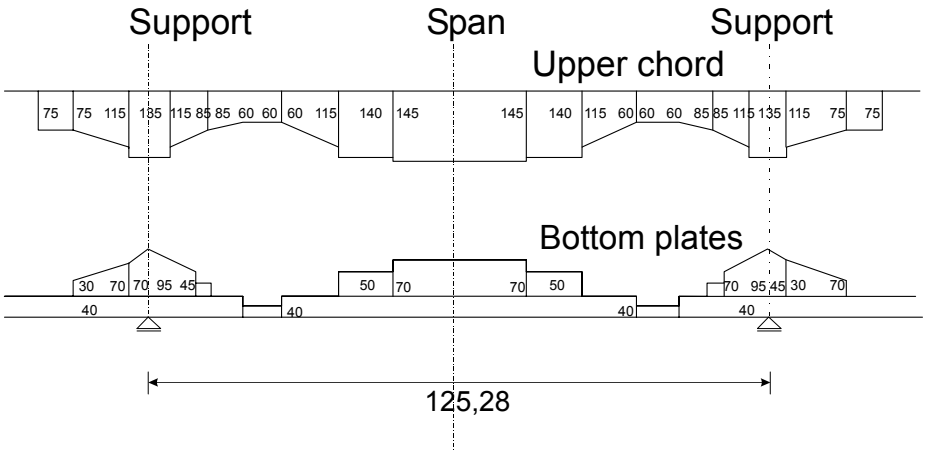


Fig. 2-82: Composite road bridge distribution of plate thickness for the upper chords and the bottom plates

2. Plate thickness of 100 mm of the horizontal girder of the ∇-pylon of a road bridge over the river Rhine, see fig. 2-83. The horizontal girder is a tension element that links the stayed cables supporting the bridge deck.

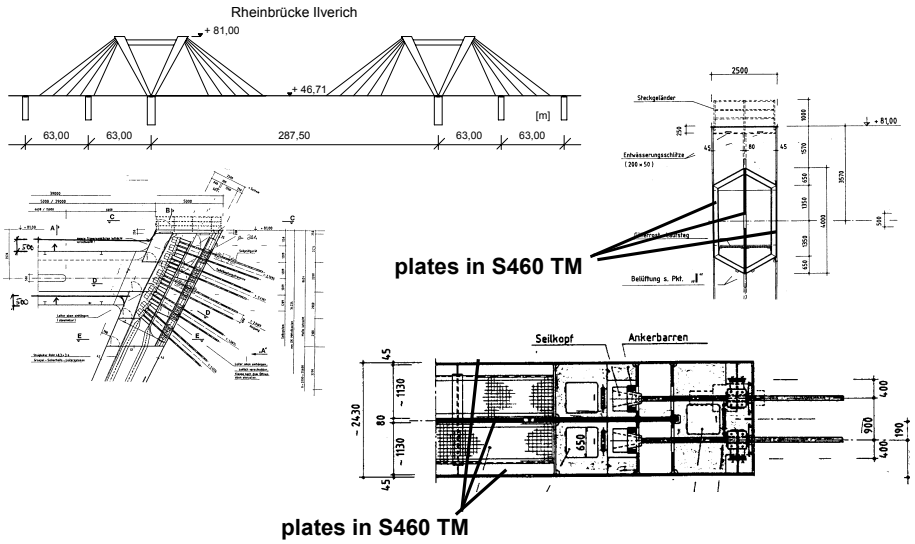


Fig. 2-83: Horizontal tension element of a ∇-pylon

3. Castor container for transporting nuclear waste. The relevant load case results from an accidental situation during transport, for which the material toughness of the thick shell had to be determined, see fig. 2-84.

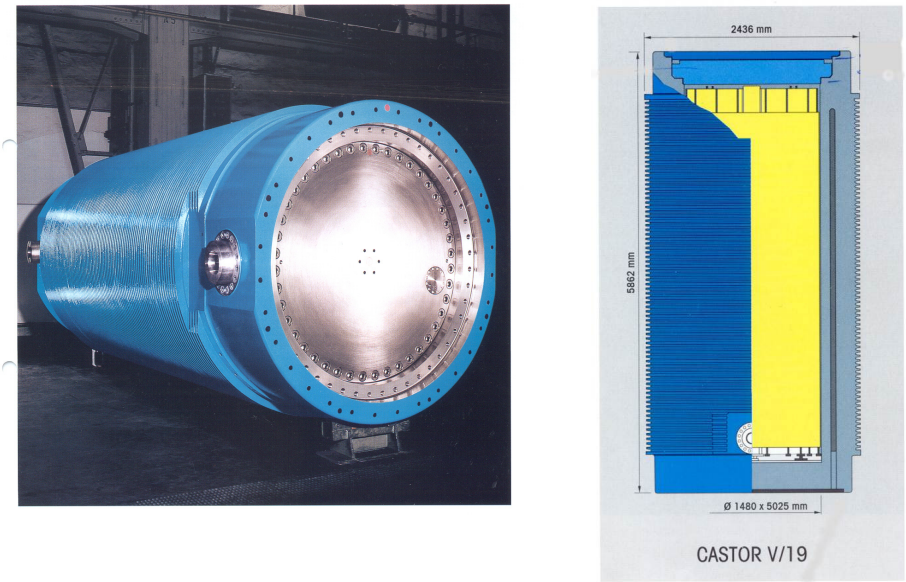
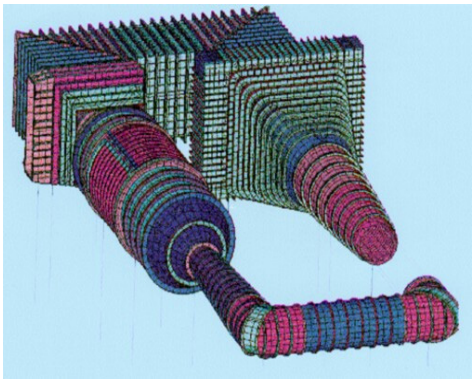


Fig. 2-84: Castor container

4. Wind tunnel for aerodynamic design. The wind tunnel is a container that is operated with low testing temperatures and air pressure, see fig. 2-85.



- Dimensions 65 x 30 m
- Volumen 5750 m^3
- Air pressure
  -110 kN/m^2 , + 95 kN/m^2
- Test temperature -40°C
- Max. plate thickness 50 mm
- Choice of material P275NL2

Fig. 2-85: Wind tunnel with technical specifications.

5. Composite bridge with a triangle cross-section and single bottom chords made of steel tubes welded to cast steel nodes, see fig. 2-86, fig. 2-87 and fig. 2-88.

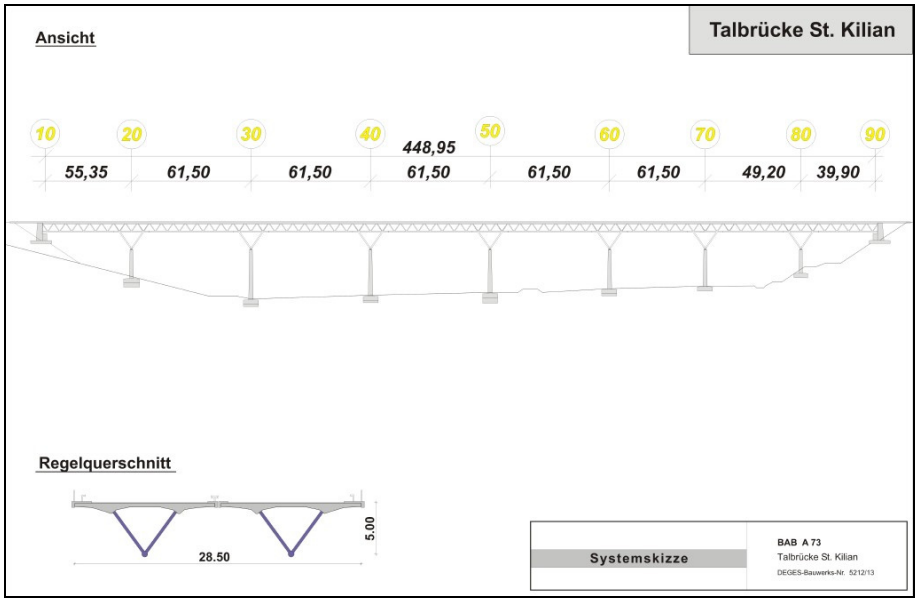
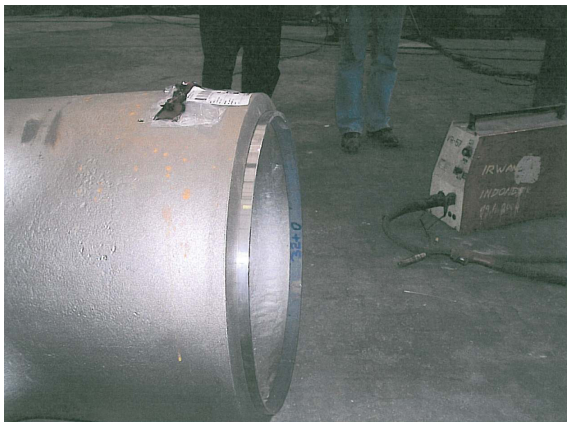


Fig. 2-86: View of the composite bridge with a cross-section made of two separate triangle girders.





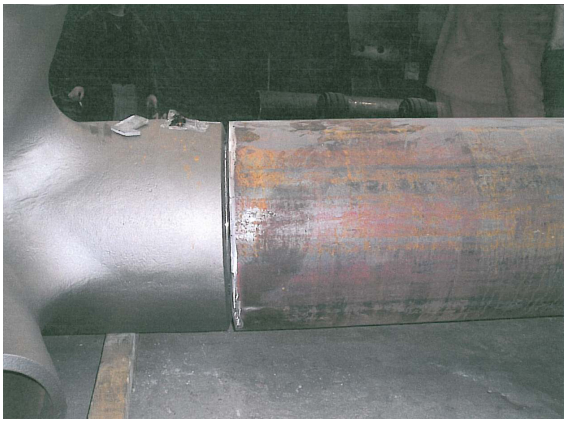


Fig. 2-87: Details of the welded connection between steel tubes and cast steel node.

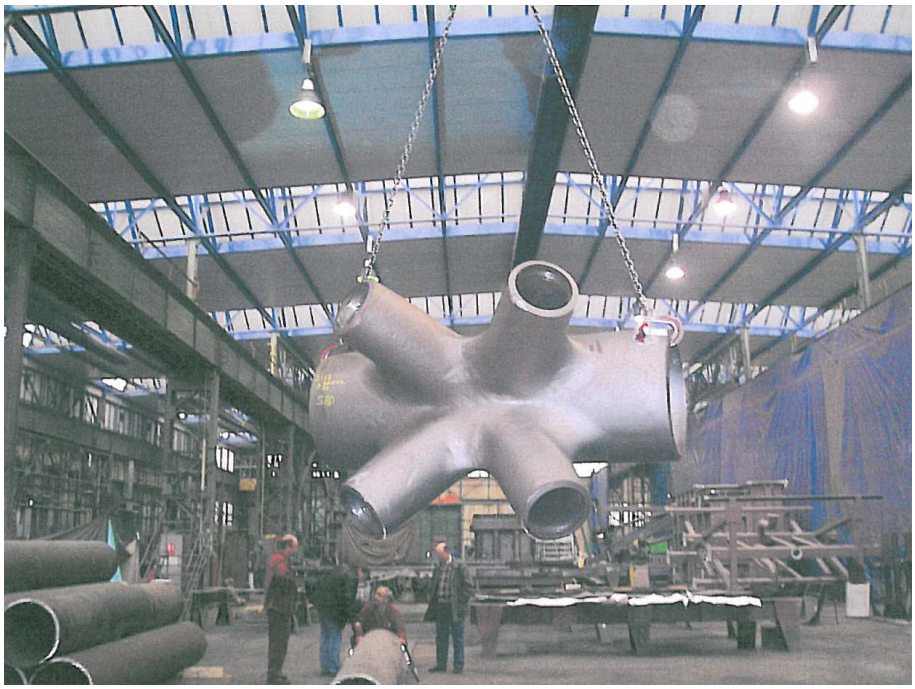


Fig. 2-88: Cast steel node in factory

2.5 Bibliography

[1] Liessem, A., Bruchmechanische Sicherheitsanalysen von Stahlbauten aus hochfesten niedriglegierten Stählen, Bericht aus dem Institut für Eisenhüttenkunde der RWTH Aachen, Shaker Verlag, Band 3/96, 1996

[2] Sedlacek G., Dahl W., Stötzel G., Liessem A., Improvement of the methods given in Eurocode 3, Annex C, for the choice of material to avoid brittle fracture, IIW-Doc. X-1274-93, 1993

[3] Wallin K., Methodology for Selecting Charpy Toughness Criteria for Thin High Strength Steels, Part 1, 2 and 3, Jernkontorets Forskning, Nr. 4013/89, VTT Manufacturing Technology, VTT Espoo, 1994

[4] Stranghöner N., Sedlacek, G., Stötzel G., Langenberg P, Dahl W., Sprödbruch-Konzept-Teilsicherheitsbeiwerte im Eurocode 3 statistisch ermitteln, Materialprüfung 39, 1997, S. 339-343

[5] Stranghöner N., Sedlacek G., Stötzel, G., Dahl W., Langenberg P., The New Eurocode 3 - Part 2 – Annex C, Approach for the Choice of Steel material to Avoid Brittle Fracture, Proc. of the Seventh (1997) International Offshore and Polar Engineering Conference, Honolulu, USA, 1997, S. 551-556

[6] Stahlgütewahl nach Betriebsfestigkeitskatalogen, DFG-Forschungsvorhaben, 1994-1997, Gemeinschaftsvorhaben des Lehrstuhls für Stahlbau mit dem Institut für Eisenhüttenkunde der RWTH Aachen und dem Lehrstuhl für Stahlbau der TU Dresden

[7] AIF Forschungsvorhaben 9044, Bruchmechanische Sicherheitsanalyse im Stahlbau, 1994

[8] EC3 Design of steel structures, Part 2 Steel Bridges, Annex C Design against brittle fracture

[9] Harrison, R.P., K. Loosemore and I. Milne, Assessment of the integrity of structures containing defects, CEGB-Report R/H/R6, Revision 3, 1986

[10] Marandet, B. und G., Sanz, Étude par la mécanique de la rupture de la ténacité d'aciers à resistance moyenne fournis en forte épaisseur, Revue de Métallurgie, S. 359-383, april 1976

[11] Liessem A., Dahl W., Effect of toughness on the failure of high and very high strength structural steels in the elasto-plastic and fully plastic range on the basis of large scale tests, EUUR 13954, European Commission Technical Steel Research

[12] Liessem A., Nießen T., Dahl W., Investigation of the effect of toughness and crack geometry on the crack propagation behaviour by tensile tests on large specimens of structural steels on different strength levels, EUR 16627, European Commission, Technical Steel Research

[13] Kalinowski B., Bruchmechanische Sicherheitsanalyse an Bauteilen mit aufgeschweißten Versteifungen, Dissertation RWTH Aachen, 1998

[14] Guerney, T.R., Fatigue of welded structures, Cambridge University press, Cambridge 2nd ed. 1978

[15] Newman, J.C. and Raju, I.S., An empirical stress intensity equation for the surface crack, Eng. Frac, Mech. 15, 1981, S. 185-192

[16] Hobbacher, Stress Intensity Factors of Welded Joints, Engineering Fracture Mechanics, Vol. 46, No. 2, pp. 173-182, 1993, and Vol. 49, No. 2, p323, 1994

[17] Zettelmoyer, N,. Fischer J.W., Stress Gradient Correction Factor for Stress Intensity of welded Stiffeners and Cover Plates, Welding Research Supplement

[19] Langenberg P, Dahl W., Sedlacek G., Stötzel G., Stranghöner N., RWTH Aachen, ANNEX C Material choice for the avoidance of brittle fracture in EUROCODE 3, Mis-Matching of Welds 96, Reinstorf-Lüneburg, April 1996

[20] J. Falk, Untersuchungen zum Einfluß der Belastungsgeschwindigkeit auf das Verformungs- und Bruchverhalten an Stählen unterschiedlicher Festigkeit und Zähigkeit, Fortschrittsberichte VDI, Reihe 18, Nr. 117, 1993

[21] Murakami, Y., Stress Intensity Factors Handbook, Pergamon Press, Frankfurt, 1987

[22] Beltrami, Chr., Numerische Analyse der lokalen Beanspruchung in Bauteilen mit Rissen und Quantifizierung der Zähigkeitsanforderungen, Bericht aus dem Institut für Eisenhüttenkunde, RWTH Aachen, Shaker Verlag, Band 5/95, 1995

[23] Colbach, Henri, diploma thesis, Institute of steel construction, RWTH Aachen, 1994, Untersuchung typischer geschweißter Konstruktionsdetails hinsichtlich ihrer Zähigkeitsanforderungen bei Vorhandensein von Oberflächenrissen

[25] DS 804, Vorschriften für Eisenbahnbrücken und sonstige Ingenieurbauwerke (VEI), Deutsche Bundesbahn, 1.1.1983, Bundesbahn Zentralamt München

[26] BS 5400 (October 1996), Draft, Design of Steel Highway Bridges, British Standard

[27] NFA 26-010 (May 1980), Choix des qualités d'aciers pour construction métalique ou chaudronée vis-a-vis au risque de rupture fragile, Association Francaise de Normalisation (AFNOR)

[28] DASt-Richtlinie 009, Empfehlung zur Wahl der Stahlsorte für geschweißte Bauteile (4/73), Deutscher Ausschuß für Stahlbau

[29] Kühn B., Sedlacek G., Höhler S., Bericht zum Stand und zur weiteren Bearbeitung der DASt-Richtlinie 009 „Empfehlungen zur Wahl der Stahlgütegruppe für geschweißte Stahlbauten", Fortlaufender Bericht Stand 11/00, Lehrstuhl für Stahlbau, RWTH Aachen

[30] Heuser, A., Abu-Zeid, O.A., Dahl, W., Änderung des Festigkeits- und Zähigkeitsverhaltens von Baustählen durch Kaltverformung, Sonderdruck aus

„Stahl und Eisen“ 107 (1987), Heft 20, Seite 952-956, Verlag Stahleisen mbH, Düsseldorf

[31] Verein Deutscher Eisenhüttenleute, STEEL- A Handbook for Materials Research and Engineering, Volume 1: Fundamentals, Springer Verlag Berlin, Verlag Stahleisen mbH, Düsseldorf

[32] Degenkolbe, J., Müsgen, B., Arch. Eisenhüttenwes. 44 (1973), Nr. 10, S. 769/74

[33] Burdekin, F.M., Lucha, P., Hadley, I., Ogle, M.H., Notch Toughness of Steel for Bridges, Final Report (DPU 9/3/38) for Highways Agency, UMIST, TWI, 1997

[34] Kühn, B., Beitrag zur Vereinheitlichung der europäischen Regelungen zur Vermeidung von Sprödbruch, Dissertation am Lehrstuhl für Stahlbau, RWTH Aachen, Shaker-Verlag, ISBN 3-8322-3901-4.

[35] Sedlacek, G., Müller, Ch., Background document on the safety and recommended γ_{Mf} factores in prEN 1993-1-9, 1st Draft, Lehrstuhl für Stahlbau, RWTH Aachen, May 2001

[36] Sedlacek, G., Stranghöner, N., Stötzel, G., Dahl, W., Langenberg, P., Wallin, K., Brozzetti, J., Nussbaumer, A., Blauel, J.G., Burdekin, F.M., Background documentation to Eurocode 3 – Design of Steel Structures – Part 2 – Bridges – for Chapter 34 – Materials – Choice of steel material to avoid brittle fracture, Document No.: II.3.1, Draft, Aachen, May 1997

[37] Verein Deutscher Eisenhüttenleute, STEEL, A Handbook for Materials Research and Engineering, Volume 2:Applications, Springer Verlag Berlin, Verlag Stahleisen mbH, Düsseldorf

[38] Halbritter, J., Mokosch, M., Beurteilung der Schweißeignung in kaltgeformten Bereichen hochfester Feinkornbaustähle, Schweissen & Schneiden, 51 (1999), Heft 6, Verlag für Schweißen und verwandte Verfahren, DVS-Verlag GmbH, Düsseldorf

[39] Hadley, I., Investigation of the Notch Toughness of Steel for Bridges, First Progress Report (220570/1/95) for Highways Agency, TWI, March 1995

[40] Hadley, I., Ogle, M.H., Burdekin, F.M., Luccha, O., Investigation of the Notch Toughness of Steel Bridges, for Highways Agency, TWI and UMIST
Progress Report No. 2 (220570/2/95) June 1995
Progress Report No. 3 (220570/3/95), October 1995
Progress Report No. 4 (220570/4/96), January 1996
Progress Report No. 5 (220570/5/96), May 1996
Progress Report No. 6 (Report on Full-Scale Testing), (220570/6/97), June 1997
Progress Report No. 7 (220570/7/97), June 1997

[41] Stranghöner, N., Werkstoffwahl im Stahlbrücken, DASt (Deutscher Ausschuß für Stahlbau), Forschungsbericht 4/2006, Stahlbau Verlags- und Service GmbH, Düsseldorf, 2006

[42] Stranghöner, N., Sedlacek, G., Stötzel, G., Dahl, W., Langenberg, P., Background Documentation to Eurocode 3, Design of Steel Structures, Part 2, bridges, for Chapter 3 – Materials, Choice of Steel Material to Avoid Brittle Fracture, Document No.: II.3.1, Draft, Aachen, May 1997

[43] Marandat, B., Sanz, G.: “Étude par la mécanique de la rupture de la ténacité d’aciers à résistance moyenne fournis en forte épaisseur”, Revue de Métallurgie, pp. 359-383, April 1976

[44] Sanz, G.: “Essai de mise au point d’une méthode quantitive de choix des qualités d’aciers vis-à-vis du risque de rupture fragile”, Revue de Métallurgie, CIT, pp. 621-642, July 1980

[45] Mangerig, I.: Minimale Oberflächentemperaturen von Stahlbrücken”, unveröffentlichtes Dokument.

[46] Silcher, H.: “Untersuchung der Einflussfaktoren auf das bruchmechanische Verhalten von Proben mit symmetrischen Fehlergeometrien”, Technisch-wissenschaftlicher Bericht, MPA Darmstadt, 91-03, 1991

Section 3

3 Selection of materials for through-thickness properties

3.1 General

(1) Section 3 of EN 1993-1-10 gives rules for the choice of Z-qualities of steels subject to requirements for deformation properties perpendicular to the surface of the steel product.

(2) Such requirements arise from welding, when shrinkage of welds is restrained locally or globally in through thickness direction, and needs compensation by local plastic through thickness strains.

(3) Damages from such excessive strains are known as lamellar tearing, see fig. 3-1.

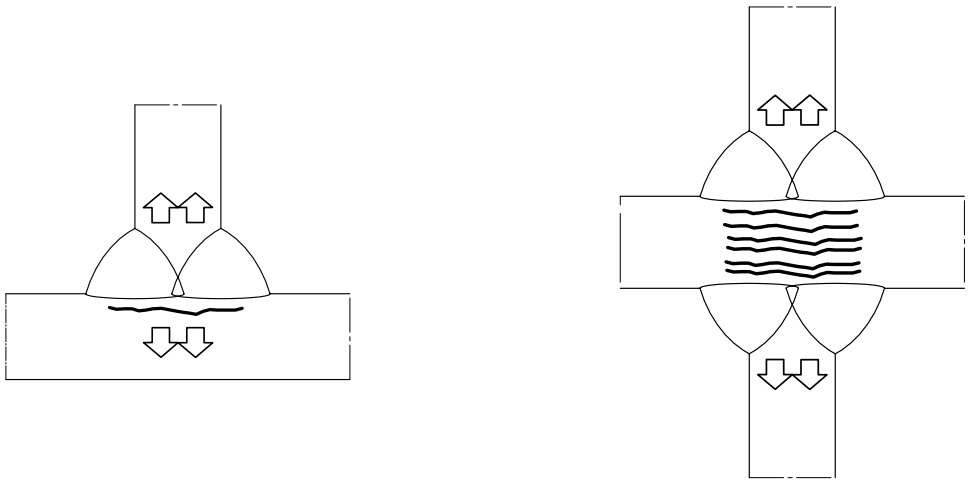


Fig. 3-1: Lamellar tearing

(4) They occur almost exclusively during fabrication, where the microstructure of steels with a certain sulphur content is segregated by tension stresses normal to the plane of the laminations, see fig. 3-2, 3-3 and 3-4 and delaminations are linked via shear steps.

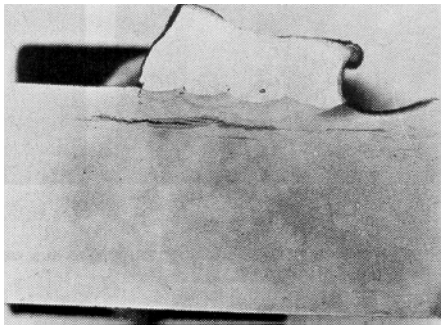


Fig. 3.2: Damage case a plate (30 mm) Made of St 52-3

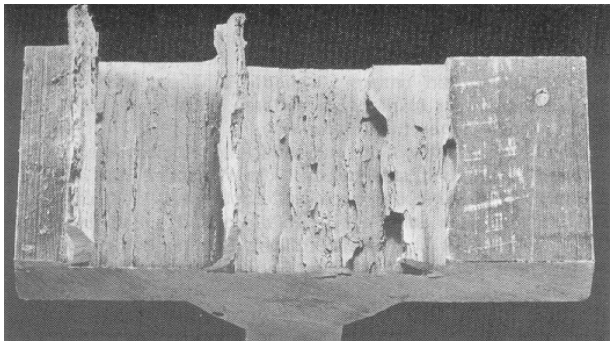


Fig. 3-3: Damage case of a plate (28 mm) of a cruciform joint made of R St37-2

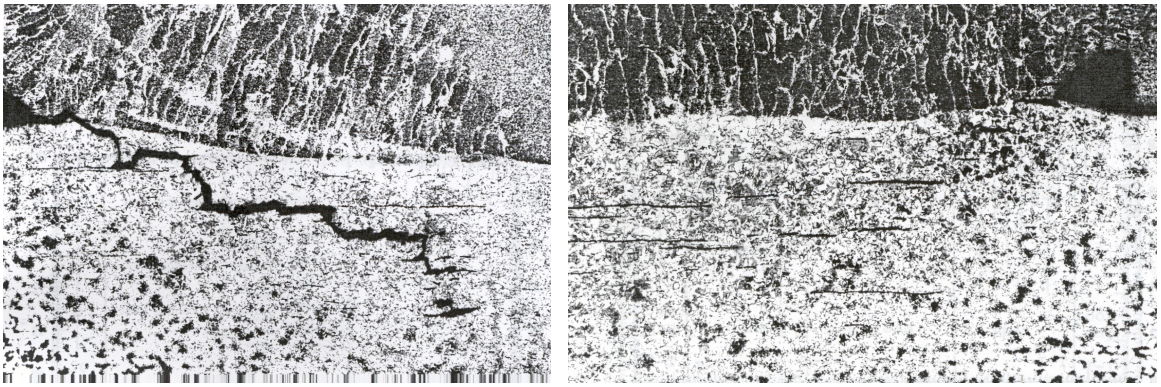


Fig. 3.4: Micrograph showing lamellar tearing

(5) Lamellar tearing is therefore a weld induced flaw in the material which generally becomes evident during ultrasonic inspection. The main risk of tearing is with cruciform, T- and corner joints and with full penetration welds.

(6) The suitability of material for through-thickness requirements should be based on the through-thickness ductility quality criterion in EN 10164, which is expressed in terms of quality classes identified by Z-values representing the percentage of short transverse reduction of area (STRA) in a tensile test.

(7) The choice of material depends on requirements affected by the design of welded connections and the execution.

(8) For the choice of quality class, EN 1993-1-10 provides two classes depending on the consequences of lamellar tearing, see fig. 3-5.

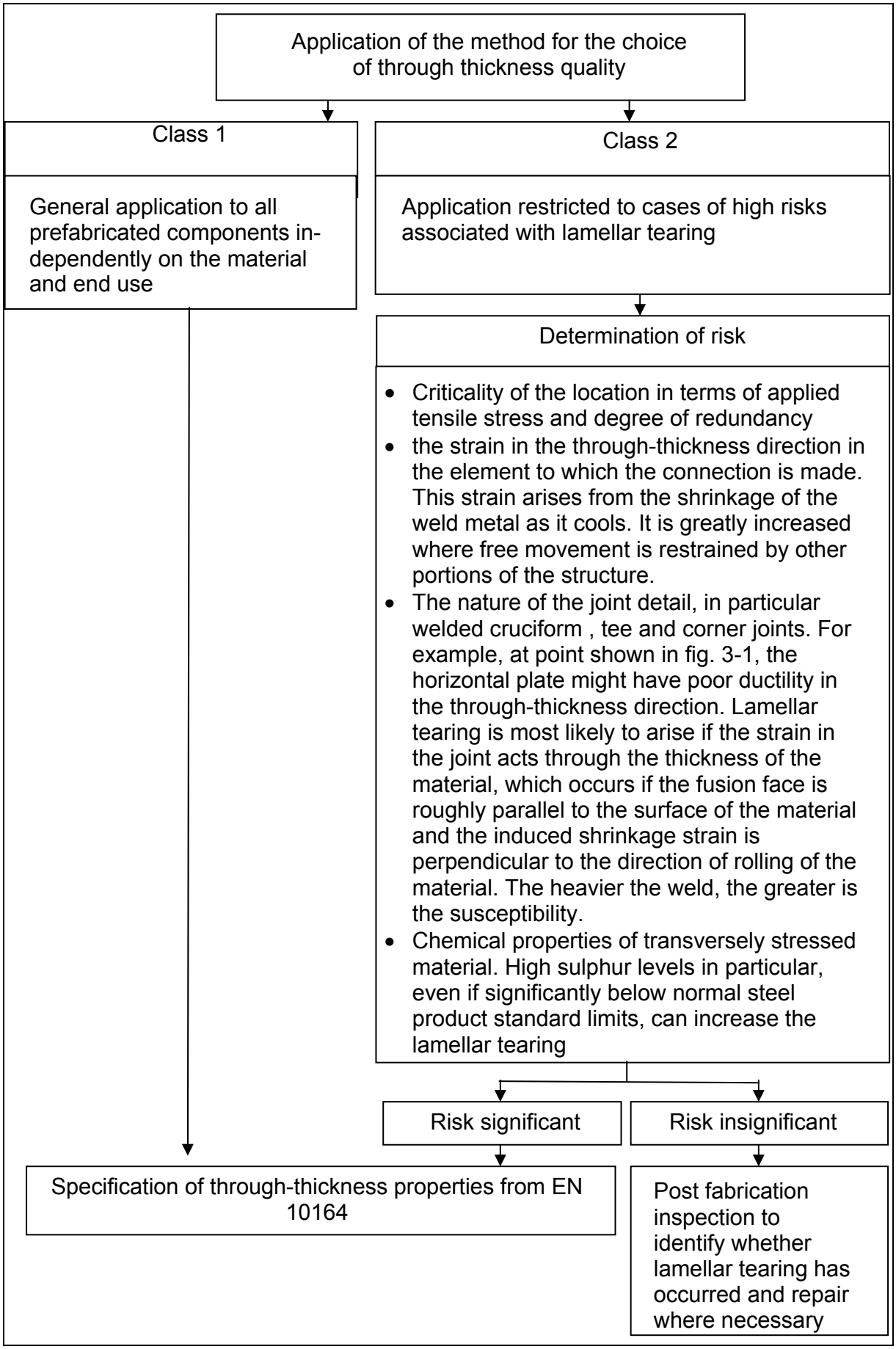


Fig. 3-5: Routes for the choice of through-thickness-quality

(9) Guidance on the avoidance of lamellar tearing during welding is given in EN 1011-2.

3.2 Procedure

(1) The limit state of lamellar tearing is expressed by the following formula

$$Z_{Ed} \leq Z_{Rd} \tag{3-1}$$

where:

Z_{Ed} is the design value of the Z-requirement resulting from the magnitude of strains from restrained metal shrinkage under the weld beads.

Z_{Rd} is the design value of the material capacity to avoid lamellar tearing expressed by the Z-classes for material according to EN 10164 e.g. Z15, Z25 or Z35.

3.2.2 Allocation of influence to the requirement Z_{Ed}

3.2.2.1 Influences

(1) The local straining which may exhaust the ductility of the material depends on the following influences:

a effective weld depth a_{eff} between through plate and incoming plate
b shape and position of weld, weld bead sequence
c effect of material thickness s of the through plate
d remote restraint of shrinkage from welding due to stiffness of other portions of the structure
e influence of preheating.

3.2.2.2 Representation of influences in the limit state equation

(1) The requirement Z_{Ed} has been allocated to the influences a to e in the form

$$Z_{Ed} = Z_a + Z_b + Z_c + Z_d + Z_e \tag{3-2}$$

using partial requirements Z_i for each influences i.

(2) The allocation is given in table 3-1 on the basis of damages reported, see table 3-2.

(3) Table 3-2 contains data from failures due to lamellar tearing which are arranged according to minimum values of STRA (short transverse reduction of area) in through-thickness direction determined from tests. In most failure cases, the mean values of STRA are below 15%, only for three cases they are between 15% and 25%. No failure case above 25% is reported. Two damage cases have been excluded in the evaluation due to the special failure case during the preheating due to internal rolling stress (case 20) and the specific test configuration (designed to provoke lamellar tearing) and additionally overstress during test (case 22). This complies with conclusions from the UK

[2] and Japan [9]. According to French data [10] lamellar tearing would not more be expected for STRA greater than 35%.

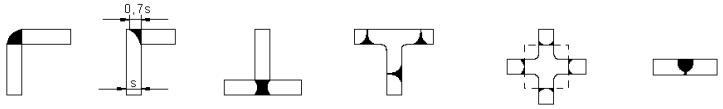
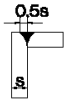
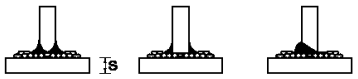
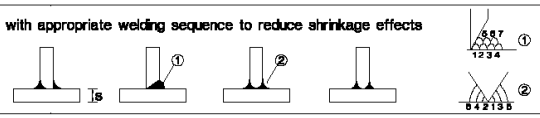
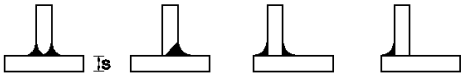
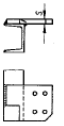
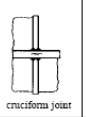
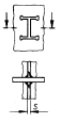
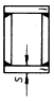
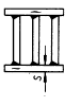
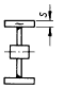
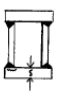
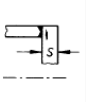
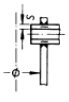
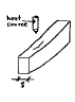
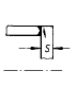
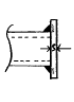
a)	Weld depth relevant for straining from metal shrinkage	Effective weld depth a_{eff} (see Figure 3.2) ≙ throat thickness a of fillet welds		**Z_i**
		$a_{eff} \leq$ 7mm	a = 5 mm	**Z_a = 0**
		7 < $a_{eff} \leq$ 10mm	a = 7 mm	**Z_a = 3**
		10 < $a_{eff} \leq$ 20mm	a = 14 mm	**Z_a = 6**
		20 < $a_{eff} \leq$ 30mm	a = 21 mm	**Z_a = 9**
		30 < $a_{eff} \leq$ 40mm	a = 28 mm	**Z_a = 12**
		40 < $a_{eff} \leq$ 50mm	a = 35 mm	**Z_a = 15**
		50 < a_{eff}	a > 35 mm	**Z_a = 15**
b)	Shape and position of welds in T- and cruciform- and corner-connections			**Z_b = -25**
		corner joints 		**Z_b = -10**
		single run fillet welds Z_a = 0 or fillet welds with Z_a > 1 with buttering with low strength weld material 		**Z_b = -5**
		multi run fillet welds 		**Z_b = 0**
		partial and full penetration welds 		**Z_b = 3**
		partial and full penetration welds 		**Z_b = 5**
		corner joints 		**Z_b = 8**
c)	Effect of material thickness *s* on restraint to shrinkage	$s \leq$ 10mm		**Z_c = 2***
		10 < $s \leq$ 20mm		**Z_c = 4***
		20 < $s \leq$ 30mm		**Z_c = 6***
		30 < $s \leq$ 40mm		**Z_c = 8***
		40 < $s \leq$ 50mm		**Z_c = 10***
		50 < $s \leq$ 60mm		**Z_c = 12***
		60 < $s \leq$ 70mm		**Z_c = 15***
		70 < s		**Z_c = 15***
d)	Remote restraint of shrinkage after welding by other portions of the structure	Low restraint:	Free shrinkage possible (e.g. T-joints)	**Z_d = 0**
		Medium restraint:	Free shrinkage restricted (e.g. diaphragms in box girders)	**Z_d = 3**
		High restraint:	Free shrinkage not possible (e.g. stringers in orthotropic deck plates)	**Z_d = 5**
e)	Influence of preheating	Without preheating		**Z_e = 0**
		Preheating ≥ 100°C		**Z_e = -8**
* May be reduced by 50% for material stressed, in the through-thickness direction, by predominantly static loads and compression only (such as baseplates)				

Table 3-1 Allocation of Z_i-values to the influences i

Case	1	2	3	4	5	6	7		8	9	10	11
σ_{th}/σ_l [3]	0,60	0,67	-	0,33	0,70	-	-	-	0,89	0,90	0,81	0,84
s [4] [mm]	32,5	10	20	8	30	41	41	41	14	25,5	25	24,5
Appl. load [2]	σ_{sh}	?	σ_{sh}	σ_{sh}	σ_{sh}	σ_{sh}	σ_{sh}	σ_{sh}	M_b dynamic	σ_{sh}	σ_{sh}	σ_{sh} + change of temp.
Detail					 orthotropic deck					 cruciform joint		
Type of seam [6]								?				
a_{eff} [5] [mm]	< 10	10	20	17	12	30	?	?	5	25	20	25
Steel	StE 390	?	WStE47N	A42	St52-3	▵ 19MN5	BS 1501 - 161		St37-2	~ StE26	St52-3	WStE 47
No. tests	1	?	2	4	10	?	15	15	2	50	2	5
STRA mean value [%] [1]	0	0	2	3	3	3	3	3	4	5	5	5
STRA min. value [%] [1]	0	?	3	1	0	1,5	?	?	4	0	3	5
Lit.	[12]	[12]	[12]	[12]	[3, 13]	[2]	[11]		[3, 13]	[6]	[3, 13]	[7]

Case	12	13	14	15	16	17	18	19	20	21	22
σ_{th}/σ_l [3]	-	0,91	0,80	-	0,88	0,82	0,96	0,92	-	0,91	0,98
s [4] [mm]	51	32	51	50	112	70	24,5	50	120	70	30
Appl. load [2]	σ_{sh}	σ_{sh}	σ_{sh}	σ_{sh}	σ_{sh}	σ_{sh}	σ_{sh}	σ_{sh}	during preheating due to internal rolling stresses	σ_{sh}	σ resulting from internal pressure
Detail											
Type of seam [6]									-		
a_{eff} [5] [mm]	30	25	28	17	40	35	25	20	-	35	12
Steel	▵ St52-3	▵ StE70 (NiCrMoB)	▵ St52-3 with Cu, V	RSt37-2	A283C	St37-2	15Mo3	SIS142106	St52-3	St37-2	St37
No. tests	?	22	?	?	2	1	2	6	?	3	15
STRA mean value [%] [1]	8	9	9	12	12	14	19	17	17	23	28
STRA min. value [%] [1]	4	2,5	8	?	11	14,5	16	10	?	17	22
Lit.	[2]	[8]	[8]	[13]	[12]	[3, 13]	[7]	[12]	[12]	[3, 13]	[13]

[1] values of STRA are valid for test specimen with diameter 10 mm. The values of tests specimen with lower diameter were converted acc. to [10; 11] as follows:
$STRA_{Dia6} \leq 15 \Rightarrow STRA_{Dia10} = STRA_{Dia6} - 1$; $STRA_{Dia6} > 15 \Rightarrow STRA_{Dia10} = STRA_{Dia6} - 2$ with STRA ▵ short transverse reduction of area

[2] σ_{sh} = stress due to shrinkage; M_b = stress due to bending moment

[3] stress ratio of the ultimate stress in through-thickness direction (σ_{th}) versus the ultimate stress in longitudinal direction (σ_l)

[4] plate thickness of the through plate

[5] weld thickness in thickness direction, see also fig. 2

[6] Type according to EN 22553

Table 3-2: Description of damage cases [15]

(4) The evaluation of damage cases according to EN 1993-10 is given in table 3-3 and table 3-4

Case	Description of test	Z_{Sd} Table 1	Z_{Rd} in test	Occurence of lamellar tearing	$Z_{requir.}$ Table 4
A	$a_{eff} \leq 7mm$ fillet welded T-connection s ~ 40mm low restraint no preheating	$Z_a = 0$ $Z_b = -5$ $Z_c = 8\ (4)$ $Z_d = 0$ $Z_e = 0$			
	for dyn. loads & tension	$Z_{Sd} = 3$	3	no	no
	for stat. loads & compression	$Z_{Sd} \sim 0$			no
B	$7mm < a_{eff} \leq 10mm$ fillet welded T-connection s ~ 40mm low restraint no preheating	$Z_a = 3$ $Z_b = 0$ $Z_c = 8\ (4)$ $Z_d = 0$ $Z_e = 0$			
	for dyn. loads & tension	$Z_{Sd} = 11$	3	yes	Z15
	for stat. loads & compression	$Z_{Sd} = 7$			no
C	$10mm < a_{eff} \leq 20mm$ fillet welded T-connection s ~ 40mm low restraint no preheating	$Z_a = 6$ $Z_b = 0$ $Z_c = 8\ (4)$ $Z_d = 0$ $Z_e = 0$			
	for dyn. loads & tension	$Z_{Sd} = 14$	3	yes	Z15
	for stat. loads & compression	$Z_{Sd} = 10$			no
D	$a_{eff} \leq 7mm$ fillet welded cruciform-conn. s ~ 40mm high restraint no preheating	$Z_a = 0$ $Z_b = -5$ $Z_c = 8\ (4)$ $Z_d = 5$ $Z_e = 0$			
	for dyn. loads & tension	$Z_{Sd} = 8$	3	no	no
	for stat. loads & compression	$Z_{Sd} = 4$			no
E	$7mm < a_{eff} \leq 10mm$ fillet welded cruciform-conn. s ~ 40mm high restraint no preheating	$Z_a = 3$ $Z_b = 0$ $Z_c = 8\ (4)$ $Z_d = 5$ $Z_e = 0$			
	for dyn. loads & tension	$Z_{Sd} = 16$	3	yes	Z15
	for stat. loads & compression	$Z_{Sd} = 12$			Z15
F	$10mm < a_{eff} \leq 20mm$ fillet welded cruciform-conn. s ~ 40mm high restraint no preheating	$Z_a = 6$ $Z_b = 0$ $Z_c = 8\ (4)$ $Z_d = 5$ $Z_e = 0$			
	for dyn. loads & tension	$Z_{Sd} = 19$	3	yes	Z15
	for stat. loads & compression	$Z_{Sd} = 15$			Z15

Table 3-3 Evaluation of test results

Case	Z_a	Z_b	Z_c	Z_d	Z_e	Z_{Sd}	$Z_{requir.}$ Table 4	measured value Z_{mean}	prEN 1993-1.10
1	3	0	8	3	-	14	Z15	0	safe
2	3	5	2	0	-	10	-	0	safe*
3	6	5	4	3	-	18	Z15	2	safe
4	6	5	2	5	-	18	Z15	3	safe
5	6	5	6	0	-	17	Z15	3	safe
6	9	0	10	0	-	19	Z15	3	safe
7	see table 3								
8	0	0	4	0	-	4	-	4	safe*
9	9	5	6	3	-	23	Z25	5	safe
10	6	0	6	5	-	17	Z15	5	safe
11	9	5	6	5	-8	17	Z15	5	safe
12	9	5	12	3	-	29	Z25	8	safe
13	9	5	8	5	-	27	Z25	9	safe
14	9	5	12	5	-8	23	Z25	9	safe
15	6	5	10	0	-	21	Z25	12	safe
16	12	5	15	5	-	37	Z35	12	safe
17	12	8	15	3	-	38	Z35	14	safe
18	9	5	6	5	-	25	Z25	19	safe
19	6	3	10	0	-	19	Z15	17	safe
20	special case								
21	12	8	15	3	-8	30	Z25	23	safe
22	special configuration (designed to provoke lamellar tearing) + overstress								

* though $Z_{required}$ according to prEN 1993-1.10 is equal or smaller than the measured values Z_{mean} of the damage cases the procedure is safe because for structural steels not classified as Z-grade according to EN 10164 a minimum Z-quality equivalent to Z=10 is assumed.

Table 3.4: Evaluation of damage cases given in table 3-2

(5) According to this evaluation, the procedure in EN 1993-1-10 gives safe results if structural steels not classified as Z-grades according to EN 10164 provide a Z-quality equivalent Z = 10.

(6) Fig. 3-6 gives a lower bound relationship between Z-values and the sulphur content of steels S355 [14].

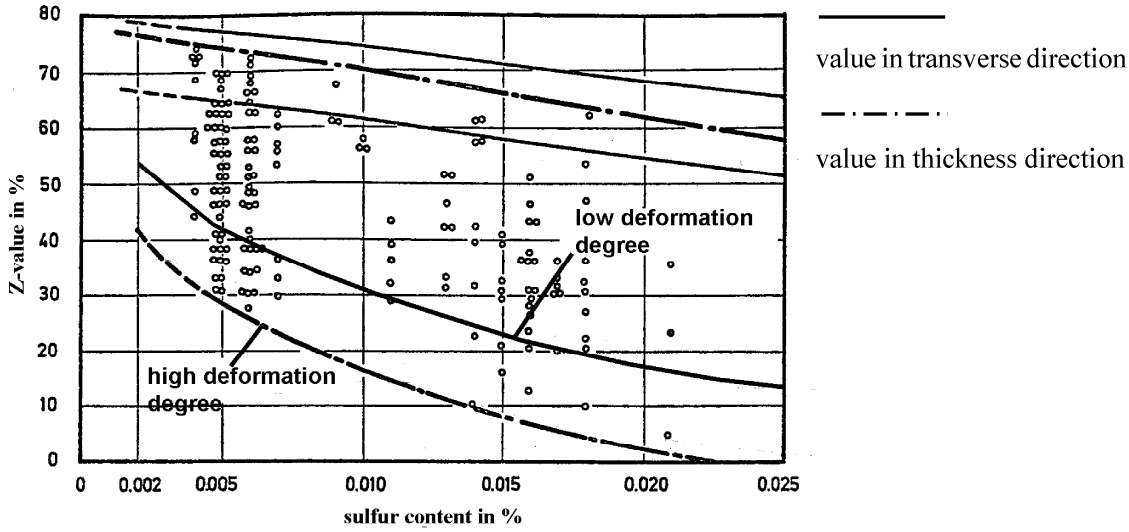


Fig. 3-6: Comparison between the percentage reduction of area in transverse direction to the reduction of area in thickness direction of steel S355 in relation to the sulphur content [14].

3.2.2.3 Influence of the effective weld depth a_{eff} (a)

(1) In Fig. 3-7, the relationship between the effective weld depth a_{eff} for straining, defined in fig. 3-8, and the percentage short transverse reduction of area (STRA) = Z_{damage} of the material, for which lamellar tearing was reported (see table 3-2), is plotted. For fillet welds the effective weld depth corresponds to the leg length of weld.

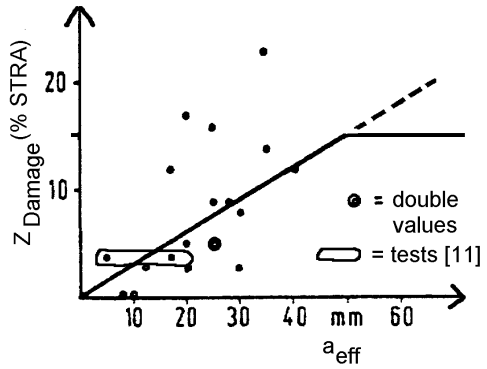


Fig. 3-7: Z_{damage} [% STRA] versus weld depth a_{eff}



Fig. 3-8: Definition of effective weld depth a_{eff} for shrinkage

(2) In the mean, a linear relationship between effective weld depth a_{eff} and damage (% STRA) can be identified for a_{eff} < 50 mm. For a_{eff} > 50 mm the damage effect is taken as constant (Z_a = 15) because of the effect of welding sequence to shrinkage.

(3) In using the mean lines (instead of an enveloping line), also the other influences need to be considered to be conservative in the choice.

(4) Table 3-1 shows for influence (a) the linear relationship between Z_a and a_{eff} from fig. 3-7.

3.2.2.4 Influence of the shape and position of weld and weld bead sequence (b)

(1) The reference case for the shape and position of weld is the case of fillet welds for T-, cruciform- and corner-joints for which $Z_b = 0$ was used.

(2) The cases above this reference case in table 3-1 are more favourable and allow to compensate unfavourable effects of other influences; the cases below the reference case are less favourable.

(3) Weld bead sequences close to buttering, balanced welding and weld bead sizes with $a_{eff} \leq 7$ mm for multipass welds reduce the risk of lamellar bearing.

3.2.2.5 Thickness s of plate with through thickness strains (c)

(1) The plot of plate thickness s versus Z_{damage} in % STRA for the material, for which lamellar bearing was reported (see table 3-2), is given in fig. 3-9.

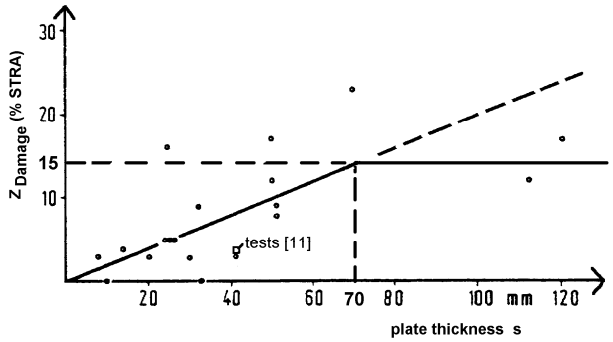


Fig. 3-9: Z_{damage} [% STRA] versus plate thickness s

(2) In the mean, a linear relationship between Z_{damage} and plate thickness s has been derived for $s \leq 80$ mm with a maximum value $Z_{damage} = 15$ for $s > 70$ mm plates.

(3) The limitation $Z_c = 15$ mm may be understood as effect from the limited St-Venant-zone affected by the straining requirement from metal shrinkage.

(4) In order to consider various consequences of potential delaminations, the Z-requirements, established for plate thickness, are reduced by 50% when external loads are predominantly static and lead to compression only.

3.2.2.6 Influence of remote restraint to shrinkage due to stiffness of other portions of the structure (d)

(1) The damage evaluation does not give a clear correlation with the global restraint effects from stiffness of the surrounding members; therefore relatively small Z_d-values have been allocated to the cases, see table 3-5:

- low restraint (e.g. built-up members with longitudinal welds, without restraints to shrinkage)
- medium restraint (e.g. for cruciform joints of members which are restrained at their ends)
- high restraint (e.g. for tubes through cut outs in plates and shells).

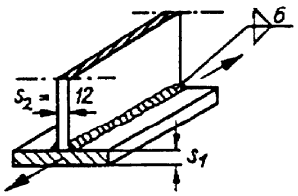
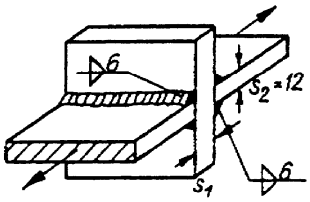
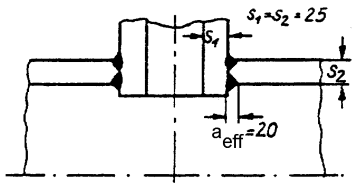
Case no	structural detail	s_1	Z_i					Z_{Sd}	required Z_{Rd}
			Z_a	Z_b	Z_c	Z_d	Z_e		
1 low restraint	Flange-web-connection of a beam 	15	3	0	4	0	0	7	-
		20	3	0	4	0	0	7	-
		30	3	0	6	0	0	9	-
		50	3	0	10	0	0	13	Z15
2 medium restraint	cruciform joint 	15	3	0	4	3	0	10	-
		20	3	0	4	3	0	10	-
		30	3	0	6	3	0	12	Z15
		50	3	0	10	3	0	16	Z15
3 high restraint	tube welded in a tube 		without preheating						
			6	5	6	5	0	22	Z25
			with preheating						
			6	5	6	5	-8	14	Z15

Table 3-5: Examples for determining Z_{Ed} and allocation to the Z_{Rd}-classes in EN 10164

3.2.2.7 Influence of preheating (e)

(1) For preheating (> 100°C), a bonus Z_e = - 8 has been adopted. This is an advantage in particular for thick plates.

(2) It should, however, be noted that where the shrinkage of the preheated material after completion of welding can provide additional strain to that arising

from cooling of the weld itself, the bonus from preheating should not be applied.

3.2.3 Minimum requirement Z_{Ed}

(1) For defining minimum requirements tests in [11] with fillet-welded T- and cruciform joints were evaluated, see table 3-3.

(2) The results of this evaluation correspond with the conclusions in [11], that for fillet-welded T- and cruciform joints with $a_{eff} \leq 7$ mm no guaranteed Z-values are necessary for s < 40 mm.

(3) This requirement applies, if hydrogen in welds is limited to 0.5 ml/100 g.

(4) The conclusions in table 3-1 also comply with the various damage cases as referred to in fig. 3-7, fig. 3-9 and table 3-2. From 7 damage cases with $Z_R \leq$ 5%, 4 cases could be allocated to low restraint and from these 4 cases 2 cases had plate-thicknesses s < 14 mm, so that for s = 10 mm, $a_{eff} \leq 10$ mm, $Z_d = 0$ and $Z_e = 0$ the minimum requirement $Z_{Ed} = Z_a$ (=3) + Z_c (=2) = 5 could be estimated.

3.2.4 Allocation of Z_{Ed} to Z-classes in EN 10164

(1) The value Z_{Ed} according to expression (3-2) should be allocated to the through thickness ductility quality classes according to EN 10164 by table 3-6.

Required value of Z	Z-quality according to EN 10164
≤ 10	—
11 to 20	Z 15
21 to 30	Z 25
> 30	Z 35

Table 3-6: Choice of quality class according to EN 10164

According to this table, it is possible that Z-values of the Z-classes according to EN 10164, which are related to the mean from 3 measurements from material tests, are smaller than Z_{Ed}.

(2) In fact the Z-classes in EN 10164 represent lower bound values which are rarely met. Therefore, the classification according to table 3-6 is sufficiently reliable and satisfies the condition of equation (3-1) with regard to design values.

(3) The allocation in table 3-6 may be modified when reliability differentiation to various design situations is applied.

3.3 Examples of application

3.3.1 Connection of the hangers of a tied-arch-bridge to the arch

(1) Fig. 3-10 gives a typical detail of the connection of a hanger of an arch-bridge to the arch. Fig. 3-10 a) shows the box-type cross-section of the arch with a diaphragm to which the hanger is welded; fig. 3-10 b) gives a section in the plane of the arch indicating the spot, where the quality of the plate of the diaphragm shall be determined.

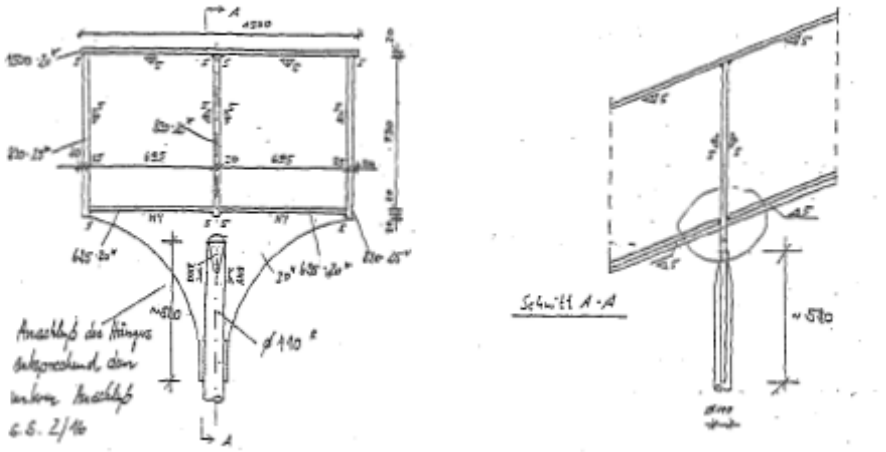
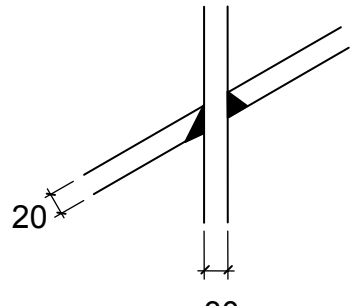


Fig. 3-10: Welded connection of hanger to the arch of an arch bridge:
a) cross-section of the arch and connection of hanger
b) section in plane of the arch

(2) The diaphragm has a plate thickness of t = 30 mm and is made of S235 J2.

(3) The Z-qualities are determined in table 3-7. For Z_e preheating of 100°C has been provided.



Z_i						
Z_a	Z_b	Z_c	Z_d	Z_e	Z_{Ed}	Z_{Rd}
6	5	6	5	-8 (pre-heating)	14	Z15

Table 3-7: Determination of Z-quality

(4) The choice made is Z15.

3.3.2 Welded connection of the arch of a tied arch bridge to the main girder

(1) Fig. 3-11 shows the connection of the end of the box-type arch to the open section main girder with stiffeners for the bearings.

Fig. 3-11 a) gives a section in the plane of the arch with the bottom flange of the main girder. Fig. 3-11 b) gives a section at the end of the arch, also with the bottom flange of the main girder and the stiffeners for the bearings.

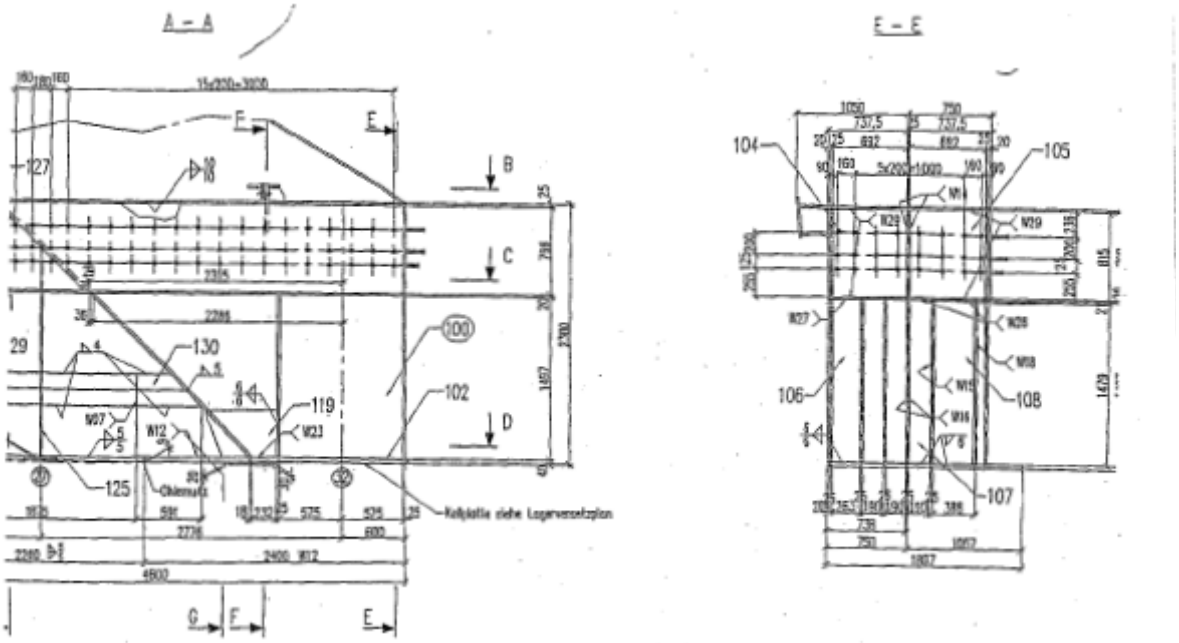
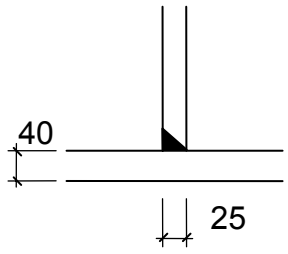


Fig. 3-11: Welded connection of the arch to the main girder
a) section in plane of the arch;
b) cross-section at the end of the arch

(2) The bottom flange has a plate thickness of t = 40 mm and is made of S355 NM; the plate-thickness of the stiffeners is t = 25 mm.

(3) The determination of Z-quality may be taken from table 3-8.



Z_i						
Z_a	Z_b	Z_c	Z_d	Z_e	Z_{Ed}	Z_{Rd}
8	5	8	3	-8	16	Z15

Table 3-8: Determination of Z-quality

(4) The choice made is Z15.

3.3.3 Connection of troughs to cross-beams in an orthotropic steel deck of a road bridge

(1) Fig. 3-12 gives the view and the cross-section of the road bridge "Kronprinzenbrücke" with an orthotropic deck plate designed by Calatrava.

(2) Due to the small construction depth of the cross-beams and cut-outs in their webs for pipes, the deck had to be designed such that the troughs are not continuously going through the webs of the cross-beams, but are inserted in between and welded to the webs.

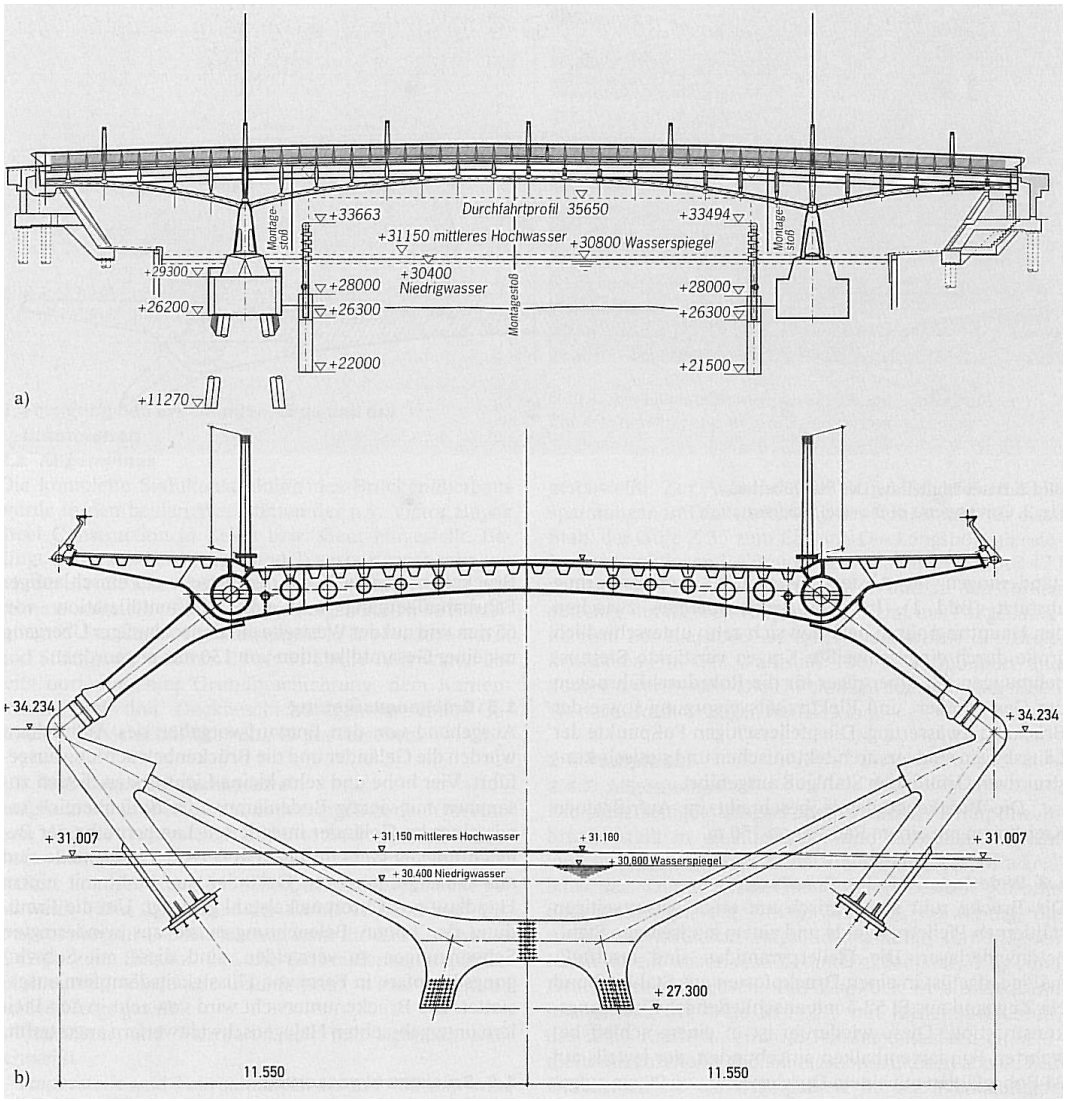


Fig. 3-12: General view and cross-section in the axis of the pier

(3) Fig. 3-13 gives details of the welded joints of the trapezoidal ribs at the cross-beams. The Z-quality of the webs of the cross-beams was questioned.

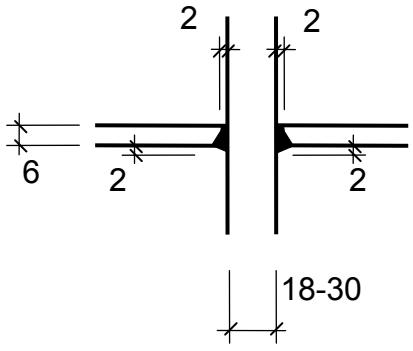


Fig. 3-13: Welded joint of troughs to webs of cross-beams

(4) The thickness of the web-plate varies between t = 18 mm and t = 30 mm. The steel is S355 NM.

(5) Table 3-9 gives the fig.s for the determination of Z-quality. The quality finally chosen was Z35.

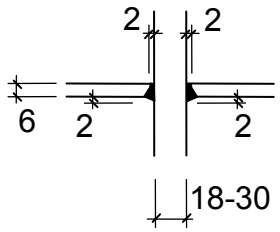
	Z_i						
	Z_a	Z_b	Z_c	Z_d	Z_e	Z_{Ed}	Z_{Rd}
	3	5	6	5	0	Z19	Z35

Table 3-9: Determination of Z-quality

3.3.4 More general examples

(1) More general examples for details in bridges are given in table 3-5.

3.4 Bibliography

[1] Schönherr, „Werkstoffliche und Konstruktive Maßnahmen zum Vermeiden von Lamellenbrücken in Schweißkonstruktionen“, DVS-Berichte, Band 50, „Schweißen und Schneiden 1978 Fortschritt und Qualität“, Düsseldorf 1978, S. 83-87

[2] Farrar, J.C. Ginn, B.J.; Dolby, R.E.: „The use of small scale destructive tests to assess susceptibility to lamellar tearing”, IIW-Doc. IX-890-74

[3] Schönherr, W.: “Beurteilung der Schweißneigung von Stahl bei Beanspruchung des Bauteils in Dickenrichtung”, Schweißen und Schneiden, Jg. 27 (1975), Heft 12, S. 491-495

[4] Dennin, G.; „Kriterien zum Festlegen der Mindestbrucheinschnürung bei Zugbeanspruchung von Erzeugnissen senkrecht zur Walzebene“, Schweißen und Schneiden, Jg. 28 (1976), Heft 10, S. 391-393

[5] Granström, A.: „The relevance of test methods for lamellar tearing“, IIW-Doc IX-1086-78

[6] König, H.; Rohweder, A.: “Schadensfall und seine Auswirkungen auf die schweißgerechte Konstruktion eines Erz-Öl-Tankers”, DVS-Bericht 31, S. 165/172, Deutscher Verlag für Schweißtechnik, Düsseldorf, 1974

[7] Kußmaul, K.; Blind, D.; „Hinweise zur werkstoff- und schweißgerechten Konstruktion anhand von Bauspielen aus dem Behälter- und Rohrleitungsbau, DVS-Bericht 31, S. 85-92, Deutscher Verlag für Schweißtechnik, Düsseldorf, 1974

[8] Heuschkel, J.: „Anisotropy and Weldability“, Wdg. J. Res. Suppl. 50 (1971), H. 3, S. 110-s/26-s

[9] Inagaki, M.; Tamura, H.; Nakazima, A.; Ito, Y.; Tanaka, J.; Shimoyama, T.: ”Japanese Report on Lamellar Tearing of Sub-Commission”, IX-F, IIW-Doc. IX-873-74

[10] Cadiou, L; Samman, J.; Leymonie, C.; ”Acoustic emission as a method for evaluating of susceptibility of a steel plate to lamellar tearing”, IIW-Doc. IX-858-73

[11] Pargeter, R.J.; Davey, T.G.; Jones, R.L.; Ogle, M.H.; Billson, D.R.; Mudge, P.J.: “Study of through thickness properties of steel for bridge construction”, The Welding Institute, Report 34048/3/91, March 1991

[12] IIW-Doc IX-1008-76

[13] The cases 5, 8, 10, 15, 17, 21 and 22 result from experts-reports or research-investigations of Bundesanstalt für Materialforschung und –prüfung (BAM)

[14] Rheinstahl Technik 11 (1973) Nr. 3, Page 180-186.

[15] Sedlacek, G.; Kühn, B.; Dahl, W.; Langenberg, P.; Schönherr, W.: Background Document 2 to Eurocode 3: design of steel structures, Part 1-10, Chapter: through-thickness properties. Sept. 2001.

Section 4

4. Complementary rules for the design to avoid brittle facture on the basis of the background to EN 1993-1-10

4.1 Assessment of the residual safety and service life of old riveted structures

4.1.1 General

(1) Section 2 of this report gives the background of the safety assessment of structural members based on toughness that has been used to develop table 2.1 of EN 1993-1-10 for the choice of material to avoid brittle fracture.

(2) This safety assessment included

- an initial flaw overlooked in inspection after fabrication and acting like an initial crack
- crack growth from fatigue taking place during a certain “safe service period” that leads to a design size of crack at the end of the “safe service period”
- fracture mechanical assessment at the end of the “safe service period” verifying that at that time the structure is still safe, even if the design size of the crack and an extremely low temperature reducing the material toughness are combined.

(3) For old riveted steel bridges, this assessment procedure may be used to verify their residual safety and residual service life by proceeding as follows:

1. It is assumed, that after an appropriate service time, fatigue has progressed in the riveted connections of the structural members to such an extent that through cracks at the heads of the rivets or cracks in inner plates exceeding cover plates have reached a certain size on the surface so that they are detectable, see fig. 4-1.

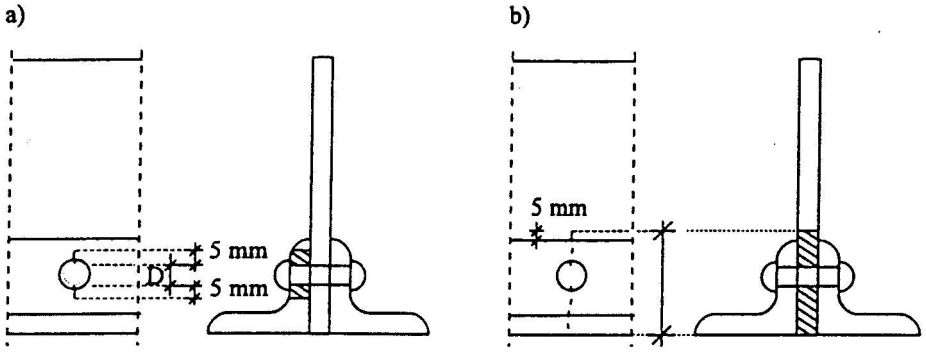


Fig. 4-1: Assumption for the initial through-crack size a_0 for a) angles, b) plates covered by angles

2. The time when these cracks may occur may not be accurately predicted by conventional fatigue calculations due to the large scatter of the fatigue strength and also due to uncertainty of the time dependent development of fatigue load. However, where the scatter can be limited (e.g. for railway bridges, where the loading is documented) the start of the period that fatigue cracks may occur may be assumed with 80% of the nominal fatigue life with a certain probability.

3. It is assumed that the initial through crack with the size a_0 has been overlooked during a main inspection of the bridge so that it propagates during the following “safe service period” due to fatigue until it reaches a critical size a_{crit} for which the ultimate limit state verification for the accidental design situation with extremely low temperatures is just fulfilled, see fig. 4-2.

4. In case the inspection after the “safe service period” shows such large crack sizes, the assumption holds and the fatigue life is going to end. In case no cracks are detected, a new “safe service period” with the same starting conditions as the old “safe service period” can start.

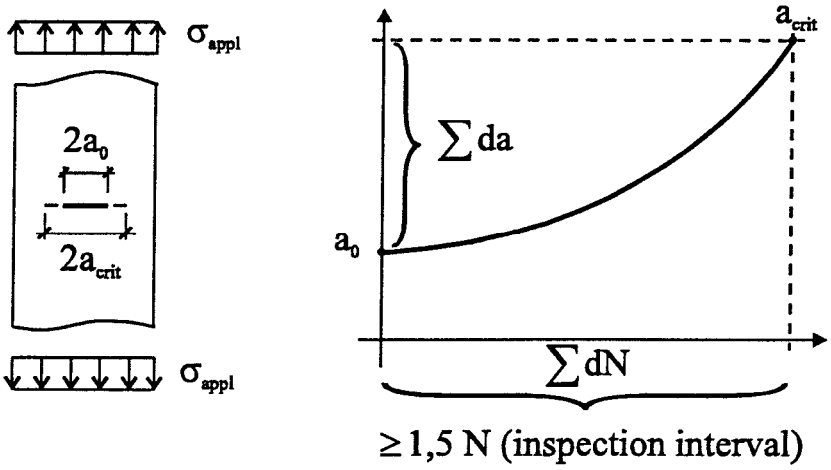


Fig. 4-2: Crack growth from through crack size a_0 to crack size a_{crit} during a “safe service period” due to the fatigue load ($\Delta\sigma^5 \cdot N$)

(4) In conclusion, the following safety assessments are necessary for old riveted bridges:

1 Conventional ultimate limit state verifications for persistent and transient design situations (assuming ductile behaviour) using the relevant load combination, however, with partial factors modified.

$$(\gamma_G \cdot G) + (\gamma_Q \cdot Q_{K1}) + (\gamma_Q \cdot \psi_{Q2} \cdot Q_{K2}) \leq \frac{R_K}{\gamma_M}$$

2. Conventional serviceability limit state verification with criteria from traffic and maintenance.

3. Conventional fatigue verifications on the basis of EN 1993-1-9, using information on fatigue loads that occurred in the past and fatigue loads expected in the future.

The partial factors $\gamma_{Ff} \cdot \gamma_{Mf}$ in these fatigue verifications depend on the outcome of an additional toughness check to avoid brittle fracture, which is specified in 4.

If the toughness check according to 4. results in a sufficiently long “safe service period”, the concept of “damage tolerance” can be applied and the $\gamma_{Ff} \cdot \gamma_{Mf}$-values for the fatigue verification may be taken as 1.0.

The conventional fatigue verification results in the following conclusions for the residual life:

a) Details for which the fatigue loading is below the fatigue threshold values for crack growth as given below, do not need further crack growth checks according to 4, because they are supposed to have an infinite fatigue life.

b) The magnitude of the residual fatigue life determined with the conventional fatigue check indicates how urgent main inspections with “safe service periods” are. If the residual fatigue life is short, uncertain or even negative, the future use of the bridge fully relies on sufficiently long “safe service periods” in combination with inspections.

4. Determination of the “safe service period” on the basis of a fracture mechanical toughness check.

This determination includes a number of action steps which are given in the flow chart in fig. 4-3.

The method presented is based on the J-integral as fracture mechanics value for the material toughness, which in the elastic range is equal to

$$J = \frac{K^2}{E} \qquad (4\text{-}1)$$

where K is the stress intensity factor.

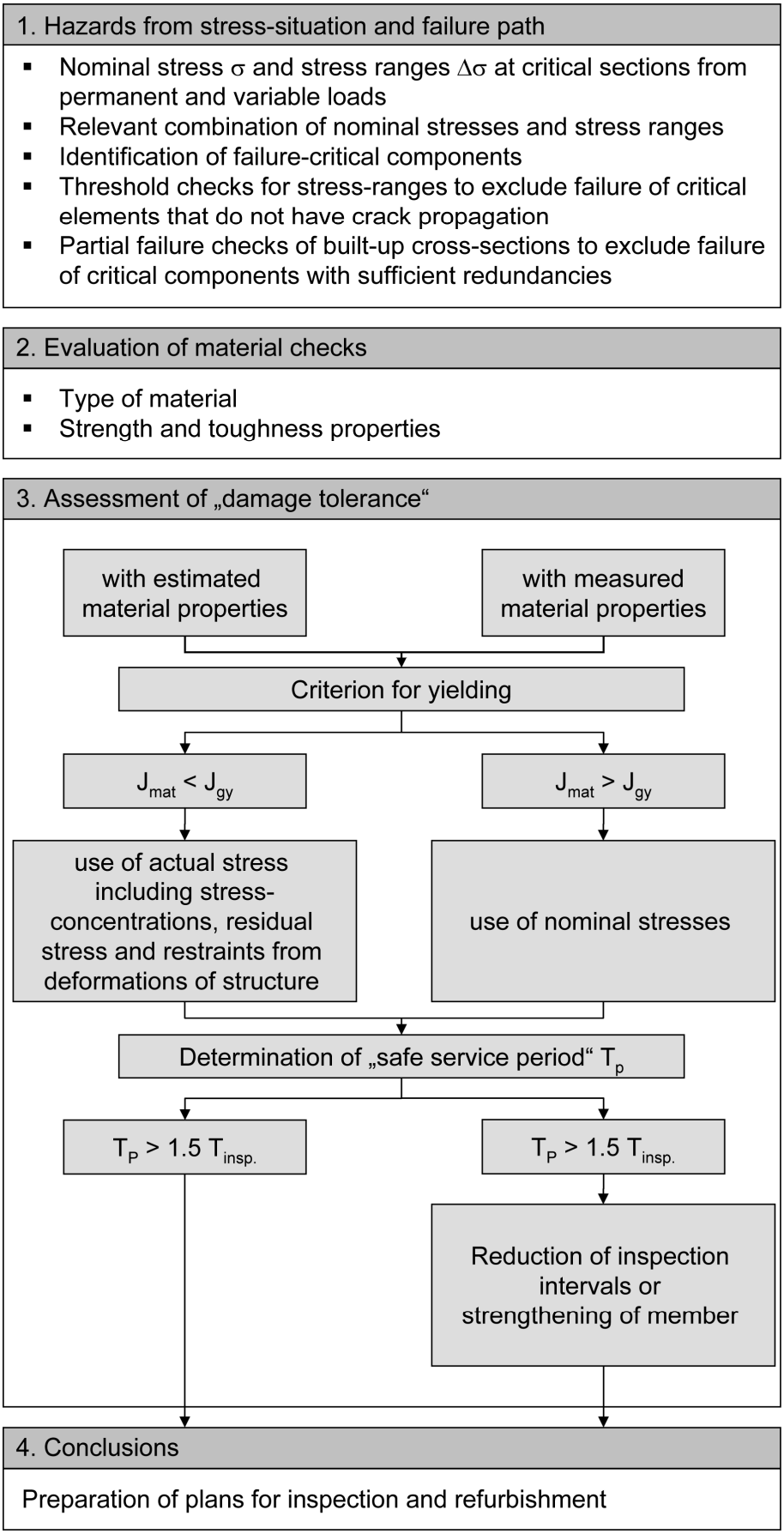


Fig. 4-3: Flow chart for the determination of “safe service periods” of existing riveted bridges with fracture mechanical values

(5) In the following, the various steps in the flow chart given in fig. 4-3 are explained.

4.1.2 Hazards from stress situation and stress ranges

4.1.2.1 Determination of nominal stresses and stress ranges

(1) Nominal stresses and nominal stress ranges are calculated from external normal forces and bending moments, neglecting stress concentration factors, e.g. due to holes or other notches.

(2) Nominal stresses in the net section are used for the conventional ultimate limit state assessments.

(3) Nominal stresses in gross sections are used for fracture mechanics assessments, where the applied stresses are gross section stresses and net section effects (effects of holes and cracks) are included in the fracture mechanical model, see fig. 4-2.

(4) Nominal stresses may, however, only be used where net-section yielding occurs before net section fracture; otherwise residual stresses and restraints that would vanish by net-section yielding have to be taken into account by increasing the external normal forces and bending moments.

(5) Nominal stress ranges result from external variable loads only; they are applied in the way indicated in EN 1993-1-9, normally to the gross sections.

4.1.2.2 Combination of permanent and variable actions

(1) For the conventional ultimate limit state verification of old riveted bridges, advantage can be taken from prior knowledge of permanent and variable loads, so that the partial factors γ_G and γ_Q can be reduced in relation to the factors applied to the design of new bridges.

(2) The recommended values for conventional ultimate limit state assessments are

γ_G = 1.15 instead of 1.35
γ_Q = 1.20 instead of 1.35 (4-2)

(3) For the fracture mechanics assessment in view of “damage tolerance”, the accidental load combination applies where the lowest temperature of the member is the leading action, whereas permanent and variable traffic loads are the accompanying actions.

Hence γ_G =1.00 is applied to permanent loads and frequent values $\psi_1 Q_{k1}$ are used for variable loads.

(4) Fatigue checks are made with traffic effects only.

4.1.2.3 Identification of failure-critical components

(1) The fracture mechanics assessment is only necessary for those components in tension of a bridge:

- which are failure critical,
- for which the stress ranges exceed the fatigue threshold values
- which have no cross-sectional redundancies.

(2) Failure critical components for the fracture mechanics assessment are those tension elements, the failure of which would cause a collapse of the structure.

(3) Fig. 4-4 gives the flow chart for the determination of the failure-critical elements by a check of the failure path.

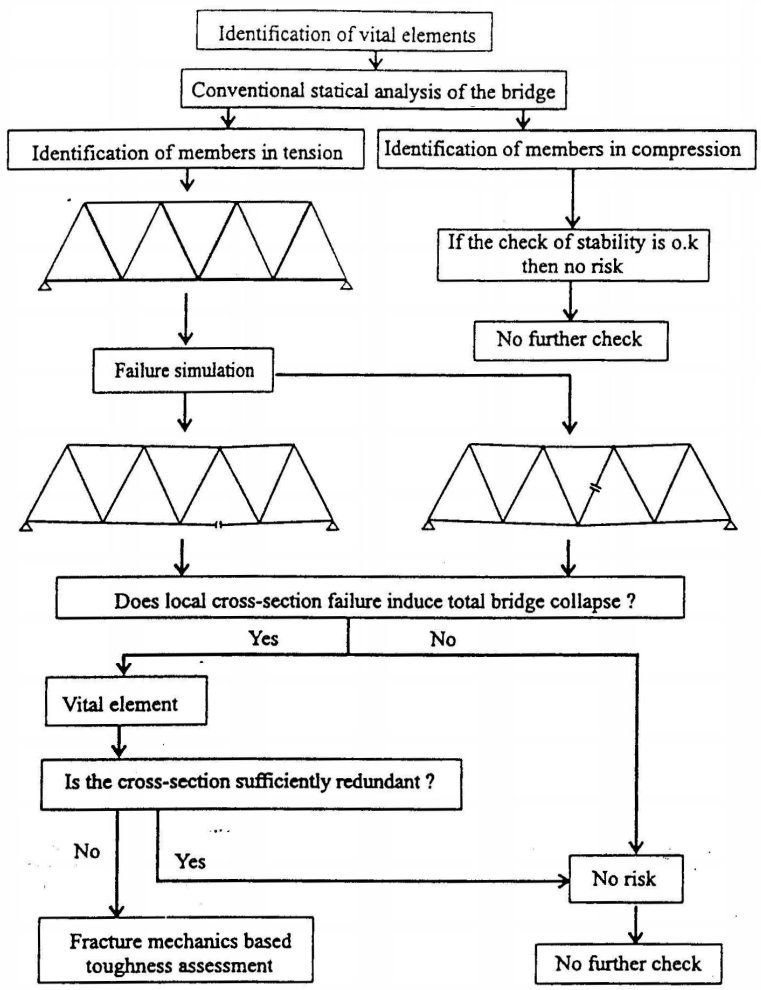


Fig. 4-4: Identification of failure-critical components

(4) Failure critical components identified by the procedure given in fig. 4.4 should be further checked in view of

a) a threshold check for stress ranges
b) redundancies

4.1.2.4 Threshold check

According to EN 1993-1-9, the S-N-curve for riveted connections is given as shown in fig. 4-5, indicating a constant amplitude endurance limit $\Delta\sigma_D$ = 52 N/mm^2.

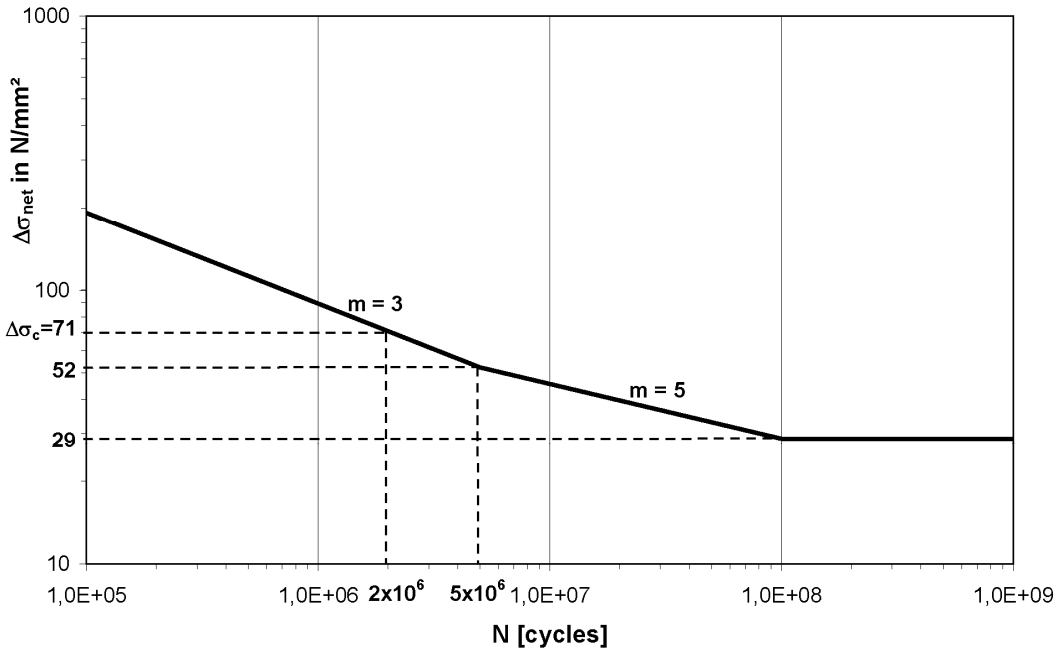


Fig. 4-5: S-N-curve for the fatigue assessment of old riveted steel bridges related to $\Delta\sigma$ for net sections

(2) A comparison with test results, see fig. 4-6, which include the loss of clamping forces in the rivets, demonstrates, however, that an endurance limit at $5 \cdot 10^6$ cycles is vague, so that threshold values $\Delta\sigma_D$ should preferably be determined from fracture mechanical modelling.

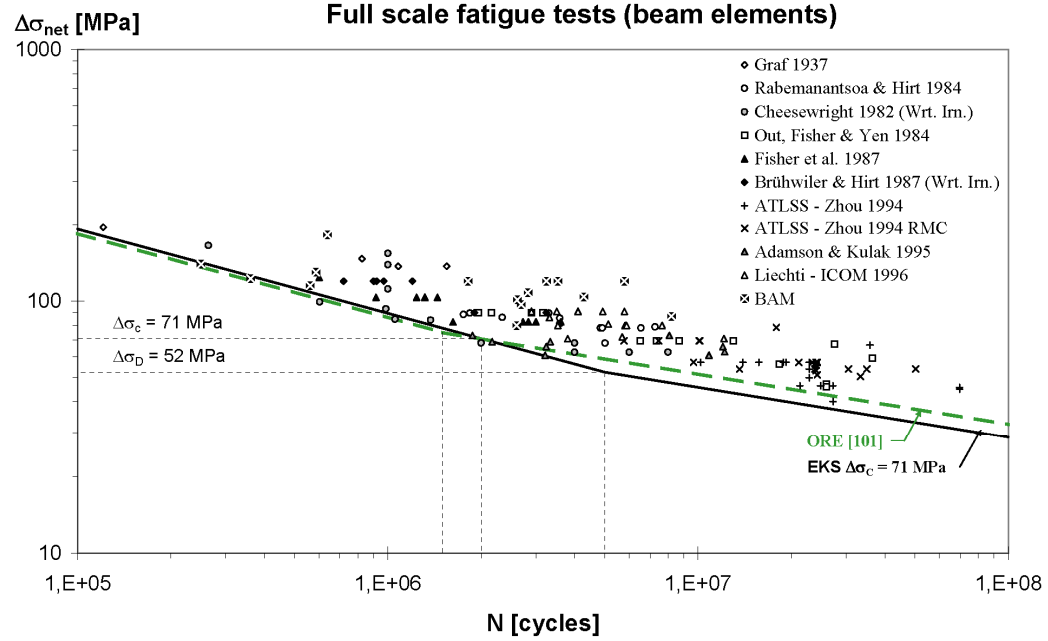


Fig. 4-6: Comparison of S-N-curve for riveted connections with test results [21]

(3) Fig. 4-7 shows in what way the threshold values $\Delta\sigma_D$ and ΔK_{th} are linked and how $\Delta\sigma_D$ can be calculated for a member with holes and cracks using ΔK_{th}-values from tests.

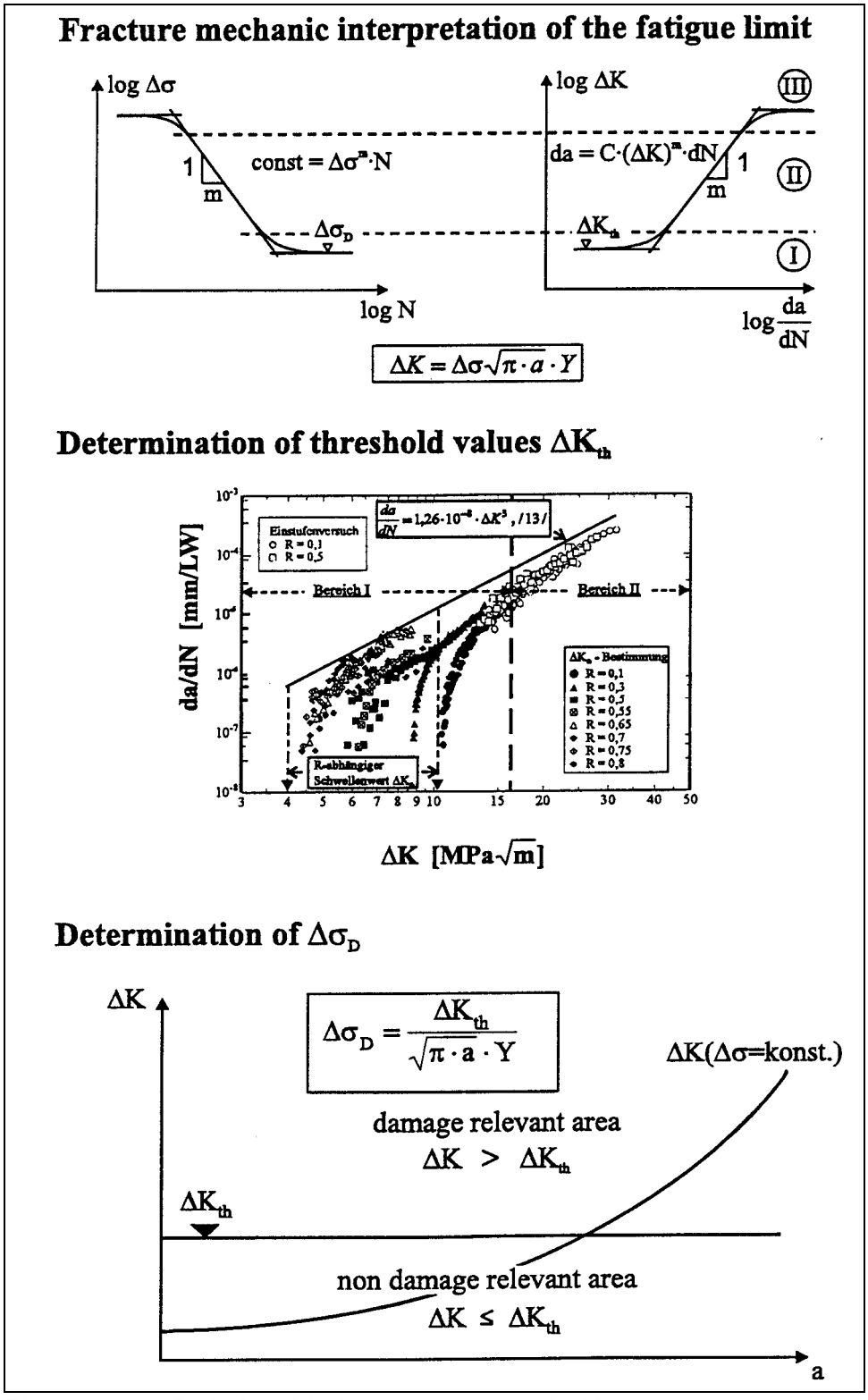
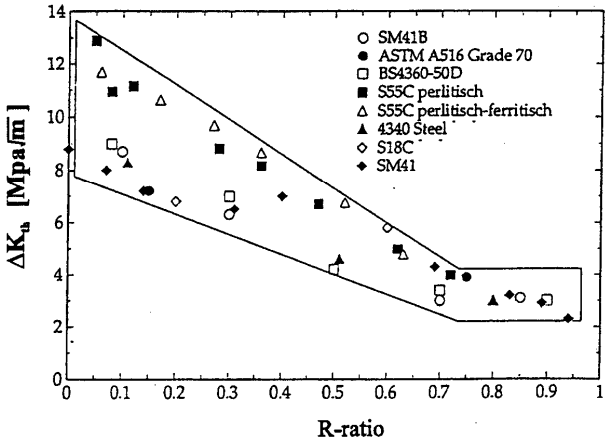


Fig. 4-7: Relationship between $\Delta\sigma_D$ and ΔK_{th}.

(4) In determining the ΔK_{th}-values, the advantageous effects of the R-ratio may be considered, see fig. 4-8.

1) IEHK



2) The Welding Institute, Cambridge

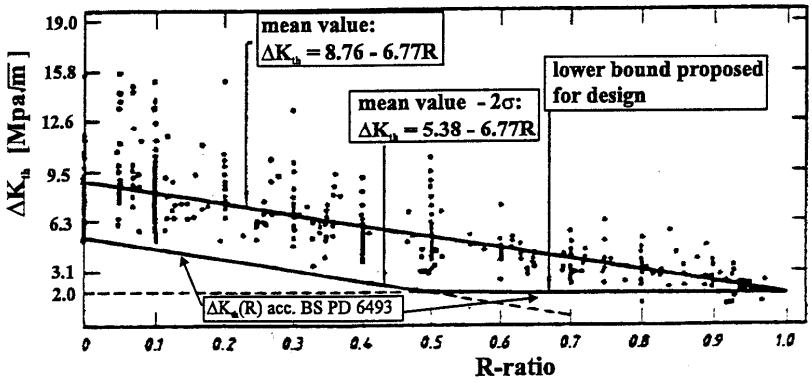


Fig. 4-8: ΔK_{th}-values dependent on of the R-ratio.

(5) Fig. 4-9 gives a survey on various recommendations together with test results related to old mild steel and also to puddle iron.

Overview

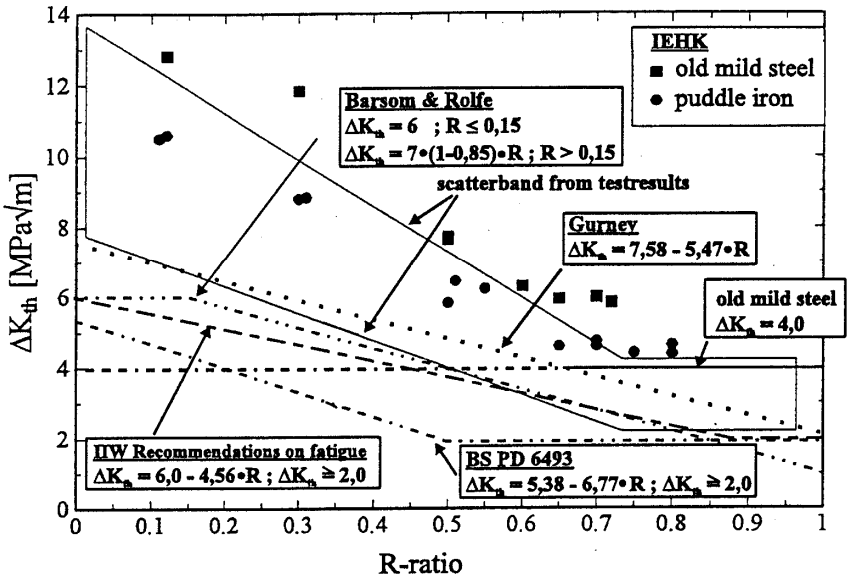


Fig. 4-9: ΔK_{th}-values according to various recommendations

(6) To demonstrate some consequences of the use of these ΔK_{th}-values, fig. 4-10 gives $\Delta\sigma_D$-values calculated with the initial crack sizes

$$2\,a = D + 2 \cdot 5\,\text{mm} \qquad (4\text{-}3)$$

where D is the diameter of the head of the rivet and $\Delta K_{th} = 4\,\text{Mpa}\sqrt{m}$ is assumed. Fig. 4-11 gives the $\Delta\sigma_D$-values for single angles, calculated according to the recommendation of BS PD-6493 for ΔK_{th} - R.

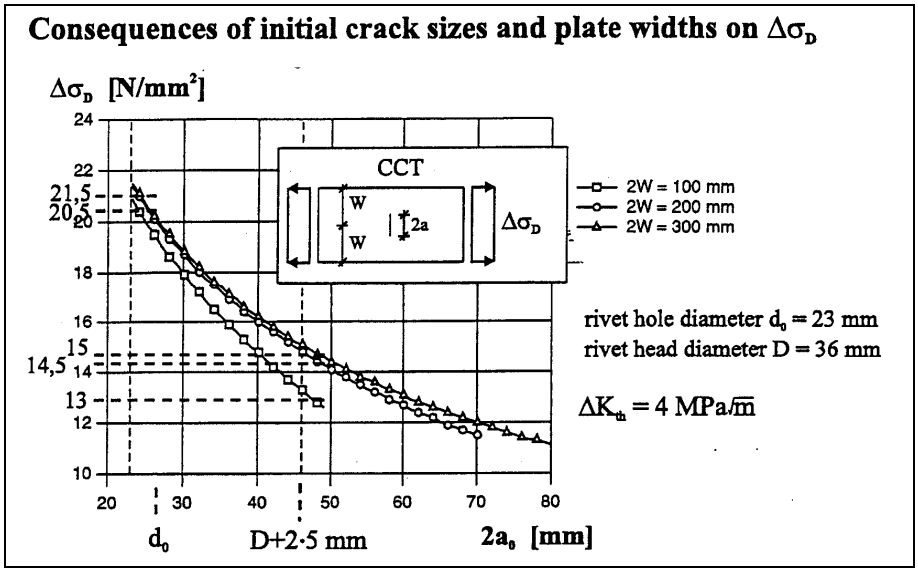


Fig. 4-10: $\Delta\sigma_D$-values in dependence of the crack-size a_0 and the plate width w for $\Delta K_{th} = 4\,\text{Mpa}\sqrt{m}$

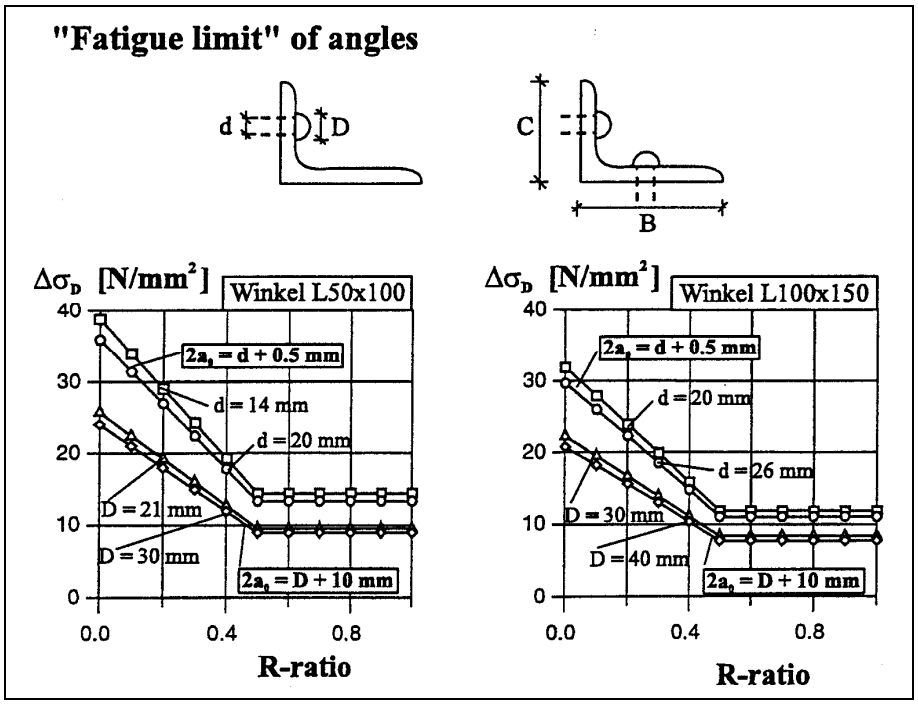


Fig. 4-11: $\Delta\sigma_D$-values for angles using the ΔK_{th}-R-function from BS PD-6493

4.1.2.5 Partial failure checks for redundancies

(1) Partial failure checks of built up cross-sections to identify redundancies should be performed for the ultimate limit state in the following way:

1. a single plate element of the cross-section is assumed to be cracked, so that all the other elements shall resist the force from that element

2. the stresses in all the other elements should not exceed the permissible stress

$$\sigma_R = \frac{f_y}{\gamma_{M0}} = \frac{f_y}{1.10} \tag{4-4}$$

(2) In case the threshold check and the safety check according to (1) is not fulfilled for failure critical components, a fracture mechanical safety check is necessary.

(3) Fig. 4-12 indicates in what way the multiple plate composition of the built up cross-section may control the hazard of brittle failure.

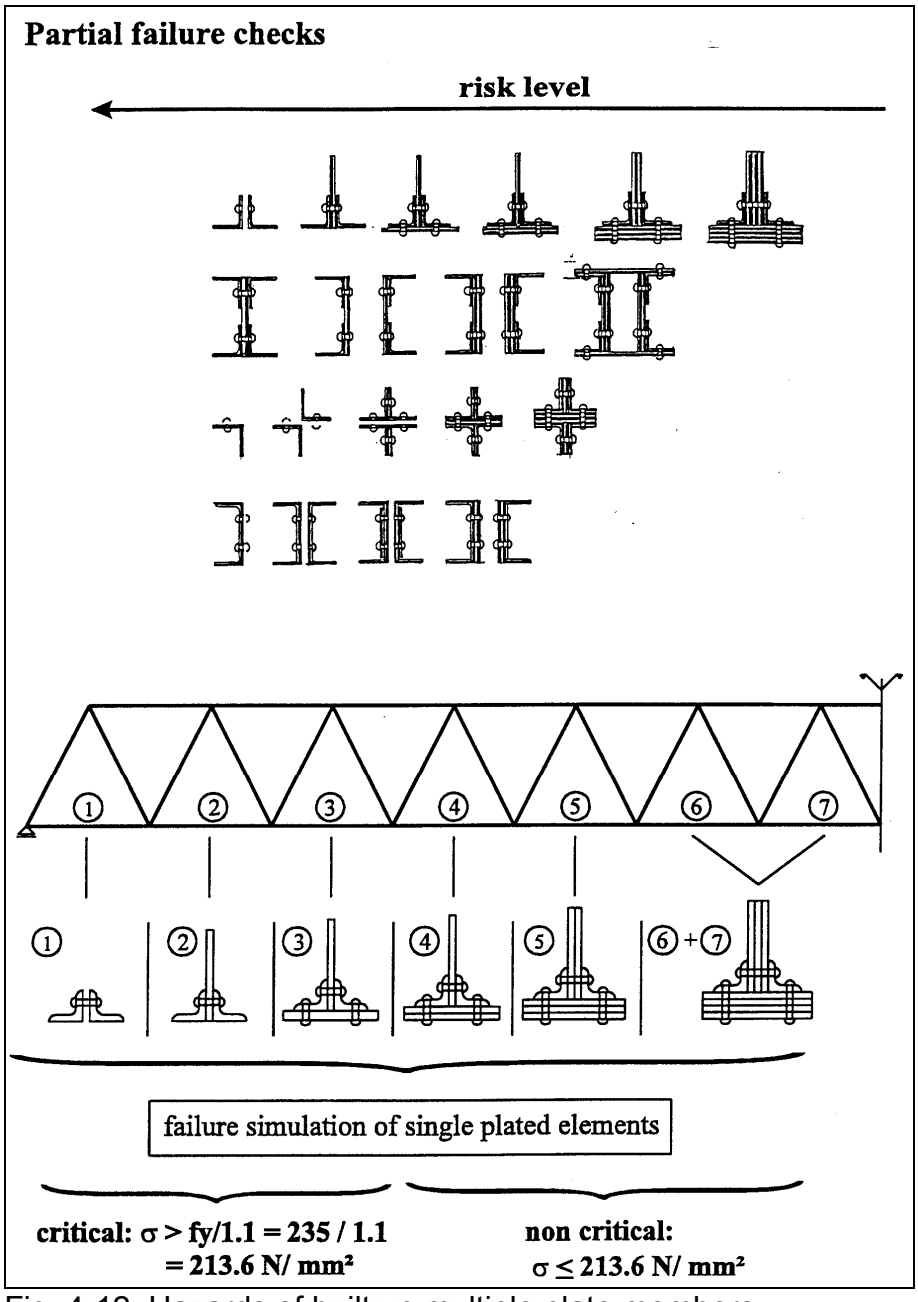


Fig. 4-12: Hazards of built up multiple plate members

4.1.3 Material check and evaluation

4.1.3.1 Type of material

(1) Sampling should be made from the failure-critical components by drilling with a pod, see fig. 4-13. The circular specimens (RCT-specimen) have a diameter of 60 to 76 mm and may be used to determine as a minimum

- the true stress-strain curve and f_y and f_u
- the J-values at the lowest temperature to be considered.

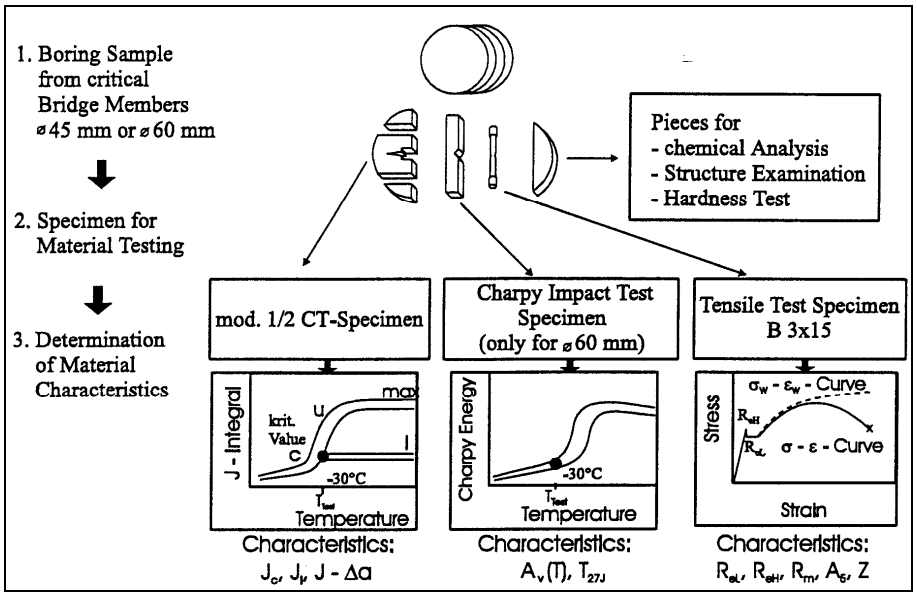


Fig. 4-13: Circular specimen for material evaluations

(2) The relevant type of old steel according to the production method may be taken from fig. 4-14.

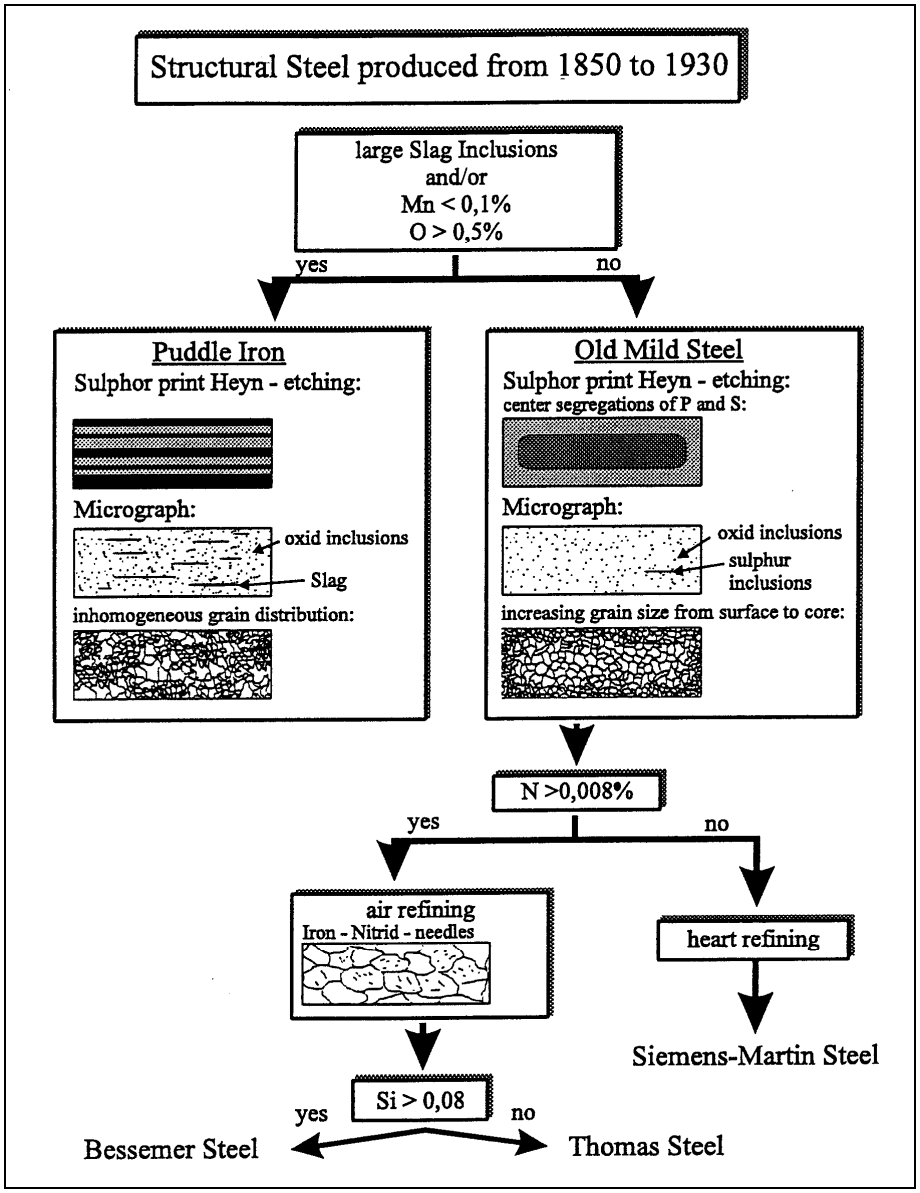


Fig. 4-14: Identification scheme for old steels

4.1.3.2 Strength and toughness properties

(1) Strength and toughness properties may be determined for the individual case or from statistics gained from the evaluation of many material tests from riveted steel bridges built with S235 in about the year 1900.

(2) Fig. 4-15 gives some values from such statistics.

	R_{eL}	R_m	R_{eL}	R_m	A	Z	J_{Mat}	J_{Mat}
T [°C]	-30	-30	0	0	0	0	-30	0
Typ	Log.	Log.	Log.	Log.	ND	ND	Weib.	Weib.
$X_{0,05}$	257	385	248	374	26	57	17	30
$X_{0,50}$	310	466	293	423	34	66	62	91

Log. = Log-normal distributed; ND = normal distributed
Weib. = Weibull distributed (3 parametric); R_{eL} = yield strength; R_m = tensile strength;
A = fracture elongation; Z = reduction of area, J_{Mat} = fracture toughness

Fig. 4-15: Statistical material data for old steel bridges

(3) The 5% fractiles for R_{el} and J_{Mat} given in fig. 4-15 may be used for fracture mechanics assessment, if no other information is available.

4.1.4 Assessment of the "safe service period"

4.1.4.1 General

(1) The assessment of the "safe service period" for components of old riveted steel bridges is performed with the following steps:

1. Definition of the initial crack size a_0 at the failure critical section that is detectible.

2. Determination of the critical crack size a_{crit}, for which the member has reached the required minimum safety for the relevant combination of actions for the lowest ambient temperature.

3. Determination of the maximum "safe service period" T_p for crack growth $\Delta a = a_{crit} - a_0$ and comparison with the regular inspection intervals T_{insp}.

(2) The relevance of "damage tolerance" for the partial factors $\gamma_{Ff} \cdot \gamma_{Mf}$ used in conventional fatigue checks may be taken from fig. 4-16, where n is the nominal number of stress cycles during the full fatigue life $T_{service}$ of the bridge and design values n_d depend on the following cases:

1. "Damage tolerance" applicable
2. "Damage tolerance" not applicable, however

   2a: Loading $\Delta\sigma_i$ and cycles n_i are controlled
   2b: only the time of fatigue life $T_{service}$ is controlled.

typ of construction		n_d/n	n_d
damage tolerant		1,5	$5{,}9 \cdot 10^7$
non damage tolerant	monitored load	2,25	$8{,}8 \cdot 10^7$
	non monitored load	6,7 - 15	$2{,}63 - 5{,}90 \cdot 10^8$

Fig. 4-16: Relevance of "damage tolerance" for the partial factors for conventional fatigue checks (right column: n = 3.927×10^7).

4.1.4.2 The J-integral assessment

(1) The J-integral safety assessment follows the procedure given in fig. 4-17 and is performed in various steps

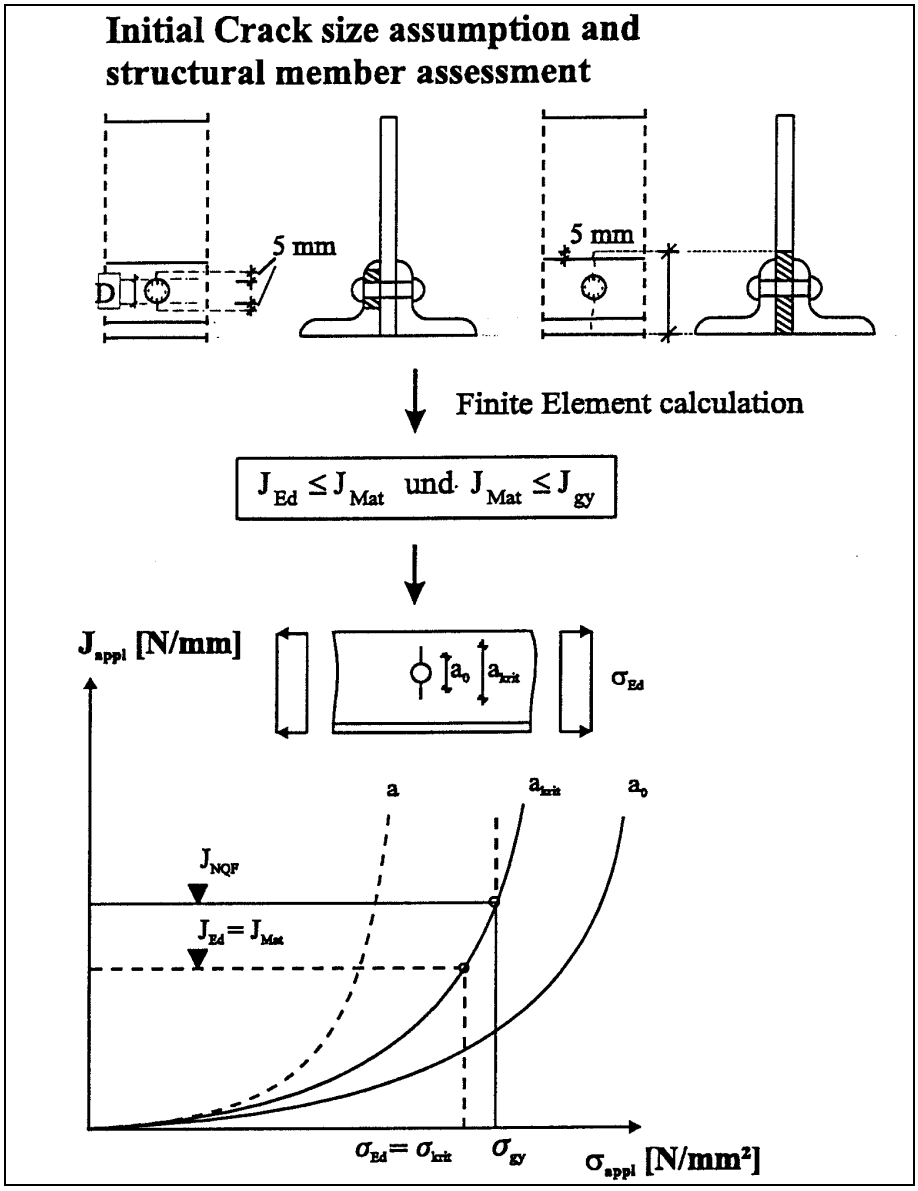


Fig. 4-17: Procedure to determine a_{crit}

(2) The steps for the assessment are the following:

1. According to fig. 4-17, a fracture mechanical model (e.g. CCT) with the initial crack size a_0 (composed of a hole with two lateral cracks) is assumed.

2. For this crack size, the J_{appl}-Integral curve versus the applied nominal stresses σ_{appl} is calculated.

3. The crack size is then increased to $a = a_0 + \Delta a$ yielding to another J_{appl} - σ_{appl}-curve, and this procedure is varied until a J_{appl} - σ_{appl}-curve is found, for which the J_{appl}-value meets the material value J_{mat} at the design value of the nominal stress $\sigma_{appl} = \sigma_{Ed}$.

   The value a pertaining to this curve is the critical crack size a_{crit}.

4. For the applied stress σ_{gy} that effects net section yielding the associated value $J_{appl} = J_{gy}$ is determined and compared with the material toughness J_{MAT}, see fig. 4-18.

If $J_{MAT} \geq J_{gy}$ (4-5)

then the use of nominal stresses σ_{Ed} is justified.

If $J_{MAT} < J_{gy}$ (4-6)

then σ_{Ed} should be increased to include residual stresses (e.g. 100 Mpa) and stresses due to restraints and deformations.

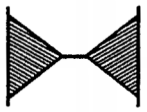
Yielding pattern	Failure Mode	Design values
	brittle fracture before net-section yielding	applied stress distribution in the net section + residual stresses + restraints
	ductile fracture with or after net-section yielding	applied nominal stress distribution in the net section

Fig. 4-18: Definition of failure mode and of applied stresses σ_{Ed} depending on ductility.

5. From a_{crit} and a_0 the maximum value of crack growth Δa due to fatigue should be determined. Using the fatigue load for the structure the "safe service period" T_p possible to effect the crack growth Δa can be calculated. T_p corresponds with a certain number n_p of stress cycles.

6. The "safe service period" T_p should be more than 1.5 times the time interval T_{insp} between regular inspections, see fig. 4-2.

(3) This procedure may be applied by using assessment aids given in the following section.

4.1.4.3 Assessment aids for the fracture mechanics assessment

4.1.4.3.1 General

(1) The following assessment aids refer to the stepwise assessment procedure given in 4.1.4.2.

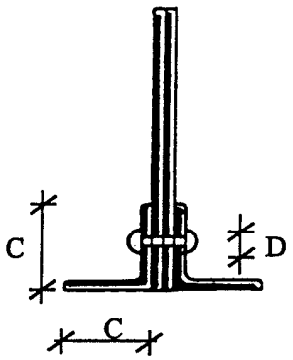
(2) The assessment aids are based on the following:

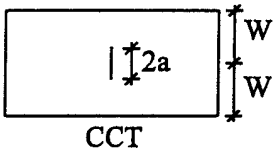
1. All structural details are represented by the following basic fracture mechanics models:

   - Central Crack Tension element (CCT)
   - Double Edge Crack Tension element (DECT)
   - Single Edge Crack Tension element (SECT),

   see example in fig. 4-19.

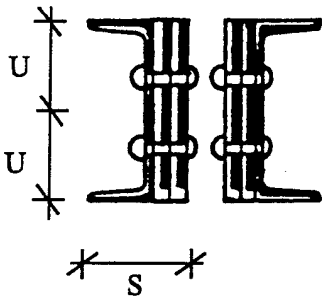
Structural Part: Angle

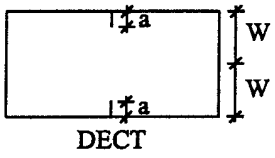




Geometrical Data
Initial Crack Size: $a_0 = (D+10)/2$
max. allowable Crack Size: $a_{max} = C/2$
Plate Width: $W = 1{,}1\ C/2$

Structural Part: U-Profile



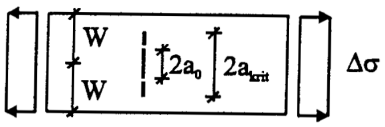


Geometrical Data
Initial Crack Size: $a_0 = (D+10)/2$
max. allowable Crack Size: $a_{max} = U/2$
Plate Width: $W = (U + 0.5\ S)/2$

Fig. 4-19: Examples for structural details represented by basic fracture mechanics models

2. The fatigue crack growth Δa may be calculated with the same fracture mechanics model as for a_{crit}, see example in fig. 4-20.

$\Delta\sigma^3 \cdot N$ – values



$$\Delta\sigma^3 \cdot \Delta N = \left[\left(a_{krit}\right) - \left(a_0\right)\right] \cdot 10^{-11}$$

a [mm] \ W [mm]	40	60	80 ↓	100
5	8.647943	19.266760	30.257930	41.474740
10	9.762876	20.416210	31.419230	42.641480
15	10.203230	20.901860	31.920640	43.150090
20	10.419290	21.170010	32.207600	43.445730
a_0 → 25	10.528390	21.333840	32.392510	43.640520
30	10.579330	21.437810	32.519000	43.777840
35	10.598210	21.503890	32.608150	43.878570
Δa 40		21.544750	32.671770	43.954210
45		21.568480	32.717080	44.011720
50		21.580730	32.748910	44.055650
a_{krit} → 55		21.585660	32.770680	44.089170
60			32.784930	44.114520
65			32.793600	44.133410
70			32.798270	44.147180
75			32.800220	44.156890
80				44.163430
85				44.167510
90				44.169760
95				44.170720

Fig. 4-20: Calculation of crack growth Δa

3. For each basic fracture mechanics model, the attainment of J_{gy} is assumed to be the ultimate limit state of the cracked element. Fig. 4-21 shows the J_{appl}-σ_{appl} curves for various a/w-ratios that do not have a significant strength increase for $\sigma_{appl} > \sigma_{gy}$.

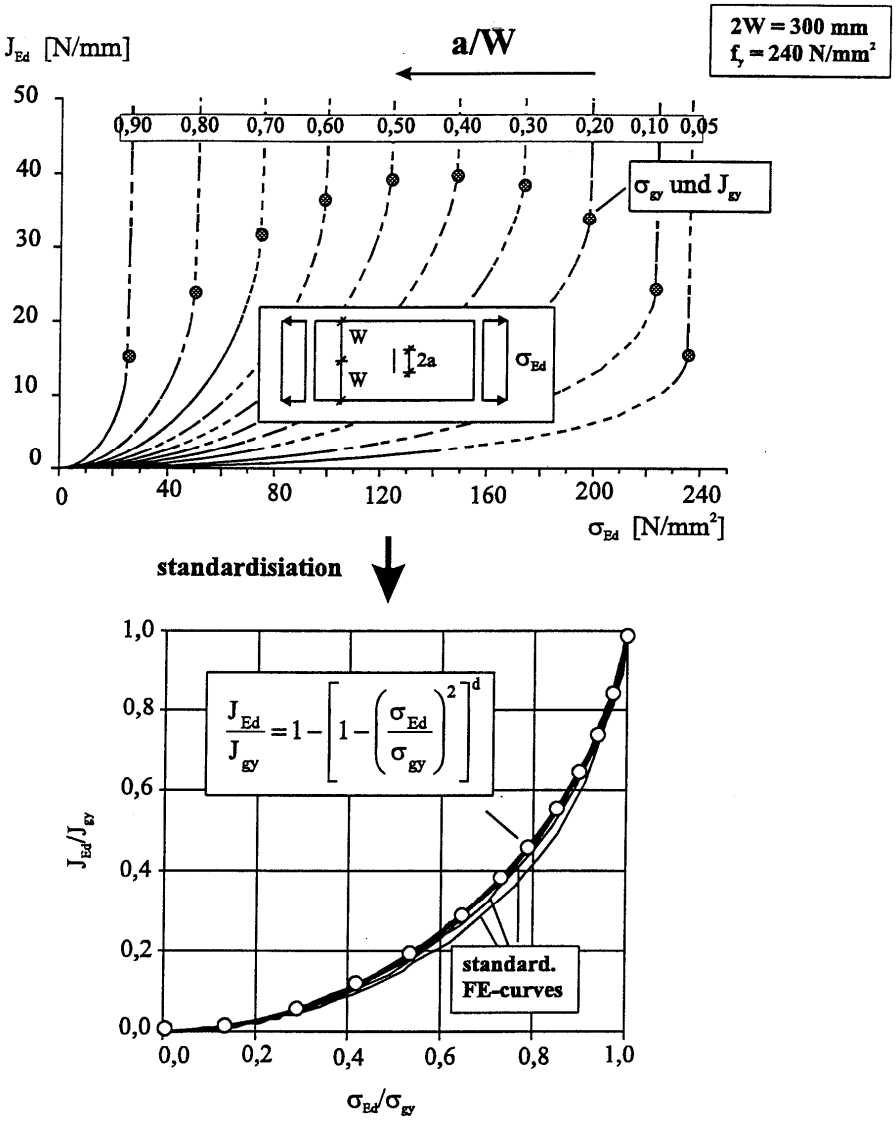
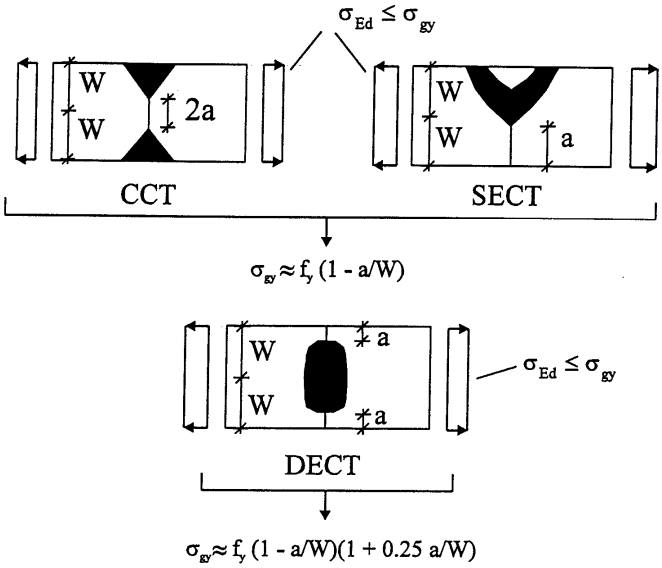


Fig. 4-21: J_{appl}-σ_{appl}-curves and standardised curves for different a/w-ratios

4. The limit values σ_{gy} and J_{gy} may be easily described by formulae for the basic fracture mechanics models, see fig. 4-22.

Definition of σ_{gy}



Definition of J_{gy}

$$J_{gy} = \frac{2W \cdot f_y^2 \cdot k_1 \cdot a/W \cdot [1 - (a/W)^{k_2}] \cdot k_3}{E \cdot (a/W + k_4)}$$

Fig. 4-22: Definition of the limit values σ_{gy} and J_{gy}

5. The function J_{appl}-σ_{appl} below the limit values σ_{gy} and J_{gy} can be described by standard functions, see fig. 4-21, so that complete sets of calculation formulae to determine critical crack sizes a_{crit} can be derived.

4.1.4.3.2 Reliability of the assessment aids

(1) Fig. 4-23 gives a comparison between the results of the formulae and more accurate FEM-calculations.

$$J_{Ed} = J_{gy}\left[1-\left(1-\left(\frac{\sigma_{Ed}}{\sigma_{gy}}\right)^2\right)^d\right]$$

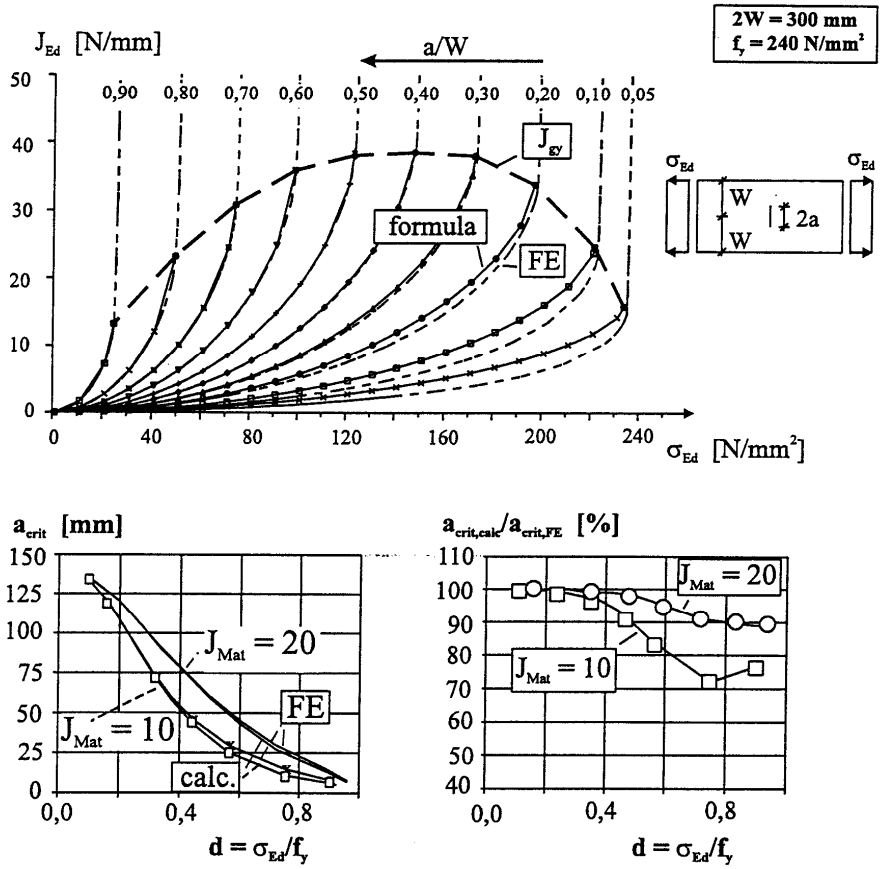


Fig. 4-23: Comparison of results of formulae and FEM-calculations

(2) In Fig. 4-24 a comparison is given between the failure loads from experiments with large scale cracked test pieces F_{exp} and the failure loads predicted by the formulae

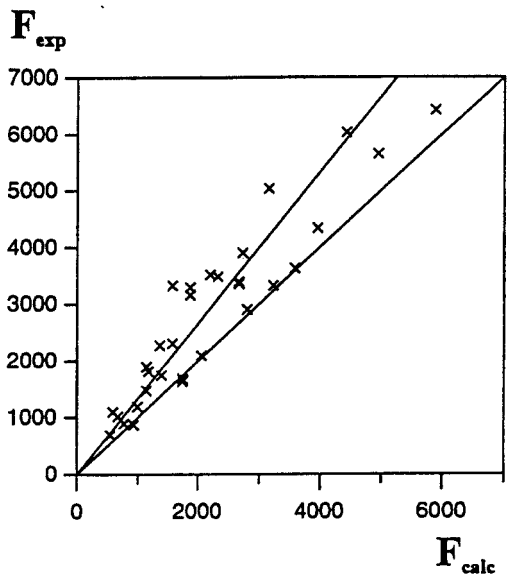


Fig. 4-24: Model uncertainty of the formulae for failure loads

(3) Fig. 4-25 gives the distribution function for the ratios F_{exp}/F_{calc} and the justification for the partial factor γ_M = 1.0, that may be applied.

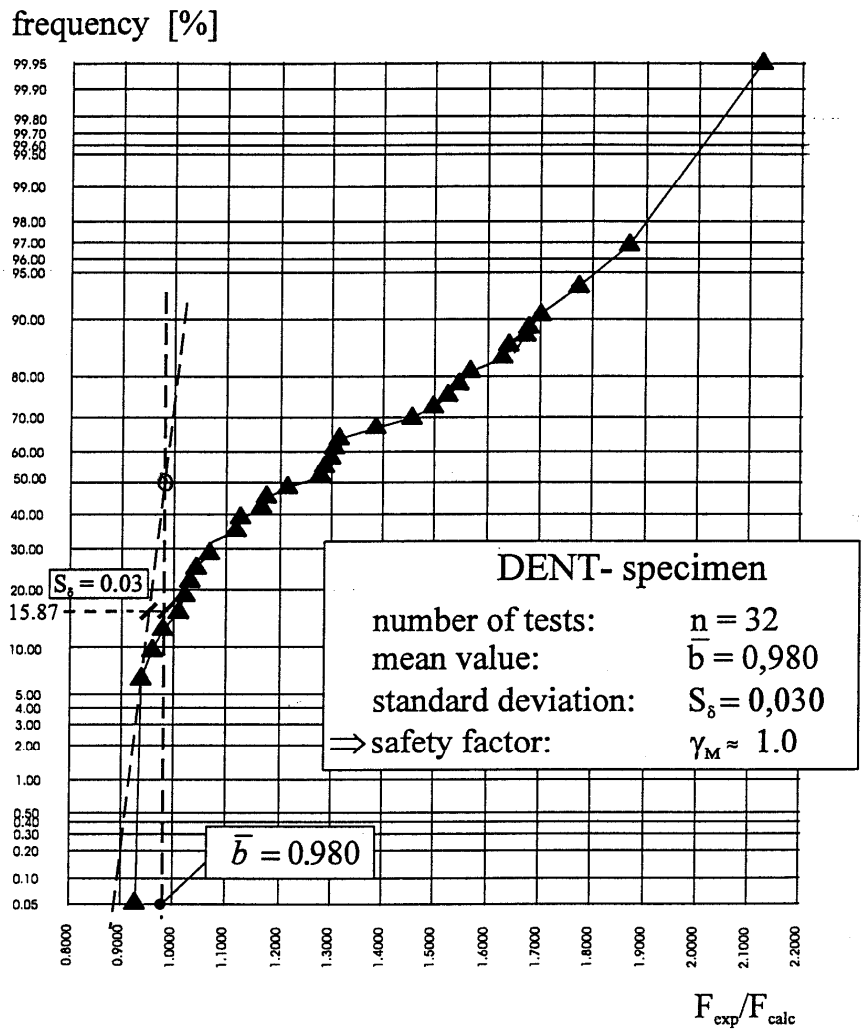


Fig. 4-25: Determination of partial factor γ_M for the application of the assessment formulae

4.1.5 Design tables

(1) A complete set of built up members and their allocation to fracture mechanics models is given in tables A.1-A.9.

(2) Tabulated values and graphs for determining a_{crit} for given values J_{Mat} and f_y and the geometrical values for the basic fracture mechanics models are presented in tables B.1-B.5 (plate with centre crack), in tables C.1-C.5 (plate with double edge crack) and tables D.1-D.5 (plate with single edge crack).

(3) Values to determine n_p for the "safe service period" for a given damage equivalent stress range $\Delta\sigma_e$ are given in tables B6-B7 (plate with centre crack), in tables C.6-C.7 (plate with double edge crack) and tables D.6 – D.7 (plate with single edge crack).

Tables A

Relevant models for the determination of the critical crack sizes a_{crit} and maximum allowable load cycles $N(a_{crit})$ for cross sections of old riveted steel bridges

In the following tables the variables are:

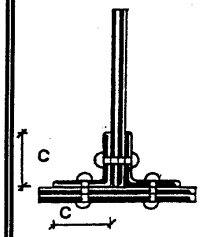
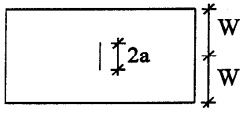
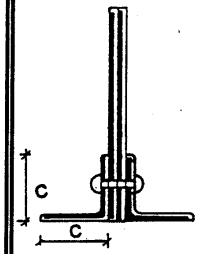
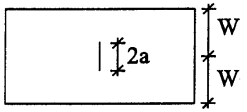
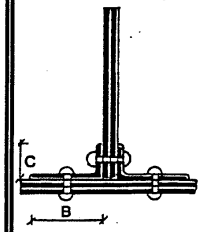
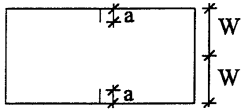
a_0 = minimum detectable crack size (initial crack size) [mm] which may have been overlooked at an inspection

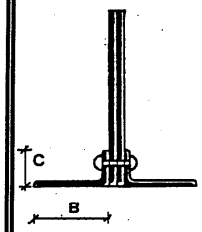
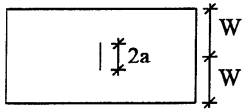
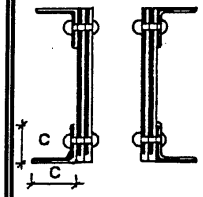
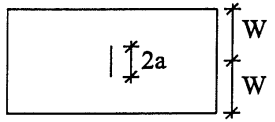
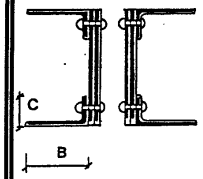
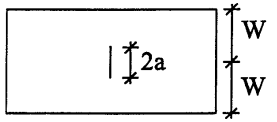
a_{max} = maximum crack size [mm] for which the member will fail
Boandary condition: $a_{crit} \leq a_{max}$

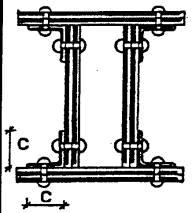
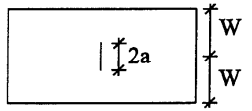
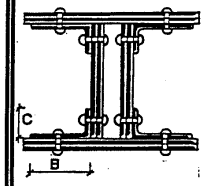
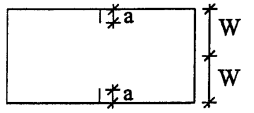
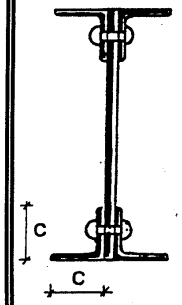
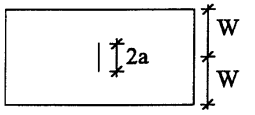
n = number of available tension chord plates

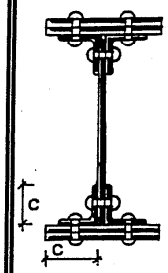
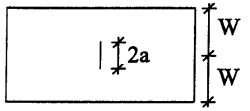
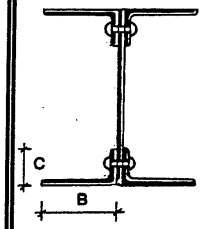
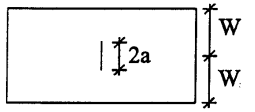
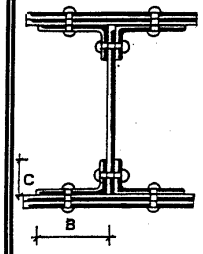
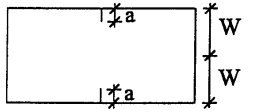
m = number of available web plates

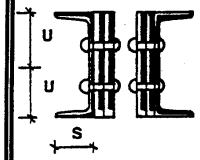
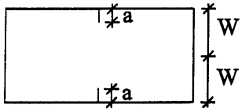
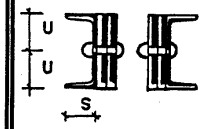
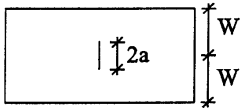
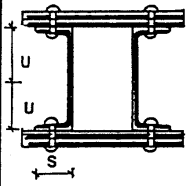
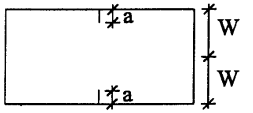
D = rivet head diameter

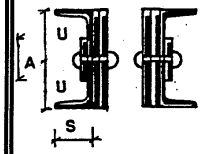
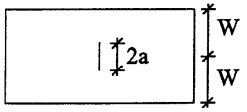
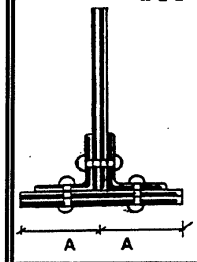
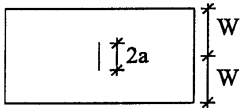
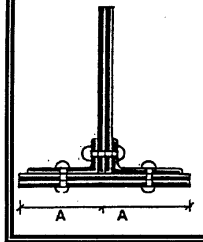
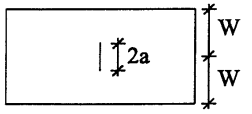
Cross section	Relevant Model and Dimensions	crit. Crack size acc. to:	max. allow. Load cycles acc. to:
Structural part: Angles			
valid for: m ≥ 1, n ≥ 1 	 Geometrical data: Initial crack size: a_0=(D+10)/2 max. allow. Crack size: a_{max} = C/2 Plate width: W = C/2	table B.2 - B.5	table B..6 - B.7
valid for: m ≥ 1 	 Geometrical data: Initial crack size: a_0=(D+10)/2 max. allow. Crack size: a_{max} = C/2 Plate width: W = 1,1 ·C/2	table B.2 - B.5	table B.6 - B.7
valid for: m ≥ 1, n ≥ 1 	 Geometrical data: Initial crack size: a_0=(D+10)/2 max. allow. Crack size: a_{max} = C/2 Plate width: W = (C + B)/2	table C.2 - C.5	table C.6 - C.7

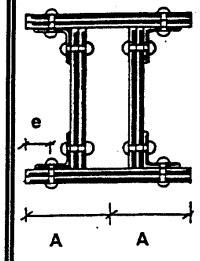
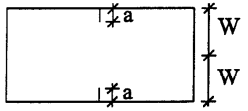
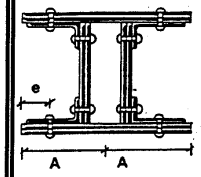
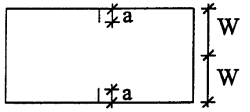
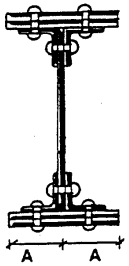
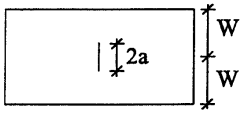
Cross section	Relevant Model and Dimensions	crit. Crack size acc. to:	max. allow. Load cycles acc. to:
Structural part: Angles			
valid for: m ≥ 1 	 Geometrical data: Initial crack size: a_0=(D+10)/2 max. allow. Crack size: a_{max} = C/2 Plate width: W = 1,2 · C/2	table B.2 - B.5	table B.6–B.7
valid for: m ≥ 1 	 Geometrical data: Initial crack size: a_0=(D+10)/2 max. allow. Crack size: a_{max} = C/2 Plate width: W = 1,1·C/2	table B.2 - B.5	table B.6 - B.7
valid for: m ≥ 1 	 Geometrical data: Initial crack size: a_0=(D+10)/2 max. allow. Crack size: a_{max} = C/2 Plate width: W = 1,2 · C/2	table B.2 - B.5	table B.6 - B.7

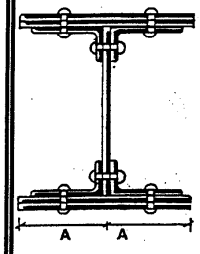
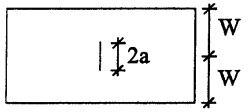
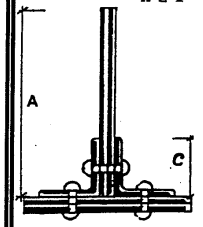
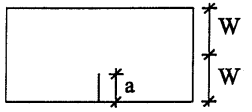
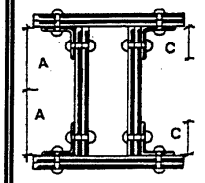
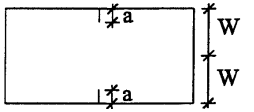
Cross section	Relevant Model and Dimensions	crit. Crack size acc. to:	max. allow. Load cycles acc. to:
Structural part: Angles			
valid for: m ≥ 1 n ≥ 1 	 Geometrical data: Initial crack size: a_0=(D+10)/2 max. allow. Crack size: a_{max} = C/2 Plate width: W = C/2	table B.2 - B.5	table B.6 - B.7
valid for: m ≥ 1 n ≥ 1 	 Geometrical data: Initial crack size: a_0=(D+10)/2 max. allow. Crack size: a_{max} = C/2 Plate width: W = (C + B)/2	table C.2 - C.5	table C.6 - C.7
	 Geometrical data: Initial crack size: a_0=(D+10)/2 max. allow. Crack size: a_{max} = C/2 Plate width: W = 1,1 · C/2	table B.2 - B.5	table B.6 - B.7

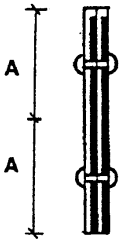
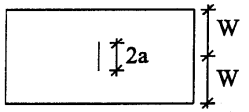
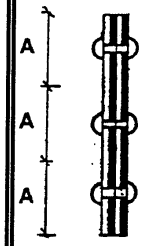
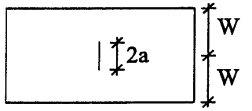
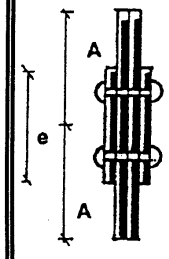
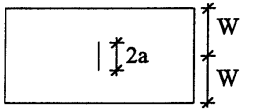
Cross section	Relevant Model and Dimensions	crit. Crack size acc. to:	max. allow. Load cycles acc. to:
Structural part: Angles			
valid for: $n \geq 1$ 	 <u>Geometrical data:</u> Initial crack size: $a_0=(D+10)/2$ max. allow. Crack size: $a_{max} = C/2$ Plate width: $W = C/2$	table B.2 - B.5	table B.6 - B.7
	 <u>Geometrical data:</u> Initial crack size: $a_0=(D+10)/2$ max. allow. Crack size: $a_{max} = C/2$ Plate width: $W = 1{,}2 \cdot C/2$	table B.2 - B.5	table B.6 - B.7
valid for: $n \geq 1$ 	 <u>Geometrical data:</u> Initial crack size: $a_0=(D+10)/2$ max. allow. Crack size: $a_{max} = C/2$ Plate width: $W = (C + B)/2$	table B.2 - B.5	table B.6 - B.7

Cross section	Relevant Model and Dimensions	crit. Crack size acc. to:	max. allow. Load cycles acc. to:
Structural part: U-Profile			
valid for: $m \geq 0$ 	 <u>Geometrical data:</u> Initial crack size: $a_0=(D+10)/2$ max. allow. Crack size: $a_{max} = U/2$ Plate width: $W=(U + 0{,}5 \cdot S)/2$	table C.2 - C.5	table C.6 - C.7
valid for: $m \geq 0$ 	 <u>Geometrical data:</u> Initial crack size: $a_0=(D+10)/2$ max. allow. Crack size: $a_{max} = U$ Plate width: $W = U + S$	table B.2 - B.5	table B.6 - B.7
valid for: $n \geq 0$ 	 <u>Geometrical data:</u> Initial crack size: $a_0=(D+10)/2$ max. allow. Crack size: $a_{max} = S$ Plate width: $W = (U + S)$	table C.2 - C.5	table C.6 - C.7

Cross section	Relevant Model and Dimensions	crit. Crack size acc. to:	max. allow. Load cycles acc. to:
Structural part: U-Profile			
valid for: m ≥ 0 	 Geometrical data: Initial crack size: a_0=(A+10)/2 max. allow. Crack size: a_{max} = U Plate width: W = U + S	table B.2 - B.5	table B.6 - B.7
Structural part: Tension chord			
valid for: m ≥ 0 n ≥ 1 	 Geometrical data: Initial crack size: a_0=(D+10)/2 max. allow. Crack size: a_{max} = A/2 Plate width: W = n · A/2 n = 1 out of the Gussets	table B.2 - B.5	table B.6 - B.7
valid for: m ≥ 0 n ≥ 1 	 Geometrical data: Initial crack size: a_0=(D+10)/2 max. allow. Crack size: a_{max} = A/2 Plate width: W = n · A/2 n = 1 out of the Gussets	table B.2 - B.5	table B.6 - B.7

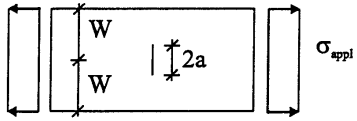
Cross section	Relevant Model and Dimensions	crit. Crack size acc. to:	max. allow. Load cycles acc. to:
Structural part: Tension chord			
valid for: m ≥ 1 n ≥ 1 	 Geometrical data: Initial crack size: a_0=e+D/2+5 max. allow. Crack size: a_{max} = A Plate width: W = n · A n = 1 out of the Gussets	table C.2 - C.5	table C.6 - C.7
valid for: m ≥ 1 n ≥ 1 	 Geometrical data: Initial crack size: a_0=e+D/2+5 max. allow. Crack size: a_{max} = A Plate width: W = n · A n = 1 out of the Gussets	table C.2 - C.5	table C.6 - C.7
valid for: m ≥ 1 n ≥ 1 	 Geometrical data: Initial crack size: a_0=(D+10)/2 max. allow. Crack size: a_{max} = A/2 Plate width: W = n · A/2 n = 1 out of the Gussets	table B.2 - B.5	table B.6 - B.7

Cross section	Relevant Model and Dimensions	crit. Crack size acc. to:	max. allow. Load cycles acc. to:
Structural part: Tension chord			
valid for: m ≥ 1 n ≥ 1 	 Geometrical data: Initial crack size: a_0=(D+10)/2 max. allow. Crack size: a_{max} = A/2 Plate width: W = n · A/2 n = 1 out of the Gussets	table B.2 - B.5	table B.6 - B.7
Structural part: Web			
valid for: m ≥ 0 n ≥ 1 	 Geometrical data: Initial crack size: a_0=D+5 max. allow. Crack size: a_{max} = A Plate width: W = m · A m = 1 out of the Gussets	table D.2 - D.5	table D.6 - D.7
valid for: m ≥ 0 n ≥ 1 	 Geometrical data: Initial crack size: a_0=C+5 max. allow. Crack size: a_{max} = A Plate width: W = m · A m = 1 out of the Gussets	table C.2 - C.5	table C.6 - C.7

Cross section	Relevant Model and Dimensions	crit. Crack size acc. to:	max. allow. Load cycles acc. to:
Structural part: Web			
valid for: m ≥ 1 	 Geometrical data: Initial crack size: a_0=(D+10)/2 max. allow. Crack size: a_{max} = A/2 Plate width: W = m · A/2 m = 1 out of the Gussets	table B.2 - B.5	table B.6 - B.7
valid for: m > 1 	 Geometrical data: Initial crack size: a_0=(D+10) max. allow. Crack size: a_{max} = A/2 Plate width: W = m · A/2 m = 1 out of the Gussets	table B.2 - B.5	table B.6 - B.7
valid for: m > 1 	 Geometrical data: Initial crack size: a_0=(e+10)/2 max. allow. Crack size: a_{max} = A Plate width: W = m · A m = 1 out of the Gussets	table B.2 - B.5	table B.6 - B.7

Tables B

Critical crack sizes a_{crit} and load cycles N(a) for the plate with Center Crack (CCT)



Use of the tables

1. Calculation of the stress relation $d = \sigma_{appl}/f_y$

2. Evaluation of the critical crack size for d and the half plate width W (the evaluation of the relevant plate width W for the considered structural part is made according tables A)

3. Calculation of the equivalent stress range $\Delta\sigma_e$

4. Evaluation of the tabulated values $N(a) \cdot \Delta\sigma_e^3 \cdot 10^{-11}$ for a_0 and a_{crit} for the half plate width W

5. Evaluation of the number of possible load cycles from a_0 to a_{krit}:

$$\Delta N = \frac{N(a_{krit})\cdot\Delta\sigma_e^3\cdot 10^{-11} - N(a_0)\cdot\Delta\sigma_e^3\cdot 10^{-11}}{\Delta\sigma_e^3\cdot 10^{-11}}$$

Interim values for a or W may be interpolated.

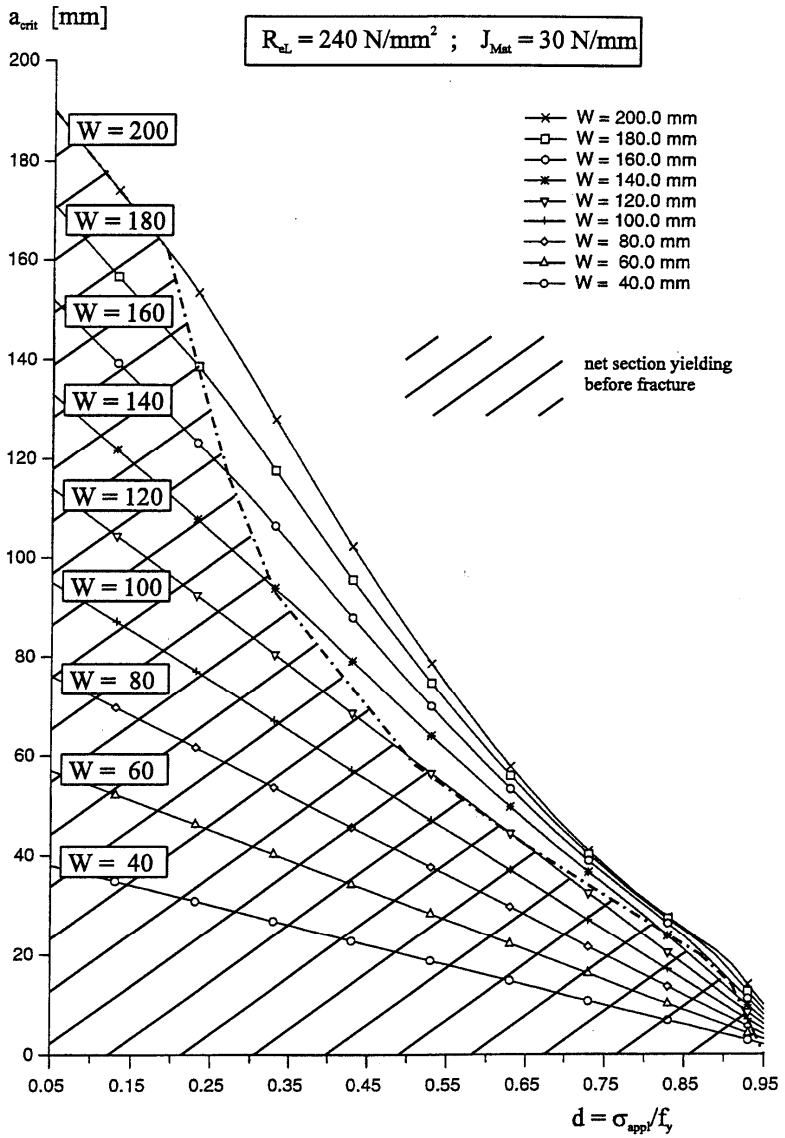
The tables for the evaluation of the number of load cycles N are based on the *Paris* crack growth relation (material constants: $C = 4\cdot 10^{-13}$ and $m = 3$).

Critical crack sizes a_{crit} [mm]

The critical crack sizes given in the following table and diagram are calculated for a fracture toughness value J_{Mat} = 30 N/mm and a yield strength value f_y = 240 N/mm².

The cases where net section yielding will occur before fracture are underlined.

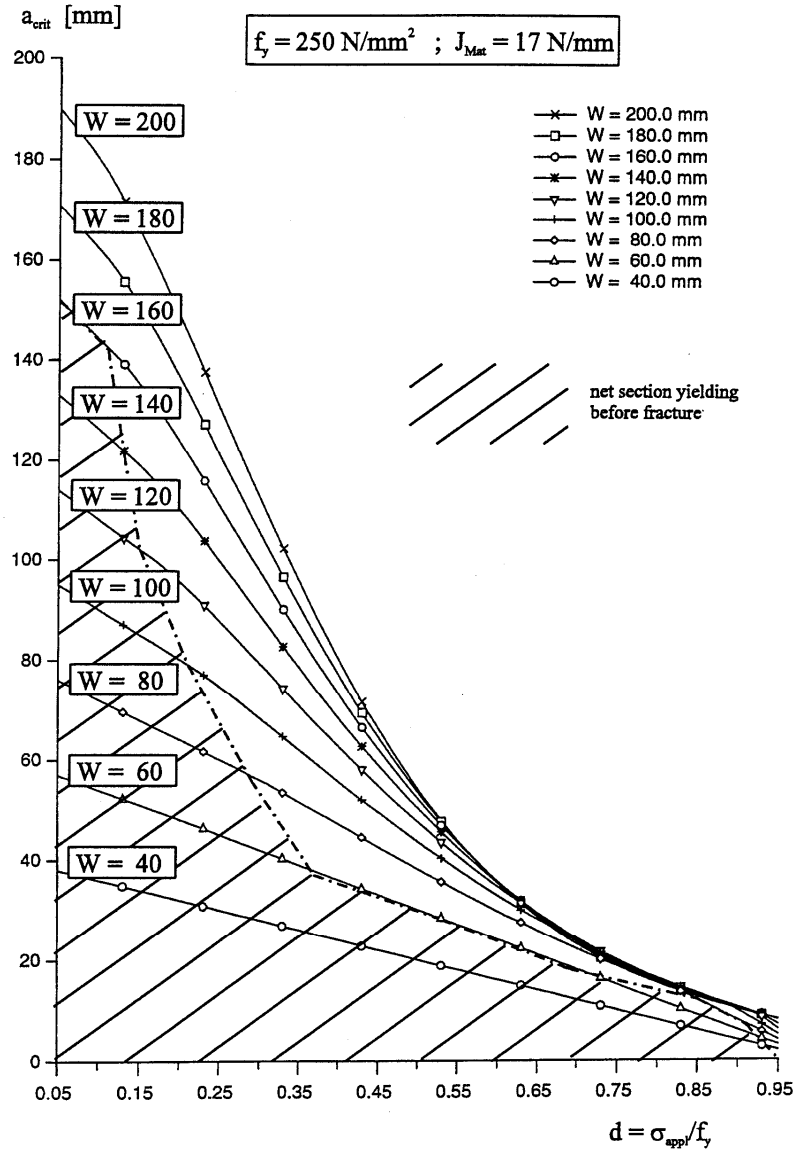
W [mm] / d [-]	40	60	80	100	120	140	160	180	200
0.05	38	57	76	95	114	133	152	171	190
0.07	37	55	74	93	111	130	148	167	186
0.09	36	54	72	91	109	127	145	163	182
0.11	35	53	71	89	106	124	142	160	178
0.13	34	52	69	87	104	121	139	156	174
0.15	34	51	68	85	102	119	136	153	170
0.17	33	49	66	83	99	116	132	149	166
0.19	32	48	64	81	97	113	129	145	162
0.21	31	47	63	79	94	110	126	142	157
0.23	30	46	61	77	92	107	123	138	153
0.25	30	45	60	75	90	105	120	134	148
0.27	29	43	58	73	87	102	116	130	143
0.29	28	42	56	71	85	99	113	126	138
0.31	27	41	55	69	82	96	109	122	133
0.33	26	40	53	67	80	93	106	117	128
0.35	26	39	52	65	78	90	102	113	122
0.37	25	37	50	63	75	88	98	108	117
0.39	24	36	48	61	73	85	95	104	112
0.41	23	35	47	59	70	82	91	99	107
0.43	22	34	45	57	68	79	87	95	102
0.45	22	33	44	55	66	75	84	91	97
0.47	21	31	42	53	63	72	80	86	92
0.49	20	30	40	50	61	69	76	82	87
0.51	19	29	39	49	58	66	73	78	82
0.53	18	28	37	47	56	63	69	74	78
0.55	18	27	36	45	53	60	66	70	74
0.57	17	25	34	43	51	58	62	66	69
0.59	16	24	32	41	49	55	59	63	65
0.61	15	23	31	38	46	52	56	59	61
0.63	14	22	29	37	44	49	53	55	57
0.65	14	21	28	35	42	46	50	52	54
0.67	13	19	26	33	39	44	47	49	50
0.69	12	18	24	30	37	41	44	46	47
0.71	11	17	23	29	34	39	41	43	43
0.73	10	16	21	26	32	36	38	40	40
0.75	10	15	20	25	30	34	36	37	37
0.77	9	13	18	23	27	31	33	34	35
0.79	8	12	16	20	25	29	31	32	32
0.81	7	11	15	19	22	26	28	29	30
0.83	6	10	13	17	20	23	26	27	27
0.85	6	9	12	15	18	21	23	24	25
0.87	5	7	10	12	15	18	20	22	23
0.89	4	6	8	11	13	15	17	19	20
0.91	3	5	7	8	10	12	14	16	17
0.93	2	4	5	7	8	9	11	12	14
0.95	2	3	4	5	6	7	8	9	10



The critical crack sizes given in the following table and diagram are calculated for a fracture toughness value J_{Mat} = 17 N/mm and a yield strength value f_y = 250 N/mm².

The cases where net section yielding will occur before fracture are underlined.

W [mm] / d [-]	40	60	80	100	120	140	160	180	200
0.05	38	57	76	95	114	133	152	171	190
0.07	37	55	74	93	111	130	148	167	186
0.09	36	54	72	91	109	127	145	163	182
0.11	35	53	71	89	106	124	142	160	177
0.13	34	52	69	87	104	121	139	155	171
0.15	34	51	68	85	102	118	134	150	165
0.17	33	49	66	83	99	115	130	144	158
0.19	32	48	64	81	96	111	125	139	151
0.21	31	47	63	79	93	107	120	133	144
0.23	30	46	61	76	90	103	115	126	137
0.25	30	45	60	74	87	99	110	120	130
0.27	29	43	58	72	84	95	105	114	122
0.29	28	42	56	69	80	91	100	108	115
0.31	27	41	55	67	77	86	94	102	108
0.33	26	40	53	64	74	82	89	96	102
0.35	26	39	51	62	70	78	84	90	95
0.37	25	37	49	59	67	74	80	85	89
0.39	24	36	48	56	64	70	75	79	83
0.41	23	35	46	54	61	66	70	74	77
0.43	22	34	44	51	57	62	66	69	71
0.45	22	33	42	49	54	58	62	64	66
0.47	21	31	40	47	51	55	58	59	61
0.49	20	30	38	44	48	51	54	55	56
0.51	19	29	37	42	46	48	50	51	51
0.53	18	28	35	40	43	45	46	47	47
0.55	18	27	33	37	40	42	43	43	43
0.57	17	25	32	35	38	39	40	40	40
0.59	16	24	30	33	35	36	37	37	36
0.61	15	23	28	31	33	34	34	34	33
0.63	14	22	27	29	31	31	31	31	31
0.65	14	21	25	27	29	29	29	28	28
0.67	13	19	24	26	26	27	26	26	26
0.69	12	18	22	24	25	25	24	24	24
0.71	11	17	21	22	23	23	22	22	22
0.73	10	16	19	21	21	21	21	20	20
0.75	10	15	18	19	19	19	19	19	18
0.77	9	13	17	18	18	18	17	17	17
0.79	8	12	16	16	17	16	16	16	15
0.81	7	11	14	15	15	15	15	14	14
0.83	6	10	13	14	14	14	14	13	13
0.85	6	9	12	13	13	13	12	12	12
0.87	5	7	10	11	12	12	11	11	11
0.89	4	6	8	10	11	11	10	10	10
0.91	3	5	7	9	9	9	9	9	9
0.93	2	4	5	7	8	8	8	8	8
0.95	2	3	4	5	6	7	7	7	7



Load cycles N(a)

tabulated values = $N \cdot \Delta\sigma_e^3 \cdot 10^{-11}$

W [mm] / a [mm]	40	60	80	100	120
5	8.647943	19.266760	30.257930	41.474740	52.846570
10	9.762876	20.416210	31.419230	42.641480	54.016250
15	10.203230	20.901860	31.920640	43.150090	54.528720
20	10.419290	21.170010	32.207600	43.445730	54.829010
25	10.528390	21.333840	32.392510	43.640520	55.029160
30	10.579330	21.437810	32.519000	43.777840	55.172430
35	10.598210	21.503890	32.608150	43.878570	55.279590
40		21.544750	32.671770	43.954210	55.362050
45		21.568480	32.717080	44.011720	55.426660
50		21.580730	32.748910	44.055650	55.477890
55		21.585660	32.770680	44.089170	55.518760
60			32.784930	44.114520	55.551410
65			32.793600	44.133410	55.577460
70			32.798270	44.147180	55.598130
75			32.800220	44.156890	55.614390
80				44.163430	55.627010
85				44.167510	55.636630
90				44.169760	55.643800
95				44.170720	55.648940
100					55.652470
105					55.654690
110					55.655960
115					55.656530

tabulated values = $N \cdot \Delta\sigma_e^3 \cdot 10^{-11}$

W [mm] a [mm]	140	160	180	200
5	64.333240	75.909210	87.557370	99.264920
10	65.504640	77.081760	88.730680	100.438700
15	66.019440	77.598080	89.247940	100.956800
20	66.322530	77.902980	89.554100	101.263700
25	66.525880	78.108400	89.760910	101.471500
30	66.672690	78.257580	89.911630	101.623300
35	66.783770	78.371160	90.026900	101.739900
40	66.870390	78.460510	90.118100	101.832400
45	66.939420	78.532420	90.192000	101.907700
50	66.995240	78.591250	90.252920	101.970100
55	67.040810	78.639980	90.303870	102.022600
60	67.078270	78.680690	90.346830	102.067200
65	67.109150	78.714890	90.383360	102.105500
70	67.134630	78.743740	90.414620	102.138400
75	67.155640	78.768110	90.441420	102.167100
80	67.172880	78.788710	90.464480	102.191900
85	67.186950	78.806120	90.484350	102.213600
90	67.198350	78.820770	90.501410	102.232600
95	67.207460	78.833040	90.516120	102.249200
100	67.214620	78.843270	90.528750	102.263700
105	67.220180	78.851740	90.539630	102.276300
110	67.224360	78.858650	90.548770	102.287400
115	67.227400	78.864280	90.556580	102.297000
120	67.229510	78.868750	90.563170	102.305300
125	67.230840	78.872210	90.568650	102.312500
130	67.231610	78.874870	90.573140	102.318700
135		78.876790	90.576830	102.324000
140		78.878140	90.579970	102.328300
145		78.879040	90.582080	102.332100
150		78.879570	90.584090	102.335300
155			90.585140	102.337800
160			90.586190	102.339900
165			90.587000	102.341600
170			90.587000	102.342600
175				102.343700
180				102.344700
185				102.344800
190				102.344800

Formulae for the calculation of critical crack sizes a_{crit}

Plate with Center Crack

application range: $50 \text{ mm} \le 2W \le 600 \text{ mm}$, $0.05 \le a/W \le 0.90$

$\mathbf{0 < \sigma_{appl} \le \sigma_{gy}}$

$\frac{J_{Mat}}{J_{gy}} < 1$: (iterative determination of a_{crit})

$$J_{appl} = J_{gy} \cdot \left(1 - \left(1 - \left(\frac{\sigma_{appl}}{\sigma_{gy}} \right)^2 \right)^{0.63} \right) = J_{Mat} \qquad \text{(I)}$$

$\frac{J_{Mat}}{J_{gy}} \ge 1$:

$$a_{crit} = W \cdot (1 - \sigma_{appl}/f_y) \qquad \text{(II)}$$

where σ_{appl} = max. stresses in the gross section

$\sigma_{gy} = f_y \cdot (1\text{-}a/W)$

f_y = yield strength

J_{Mat} = fracture mechanic toughness

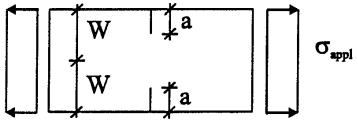
$$J_{gy} = \frac{2W \cdot f_y^2 \cdot 0.640 \cdot a/W \cdot (1 \quad a/W^3)}{210000 \cdot (a/W \quad 0.125)}$$

a/W = crack width/plate width -ratio

Calculation formulae for the calculation of critical crack sizes a_{crit} of the plate with Center Crack

Tables C

Critical crack sizes a_{crit} and load cycles N(a) for the plate with Double Edge Crack (DECT)



Use of the tables

1. Calculation of the stress relation $d = \sigma_{appl}/f_y$

2. Evaluation of the critical crack size for d and the half plate width W (the evaluation of the relevant plate width W for the considered structural part is made according tables A)

3. Calculation of the equivalent stress range $\Delta\sigma_e$

4. Evaluation of the tabulated values $N(a) \cdot \Delta\sigma_e^3 \cdot 10^{-11}$ for a_0 and a_{crit} for the half plate width W

5. Evaluation of the number of possible load cycles from a_0 to a_{krit}:

$$\Delta N = \frac{N(a_{krit})\cdot\Delta\sigma_e^3\cdot 10^{-11} - N(a_0)\cdot\Delta\sigma_e^3\cdot 10^{-11}}{\Delta\sigma_e^3\cdot 10^{-11}}$$

Interim values for a or W may be interpolated.

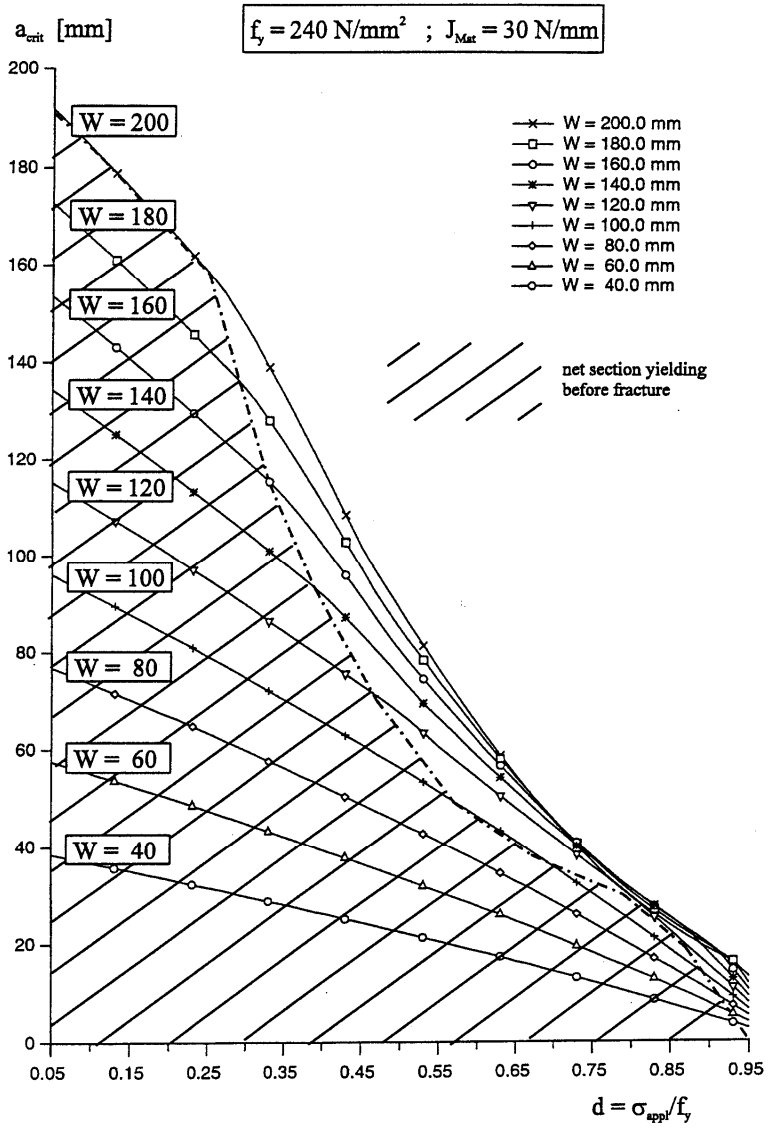
The tables for the evaluation of the number of load cycles N are based on the *Paris* crack growth relation (material constants: $C = 4\cdot 10^{-13}$ and $m = 3$).

Critical crack sizes a_{crit} [mm]

The critical crack sizes given in the following table and diagram are calculated for a fracture toughness value J_{Mat} = 30 N/mm and a yield strength value f_y = 240 N/mm².

The cases where net section yielding will occur before fracture are underlined.

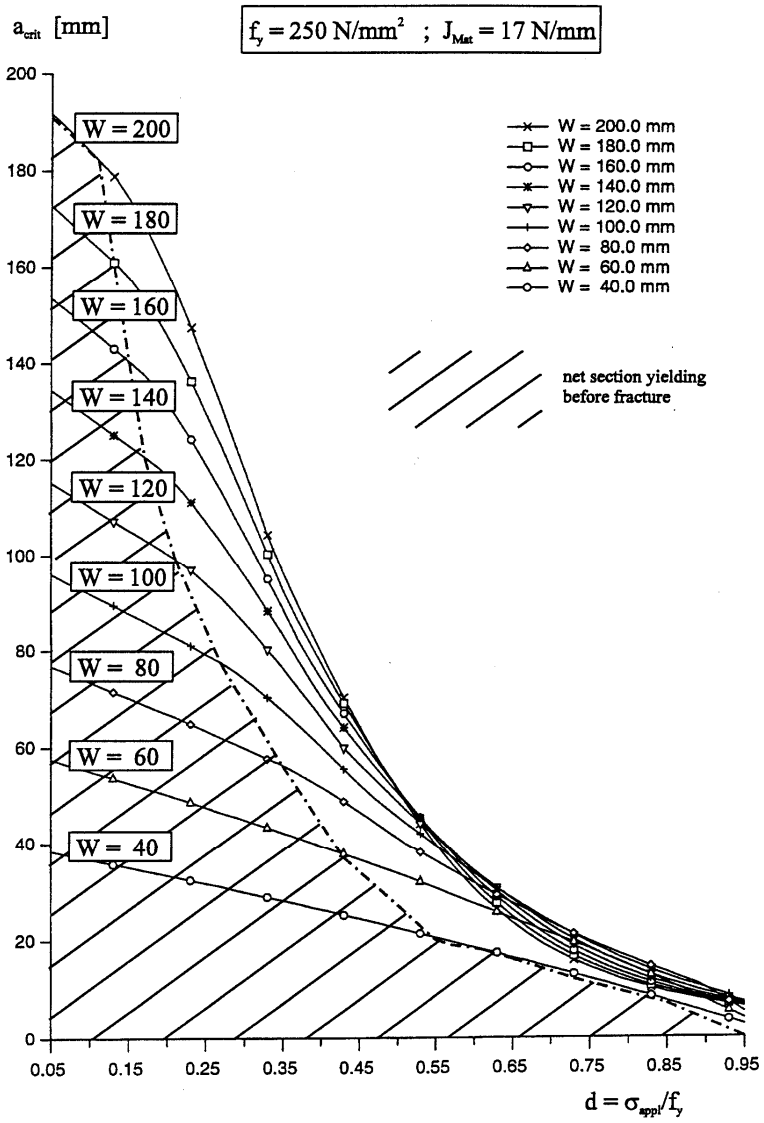
W [mm] / d [-]	40	60	80	100	120	140	160	180	200
0.05	38	57	76	95	115	134	153	172	191
0.07	37	56	75	94	113	132	150	169	188
0.09	37	55	74	92	111	129	148	166	185
0.11	36	54	72	91	109	127	145	163	182
0.13	35	53	71	89	107	125	142	160	178
0.15	35	52	70	87	105	122	140	157	175
0.17	34	51	68	86	103	120	137	154	172
0.19	33	50	67	84	101	118	134	151	168
0.21	33	49	66	82	99	115	132	148	165
0.23	32	48	64	80	97	113	129	145	161
0.25	31	47	63	79	94	110	126	142	158
0.27	30	46	61	77	92	108	123	139	154
0.29	30	45	60	75	90	105	120	136	149
0.31	29	44	59	73	88	103	118	132	144
0.33	28	43	57	72	86	100	115	127	138
0.35	28	42	56	70	84	98	111	123	133
0.37	27	41	54	68	82	95	108	118	127
0.39	26	39	53	66	79	93	104	113	120
0.41	25	38	51	64	77	90	100	108	114
0.43	25	37	50	62	75	87	95	102	108
0.45	24	36	48	60	73	83	91	97	101
0.47	23	35	47	59	70	80	86	91	96
0.49	22	34	45	57	68	76	82	86	91
0.51	22	33	44	55	65	72	78	82	86
0.53	21	31	42	53	63	69	74	78	81
0.55	20	30	40	51	60	66	70	73	76
0.57	19	29	39	49	57	63	66	69	71
0.59	18	28	37	47	55	60	63	65	67
0.61	18	27	36	45	52	57	59	61	62
0.63	17	25	34	43	50	54	56	57	58
0.65	16	24	32	41	47	51	53	54	54
0.67	15	23	31	38	45	48	49	50	50
0.69	14	22	29	36	42	45	46	47	46
0.71	13	20	27	34	40	42	43	43	43
0.73	12	19	25	32	38	40	40	40	39
0.75	12	18	24	30	35	37	37	37	36
0.77	11	16	22	28	33	35	35	34	33
0.79	10	15	20	25	30	32	32	31	31
0.81	9	14	18	23	28	30	30	29	28
0.83	8	12	16	21	25	27	27	26	26
0.85	7	11	15	18	22	25	25	24	23
0.87	6	9	13	16	19	22	23	22	21
0.89	5	8	11	14	16	19	20	20	19
0.91	4	6	9	11	13	16	18	18	17
0.93	3	5	7	9	10	12	14	16	16
0.95	2	3	5	6	7	9	10	11	13



The critical crack sizes given in the following table and diagram are calculated for a fracture toughness value J_{Mat} = 17 N/mm and a yield strength value f_y = 250 N/mm².

The cases where net section yielding will occur before fracture are underlined

W [mm] / d [-]	40	60	80	100	120	140	160	180	200
0.05	38	57	76	95	115	134	153	172	191
0.07	37	56	75	94	113	132	150	169	188
0.09	37	55	74	92	111	129	148	166	185
0.11	36	54	72	91	109	127	145	163	182
0.13	35	53	71	89	107	125	142	160	178
0.15	35	52	70	87	105	122	140	157	173
0.17	34	51	68	86	103	120	137	153	168
0.19	33	50	67	84	101	117	133	148	161
0.21	33	49	66	82	99	114	129	142	154
0.23	32	48	64	80	96	111	124	136	147
0.25	31	47	63	79	94	107	118	129	139
0.27	30	46	61	77	90	102	113	122	130
0.29	30	45	60	75	87	98	107	115	122
0.31	29	44	59	72	83	93	101	107	113
0.33	28	43	57	70	80	88	94	100	104
0.35	28	42	56	67	76	83	88	92	96
0.37	27	41	54	64	72	77	82	85	89
0.39	26	39	52	61	68	72	76	80	82
0.41	25	38	50	58	63	67	71	74	76
0.43	25	37	48	55	59	63	66	68	70
0.45	24	36	46	52	56	59	62	63	64
0.47	23	35	44	49	53	55	57	58	58
0.49	22	34	42	46	50	52	53	53	53
0.51	22	33	39	44	47	48	49	49	48
0.53	21	31	37	41	44	45	45	44	43
0.55	20	30	36	39	41	41	41	40	39
0.57	19	29	34	37	38	38	37	36	35
0.59	18	28	32	34	35	35	34	33	32
0.61	18	26	30	32	33	32	31	30	28
0.63	17	25	29	30	30	29	28	27	26
0.65	16	24	27	28	28	27	26	24	23
0.67	15	23	25	26	25	24	23	22	21
0.69	14	21	24	24	23	22	21	20	19
0.71	13	20	22	22	21	20	19	18	17
0.73	12	19	21	21	20	18	17	16	15
0.75	12	18	19	19	18	17	16	15	14
0.77	11	16	18	17	16	15	14	13	13
0.79	10	15	17	16	15	14	13	12	12
0.81	9	14	15	15	14	13	12	11	11
0.83	8	12	14	13	12	11	11	10	10
0.85	7	11	13	12	11	10	10	9	9
0.87	6	9	12	11	10	9	9	8	8
0.89	5	8	10	10	9	9	8	8	7
0.91	4	6	9	9	8	8	7	7	7
0.93	3	5	7	8	8	7	7	6	6
0.95	2	3	5	6	7	6	6	6	6



Load cycles N(a)

tabulated values = $N \cdot \Delta\sigma_e^3 \cdot 10^{-11}$

W [mm] / a [mm]	40	60	80	100	120
5	6.139167	13.851900	21.797010	29.881360	38.060850
10	6.959291	14.679570	22.627030	30.712390	38.892440
15	7.308389	15.041020	22.992090	31.078950	39.259780
20	7.500139	15.250860	23.206960	31.295840	39.477700
25	7.612514	15.387980	23.350710	31.442230	39.625360
30	7.675346	15.482610	23.453810	31.548580	39.733270
35	7.703868	15.549100	23.530740	31.629470	39.816050
40		15.595210	23.589380	31.692860	39.881650
45		15.625660	23.634430	31.743460	39.934830
50		15.643710	23.668850	31.784290	39.978610
55		15.652110	23.694650	31.817360	40.015030
60			23.713290	31.844070	40.045520
65			23.725890	31.865440	40.071110
70			23.733450	31.882250	40.092540
75			23.736990	31.895100	40.110410
80				31.904500	40.125150
85				31.910910	40.137140
90				31.914780	40.146680
95				31.916590	40.154040
100					40.159450
105					40.163150
110					40.165390
115					40.166430

tabulated values = $N \cdot \Delta\sigma_e^3 \cdot 10^{-11}$

W [mm] a [mm]	140	160	180	200
5	46.310710	54.615220	62.963910	71.349210
10	47.142580	55.447330	63.796120	72.181530
15	47.510360	55.815390	64.164400	72.549900
20	47.728860	56.034240	64.383510	72.769170
25	47.877220	56.183060	64.532630	72.918470
30	47.985980	56.292370	64.642290	73.028390
35	48.069800	56.376790	64.727130	73.113480
40	48.136600	56.444310	64.795090	73.181770
45	48.191160	56.499680	64.850980	73.238010
50	48.236520	56.545960	64.897840	73.285290
55	48.274730	56.585210	64.937740	73.325640
60	48.307220	56.618860	64.972120	73.360490
65	48.335020	56.647960	65.002010	73.390920
70	48.358910	56.673260	65.028210	73.417690
75	48.379460	56.695380	65.051280	73.441410
80	48.397120	56.714740	65.071710	73.462510
85	48.412260	56.731720	65.089830	73.481380
90	48.425160	56.746600	65.105930	73.498310
95	48.436040	56.759590	65.120260	73.513510
100	48.445130	56.770920	65.133000	73.527170
105	48.452560	56.780750	65.144330	73.539470
110	48.458500	56.789170	65.154340	73.550540
115	48.463130	56.796360	65.163190	73.560490
120	48.466530	56.802360	65.170940	73.569430
125	48.468870	56.807310	65.177700	73.577450
130	48.470240	56.811260	65.183550	73.584550
135		56.814320	65.188530	73.590880
140		56.816620	65.192720	73.596430
145		56.818160	65.196160	73.601330
150		56.819100	65.198950	73.605570
155			65.201130	73.609150
160			65.202740	73.612180
165			65.203810	73.614700
170			65.204440	73.616740
175				73.618320
180				73.619430
185				73.620230
190				73.620760

Formulae for the calculation of critical crack sizes a_{crit}

Plate with Double Edge Crack

application range: $50 \text{ mm} \le 2W \le 600 \text{ mm}$, $0.05 \le a/W \le 0.90$

$0 < \sigma_{appl} \le \sigma_{gy}$

$\frac{J_{Mat}}{J_{gy}} < 1$: (iterative determination of a_{crit})

$$J_{appl} = J_{gy} \cdot \left[1 - \left(1 - \left(\frac{\sigma_{appl}}{\sigma_{gy}}\right)^2\right)^{0.75}\right] = J_{Mat} \qquad (I)$$

$\frac{J_{Mat}}{J_{NQF}} \ge 1$:

$$a_{crit} = W \cdot \left(\sqrt{2.25 + 4 \cdot \left(1 - \frac{\sigma_{appl}}{f_y}\right)} - 1.5\right) \qquad (II)$$

mit σ_{appl} = max. stresses in the gross section

$\sigma_{gy} = f_y \cdot (1-a/W) \cdot (1 + 0.25 \cdot a/W)$

f_y = yield strength

J_{Mat} = fracture mechanic toughness

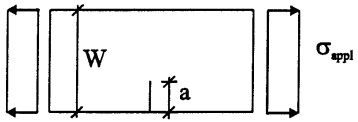
$$J_{gy} = \frac{2W \cdot f_y^2 \cdot 0.64 \cdot a/W \cdot (1 - a/W^3)}{210000 \cdot (a/W + 0.07)} \cdot \ln(e - |a/W - 0.5|)$$

a/W = crack width/plate width -ratio

Calculation formulae for the calculation of critical crack sizes a_{crit} of the plate with Double Edge Crack

Tables D

Critical crack sizes a_{crit} and load cycles N(a) for the plate with Single Edge Crack (SECT)



Use of the tables

1. Calculation of the stress relation $d = \sigma_{appl}/f_y$
2. Evaluation of the critical crack size for d and the half plate width W (the evaluation of the relevant plate width W for the considered structural part is made according tables A)
3. Calculation of the equivalent stress range $\Delta\sigma_e$
4. Evaluation of the tabulated values $N(a) \cdot \Delta\sigma_e^3 \cdot 10^{-11}$ for a_0 and a_{crit} for the half plate width W
5. Evaluation of the number of possible load cycles from a_0 to a_{krit}:

$$\Delta N = \frac{N(a_{krit})\cdot\Delta\sigma_e^3\cdot 10^{-11} - N(a_0)\cdot\Delta\sigma_e^3\cdot 10^{-11}}{\Delta\sigma_e^3\cdot 10^{-11}}$$

Interim values for a or W may be interpolated.

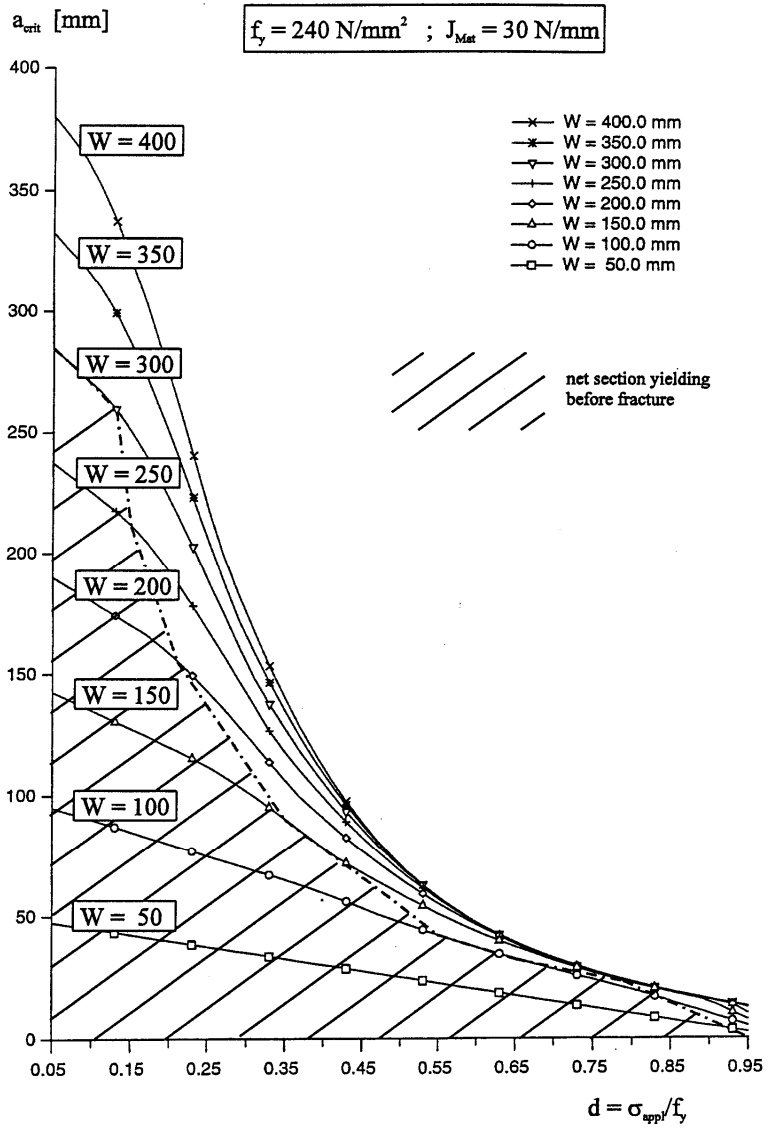
The tables for the evaluation of the number of load cycles N are based on the *Paris* crack growth relation (material constants: $C = 4\cdot 10^{-13}$ and $m = 3$).

Critical crack sizes a_{crit} [mm]

The critical crack sizes given in the following table and diagram are calculated for a fracture toughness value J_{Mat} = 30 N/mm and a yield strength value f_y = 240 N/mm².

The cases where net section yielding will occur before fracture are underlined.

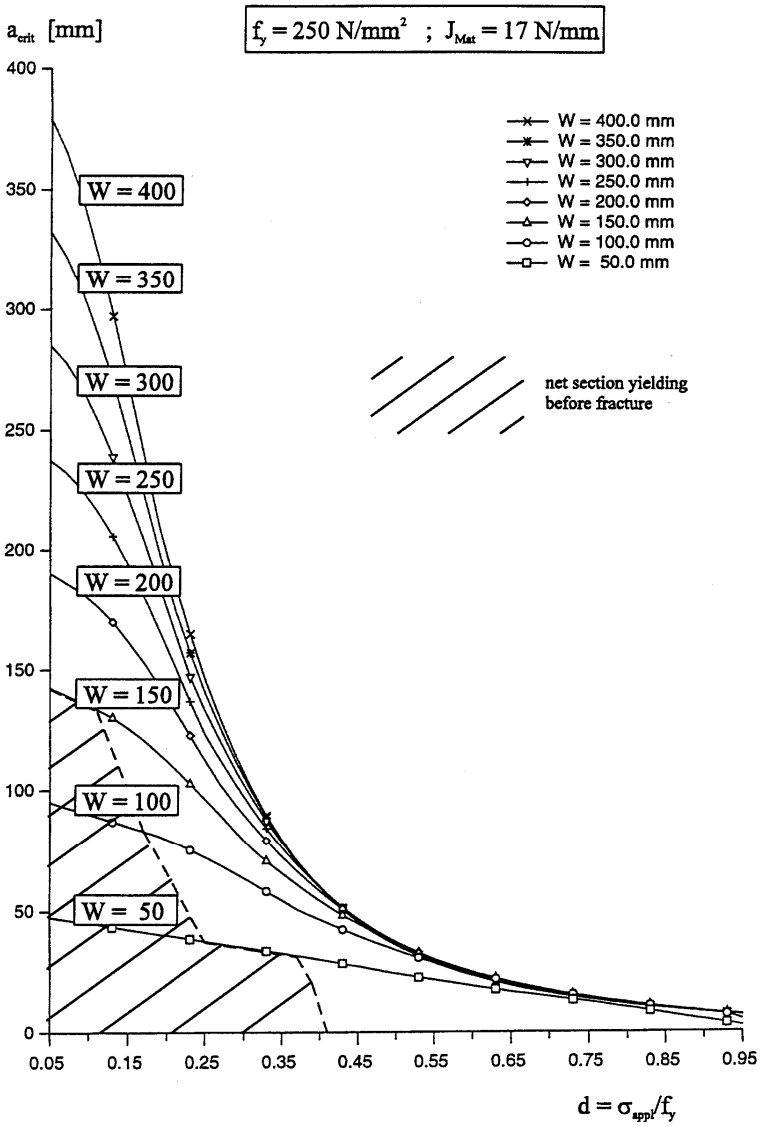
W [mm] / d [-]	50	100	150	200	250	300	350	400
0.05	47	95	142	190	237	285	332	380
0.07	46	93	139	186	232	279	325	372
0.09	45	91	136	182	227	273	318	363
0.11	44	89	133	178	222	266	310	351
0.13	43	87	130	174	217	259	299	337
0.15	42	85	127	170	211	250	286	320
0.17	41	83	124	165	204	239	272	302
0.19	40	81	121	161	196	228	256	282
0.21	39	79	118	155	187	215	240	261
0.23	38	77	115	149	177	202	223	240
0.25	37	75	111	142	168	188	205	219
0.27	36	73	108	135	157	174	188	198
0.29	35	71	103	128	147	161	171	182
0.31	34	69	99	121	136	148	158	167
0.33	33	67	94	113	126	137	146	153
0.35	32	65	90	106	118	127	134	140
0.37	31	62	85	99	110	118	123	127
0.39	30	60	80	93	102	109	113	116
0.41	29	58	75	87	95	100	104	106
0.43	28	55	71	82	88	93	95	97
0.45	27	53	68	77	82	86	87	88
0.47	26	50	64	72	76	79	80	81
0.49	25	48	60	67	71	73	74	74
0.51	24	46	57	63	66	67	68	68
0.53	23	44	54	58	61	62	62	62
0.55	22	42	50	55	56	57	57	57
0.57	21	40	47	51	52	53	53	52
0.59	20	38	45	47	49	49	49	48
0.61	19	36	42	44	45	45	45	44
0.63	18	34	39	41	42	42	41	41
0.65	17	32	37	38	39	39	38	38
0.67	16	30	34	36	36	36	36	35
0.69	15	28	32	33	33	33	33	33
0.71	14	27	30	31	31	31	31	30
0.73	13	25	28	29	29	29	28	28
0.75	12	23	26	27	27	27	26	26
0.77	11	22	25	25	25	25	25	24
0.79	10	20	23	23	23	23	23	23
0.81	9	19	21	22	22	22	21	21
0.83	8	17	20	20	20	20	20	20
0.85	7	15	18	19	19	19	19	18
0.87	6	12	17	17	17	17	17	17
0.89	5	11	15	16	16	16	16	16
0.91	4	8	13	15	15	15	15	15
0.93	3	7	10	13	14	14	14	14
0.95	2	5	7	10	12	12	12	12



The critical crack sizes given in the following table and diagram are calculated for a fracture toughness value J_{Mat} = 17 N/mm and a yield strength value f_y = 250 N/mm².

The cases where net section yielding will occur before fracture are underlined.

W [mm] / d [-]	50	100	150	200	250	300	350	400
0.05	47	95	142	190	237	285	332	379
0.07	46	93	139	186	232	277	321	365
0.09	45	91	136	181	225	267	307	346
0.11	44	89	133	176	216	254	289	323
0.13	43	87	130	169	205	238	269	297
0.15	42	85	125	161	193	221	246	268
0.17	41	83	120	152	180	203	222	238
0.19	40	80	115	143	165	184	198	209
0.21	39	78	109	133	151	164	174	185
0.23	38	75	102	122	136	146	156	164
0.25	37	72	96	112	122	132	140	145
0.27	36	68	89	101	112	119	125	128
0.29	35	65	82	93	101	107	111	114
0.31	34	61	75	85	92	96	99	100
0.33	33	57	70	78	84	86	88	89
0.35	32	54	65	72	76	78	79	79
0.37	31	50	60	66	68	70	70	70
0.39	30	47	56	60	62	63	63	62
0.41	29	44	52	55	56	56	56	56
0.43	28	42	48	50	51	51	51	50
0.45	27	39	44	46	46	46	46	45
0.47	25	37	41	42	42	42	41	41
0.49	24	34	38	38	38	38	37	37
0.51	23	32	35	35	35	34	34	33
0.53	22	30	32	32	32	31	31	31
0.55	21	28	30	30	29	29	28	28
0.57	20	26	27	27	27	26	26	26
0.59	19	24	25	25	25	24	24	24
0.61	18	23	23	23	23	22	22	22
0.63	17	21	22	21	21	21	20	20
0.65	16	20	20	20	19	19	19	18
0.67	15	18	19	18	18	18	17	17
0.69	14	17	17	17	17	16	16	16
0.71	13	16	16	16	15	15	15	15
0.73	13	15	15	15	14	14	14	14
0.75	12	14	14	13	13	13	13	13
0.77	11	13	13	13	12	12	12	12
0.79	10	12	12	12	11	11	11	11
0.81	9	11	11	11	11	11	10	10
0.83	8	10	10	10	10	10	10	10
0.85	7	10	10	9	9	9	9	9
0.87	6	9	9	9	9	9	8	8
0.89	5	8	8	8	8	8	8	8
0.91	4	7	8	7	7	7	7	7
0.93	3	6	7	7	7	7	7	7
0.95	2	5	6	6	6	6	6	6



Load cycles N(a)

tabulated values = $N \cdot \Delta\sigma_e^3 \cdot 10^{-11}$

W [mm] / a [mm]	50	100	150	200
10	1.865795	21.260500	41.104380	61.206200
20	2.073999	21.667710	41.582980	61.717920
30	2.094211	21.779480	41.748340	61.911460
40	2.095473	21.815000	41.819930	62.005940
50		21.826130	41.853080	62.056660
60		21.829300	41.868620	62.084980
70		21.830070	41.875780	62.101030
80		21.830200	41.878960	62.110120
90		21.830210	41.880290	62.115190
100			41.880800	62.117970
110			41.880970	62.119460
120			41.881030	62.120230
130			41.881030	62.120600
140			41.881030	62.120760
150				62.120840
160				62.120840
170				62.120840
180				62.120840
190				62.120840

tabulated values = $N \cdot \Delta\sigma_e^3 \cdot 10^{-11}$

W [mm] / a [mm]	250	300	350	400
10	81.475360	101.863400	122.341000	142.889600
20	82.005540	102.405100	122.890700	143.444900
30	82.215410	102.625400	123.118000	143.677300
40	82.324220	102.743600	123.242800	143.806800
50	82.387090	102.814900	123.320100	143.888500
60	82.425410	102.860500	123.371100	143.943700
70	82.449370	102.890700	123.406200	143.982500
80	82.464550	102.911100	123.430800	144.010500
90	82.474170	102.925000	123.448400	144.031100
100	82.480280	102.934600	123.461000	144.046300
110	82.484100	102.941100	123.470200	144.057800
120	82.486480	102.945500	123.476800	144.066400
130	82.487950	102.948600	123.481500	144.072800
140	82.488820	102.950600	123.485000	144.077700
150	82.489320	102.952000	123.487400	144.081400
160	82.489600	102.952900	123.489200	144.084100
170	82.489750	102.953400	123.490400	144.086200
180	82.489850	102.953800	123.491300	144.087700
190	82.489850	102.954000	123.491900	144.088900
200	82.489850	102.954200	123.492300	144.089700
210	82.489850	102.954200	123.492600	144.090300
220	82.489850	102.954200	123.492800	144.090800
230	82.489850	102.954200	123.492900	144.091100
240		102.954200	123.492900	144.091300
250		102.954200	123.492900	144.091500
260		102.954200	123.492900	144.091600
270		102.954200	123.492900	144.091600
280		102.954200	123.492900	144.091600
290			123.492900	144.091600
300			123.492900	144.091600
310			123.492900	144.091600
320			123.492900	144.091600
330			123.492900	144.091600
340				144.091600
350				144.091600
360				144.091600
370				144.091600
380				144.091600

Formulae for the calculation of critical crack sizes a_{crit}

Plate with Single Edge Crack

application range: $50 \text{ mm} \le W \le 600 \text{ mm}$, $0.05 \le a/W \le 0.90$

$0 < \sigma_{appl} \le \sigma_{gy}$

$\frac{J_{Mat}}{J_{gy}} < 1$: (iterative determination of a_{crit})

$$J_{appl} = J_{gy} \cdot \left[1 - \left(1 - \left(\frac{\sigma_{appl}}{\sigma_{gy}}\right)^2\right)^{0.65}\right] = J_{Mat} \qquad (I)$$

$\frac{J_{Mat}}{J_{gy}} \ge 1$:

$$a_{crit} = W \cdot (1-\sigma_{appl}/f_y) \qquad (II)$$

where σ_{appl} = max. stresses in the gross section

$\sigma_{gy} = f_y \cdot (1-a/W)$

f_y = yield strength

J_{Mat} = fracture mechanic toughness

$$J_{gy} = \frac{2W \cdot f_y^2 \cdot 2.48 \cdot a/W \cdot (1-a/W^2)}{210000 \cdot (a/W + 0.18)} \cdot \ln(e - |a/W - 0.5|)$$

a/W = crack width/plate width -ratio

Calculation formulae for the calculation of critical crack sizes a_{crit} of the plate with Single Edge Crack

4.1.6 Example for the fracture mechanics based safety assessment

(1) For a tension member of a truss system, as given in fig. 4-26, the following data are given:

1. Material values (lower bound values for -30°C)

f_y = 250 N/mm^2
J_{Mat} = 17 N/mm

2. Nominal stresses and stress cycles

permanent	σ_G = 45 N/mm^2
variable	$\sigma_G = \Delta\sigma$ = 60 N/mm^2
stress cycles	n_{Sd} = 1,5 n = 270000 LC
residual	σ_s = 25 N/mm^2
stress ratio	$d = \frac{(45\,N/mm^2 + 60\,N/mm^2 + 25\,N/mm^2)}{250\,N/mm^2} = 0{,}52$

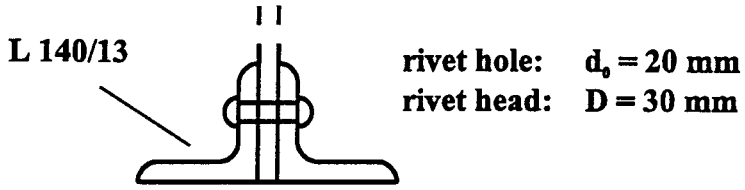


Fig. 4-26: Cross-section of tension member

(2) The equivalent fracture mechanics model is according to table A.2 (middle line):

CCT: w = 1,10 · c/2 = 77 mm

(3) The initial crack size is a_0 = 20 mm, see fig. 4-27.

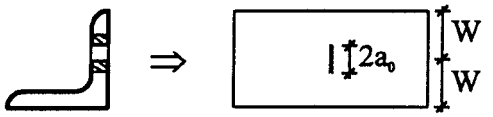


Fig. 4-27: Fracture mechanics model and initial crack size.

(4) Using table B.4 the critical size a_{crit} is

a_{crit} = 34 mm

(5) Using table B.6 the load cycles for Δa = 34 – 21 = 13 mm are

n_R = 132244 LC < n_{Insp}

(6) In conclusion, the cross-section should either be reinforced or the inspection interval t_{Insp} reduced to
T^*_{Insp} = 132244/270000 ≈ 0.5 t_{Insp}, t_{Insp} = normal inspection interval

4.1.7 Bibliography

[1] HENSEN W. Grundlagen für die Beurteilung der Weiterverwendung alter Stahlbrücken. Dissertation, RWTH Aachen 1992

[2] DAHL W., SCHUMANN O., SEDLACEK G. Method to Back Decision on Residual Safety of Bridges, IABSE Workshop Remaining Fatigue life of Steel Structures Lausanne 1990, IABSE Report Vol. 59, 1990, S. 313-326

[3] SEDLACEK G., HENSEN W., BILD J., DAHL W., LANGENBERG, P. Verfahren zur Ermittlung der Sicherheit von alten Stahlbrücken unter Verwendung neuester Erkenntnisse der Werkstofftechnik, Bauingenieur, 1992.

[4] SEDLACEK G., HENSEN W. Nouvelles Methodes de calcul pour la rehabilitation des Ponts métalliques anciens. Construction Métallique, No. 3, 1992.

[5] SEDLACEK G., HENSEN W. New assessment methods for the residual safety of old steel bridges. Steel Research 64, No. 8/9, 1993.

[6] DAHL W., SEDLACEK G. Untersuchungen zur Ermittlung der Sicherheit und Restnutzungsdauer der Karl-Lehr-Brücke in Duisburg. Expertise for the town Duisburg, 1986.

[7] DAHL W., SEDLACEK G. Untersuchungen zur Ermittlung der Sicherheit und Restnutzungsdauer der Anhalter-Bahn-Brücke in Berlin. Expertise for the railway authority in Berlin, 1989.

[8] DAHL W., SEDLACEK G. Untersuchungen zur Ermittlung der Sicherheit und Restnutzungsdauer der U-Bahnbrücken zwischen Gleisdreieck und Bahnhof Möckernbrücke in Berlin. Expertise for the railway authority in Berlin, 1990.

[9] DAHL W., LANGENBERG P., SEDLACEK G., STÖTZEL G. Sicherheitsüberprüfung von Stahlbrücken. DFG-Forschungsvorhaben Da85/62 und Se351/9.

[10] EUROCODE 3, PART 1.1 Design of steel structures: General rules and rules for buildings – ANNEX Determination of design resistance from tests. Document CEN/TC250/SC3/ N361E, Sept. 1993.

[11] BRÜHLWILER E. Essais de Fatigue sur des Poutres a Tripplis Double en fer Puddle. Publication ICOM 159/1986.

[12] BILD J. Beitrag zur Anwendung der Bruchmechanik bei der Lösung von Sicherheitsproblemen im Stahlbau. Dissertation, RWTH Aachen, 1988.

[13] CHEREPANOW G.P. PMM 31 (1967) No. 3, p. 476/88.

[14] RICE J.R., TRANCEY D.M.J. Mech. Phys. Solids 17 (1969), p. 201/17.

[15] LANGENBERG P., DAHL W., HAN S. Bruchverhalten alter Stähle in genieteten Brücken – Bruchmechanische Sicherheitsanalyse und Bauteilversuche. DVM Tagung des AK Bruchvorgänge, 2/1996.

[16] LANGENBERG P. Bruchmechanische Sicherheitsanalyse anrissgefährdeter Bauteile im Stahlbau, Dissertation, RWTH Aachen 1995.

[17] STÖTZEL G. Verfahren zur zuverlässigen Bestimmung der Sicherheit bei Weiterverwendung alter Stahlbrücken. Dissertation, RWTH Aachen.

[18] EHRHARDT H. Untersuchung zum Einfluss unterschiedlicher Fehlergeometrien auf das Versagensverhalten von Stahl auf der Grundlage von Großzugversuchen. Dissertation, RWTH Aachen 1988.

[19] PARIS P., ERDOGAN F. A critical analysis of crack propagation laws. Journal of Basic Engineering, Trans ASME Series D, Vol. 85, pp. 528-534 (1963)

[20] STÖTZEL G., SEDLACEK G., LANGENBERG P., DAHL W. Material Identification and Verification Method for the Residual Safety of Old Bridges, IABSE-Report.

[21] KÜHN, B. et al. “Assessment of existing steel structures: Recommendations for Estimation of Remaining Fatigue Life”, Joint Report JRC, ECCS, 1st Edition, Feb. 2008, EUR 23252 EN-2008, ISSN 1018-5593.

4.2 Choice of material for welded connections in buildings

4.2.1 Objective

(1) EN 1993-1-10 gives in its table 2.1 permissible plate thicknesses depending on the steel-grade, the lowest temperature of the member and the stress applied from external actions covering fracture mechanical assessments for all details specified with fatigue categories in EN 1993-1-9.

(2) The background of EN 1993-1-10 as laid down in section 2 of this commentary reveals that a basic assumption for the fracture mechanics assessment is that cracks with the initial size a_0 may have propagated by fatigue during a "safe service period" equivalent to ¼ of the full service life to their design size a_d. Hence it is applicable to all structures loaded in fatigue.

(3) Table 2-1 of EN 1992-1-10 may also be used on the safe-side for details that are specified in EN 1993-1-9, but are not subjected to fatigue, as is the case for buildings, assuming that the design size of crack a_d may originate from larger initial cracks a_0, that may have been overlooked in inspections, and smaller contributions from crack propagation.

(4) However, often in buildings welded connections are used that are not classified for fatigue in EN 1993-1-9, and that have such a poor fatigue behaviour that special consideration are necessary.

(5) Fig. 4-28 gives examples of such connections, that are frequently used because of the possibility to accept large tolerances of length from fabrication and erection in a residual slot, and for which in the following specific rules for the choice of material to avoid brittle fracture are given.

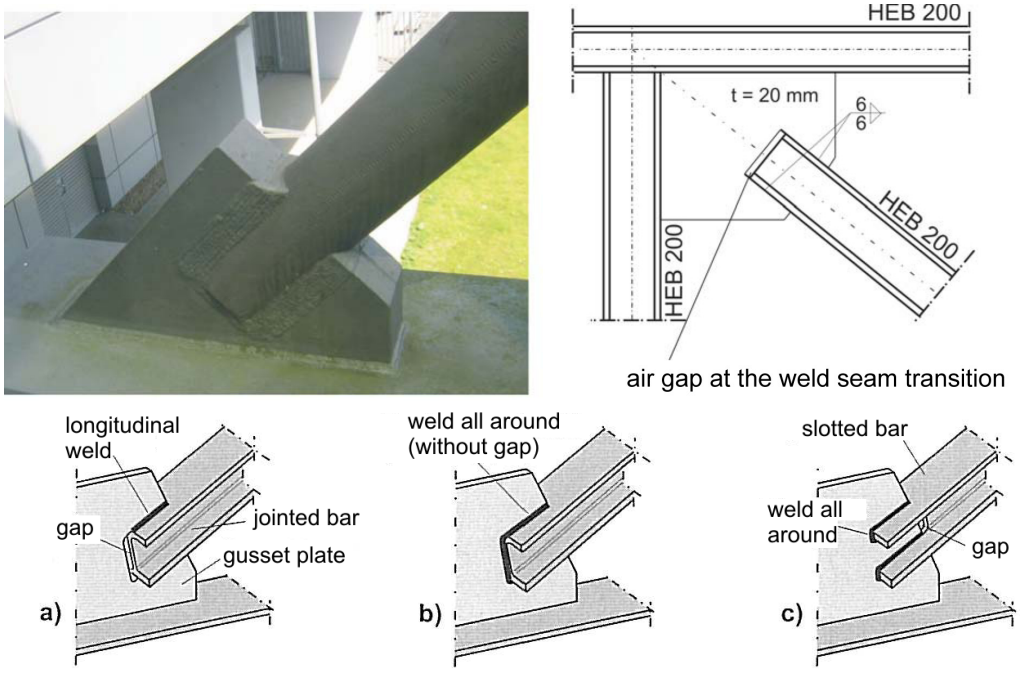


Fig. 4-28: Welded connections with thick plates and slots in buildings

4.2.2 Basis of fracture mechanical assessment

(1) The fracture mechanical assessment is performed for a design situation as given in fig. 4-29.

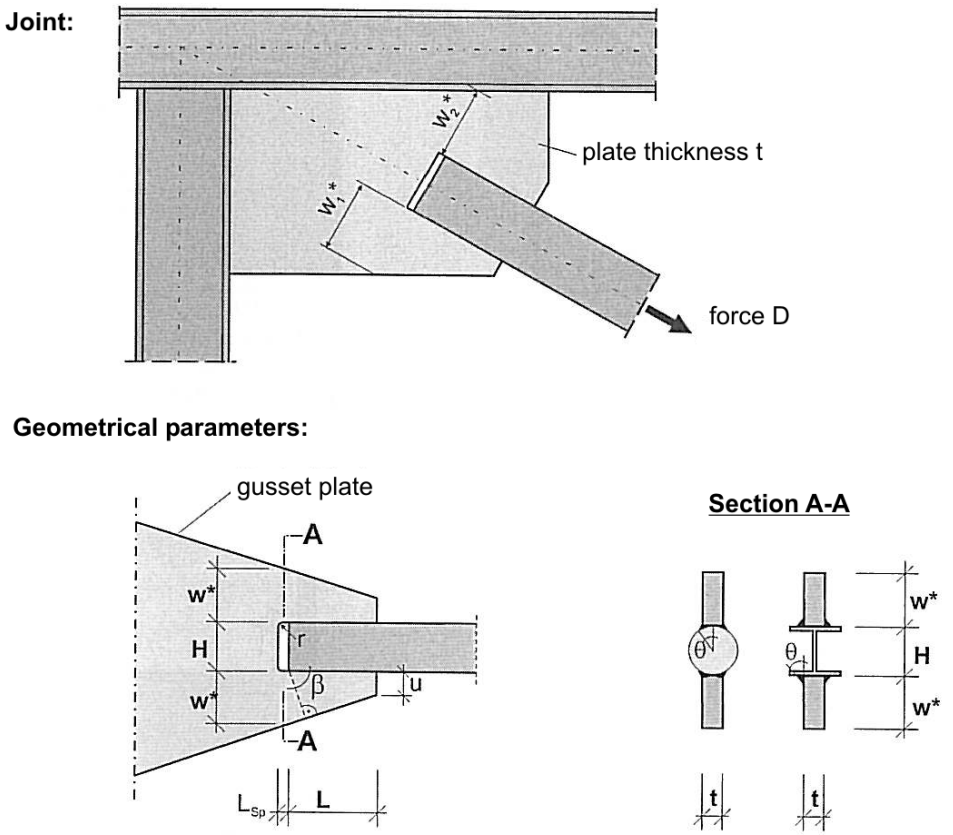


Fig. 4-29: Definition of geometric parameters and relevant cross-section A-A

(2) In Fig. 4-29 also the relevant geometrical parameters influencing the stress state at the critical section A-A are indicated:

- thickness of gusset plate t
- net width of gusset plate at section A-A $2w^*$
- slot width at section A-A H/2w*
- length of welded connection L/w^*

(3) Cracks are supposed to be at the ends of the slot.

(4) To limit the parameter variation particular ranges of parameters that are frequently used (common plate dimensions) and that represent limits of favourable or unfavourable toughness requirements, are given in table 4-1.

parameter	unfavourable	common	favourable
edge distance w* [mm]	300	130	80
length of weld L/w* [-]	0,8	1,3	1,6
width of slot H/2w* [-]	1,2	0,55	0,4

Table 4-1: Geometric parameter combinations

(5) The procedure to develop tables for the choice of material is similar to the one used to prepare table 2-1 of EN 1993-1-10, however, with the following differences:

1. The initial crack is quarter-elliptic with the same dimensions as in EN 1993-1-10

$a_0 = 0{,}5 \ln(t)$

$c_0 = \frac{a_0}{0{,}4} = 1{,}25 \ln(t)$

see fig. 4-30.

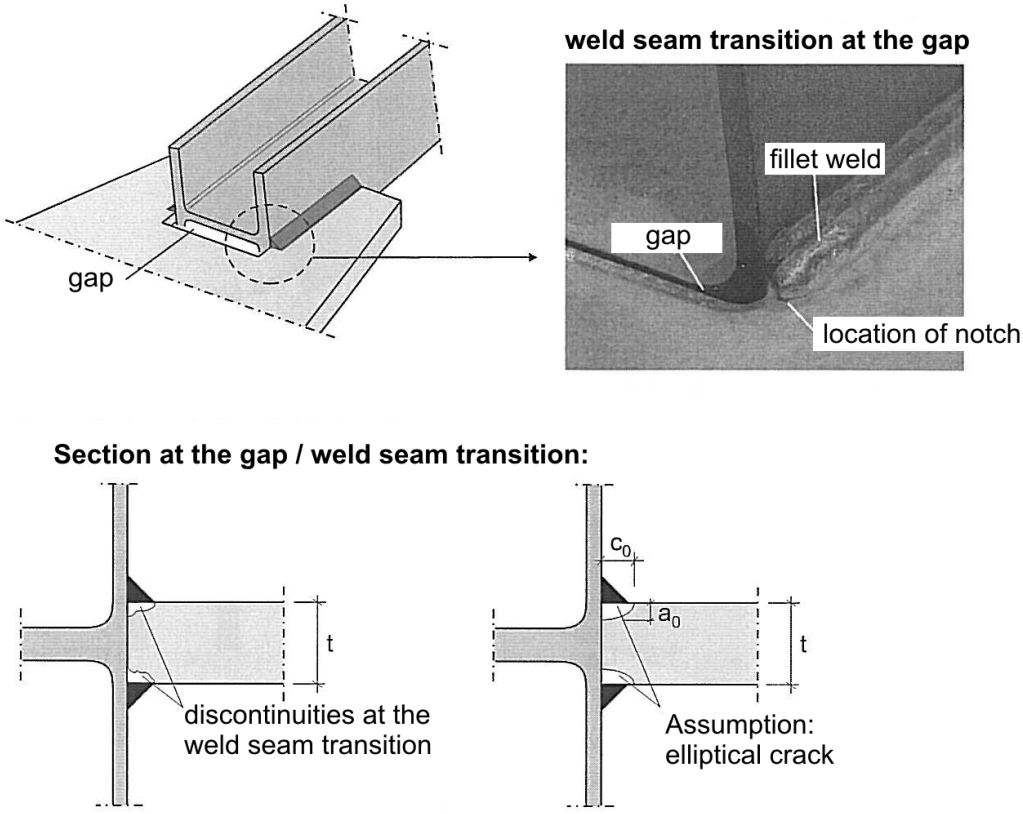


Fig. 4-30: Notches from fabrication and assumption for initial crack

2. A crack propagation is assumed under the fatigue load usually used to distinguish between structures with predominantly static load and structures susceptible to fatigue, i.e.

$\gamma_{Ff} \ \Delta\sigma \leq 26\,N/mm^2 / \gamma_{Mf}$.

As fatigue assessments are also only relevant if the number of load cycles is

$n \geq 20.000$

the fatigue loading assumed reads

$D = 26^3 \cdot 20{,}000$

3. During the fatigue life, crack propagation takes place in two steps, see fig. 4-31.

   1. First the quarter-elliptic cracks grow into the thickness direction to form a through-thickness crack.
   2. Then the through-thickness crack grows into the width direction.

   Instead of considering the two steps, only a single step is taken into account by assuming that the initial crack is a through-thickness crack and has the initial crack-size

   $a_0^* = 1{,}25 \ln(1 + t)$ for t < 15 mm

   $a_0^* = 1{,}25 \ln(t)$ for $\geq$ 15 mm.

   For the crack growth from this initial crack, a reduced fatigue load for determining the design crack

   $a_d = a_0^* + \Delta a^*$

   is assumed, which reads

   $D^* = 26^3 \cdot 10.000$

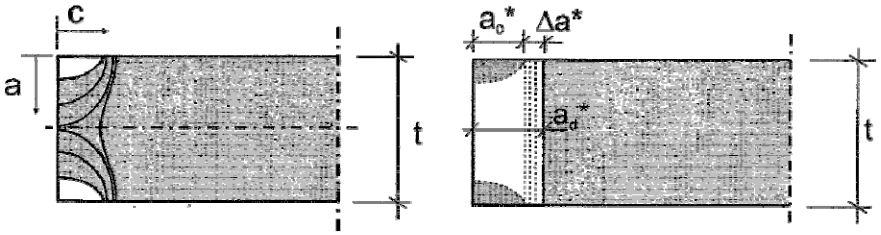


Fig. 4-31: Growth of the elliptical corner crack until a through thickness crack has formed (left) and assumption for edge-crack (right).

4. The calculation of the toughness requirement K_{appl} for the accidental design situation with

   - the extremely low temperature T_{Ed}
   - the "frequent" stress σ_{Ed}
   - the design size of crack a_d and sharp corners of the slot

   and the geometric conditions in table 4-1 lead to functions K_{appl} (t) as given in fig. 4-32. In this fig., also the standard function K_{appl}(t) as used for preparing table 2-1 of EN 1993-1-10 is indicated.

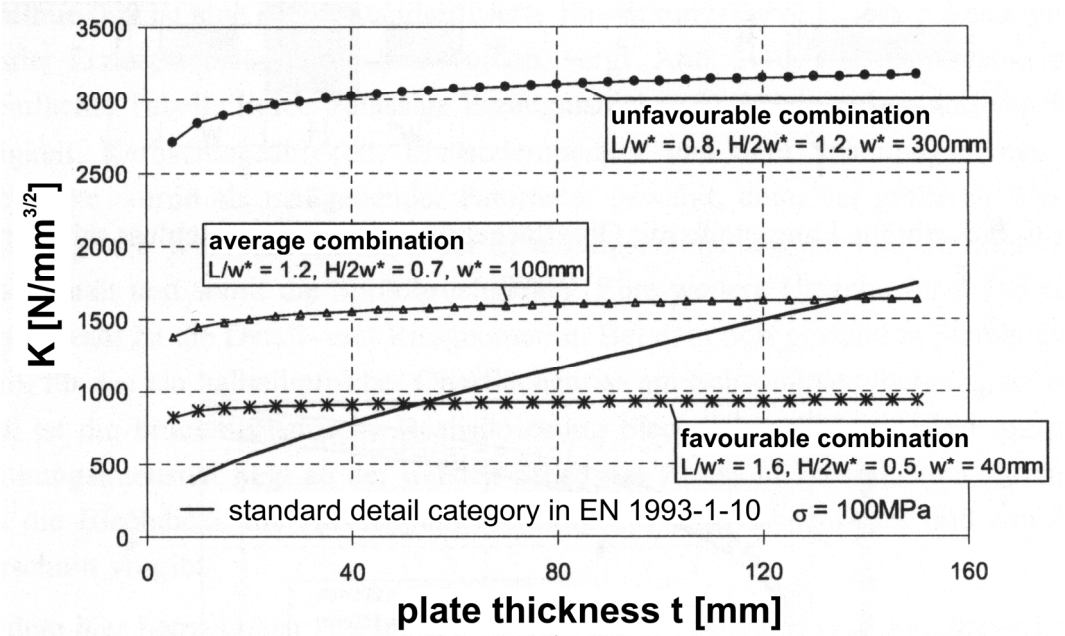


Fig. 4-32: K_{appl} depending on the gusset plate thickness for various dimensions.

5. Fig. 4-32 shows that for the welded connection with slots according to fig. 4-28 the function K_{appl} is almost independent of the plate-thickness t, but differs with the parameter w^*. Therefore, the tables for the choice of material have to be referred to the gusset-plate-width w^* and not to their thickness t.

Fig. 4-33 and fig. 4-34 give the full picture on the toughness requirement depending on the gusset plate width w^* and the weld-length L.

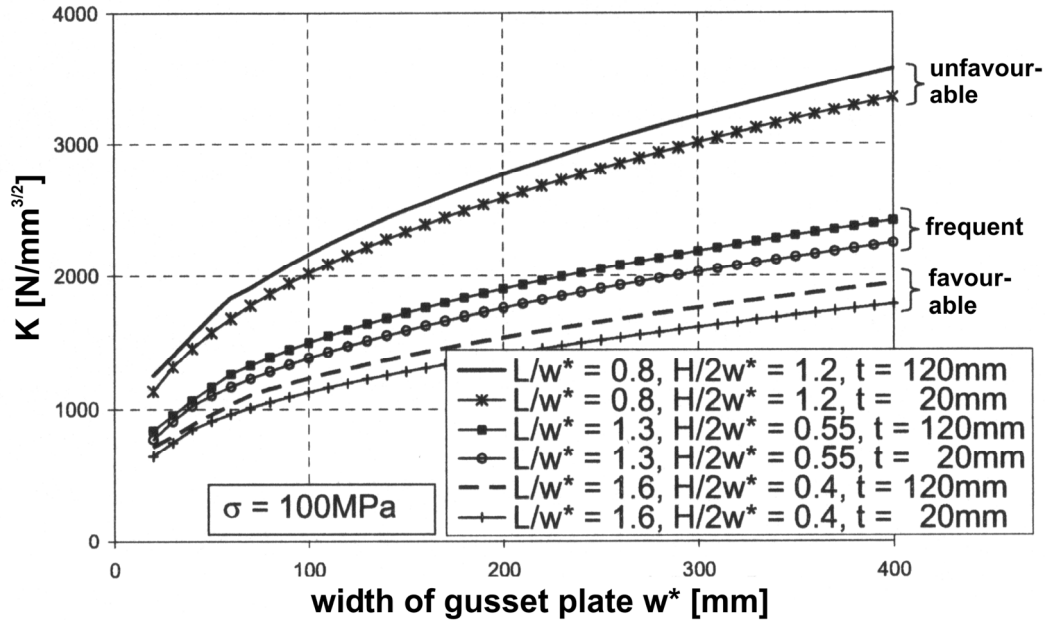


Fig. 4-33: K_{appl} depending on the gusset-plate width w^*

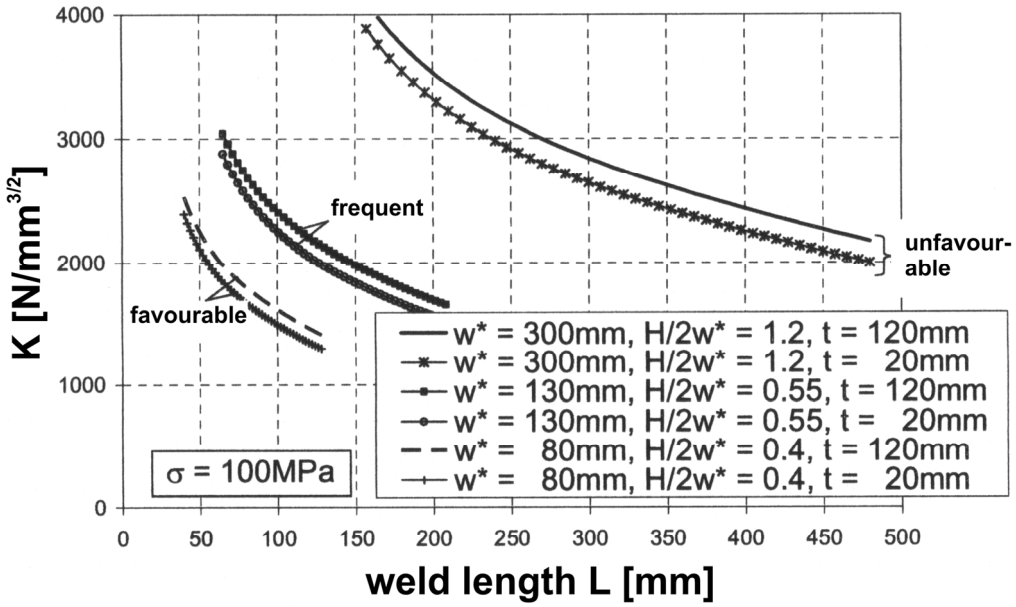


Fig. 4-34: K_{appl} depending on the weld length L

4.2.3 Tables for the choice of material to avoid brittle fracture

(1) Tables 4-2 to 4-5 give the allowable gusset plate widths w* for the different limits of parameters according to table 4-1.

L/w* **≥ 1.3** **t ≤ 120mm** - safety verification not fulfilled, special examination required																									
H/2w* ≤ 0.55 all: all widths of gusset plates permitted																									
steel grade	sub grade	Charpy energy CVN		reference temperature T_{Ed} in °C																					
		at T [°C]	J min.	10	0	-10	-20	-30	-40	-50	10	0	-10	-20	-30	-40	-50	10	0	-10	-20	-30	-40	-50
				σ_{Ed}=0,75*f_y(t)							σ_{Ed}=0,50*f_y(t)							σ_{Ed}=0,25*f_y(t)							
				Maximum allowable gusset plate widths **w*** in mm																					
S235	JR	20	27	-	-	-	-	-	-	-	20	-	-	-	-	-	-	60	50	30	30	20	-	-
	J0	0	27	-	-	-	-	-	-	-	50	30	20	-	-	-	-	140	90	60	50	30	30	20
	J2	-20	27	40	30	-	-	-	-	-	120	70	50	30	20	-	-	340	220	140	90	60	50	30
S275	JR	20	27	-	-	-	-	-	-	-	-	-	-	-	-	-	-	50	40	30	20	-	-	-
	J0	0	27	-	-	-	-	-	-	-	40	20	-	-	-	-	-	120	80	50	40	30	20	-
	J2	-20	27	30	20	-	-	-	-	-	90	50	40	20	-	-	-	280	180	120	80	50	40	30
	M,N	-20	40	50	30	20	-	-	-	-	140	90	50	40	20	-	-	440	280	180	120	80	50	40
	ML,NL	-50	27	140	80	50	30	20	-	-	380	230	140	90	50	40	20	all	all	440	280	180	120	80
S355	JR	20	27	-	-	-	-	-	-	-	-	-	-	-	-	-	-	40	30	20	-	-	-	-
	J0	0	27	-	-	-	-	-	-	-	20	-	-	-	-	-	-	80	50	40	30	20	-	-
	J2	-20	27	-	-	-	-	-	-	-	50	30	20	-	-	-	-	190	120	80	50	40	30	20
	K2,M,N	-20	40	30	-	-	-	-	-	-	80	50	30	20	-	-	-	310	190	120	80	50	40	30
	ML,NL	-50	27	80	40	30	-	-	-	-	230	140	80	50	30	20	-	all	480	310	190	120	80	50
S420	M,N	-20	40	-	-	-	-	-	-	-	50	40	20	-	-	-	-	240	150	90	60	40	30	20
	ML,NL	-50	27	50	30	-	-	-	-	-	160	90	50	40	20	-	-	all	380	240	150	90	60	40
S460	Q	-20	30	-	-	-	-	-	-	-	30	20	-	-	-	-	-	130	80	50	40	30	20	-
	M,N	-20	40	-	-	-	-	-	-	-	50	30	20	-	-	-	-	200	130	80	50	40	30	20
	QL	-40	30	20	-	-	-	-	-	-	80	50	30	20	-	-	-	330	200	130	80	50	40	30
	ML,NL	-50	27	40	20	-	-	-	-	-	130	80	50	30	20	-	-	520	330	200	130	80	50	40
	QL1	-60	30	70	40	20	-	-	-	-	220	130	80	50	30	20	-	all	520	330	200	130	80	50
S690	Q	0	40	-	-	-	-	-	-	-	-	-	-	-	-	-	-	40	30	-	-	-	-	-
	Q	-20	30	-	-	-	-	-	-	-	-	-	-	-	-	-	-	60	40	30	-	-	-	-
	QL	-20	40	-	-	-	-	-	-	-	-	-	-	-	-	-	-	90	60	40	30	-	-	-
	QL	-40	30	-	-	-	-	-	-	-	30	-	-	-	-	-	-	150	90	60	40	30	-	-
	QL1	-40	40	-	-	-	-	-	-	-	50	30	-	-	-	-	-	250	150	90	60	40	30	-
	QL1	-60	30	20	-	-	-	-	-	-	80	50	30	-	-	-	-	420	250	150	90	60	40	30

Table 4-2: Maximum allowable gusset plate width w* for common plate dimensions according to Table 4-1 for t ≤ 120 mm

L/w* ≥ 1.3			**t ≤ 40mm**	- safety verification not fulfilled, special examination required																						
H/2w* ≤ 0.55				all: all widths of gusset plates permitted																						
steel grade	sub grade	Charpy energy CVN		reference temperature T_{Ed} in °C																						
		at T [°C]	J min.	10	0	-10	-20	-30	-40	-50	10	0	-10	-20	-30	-40	-50	10	0	-10	-20	-30	-40	-50
				σ_{Ed}=0,75*f_y(t)							σ_{Ed}=0,50*f_y(t)							σ_{Ed}=0,25*f_y(t)						
				Maximum allowable gusset plate widths **w*** in mm																						
S235	JR	20	27	20	-	-	-	-	-	-	60	40	30	20	-	-	-	190	120	80	60	40	30	30
	J0	0	27	50	30	20	-	-	-	-	150	90	60	40	30	20	-	440	280	190	120	80	60	40
	J2	-20	27	150	90	50	30	20	-	-	380	240	150	90	60	40	30	all	all	440	280	190	120	80
S275	JR	20	27	-	-	-	-	-	-	-	40	30	20	-	-	-	-	150	100	70	50	30	30	20
	J0	0	27	40	20	-	-	-	-	-	110	70	40	30	20	-	-	360	230	150	100	70	50	30
	J2	-20	27	110	60	40	20	-	-	-	290	180	110	70	40	30	20	all	all	360	230	150	100	70
	M,N	-20	40	180	110	60	40	20	-	-	460	290	180	110	70	40	30	all	all	all	360	230	150	100
	ML,NL	-50	27	all	300	180	110	60	40	20	all	all	460	290	180	110	70	all	all	all	all	all	360	230
S355	JR	20	27	-	-	-	-	-	-	-	30	20	-	-	-	-	-	110	70	50	30	30	20	-
	J0	0	27	20	-	-	-	-	-	-	70	40	30	20	-	-	-	260	160	110	70	50	30	30
	J2	-20	27	60	30	20	-	-	-	-	180	110	70	40	30	20	-	all	400	260	160	110	70	50
	K2,M,N	-20	40	100	60	30	20	-	-	-	290	180	110	70	40	30	20	all	all	400	260	160	110	70
	ML,NL	-50	27	290	170	100	60	30	20	-	all	480	290	180	110	70	40	all	all	all	all	400	260	160
S420	M,N	-20	40	60	40	20	-	-	-	-	210	120	70	40	30	20	-	all	all	310	200	130	80	50
	ML,NL	-50	27	190	110	60	40	20	-	-	all	340	210	120	70	40	30	all	all	all	all	310	200	130
S460	Q	-20	30	30	20	-	-	-	-	-	100	60	40	20	-	-	-	440	270	170	110	70	50	30
	M,N	-20	40	50	30	20	-	-	-	-	170	100	60	40	20	-	-	all	440	270	170	110	70	50
	QL	-40	30	90	50	30	20	-	-	-	280	170	100	60	40	20	-	all	all	440	270	170	110	70
	ML,NL	-50	27	150	90	50	30	20	-	-	460	280	170	100	60	40	20	all	all	all	440	270	170	110
	QL1	-60	30	270	150	90	50	30	20	-	all	460	280	170	100	60	40	all	all	all	all	440	270	170
S690	Q	0	40	-	-	-	-	-	-	-	20	-	-	-	-	-	-	130	80	50	30	20	-	-
	Q	-20	30	-	-	-	-	-	-	-	40	20	-	-	-	-	-	210	130	80	50	30	20	-
	QL	-20	40	20	-	-	-	-	-	-	60	40	20	-	-	-	-	340	210	130	80	50	30	20
	QL	-40	30	30	20	-	-	-	-	-	110	60	40	20	-	-	-	all	340	210	130	80	50	30
	QL1	-40	40	50	30	20	-	-	-	-	190	110	60	40	20	-	-	all	all	340	210	130	80	50
	QL1	-60	30	90	50	30	20	-	-	-	320	190	110	60	40	20	-	all	all	all	340	210	130	80

Table 4-3: Maximum allowable gusset plate width w* for common plate dimensions according to Table 4-1 for t ≤ 40 mm

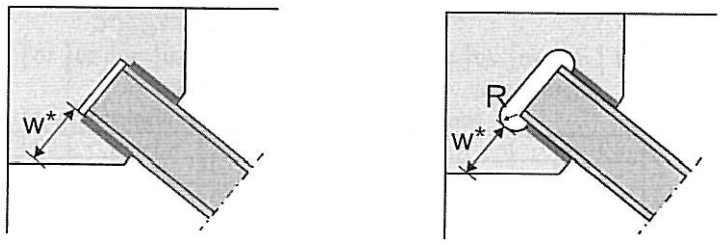
L/w* ≥ 1.6			**t ≤ 40mm**	- safety verification not fulfilled, special examination required																						
H/2w* ≤ 0.4				all: all widths of gusset plates permitted																						
steel grade	sub grade	Charpy energy CVN		reference temperature T_{Ed} in °C																						
		at T [°C]	J min.	10	0	-10	-20	-30	-40	-50	10	0	-10	-20	-30	-40	-50	10	0	-10	-20	-30	-40	-50
				σ_{Ed}=0,75*f_y(t)							σ_{Ed}=0,50*f_y(t)							σ_{Ed}=0,25*f_y(t)						
				Maximum allowable gusset plate widths **w*** in mm																						
S235	JR	20	27	40	30	20	-	-	-	-	120	70	50	30	30	20	-	380	250	170	110	80	60	40
	J0	0	27	110	60	40	30	20	-	-	300	190	120	70	50	30	30	all	all	380	250	170	110	80
	J2	-20	27	310	180	110	60	40	30	20	all	all	300	190	120	70	50	all	all	all	all	380	250	170
S275	JR	20	27	30	20	-	-	-	-	-	90	50	40	30	20	-	-	310	200	140	90	60	50	40
	J0	0	27	70	40	30	20	-	-	-	220	140	90	50	40	30	20	all	all	310	200	140	90	60
	J2	-20	27	220	130	70	40	30	20	-	all	370	220	140	90	50	40	all	all	all	all	310	200	140
	M,N	-20	40	370	220	130	70	40	30	20	all	all	370	220	140	90	50	all	all	all	all	all	310	200
	ML,NL	-50	27	all	all	370	220	130	70	40	all	all	all	all	370	220	140	all	all	all	all	all	all	all
S355	JR	20	27	-	-	-	-	-	-	-	50	30	20	-	-	-	-	210	140	90	60	40	30	30
	J0	0	27	40	20	-	-	-	-	-	130	80	50	30	20	-	-	all	340	210	140	90	60	40
	J2	-20	27	110	70	40	20	-	-	-	370	220	130	80	50	30	20	all	all	all	340	210	140	90
	K2,M,N	-20	40	200	110	70	40	20	-	-	all	370	220	130	80	50	30	all	all	all	all	340	210	140
	ML,NL	-50	27	all	350	200	110	70	40	20	all	all	all	370	220	130	80	all	all	all	all	all	all	340
S420	M,N	-20	40	130	70	40	30	-	-	-	420	250	150	90	50	30	20	all	all	all	400	250	160	100
	ML,NL	-50	27	400	230	130	70	40	30	-	all	all	420	250	150	90	50	all	all	all	all	all	400	250
S460	Q	-20	30	60	30	20	-	-	-	-	200	120	70	40	30	20	-	all	all	350	220	140	90	60
	M,N	-20	40	100	60	30	20	-	-	-	350	200	120	70	40	30	20	all	all	all	350	220	140	90
	QL	-40	30	180	100	60	30	20	-	-	all	350	200	120	70	40	30	all	all	all	all	350	220	140
	ML,NL	-50	27	320	180	100	60	30	20	-	all	all	350	200	120	70	40	all	all	all	all	all	350	220
	QL1	-60	30	all	320	180	100	60	30	20	all	all	all	350	200	120	70	all	all	all	all	all	all	350
S690	Q	0	40	-	-	-	-	-	-	-	40	30	-	-	-	-	-	260	160	100	60	40	30	20
	Q	-20	30	20	-	-	-	-	-	-	70	40	30	-	-	-	-	440	260	160	100	60	40	30
	QL	-20	40	30	20	-	-	-	-	-	130	70	40	30	-	-	-	all	440	260	160	100	60	40
	QL	-40	30	50	30	20	-	-	-	-	220	130	70	40	30	-	-	all	all	440	260	160	100	60
	QL1	-40	40	100	50	30	20	-	-	-	390	220	130	70	40	30	-	all	all	all	440	260	160	100
	QL1	-60	30	190	100	50	30	20	-	-	all	390	220	130	70	40	30	all	all	all	all	440	260	160

Table 4-4: Maximum allowable gusset plate width w* for favourable plate dimensions according to Table 4-1 for t ≤ 40 mm

L/w* ≥ 1.6			t ≤ 20mm	- safety verification not fulfilled, special examination required																					
H/2w* ≤ 0.4				all: all widths of gusset plates permitted																					
steel grade	sub grade	Charpy energy CVN		reference temperature T_{Ed} in °C																					
		at T [°C]	J min.	10	0	-10	-20	-30	-40	-50	10	0	-10	-20	-30	-40	-50	10	0	-10	-20	-30	-40	-50
				σ_{Ed}=0,75*f_y(t)							σ_{Ed}=0,50*f_y(t)							σ_{Ed}=0,25*f_y(t)							
				Maximum allowable gusset plate widths **w*** in mm																					
S235	JR	20	27	140	90	50	30	20	-	-	all	250	160	100	70	40	30	all	all	all	330	220	150	110
	J0	0	27	all	240	140	90	50	30	20	all	all	all	250	160	100	70	all	all	all	all	all	330	220
	J2	-20	27	all	all	all	240	140	90	50	all	all	all	all	all	250	160	all	all	all	all	all	all	all
S275	JR	20	27	100	60	30	20	-	-	-	300	180	120	70	50	30	20	all	all	all	270	180	120	90
	J0	0	27	280	170	100	60	30	20	-	all	all	300	180	120	70	50	all	all	all	all	all	270	180
	J2	-20	27	all	all	280	170	100	60	30	all	all	all	all	300	180	120	all	all	all	all	all	all	all
	M,N	-20	40	all	all	all	280	170	100	60	all	all	all	all	all	300	180	all	all	all	all	all	all	all
	ML,NL	-50	27	all	all	all	all	all	280	170	all	all	all	all	all	all	all	all	all	all	all	all	all	all
S355	JR	20	27	50	30	20	-	-	-	-	180	110	70	40	30	20	-	all	all	290	190	120	80	60
	J0	0	27	150	90	50	30	20	-	-	all	290	180	110	70	40	30	all	all	all	all	290	190	120
	J2	-20	27	all	270	150	90	50	30	20	all	all	all	290	180	110	70	all	all	all	all	all	all	290
	K2,M,N	-20	40	all	all	270	150	90	50	30	all	all	all	all	290	180	110	all	all	all	all	all	all	all
	ML,NL	-50	27	all	all	all	all	270	150	90	all	all	all	all	all	all	290	all	all	all	all	all	all	all
S420	M,N	-20	40	all	310	170	100	60	30	20	all	all	all	340	200	120	70	all	all	all	all	all	all	340
	ML,NL	-50	27	all	all	all	310	170	100	60	all	all	all	all	all	340	200	all	all	all	all	all	all	all
S460	Q	-20	30	240	140	80	40	30	20	-	all	all	270	160	100	60	30	all	all	all	all	all	290	190
	M,N	-20	40	all	240	140	80	40	30	20	all	all	all	270	160	100	60	all	all	all	all	all	all	290
	QL	-40	30	all	all	240	140	80	40	30	all	all	all	all	270	160	100	all	all	all	all	all	all	all
	ML,NL	-50	27	all	all	all	240	140	80	40	all	all	all	all	all	270	160	all	all	all	all	all	all	all
	QL1	-60	30	all	all	all	all	240	140	80	all	all	all	all	all	all	270	all	all	all	all	all	all	all
S690	Q	0	40	40	20	-	-	-	-	-	170	100	60	30	20	-	-	all	all	350	210	130	80	50
	Q	-20	30	80	40	20	-	-	-	-	300	170	100	60	30	20	-	all	all	all	350	210	130	80
	QL	-20	40	140	80	40	20	-	-	-	all	300	170	100	60	30	20	all	all	all	all	350	210	130
	QL	-40	30	250	140	80	40	20	-	-	all	all	300	170	100	60	30	all	all	all	all	all	350	210
	QL1	-40	40	all	250	140	80	40	20	-	all	all	all	300	170	100	60	all	all	all	all	all	all	350
	QL1	-60	30	all	all	250	140	80	40	20	all	all	all	all	300	170	100	all	all	all	all	all	all	all

Table 4-5: Maximum allowable gusset plate width w* for favourable plate dimensions according to Table 4-1 for t ≤ 20 mm

(2) If the slot has no sharp corners by rounding the ends, this would enhance the fatigue resistance and therefore also reduce the toughness requirement, see fig. 4-35.



reference detail air gap and cut out

Fig. 4-35: Alternative gusset plate connection

(3) Table 4-6 gives the allowable plate width w* for a cut out with a radius of 30 mm.

L/w* ≥ 1.3			t ≤ 40mm								- safety verification not fulfilled, special examination required														
H/2w* ≤ 0.55			radius R = 30 mm								all: all widths of gusset plates permitted														
steel grade	sub grade	Charpy energy CVN at T [°C]	J min.	reference temperature T_{Ed} in °C 10	0	-10	-20	-30	-40	-50	10	0	-10	-20	-30	-40	-50	10	0	-10	-20	-30	-40	-50
				σ_{Ed}=0,75*f_y(t)							σ_{Ed}=0,50*f_y(t)							σ_{Ed}=0,25*f_y(t)						
				Maximum allowable gusset plate widths **w*** in mm																					
S235	JR	20	27	50	30	20	-	-	-	-	100	70	50	40	30	20	20	240	180	130	100	80	60	50
	J0	0	27	100	70	50	30	20	-	-	210	140	100	70	50	40	30	all	340	240	180	130	100	80
	J2	-20	27	210	140	100	70	50	30	20	all	300	210	140	100	70	50	all	all	all	340	240	180	130
S275	JR	20	27	30	20	-	-	-	-	-	80	60	40	30	20	20	-	210	150	120	90	70	50	40
	J0	0	27	70	50	30	20	-	-	-	170	120	80	60	40	30	20	all	290	210	150	120	90	70
	J2	-20	27	160	110	70	50	30	20	-	350	240	170	120	80	60	40	all	all	all	290	210	150	120
	M,N	-20	40	240	160	110	70	50	30	20	all	350	240	170	120	80	60	all	all	all	all	290	210	150
	ML,NL	-50	27	all	360	240	160	110	70	50	all	all	all	350	240	170	120	all	all	all	all	all	all	290
S355	JR	20	27	20	-	-	-	-	-	-	50	40	30	20	-	-	-	160	120	90	70	50	40	30
	J0	0	27	50	30	20	-	-	-	-	110	80	50	40	30	20	-	310	220	160	120	90	70	50
	J2	-20	27	100	70	50	30	20	-	-	240	160	110	80	50	40	30	all	all	310	220	160	120	90
	K2,M,N	-20	40	150	100	70	50	30	20	-	350	240	160	110	80	50	40	all	all	all	310	220	160	120
	ML,NL	-50	27	350	230	150	100	70	50	30	all	all	350	240	160	110	80	all	all	all	all	all	310	220
S420	M,N	-20	40	110	70	50	30	20	-	-	270	180	120	80	60	40	30	all	all	370	260	180	130	100
	ML,NL	-50	27	250	170	110	70	50	30	20	all	all	270	180	120	80	60	all	all	all	all	370	260	180
S460	Q	-20	30	60	40	30	20	-	-	-	150	110	70	50	30	20	20	all	330	230	160	120	80	60
	M,N	-20	40	90	60	40	30	20	-	-	230	150	110	70	50	30	20	all	all	330	230	160	120	80
	QL	-40	30	140	90	60	40	30	20	-	340	230	150	110	70	50	30	all	all	all	330	230	160	120
	ML,NL	-50	27	210	140	90	60	40	30	20	all	340	230	150	110	70	50	all	all	all	all	330	230	160
	QL1	-60	30	330	210	140	90	60	40	30	all	all	340	230	150	110	70	all	all	all	all	all	330	230
S690	Q	0	40	-	-	-	-	-	-	-	50	30	20	-	-	-	-	190	130	90	60	50	30	20
	Q	-20	30	20	-	-	-	-	-	-	70	50	30	20	-	-	-	270	190	130	90	60	50	30
	QL	-20	40	40	20	-	-	-	-	-	110	70	50	30	20	-	-	all	270	190	130	90	60	50
	QL	-40	30	60	40	20	-	-	-	-	160	110	70	50	30	20	-	all	all	270	190	130	90	60
	QL1	-40	40	90	60	40	20	-	-	-	250	160	110	70	50	30	20	all	all	all	270	190	130	90
	QL1	-60	30	140	90	60	40	20	-	-	380	250	160	110	70	50	30	all	all	all	all	270	190	130

Table 4-6: Maximum allowable gusset-plate width w^* for a cut out with a radius of 30 mm.

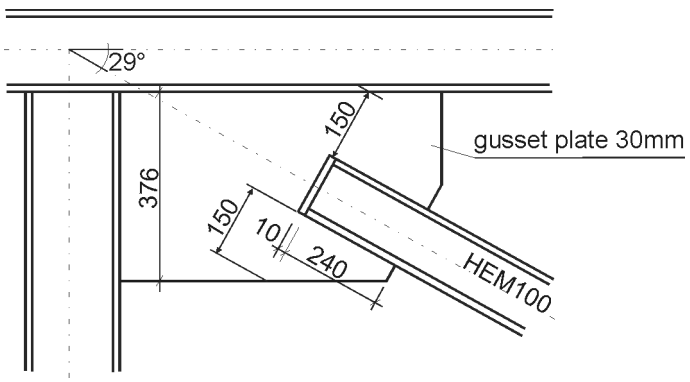
4.2.4 Example

(1) For a design situation as given in fig. 4-36, the following geometric data apply:

- Gusset plate thickness t = 30 mm
- Weld length L = 240 mm
- Slot width H = 120 mm
- Net width w* of gusset plate w* = 150 mm

giving the following parameters for Table 4-4

$L / w^* = 1{,}6$
$H / 2w^* = 0{,}4$
$t \leq 40\,mm$



From static design:

Force of diagonal bar D_d

1310 kN

Steel grade S355

Fig. 4-36: Example for a gusset plate connection

(2) In case the cut out of the gusset plate would not be symmetrical $\left(w_1^* \neq w_2^*\right)$ the verification should be performed independently for both sides of the connection using

$L/w_1^*, L/w_2^*$
$H/2w_1^*, H/w_2^*$

(3) The loading situation for the ultimate limit state verification is

D_{Ed} = 1310 kN

which yields

$$\sigma_{ULS} = \frac{D_{EdLS}}{A_{net}} = \frac{D_d}{2w * t} = \frac{1310}{2 \cdot 150 \cdot 30} = 144 N/mm^2$$

The reference stress σ_{Ed} for the choice of material should be determined for the "frequent" loading situation, for which (on the safe side) the characteristic value of stress is taken:

$$\sigma_{ULS} = \frac{\sigma_{ULS}}{\gamma_F} = \frac{144}{1{,}35} = 107 N/mm^2$$

which gives for Table 4-4:

$$\sigma_{Ed} = \frac{\sigma_{Ed}^*}{f_y(t)} = \frac{107}{347{,}5} f_y(t) = 0{,}31 f_y(t)$$

(4) The design temperature T_{Ed} is defined by

$$T_{Ed} = T_{mdv} + \Delta T_{\dot{\varepsilon}} + \Delta T_{\varepsilon cf}$$

for which T_{Ed} = - 30°C

is specified (strain-rate effects and cold forming are not considered).

(5) Using Table 4-4, the allowable gusset-plate width can be interpolated as follows for steel grade S355 J2:

allow. w^* for σ_{Ed} = 0,25 f_y (t) = 210 mm
allow. w^* for σ_{Ed} = 0,50 f_y (t) = 50 mm
allow. w^* for σ_{Ed} = 0,32 f_y (t) = 171 mm

which is larger than the choice made (150 mm).

4.2.5 Bibliography

[1] Kühn, B.: Beitrag zur Vereinheitlichung der europäischen Regelungen zur Vermeidung von Sprödbruch, Diss. RWTH Aachen, Heft 54, Shaker Verlag, Aachen 2005, ISBN 3-8322-3901-4

[2] Höhler, S.: Beitrag zur Erweiterung der Regelungen der Stahlsortenwahl zur Vermeidung von Sprödbruch auf Anschlüsse unter vorwiegend ruhender Beanspruchung, Diss. RWTH Aachen, Heft 58, Shaker Verlag, Aachen 2006, ISBN 3-8322-5399-8

[3] Klinkenberg, A., Peter, A., Saal, H., Volz, M.: Berechnungsmodelle für geschweißte Anschlüsse in ausgeschnittenen Knotenblechen, Stahlbau 68 (1999), S. 173-180, und Berichtigungen/Ergänzungen S. 688-689

Section 5

5. Other toughness-related rules in EN 1993

5.1 The role of upper-shelf toughness

5.1.1 Resistance rules in Eurocode 3 and upper-shelf toughness

(1) The strength-related design rules in the various parts of EN 1993 have been presented in such a way that ductile behaviour of the material is assumed and the material toughness seems to have no significant effect on the attainment of the ultimate limit state, see fig. 1-2.

(2) Material toughness is only explicitly addressed in EN 1993-1-10 for the choice of material to avoid brittle fracture, but not any more in other parts of Eurocode 3.

(3) As, however, the rules in EN 1993-1-10 exclude only brittle fracture in the temperature-transition range of the material toughness, see fig. 2-11, a basic prerequisite of the strength related design rules in view of toughness is, that the toughness properties in the upper-shelf region of the toughness temperature diagram are sufficient to attain these strengths.

(4) EN 1993-1-10 does not address the toughness properties in the upper-shelf region. Therefore toughness limits in the upper-shelf region have been implicitly taken into account in the strength rules of the various parts of Eurocode 3, so that they reflect the requirements from both strength and toughness.

(5) Fig. 5-1 explains the principle underlying the involvement of the upper-shelf toughness in the strength rules in Eurocode 3.

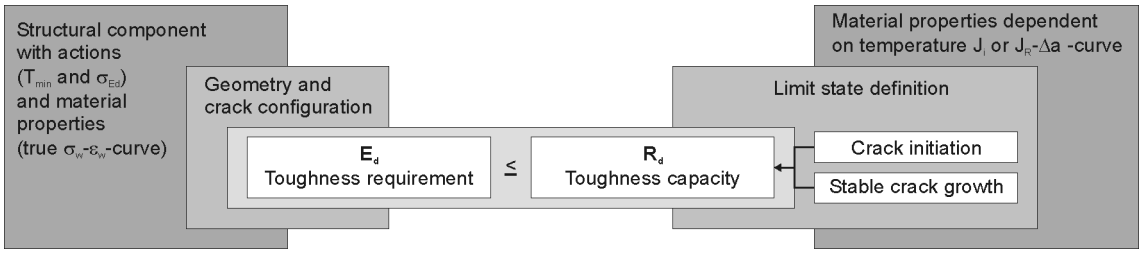


Fig. 5-1: Principle underlying the involvement of upper-shelf toughness in the strength rules in Eurocode 3.

(6) A basic safety criterion for all strength rules in Eurocode 3 is, that for any resistance in tension, the accidental presence of crack-like flaws is assumed independently of the execution requirement in EN 1090-2, which does not permit any detectable cracks in inspections after execution.

(7) This assumption makes it possible to link the resistance rules in Eurocode 3 with toughness requirements and to make this link accessible to numerical checks where appropriate numerical models for the toughness verification in the upper-shelf region are available.

(8) The safety criteria for the toughness verification in the various parts of Eurocode 3 are the following:

1. For any of the rules, the ductility requirement is that net section yielding shall be reached before fracture in the net section.
2. For some of the rules (where capacity design applies) the ductility requirement is that gross section yielding must occur before fracture in the net section.

5.1.2 Appropriate models for calculation of upper shelf toughness requirements

5.1.2.1 General

(1) There are two mechanical approaches for determining the ultimate resistance of steel components in tension in the upper-shelf region of the toughness temperature diagram:

1. fracture mechanics
2. damage mechanics

(2) Fracture mechanics procedures are well established. International guidelines such as BS7910 or FITNET procedure have been published. Therefore, the application is recommended in such areas where crack like defects may be assumed in constructions.

(3) Damage mechanics allows to determine the fracture behaviour of structural components in tension also without the assumption of crack-like imperfections, because structural response to load is modelled on the microscopic level where void nucleation, void growth and void coalescence leads to crack initiation and to further stable crack growth. Such models employ material parameters which can be determined from tests. More details of this approach, which is in the state of development for practical applications, are given in section 6.

5.1.2.2 Fracture mechanics approach for upper-shelf behaviour

(1) In case of upper shelf behaviour the development of a fracture is governed by local and global plasticity of the material. Fig. 2-1 shows that temperatures higher than the transition temperature for instable crack growth initiate cracks in a stable manner and crack growth consumes further energy, different to the instable behaviour in the brittle area. On a global scale the net section reaches yielding and plasticity starts to spread over the gross section and may reach gross section yielding before a crack initiates, when toughness is high and initial damage is small.

(2) In many design rules for steels structures the relation between the tensile strength R_m and the yield strength R_e is assumed to represent ductility and resistance against fracture. This assumption can be interpreted as follows.

(3) The tensile strength $f_u = R_m$ of the material is considered to be the limit where fracture in the net section occurs and the yield strength, $f_y = R_{el}$ is used to determine the stress σ_{gy} for net section yielding.

(4) The fracture stress $\sigma_{fracture}$ and the yield stress σ_{gy} applied to the gross section could be determined for a plate with a center crack as given in fig. 5-2, if infinite material toughness is presumed.

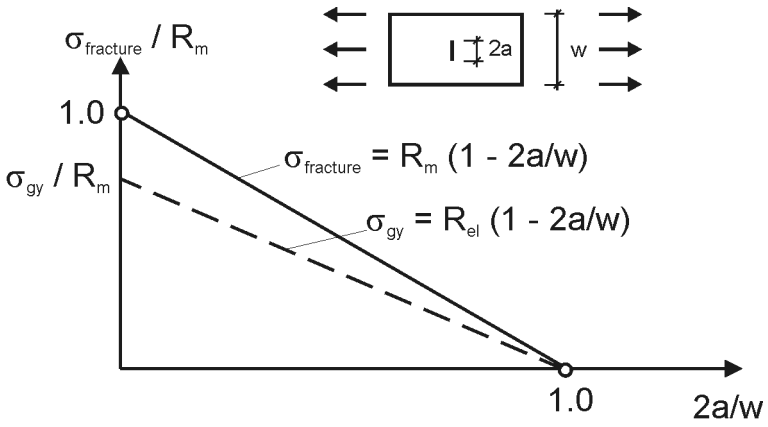


Fig. 5-2: Limits for $\sigma_{fracture}$ and σ_{gy} dependent on A_{net}/A_{gross}

(5) In practice many tests have been performed on wide plates with defined cracks of different geometry and position made from structural steels with yield strength between 235 and 890 MPa and representing different toughness levels (steel quality). Typical Wide Plate test components are shown in Fig. 5-3. Such cracks have normally been introduced by sawing or sawing plus fatigue.

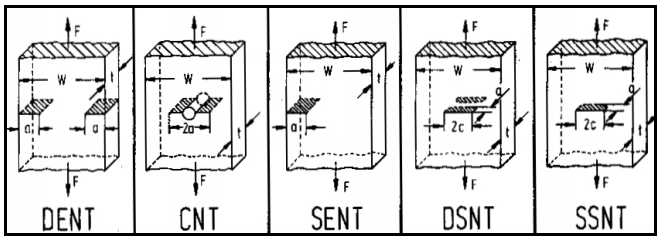


Fig. 5-3: Typical Wide Plate test components with different position and geometry of defined cracks. The short name is explained following:

DENT (Double Edge Notched Tension)
CNT (Centre Notched Tension)
SENT (Single Notched Tension)
DSNT (Double Surface Notched Tension)
SSNT (Single Surface Notched Tension)

(6) From such tests the influence of the material toughness in the upper-shelf region and the strength R_m and R_e together with the geometry of the test specimens and the crack geometry on the fracture stress has been studied. Fig. 5-4 gives some typical test results for a steels grade S355 J2 and for different specimen types. .

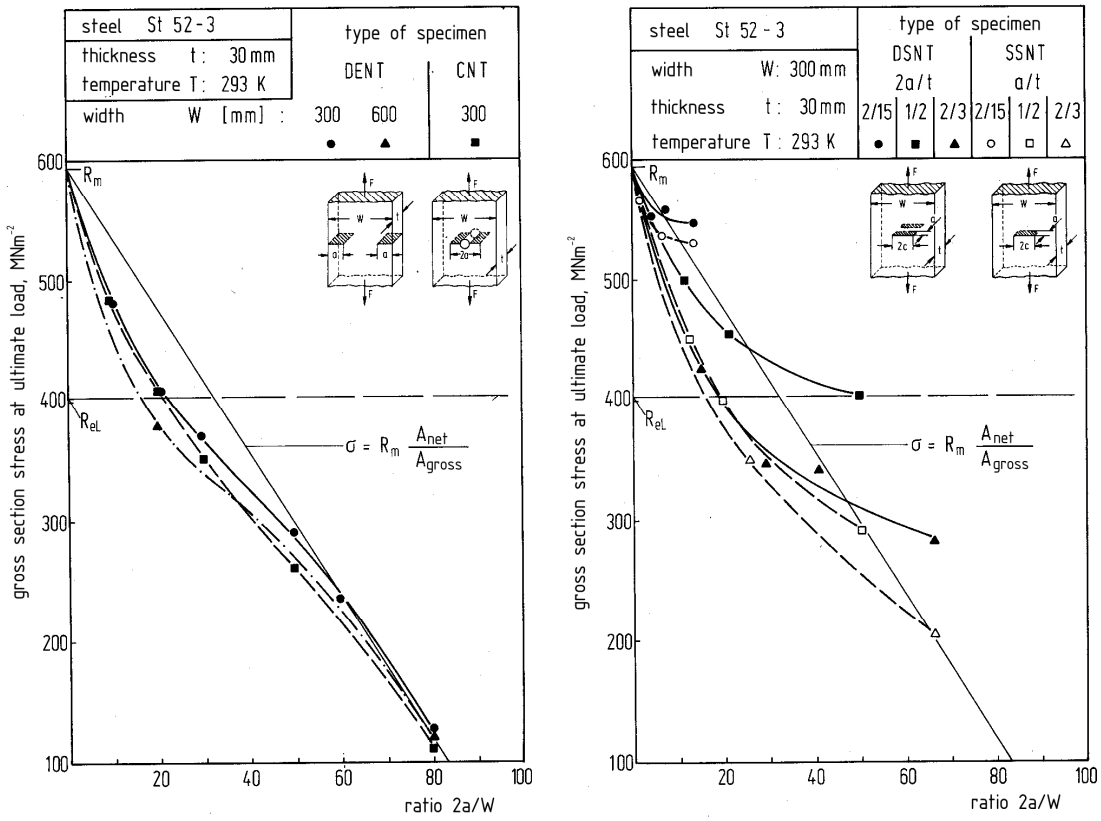


Fig. 5-4: Actual fracture stresses dependent on $\frac{A_{net}}{A_{gross}}$

(7) The result shows, that only for crack-free structures the theoretical fracture stress $f_u = R_m$ (1-2a/W) may be reached. In case of cracks the real fracture stress is lower. How low the real fracture stress is depends on the material toughness and the geometry of the defect.

5.1.2.3 Basis for the calculation of the upper shelf fracture resistance

(1) For the fracture mechanics based failure analysis in the upper-shelf region ideally the elastic plastic J-Integral is used. However the Failue Assessment Diagram can also be used beyond net section yielding.

(2) The toughness requirement for a structural member with cracks expressed in terms of the J-Integral may be obtained from FEM (e.g. with ABAQUS) calculations using the following input parameters:

- the true stress-strain curve valid for the temperature considered, including the Lueders strain where necessary.
- the von Mises yield criterion and isotropic material considered
- elasto-plastic-calculations with deformation control

A result from such a calculation for different stress strain curves is shown in fig. 5-5.

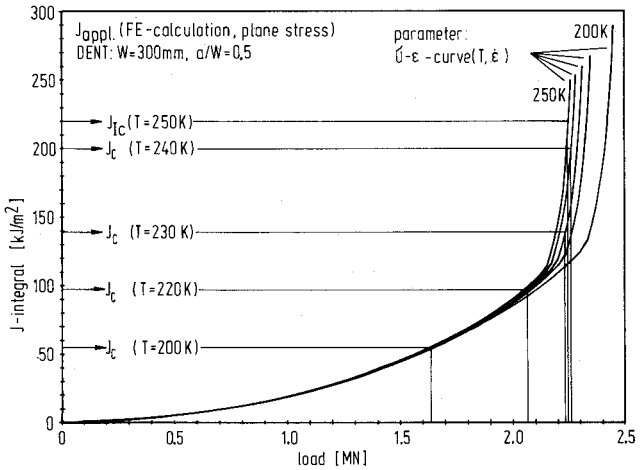


Fig. 5-5: Example for J_{appl}-curves as a function of applied load and different temperatures

(3) For resistances J_{Mat} the J_i-values, which represent the start of stable crack growth, may be used. They may be based on standard CT-tests, see fig. 2-4.

(4) Fig. 5-6 gives an example for the results of such a calculation.

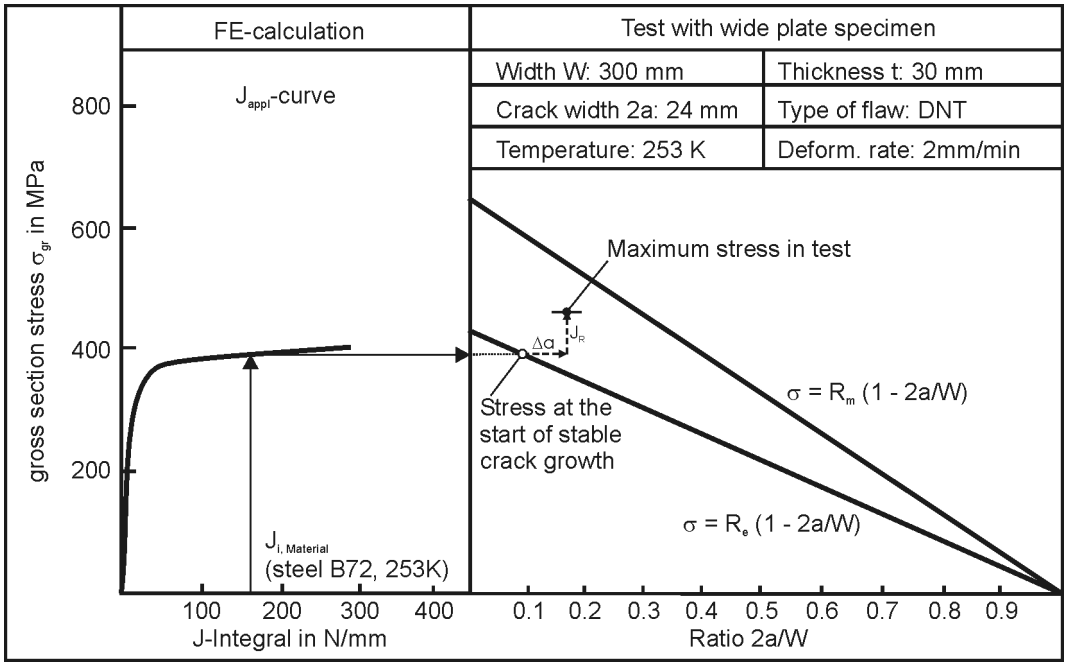


Fig. 5-6: Fracture mechanical assessment in the upper-shelf region

(5) On the left hand side of fig. 5-6, the J_{appl}-curve is given versus the stresses applied to the gross section of a test specimen (made of steel S355 N) tested at T = -20°C, for which a J_i-value of 170 KN/m had been determined.

(6) On the right hand side of fig. 5-6, the fracture strength as calculated with J_i is indicated; it is below the theoretical resistance curve

$$\sigma_{ult} = R_m \left(1 - \frac{2a}{w}\right) \tag{5-1}$$

but above the stress for net section yielding

$$\sigma_{gy} = R_{el}\left(1-\frac{2a}{w}\right) \qquad (5\text{-}2)$$

(7) The experimental value of resistance is also indicated; it requires a higher toughness value $J_{R,}$ that results from a certain amount Δa of stable crack growth.

(8) Above the temperature T_i, where failure occurs after a certain amount of stable crack growth, the failure analysis on the basis of J_i is conservative. But it may be based on the tearing instability concept.

(9) Herein the J-integral J_{appl} as a function of crack length and load F is compared with the J_R - Δa crack resistance curve, for which fig. 5-7 gives examples

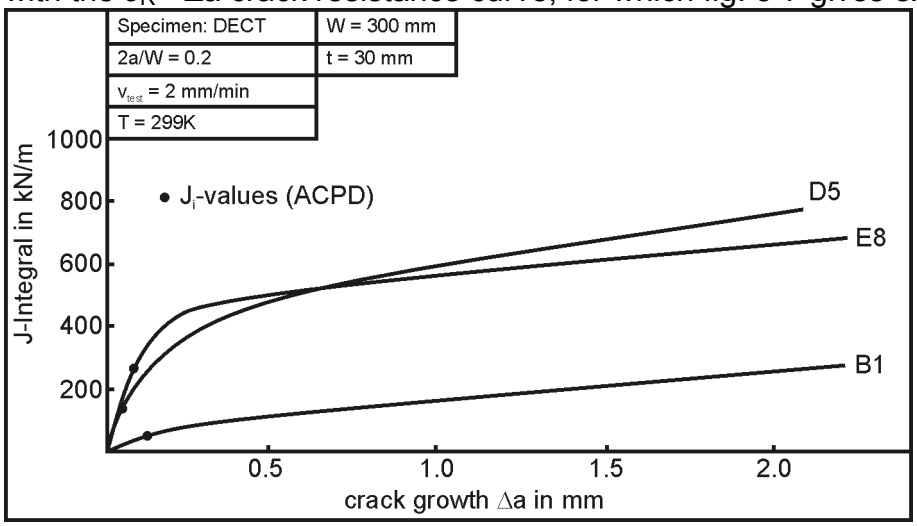


Fig. 5-7: J_R - Δa curves and J_i-values

(10) The tearing instability concept uses the point of instability defined by

$$J_{appl}(a, F) = J_R(\Delta a) \qquad (5\text{-}3)$$

and

$$\frac{\partial J_{appl}}{\partial a} \geq \frac{\partial J_R}{\partial a}. \qquad (5\text{-}4)$$

This means that the limit state is reached, where the J_{appl} (a, F)-curve has a common tangent point with the J_R (Δa)-curve, see fig. 5-8.

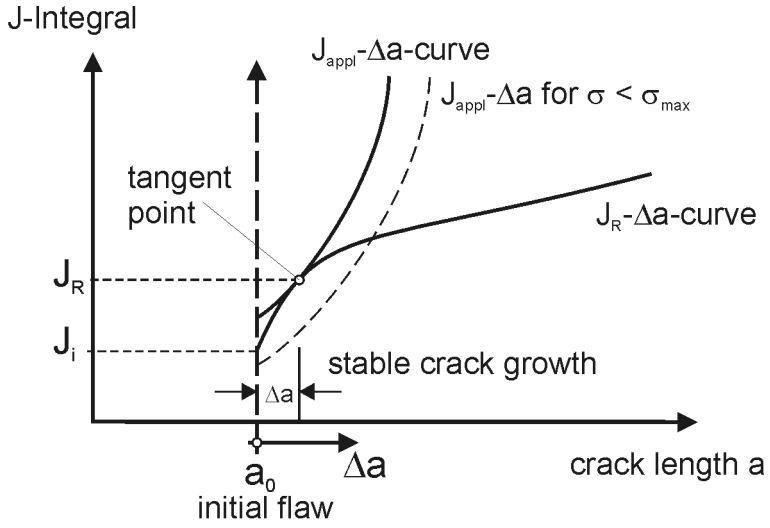


Fig. 5-8: Determination of fracture resistance with stable crack growth

(11) The J_R - Δa-curve is a material property independent on the stress-state (as the J_i-value is), if the curve is determined from a test specimen with a stress situation which is equal to and more severe than the stress state of the structural component considered; this applies to CT-test specimens.

(12) This concept can also be used in conjunction with the FAD concept.

5.1.3 Transfer of upper shelf toughness models into practice

(1) In the following, results of toughness checks that are either experimental or calculative, are presented to explain in what way toughness criteria have influenced the design rules for resistances in the various parts of Eurocode 3.

(2) Section 5.2 explains the background of the recommendation for sufficient upper-shelf toughness in table 3-1 of EN 1993-2 – Design of steel bridges.

(3) Section 5.3 gives explanations of net section resistances in EN 1993-1-1, 6.23 (2) b) and 6.2.5 (4).

(4) Section 5.4 addresses the choice of material for “capacity design” as used for plastic hinges or for seismic resistant structures.

5.2 Empirical rules for minimum upper-shelf toughness

5.2.1 General

(1) Whereas the mechanical modelling for the fracture-mechanical assessment in the temperature transition range of the toughness temperature diagram can be based on geometrically independent material values determined from small-scale tests (applicable to $T \leq T_i$ with the limit state of crack initiation), the verification in the upper-shelf region of the temperature needs the stable crack growth to be considered by the J_R-Δa-curves, that for accuracy reasons need tests on large scale members with geometries similar to the one for the member in question.

(2) Before such methods for the quantitative toughness assessment in the upper-shelf region were developed, particular qualitative assessment methods were

used which were based on test pieces with initial cracks that were subjected to large plastic strains.

(3) An example for such a test was the AUBI-test according to the German specification SEP 1390 (1996), which was required for plate thicknesses larger than 30 mm for welded structures subjected to tensile stresses for steel grades S235, S275 and S355, see fig. 5-9.

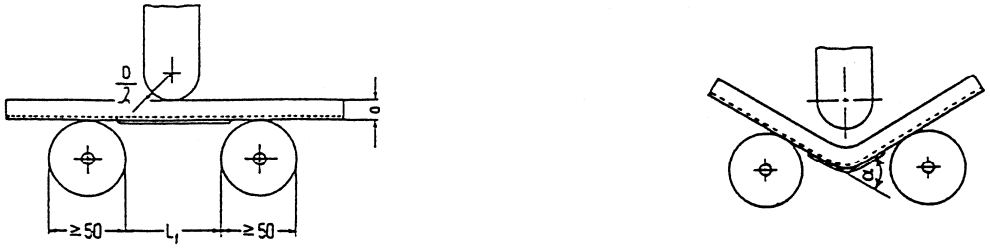


Fig. 5-9: AUBI-test according to SEP 1390 (1996)

(4) The principles of the AUBI-test are:

1. On the tension side of the test piece, a weld bead is applied that is brittle enough to act as crack starter when the test piece is bent.
2. The test piece is bent “quasi-statically” to an angle of 60°.
3. The material is accepted if the crack growth initiated from the brittle weld bead and driven by the tensile strains from plastic bending is stopped in the heat affected zone or in the base material without exceeding a certain crack length at the angle of 60°.

(5) The test has the disadvantage that it cannot be correlated quantitatively with any member loading nor with a realistic member resistance, so that no relation can be established with the realistic member performance in the ultimate limit state. Insofar, the test gave only empirical data, which, however, have lead to an enhancement of the product quality of structural steels now represented by fine grain steels according to EN 10025-3/4. Because of their production technology, these fine grain steels have better toughness properties than classical steels.

(6) In order to maintain this quality standard in the upper-shelf region without applying the AUBI-test, it was necessary to correlate the results of the AUBI-test with the methods used in Eurocode 3.

5.2.2 AUBI-quality and correlations

5.2.2.1 Correlation to Charpy-V-impact energies

(1) To identify an equivalence between the acceptance of material by the AUBI-test and associated values A_V of Charpy-V-impact tests at T = -20°C, particular tests were carried out with a selection of 13 steel plates that were considered to be critical in view of AUBI acceptance.

(2) Fig. 5-10 shows the results of the AUBI-tests with failure before an angle of 60° was reached and without failure at an angle of 60°, as well as some results (non fracture) at an angle of 90°. The fig. also indicates the plate thicknesses tested.

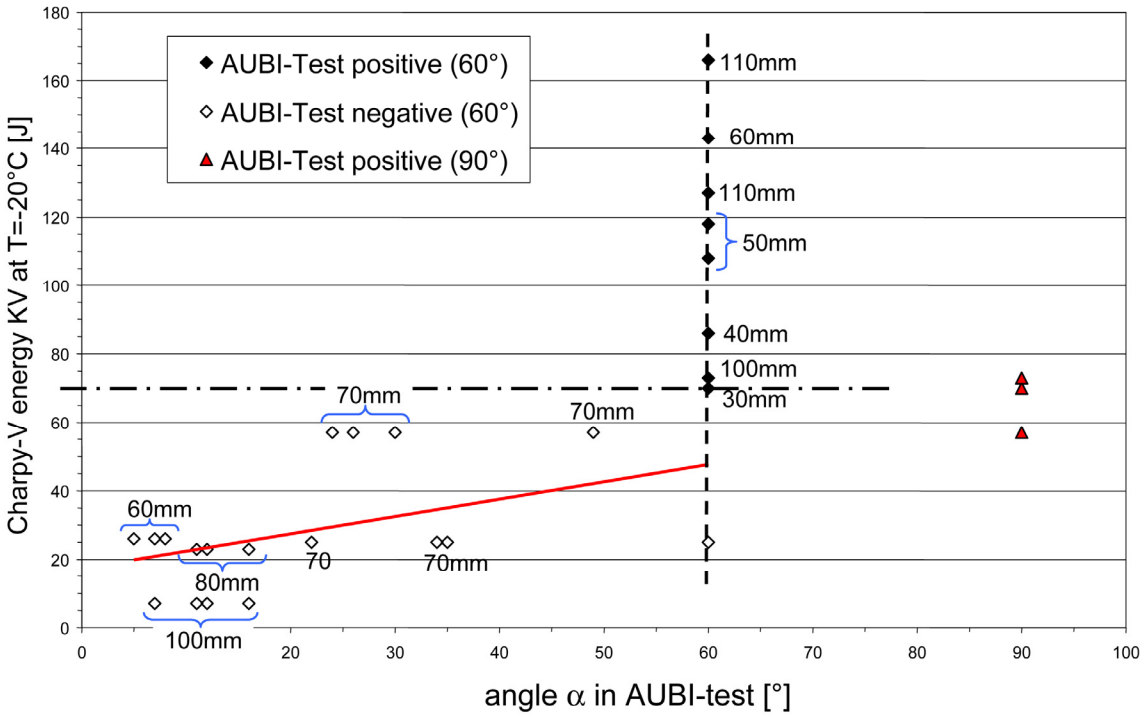


Fig. 5-10: Comparison of AUBI-tests and Charpy-V energy results in Joule

(3) Fig. 5-10 gives a trend relationship between K_v at T_{Kv} = -20°C and the attainable bending angle α in the AUBI-test. But the small number of tests and the large scatter do not allow the development of an acceptable correlation. The K_v-values allocated to AUBI-tests with different plate thicknesses that were accepted at an angle of 60°, do not give any correlation either.

(4) Hence it is not possible to apply any reliability evaluation to the tests; the only conclusion is the engineering judgement that the borderline between AUBI-tests accepted and non-accepted may be estimated at $T_{70J} \leq$ - 20°C. A dependence on thickness of the material cannot be found.

(5) The conclusion was, that it would be preferable to correlate the acceptance and non-acceptance by the AUBI-test directly with the toughness qualities of modern steels according to EN 10025 Parts 3 and 4 instead of developing equivalence criteria for Charpy-energy testing that shall lead to such qualities.

(6) In the following, such a correlation is developed.

5.2.2.2 Correlation to steel qualities

(1) For the correlation between the acceptance and non-acceptance of the AUBI-test and the steel quality according to EN 10025, the quality control data for 4 different steel producers for the production period after 1996 for steels S355 J2 G3, were evaluated. In total 1133 AUBI-tests were carried out, from which 18 tests (1,59%) failed in the production control.

(2) The analysis of those AUBI-tests that did not fail revealed that those steels complied both in their chemical analysis and their mechanical properties with fine-grain-steels according to EN 10025-2/4. This means that the AUBI-test indirectly requires higher qualities of S355 according to EN 10025.

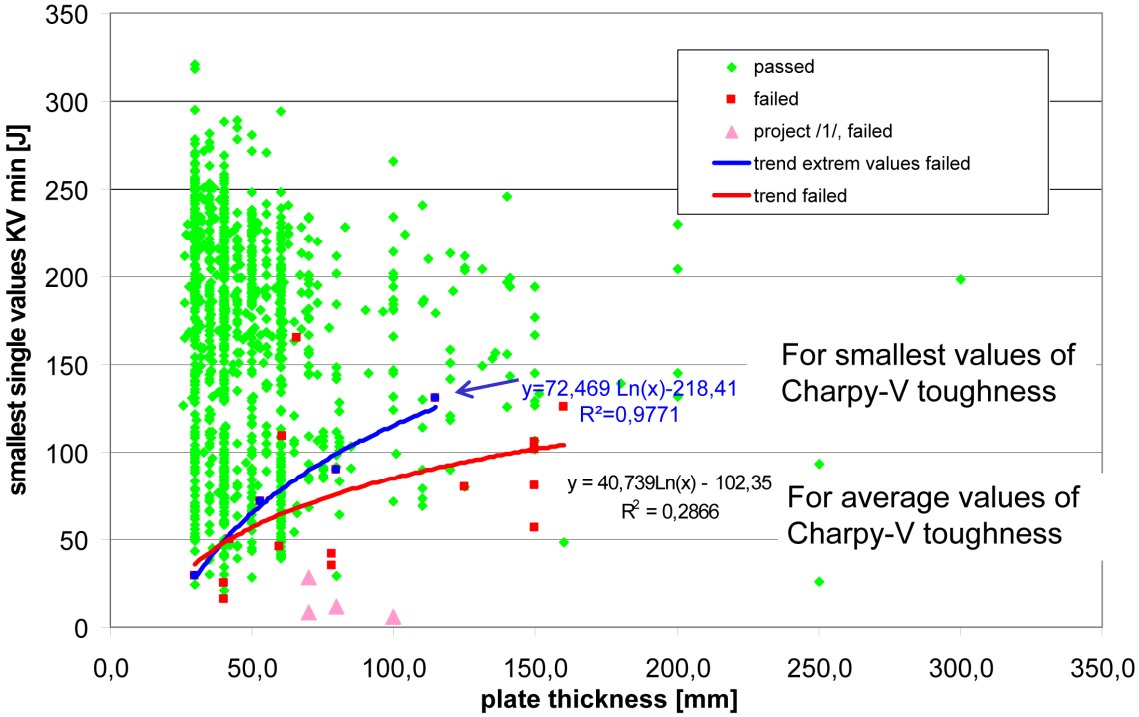


Fig. 5-11: trend analysis for the AUBI correlation

(3) Fig. 5-11 shows the trend analysis for average values and for the lowest single values of Charpy-energies for AUBI-tests, that passed and that failed independent of the plate-thickness: It becomes clear that the correlation between the K_V-values and the AUBI-test results suffers from a large scatter. A certain tendency is related to the thickness influence.

(4) For further evaluation in a first step, a safe-sided equivalence criterion was developed in assuming that the portion of AUBI-tests that failed (1.8 %) is weighed in the same way as those that passed (98.4 %). Table 5-1 shows the results in the column “equal weighing”.

Range of thickness in mm	Passed AUBI-tests Lower distribution free tolerance limit T_U		Failed AUBI-tests Extreme values T_E	Equivalence criterium			
				Equal weighting		Weighting acc. to failure probability	
				Smallest single value	Average value	Smallest single value	Average value
	$K_{v,min}$ in J at T = -20 °C	Proportion of population in %	K_v in J at T = -20 °C	$K_{v,min}$ in J at T = -20 °C	K_v in J at T = -20 °C	$K_{v,min}$ in J at T = -20 °C	K_v in J at T = -20 °C
(=30)			(=29)				
30 ≤ t < 50	21	98,68	49	35	50	21	30
50 ≤ t < 80	29	97,36	85	57	81	30	43
≥ 80	26	96,76	100	63	90	31	45

Table 5-1: Equivalence criteria from steel quality control data; the results of Charpy-energy tests refer to the test temperature of -20°C

(5) If the weighing of the portion that failed is assumed to be according to the failure probability as indicated in fig. 5-12, the equivalence values are reduced accordingly. These results are more realistic and therefore are used for the following conclusion.

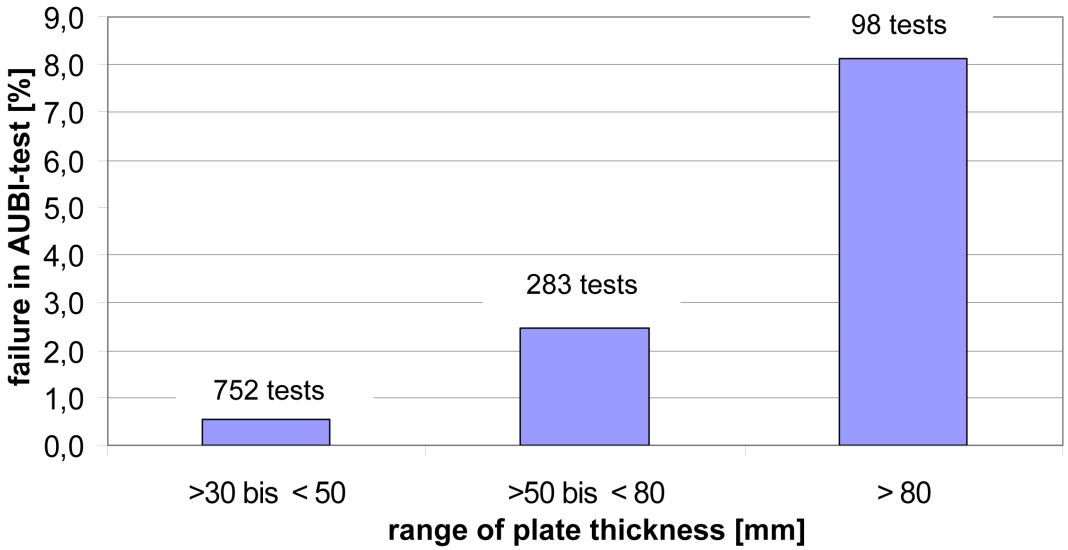


Fig. 5-12: Failure probability of AUBI-tests in steel production control

5.2.2.3 Conclusions

(1) The results in Table 5-1 show that for plate-thicknesses t < 30 mm no AUBI-tests are necessary, as the T_{27J}-values according to EN 10025 are sufficient to reach the acceptance of AUBI-tests.

(2) For plate thicknesses 30 mm ≤ t ≤ 80 mm, the requirements from the column "Weighing according to the failure-probability" of table 5-1 are close to those specified for T = -20°C for fine-grain steels in EN 10025.

(3) In conclusion, a sufficient steel quality to stop crack growth from initial cracks due to large straining as carried out in the AUBI-tests, can be achieved by applying the choice of material given in table 3.1 of EN 1993 – Part 2, see table 5-2.

Example	Nominal plate thickness	Additional requirement
1	t ≤ 30 mm	T_{27J} = -20 °C acc. to EN 10025
	30 < t ≤ 80 mm	Fine grained steel acc. to EN 10025, e.g. S355N/M
	t > 80 mm	Fine grained steel acc. to EN 10025, e.g. S355NL/ML

Table 5-2: Choice of material given in table 3.1 of EN 1993-2

(4) The consequence of such a choice is given in fig. 5-13

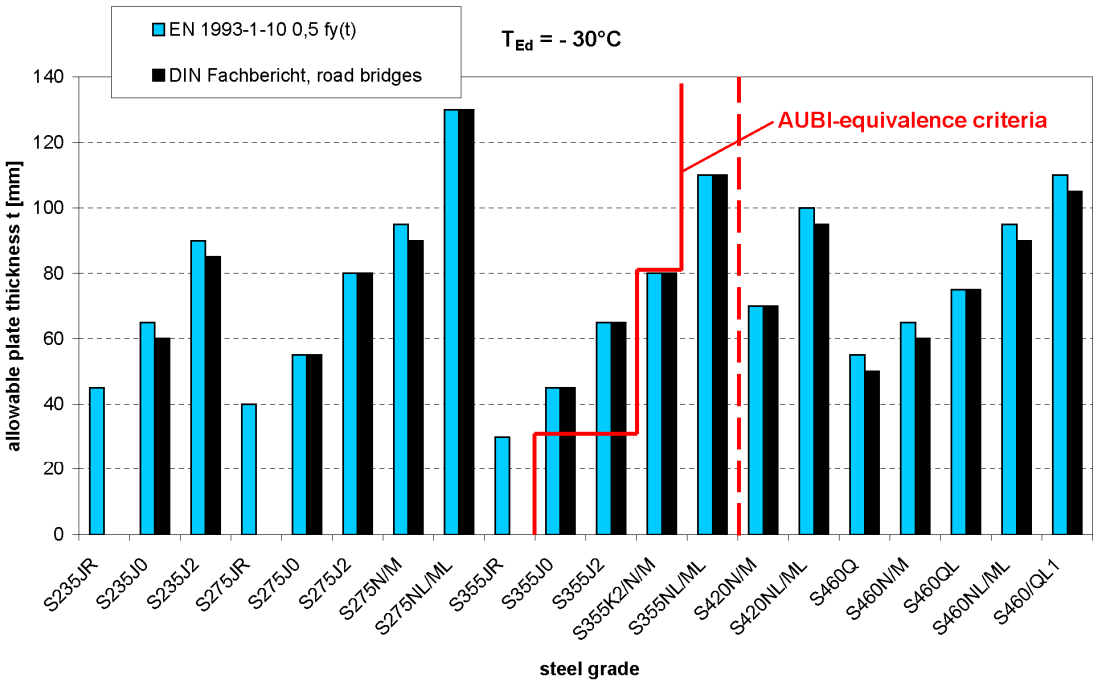


Fig. 5-13: Comparison of permissible plate thicknesses for road-bridges with σ_{Ed} = 0,5 f_y (t) according to EN 1993-1-10 and the AUBI-equivalence criteria

(5) The conclusions from Table 5.2 are given in detail in Table 5-3.

Steel grade	Product thickness [mm]		
	t ≤ 30	30 < t ≤ 80	t > 80
S355	No additional requirements	Fine grained steel type N or M acc. to EN 10025-3/-4	Fine grained steel type NL or ML acc. to EN 10025-3/-4
S275	No additional requirements	Fine grained steel type N or M acc. to EN 10025-3/-4	Fine grained steel type NL or ML acc. to EN 10025-3/-4
S235	No additional requirements	type +N or +M acc. to EN 10025-2	type +N or +M acc. to EN 10025-2

Table 5-3: Additional requirements to EN 1993-10 to fulfil the AUBI-requirement

(6) In general, the AUBI-test is a traditional test not related to any quantified structural performance and subsequent numerical verification. Therefore it should be fully abandoned to give room for performance oriented test & verification methods.

5.3 Explanations of net-section resistances in EN 1993-1-1

5.3.1 General

(1) EN 1993 specifies in Part 1-1, 6.2.3 (2) b) and 6.2.5 (4) and in Part 1-12, 6.2.3, the ultimate resistance of net sections to tension:

$$N_{Rd} = \frac{0.9\ A_{net} \cdot f_y}{\gamma_{M2}} \tag{5-4}$$

where γ_{M2} is recommended to be

$$\gamma_{M2} = 1.25. \tag{5-5}$$

(2) The reasons for the factor 0.9 in the resistance formula are the following:

1. test evaluation of tension tests with bolted connections, see commentary to EN 1993-1-1,
2. consistency with resistance formula for bolts in tension from test evaluations of bolt tests, see commentary to EN 1993-1-8,
3. fracture mechanics safety assessments.

(3) In this section, the reasoning from fracture mechanics safety assessments is given.

5.3.1 Influence of upper-shelf toughness on net-section resistance to tension

5.3.2.1 Tensile strength from the stability criterion

(1) The tensile strength $f_u = R_m$ is defined as the maximum stress related to the initial gross section area A_o of the tension test specimen, as specified for the determination of the conventional stress-strain curve, see fig. 5-14 b)

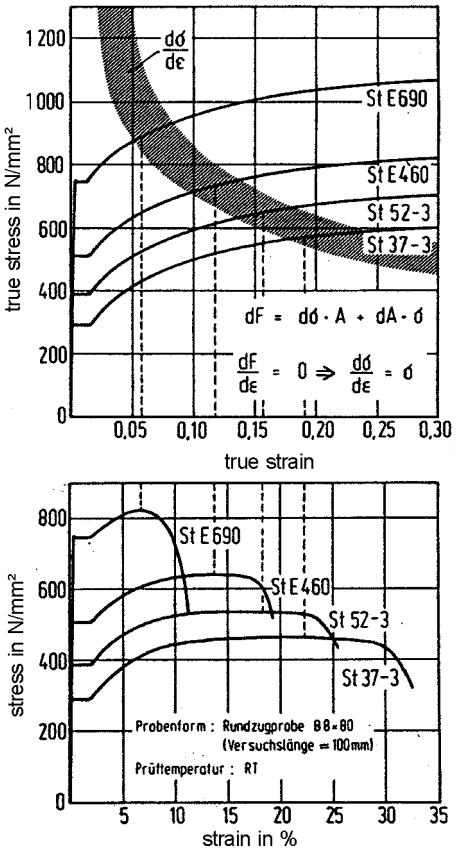


Fig. 5-14: Stress-strain curve:
a) true stress-strain curve
b) conventional stress-strain curve

(2) The true stress-strain curve relates to the actual stress σ_w related to the actual gross-section A and the actual strain ε_w, see fig. 5-14 a) and is a real material constant independent of the test specimen.

(3) The maximum $f_u = R_m$ is reached where the differential dF of the applied force with increasing deformation attains the value

$$\partial F = \partial\sigma_w \cdot A + d A \cdot \sigma_w = 0 \qquad (5\text{-}7)$$

which leads to the stability criterion for the ultimate stress f_u:

$$\frac{\partial\sigma_w}{\partial\varepsilon_w} = \sigma_w \qquad (5\text{-}8)$$

(4) Fig. 5-14 a) demonstrates that the "stability strength" f_u resulting from this criterion leads to ultimate strains ε_u which automatically are the smaller, the higher the yield strength of the material is.

(5) A consequence of this behaviour is that the yield-strength ratio $\frac{f_y}{f_u}$ automatically depends on the magnitude of the yield strength, see fig. 5-15.

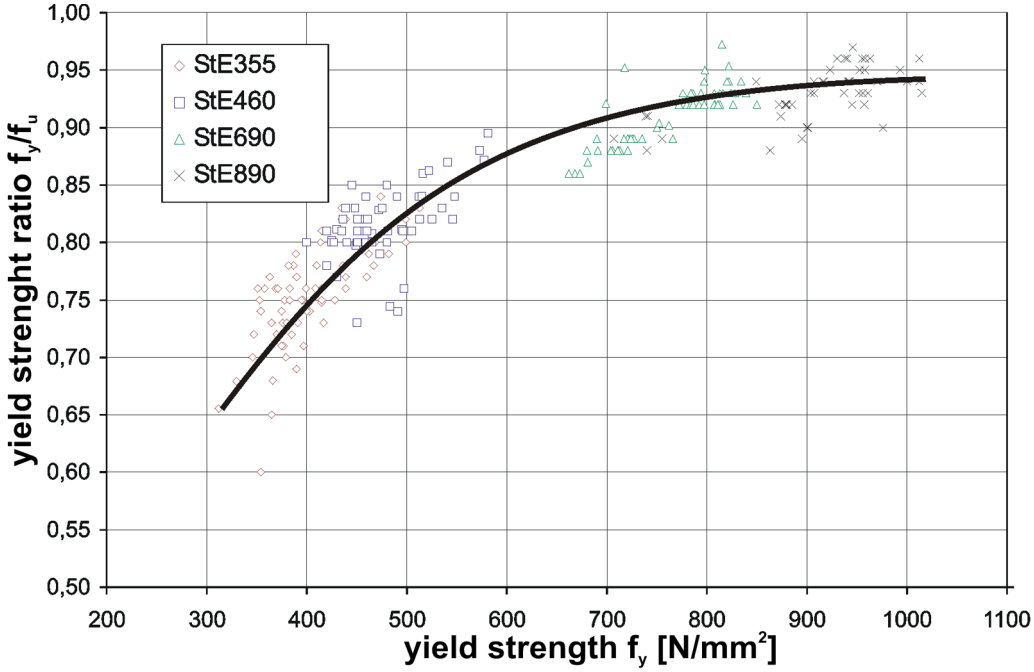


Fig. 5-15: Relationship between yield strength ratio $\frac{f_y}{f_u}$ and the yield strength

(6) EN 1993-1-1 limits the yield strength ratio to $\frac{f_y}{f_u} \le \frac{1}{1.10} = 0.90$; EN 1993-1-12 recommends a limit $\frac{f_y}{f_u} \le \frac{1}{1.05} = 0.95$ to get the nominal values of higher strength steels included.

(7) Such limitations have no direct mechanical impact on the reliability of structures resulting from design rules in EN 1993; they only have an indirect impact by permissible tolerances for defects from production and fabrication as indicated in 5.3.2.2.

5.3.2.2 Impact of material toughness

(1) In the upper-shelf region for temperatures above T_{gy} it can be assumed that in any case net section yielding σ_{gy} will be reached before fracture occurs in the net section.

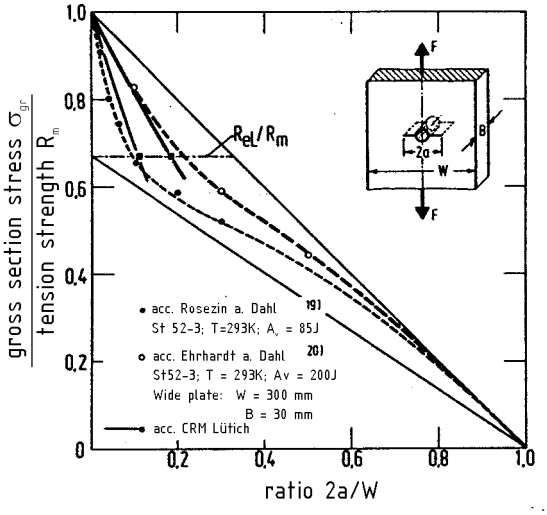


Fig. 5-16: Comparison of fracture stresses from large scale mechanical tests with $\sigma_{fracture}$ from "stability strength" and net section yield strength

(2) Fig. 5-16 gives the results of large scale fracture tests for CNT-test specimens for S355 J2 with two different toughness values A_v = 85 J and A_v = 200 J from Charpy-V-impact tests that reveal that

1. the fracture stress $\sigma_{fracture}$ is above the net section yield curve for any value 2a/w.
   High values 2a/w are not unrealistic, because for structural components the value 2a does not signify the actual length of a crack, but the effective length of crack, which may be far higher than the actual length of crack through structural detailing, see fig. 5-17.

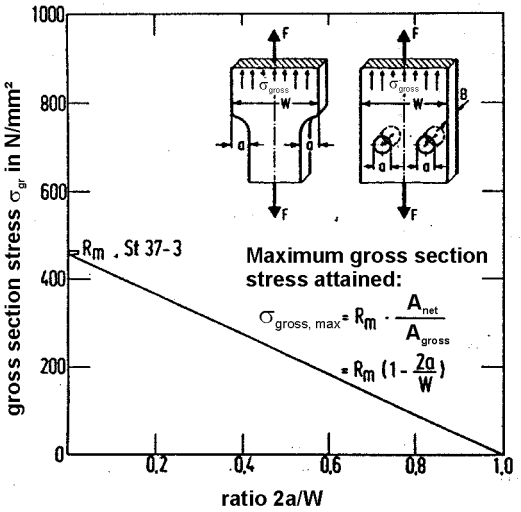


Fig. 5-17: Effect of structural detailing to net section area

   This means that the criterion applies realistically to the whole 2a/w-range with particular importance of 2a/w ~ 1/3 for the net section of bolted connections, where the decrease of "stability strength" by toughness attains about the maximum.

2. The linear "stability strength" f_u cannot be fully reached due to the decrease of fracture strength by toughness, so that the definition

$N_{RK} = 0.9 \cdot f_u \cdot A_{net}$

is based on the assumption that either, see fig 5-18

case a): the material toughness is sufficient to cover

$\sigma_{fracture} = 0.90 \cdot f_u$

for any value 2a/w or

or

case b): the interaction of material toughness with the magnitude of effective cracks 2a/w is such that a certain permissible value 2a/w is not exceeded.

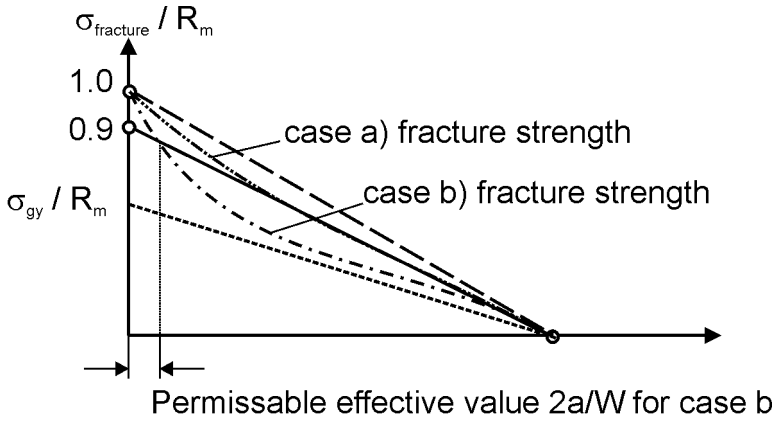


Fig. 5-18: Conclusions from $\sigma_{fracture} = 0.9\ f_u$

3. The decrease of the toughness controlled fracture stress at $2a/w \approx 0$ is the steeper, the lower the toughness values are, see fig. 5-16. The slope of the tangents at $2a/w = 0$ are indicators for permissible 2a/w values from the inter-section points of these tangents with the fracture line $0.9\ f_u \cdot A_{net}$.

(3) Fig. 5-19 shows the role of the steel grade for the theoretical values σ_{ult} according to equation (5-1) and σ_{gy} according to equation (5-2) for S690 and S235. It also shows the $\sigma_{fracture}$-curves, which were calculated with the hypothesis that S690 would have the same toughness value as S235.

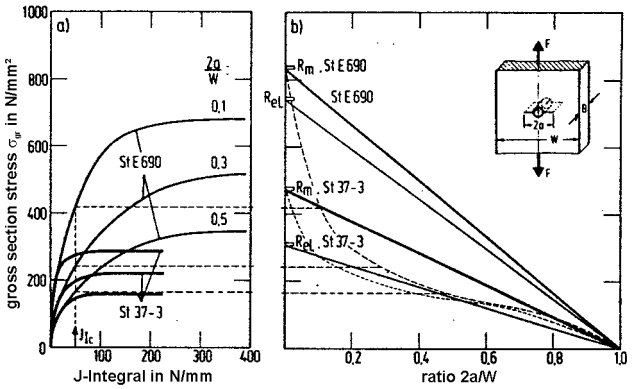


Fig. 5-19: Determination of $\sigma_{fracture}$ using the same toughness values for S690 as for S235

(4) From fig. 5-19 it is evident that for reaching the criteria

- net section yielding before net-section fracture and
- $\sigma_{fracture} = 0.9\ f_u$

the toughness-requirements for high strength steels are significantly higher than for mild steels.

(5) Fig. 5-20 gives fracture stresses $\sigma_{fracture}$ in relation to the net section yield stresses, which are based on the assumption that the toughness of high strength steels is increased in relation to the toughness of mild steels by a factor equal to the square of the yield strengths.

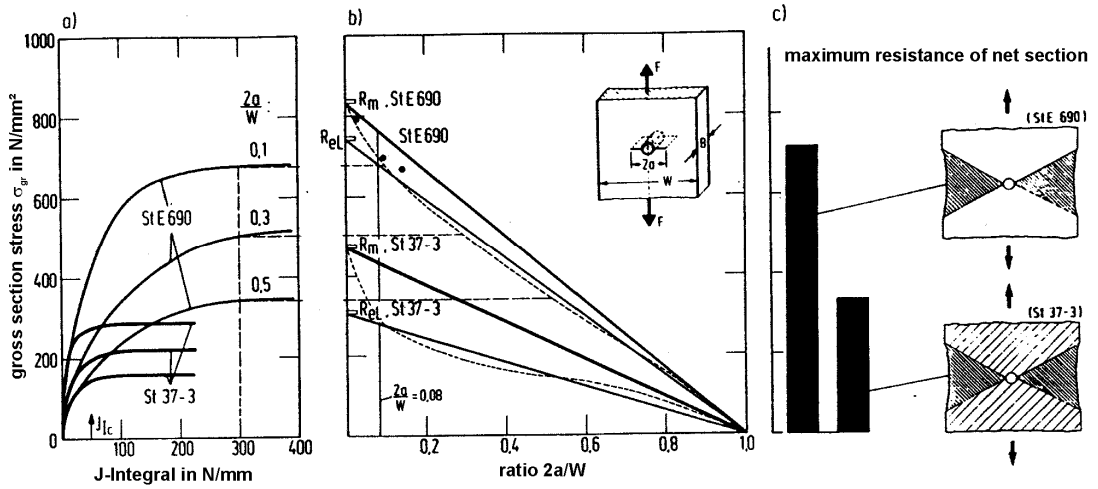


Fig. 5-20: $\sigma_{fracture}$-curves for material toughness adjusted to the yield strength of material

(6) The choice of the yield-strength ratio in EN 1993-1-1: $\frac{f_y}{f_u} \leq 0.9$ is related to the fracture strength criterion

$\sigma_{fracture} \geq 0.9\ f_u$

see fig. 5-18, by which it shall be secured for steel grades S235 to S460 that for the upper-shelf toughness of material adjusted to the yield strength, the criterion

- net section yielding before net-section fracture

can be achieved for all 2a/w-values.

The structural detailing for high strength steels as S690, see fig. 5-20, should be such that the effective crack sizes 2a/w are small if (2) 2. case b) applies, so that the net section criterion can also be reached where, due to lower toughness or a higher yield strength ratio, the $\sigma_{fracture}$-curve may have intersections with the σ_{gy}-line.

(7) For steels according to EN 1993-12 and yield strength ratios $\frac{f_y}{f_u}$ ~ 0.95, see fig. 5-15, the requirement to keep small values 2a/w by appropriate detailing is even more important, see fig. 5-18. Otherwise the criterion net section yielding before net section fracture cannot be maintained with the consequence that residual stresses and deformation controlled secondary stresses have to be taken into account in the design.

5.4 Choice of material for capacity design

5.4.1 General requirement

(1) “Capacity design” is needed where yielding of the gross-section of a structural element is required before the ultimate limit state is reached, e.g. for the formation of plastic hinges for moment redistribution or for limiting action effects by energy dissipation as in seismic design or in accidental situations.

(2) “Capacity design” requires that gross section yielding proceeds to net section fracture, so that plastic zones can form in the gross sections before a structural component can fail due to insufficient resistance capacity in the net section.

5.4.2 Conclusions for „capacity design“

(1) In the diagram for stability strength and yield strength, see fig 5-3, “capacity design” requires that the intersection of the fracture curve

$$\sigma_{fracture} = R_m \left(1 - \frac{2a}{w}\right)$$

with the gross section yield line

R_{el} = const.

is of importance, see fig 5-21.

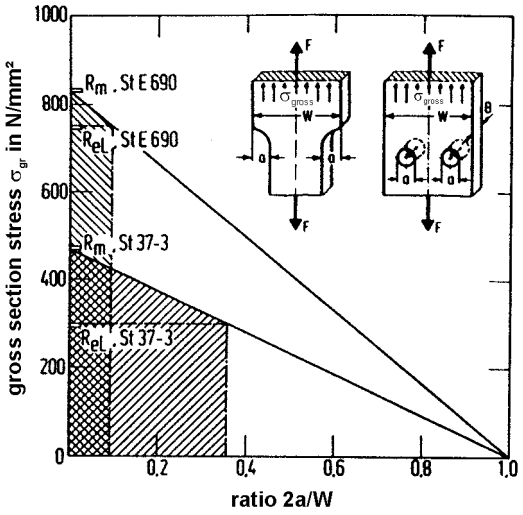


Fig 5-21 Permissible values 2a/w for gross section yielding for different steel grades

(2) Fig 5-21 makes clear that independently of toughness considerations, the possibilities for structural detailing (e. g. for choice of net sections by bolted connections) are the greater, the smaller the yield strength and the higher the yield strength ratio is.

That is the reason why low grade steels should be preferably used for seismic resistant structural components according to chapter 6 of EN 1998-1, where energy dissipation by hysteretic yielding is required.

(3) When looking at the toughness effects, the conclusions are even more pronounced, because the possibilities for structural detailing are even more reduced, see intersection points of fracture curves with R_{el}/R_m in fig 5-16, so that the conclusion is, that the permissible values 2a/w are a function of yield strength ratio and toughness of material.

(4) The conclusions for design are therefore:

1. There should be no geometric notches in the plastic zones that would enhance the size of effective initial cracks (e.g. by holes or attachments).
   The rules for good design for energy dissipation are equivalent to good design for fatigue.
2. The size of permissible cracks is the smaller, the higher the yield strength ratio is; higher yield strength ratios as for S235 and S355 should be preferred.

5.4.3 Behaviour of components subject to capacity design in the temperature-transition area

(1) Where the formation of plastic zones (e.g. for earthquakes) is combined with the occurrence of low temperatures, EN 1993-1-10 may be applied to protect the structural component from brittle failure during the time period, where it is still in the elastic range and before the yield strength $f_y(t)$ is reached.

(2) This also affects the structural detailing of energy dissipation components. The design, production and erection should be such that

- steel-grade should be up to S355,
- fabrication and erection should be such that residual stresses may be neglected,
- the upper value of yield strength should be specified according to chapter 6 of EN 1998-1 for delivery,
- notch effects should be reduced.

(3) In this case, table 2.1 of EN 1993-1-10 may be used for the choice of material in conjunction with $\sigma_{Ed} = 0.75\ f_y$, as the permissible plate thicknesses for $\sigma_{Ed} = 0.75\ f_y$ are actually related to the attainment the yield strength:

$$\sigma_{Ed} = 0.75\ f_y + 100\ Mp \approx f_y$$

(4) Under certain conditions (adiabatic or large strain rates) the temperature of a dissipative component may increase with yielding once during the hysteretic deformations the yield strength is exceeded. Fig. 5-22 gives an example for a possible temperature development that may cause a temperature shift in the toughness temperature diagram so that the behaviour is more favourable.

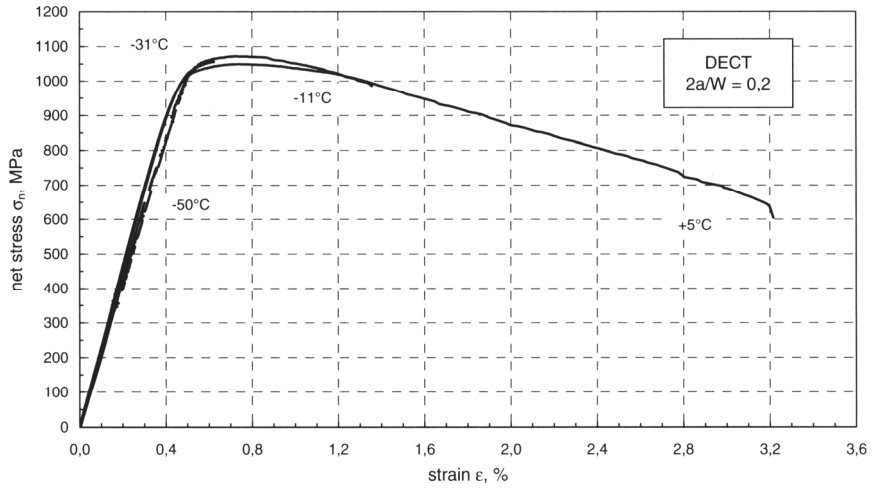


Fig 5-22: Typical net stress-temperature yielding curve for steel

5.5 Bibliography

[1] Kühn, B.: Beitrag zur Vereinheitlichung der europäischen Regelungen zur Vermeidung von Sprödbruch, Schriftenreihe Stahlbau – RWTH Aachen, Heft 54 (2005), Shaker Verlag

[2] Hubo, R.: Bruchmechanische Untersuchungen zum Einsatz von Stählen unterschiedlicher Festigkeit und Zähigkeit, VDI-Verlag: Fortschritt-Berichte-VDI, Reihe 18 – Mechanik/Bruchmechanik, Nr. 80 (1990)

[3] Sedlacek, G., Müller, Chr., Nußbaumer, A.: Toughness-Requirements in Structural Applications, Structural Engineering Document (SED): Use and application of high-performance Steels for Steel Structures, No. 8, IABSE 2005

[4] Sedlacek, G., Höhler, S,. Dahl, W., Kühn, B., Langenberg, P., Finger, M., Floßdorf, F.-J., Schröter, F. Hocké, A.,: Ersatz des Aufschweißbiegeversuchs durch äquivalente Stahlgütewahl, Stahlbau 74 (2005), S. 539-546

[5] Stranghöner, N.: Werkstoffwahl im Brückenbau, DASt-Forschungsbericht 4/2006

[6] Dahl, W., Ehrhardt, H.: „Einfluß des Spannungszustandes auf das Verformungs- und Bruchverhalten von Stählen in Großzugversuchen", Stahl und Eisen 108 (1983), Heft 6, Seite 289-292.

[7] Dahl, W.: "Application of fracture mechanics concepts to the failure of steel constructions", Steel research, Issue No 3/86, pages 131-134.

[8] Dahl, W., Hesse, W.: „Auswirkung der Beurteilung von Stählen auf die Anwendung im Hoch- und Anlagenbau", Stahl und Eisen 106 (1986), Heft 12, Seite 695-702.

Section 6

6. Damage Mechanics – Calculation of limit state condition of fracture in the upper shelf with local models

6.1 Introduction

(1) Finite element methods combined with the use of the true stress-strain curve for steel, see fig. 5-14, and the von Mises-yield criterion, expressed by the yield potential

$$\Phi = \left(\frac{\sigma_v}{\sigma_y} \right)^2 - 1 = 0$$

where σ_v is the von-Mises-equivalent stress
σ_y is the yield stress

allow to determine the ultimate resistance of tension elements in terms of "stability" resistance, see equation (5-7) for monotonic loading. In this case only the limit condition of plastic yielding but not that of the final fracture developing from local damage can be obtained.

These tools are based on fully ductile behaviour without damage and therefore do not give any indication when cracks will occur and induce rupture,

(2) In order to be able to predict the failure of a tension element by rupture, the damage mechanics approaches have been developed which are capable of simulating the following behaviour more realistically:

1. Description of the local microcstructural behaviour leading to rupture which is expressed as development of voids in the material with the onset of yielding, growth of voids and coalescence that leads to a critical limit from where cracks are initiated (continuum models suplemented by the GNT-model).

   These approaches are both appropriate for determining component behaviour or fracture mechanical resistance values like J_i for crack initiation (see chapter 5) and the growth of a stable crack associated with the J_R resistance curve .

(3) Whereas fracture mechanics models use a single, one-dimensional parameter (e.g. by the fracture mechanics parameter K or J or CTOD) and are based on the assumption of crack-like imperfections for the safety assessment, damage mechanics approaches are based on a set of parameters representing the microstructure of steel. Such approaches can be applied to all type of structural elements with initial cracks or without initial cracks and therefore represent the most realistic attempt to predict the rupture which works without the safe-sided assumption of the presence of initial cracks (see chapter 5).

(4) In the following some basics and first applications of damage mechanics are demonstrated. However, it must be noted that this method requires the use of Finite Elements together with model parameters derived from experiments.

(5) The aspects of reliability in relation to requirements, model uncertainties, imperfections and scatter of input data as well as the relation of measured data to data specified in product standards, which all are necessary for the use of damage mechanics in practical safety assessments, is not addressed in this section.

6.2 Model for determining crack initiation

(1) Fig. 6-1 illustrates the role of the microstructural development of microvoids at the crack tip of a fracture mechanics model under tension in the upper-shelf region.

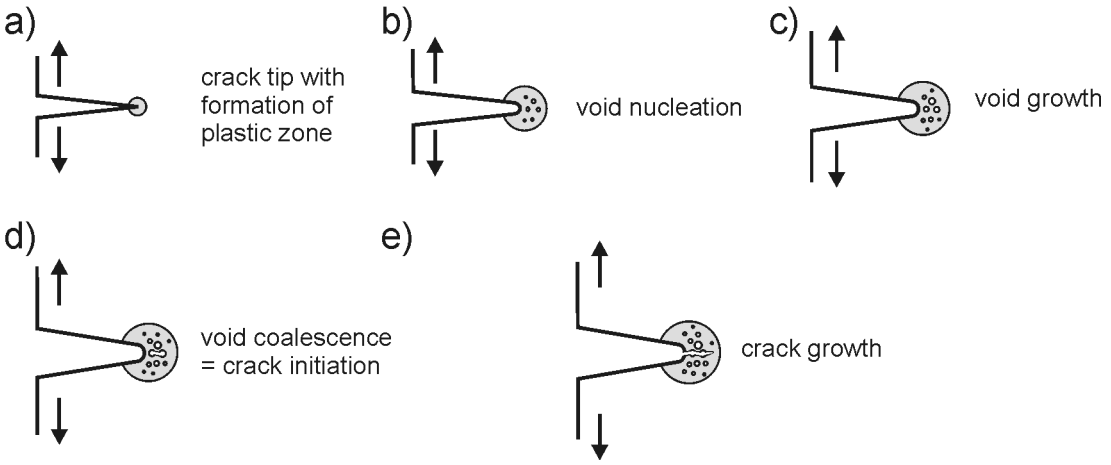


Fig. 6-1: Schematic presentation of ductile damage development at a crack tip

(2) The phases of the development of voids develop from void nucleation to void growth and to void coalescence, which is identical with crack initiation, see fig. 6-2.

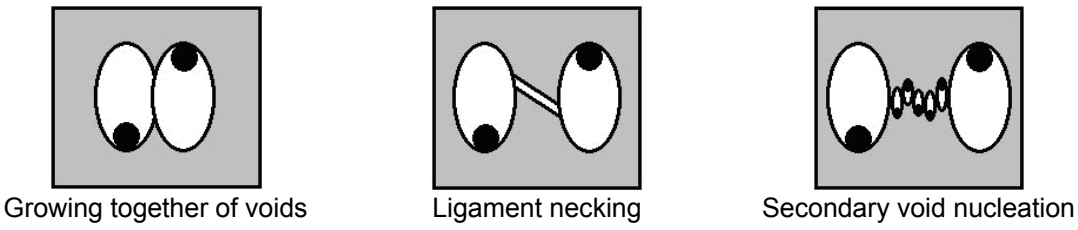


Fig. 6-2: Different types of void coalescence

(3) The conclusion of the use of the porous metal plasticity model, see section 6.3, is that the stress and the strain for crack initiation can be determined, see fig. 6-3.

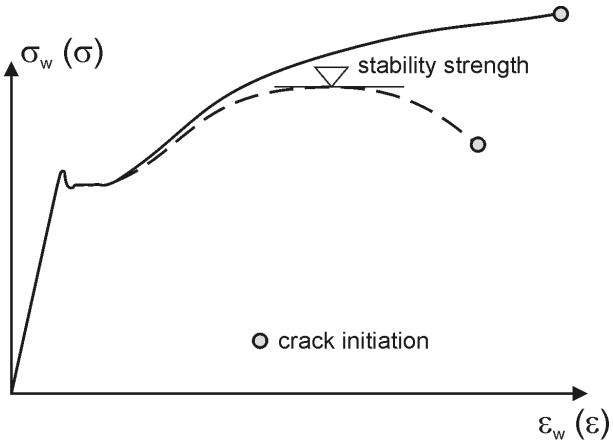


Fig. 6-3: Determination of the limit state of crack initiation

(4) The simulation of further development from crack initiation to failure requires the use of an effective behaviour law for damaged elements, that regulates the stress transfer through damaged elements, see section 6-5.

6.3 The GTN – Damage model

6.3.1 General

(1) The GTN – Damage model of Gurson, Tvergaard and Needleman modifies the von Mises yield model in such a way that the effects of micro voids (micro-structural damage) are included.

(2) The modified yield potential reads

$$\Phi = \left(\frac{\sigma_v}{\sigma_y}\right)^2 + 2\, q_1\, f^*\, \cosh\left(\frac{3}{2}\, q_2\, \frac{\sigma_H}{\sigma_y}\right) - \left(1 - q_3\, f^{*2}\right) = 0$$

with the additional parameters

σ_H = hydrostatic stress components

$q_1 = 1.5$
$q_2 = 1.0$ } model parameters
$q_3 = 2.25$

f* = modified void volume fraction

(3) In each element of the FE-calculation, a void is considered which is supposed to grow due to local stresses and strains resulting in a void volume fraction f. This gives

$$f^*(f) = \begin{cases} f; & \text{for } f \le f_c \\ f_c + \kappa(f - f_c); & \text{for } f > f_c \end{cases}$$

where

f_c = critical void volume fraction, at the load drop point of a tension test depending on the stress triaxiality of the spot considered,

κ = acceleration factor (often determined directly in the range of 4 to 8) or determined from

$$\kappa = \frac{0.667 - f_c}{f_f - f_c}$$

with

f_f = final void volume fraction at microscopic failure at which the stress transfer through an element is interrupted.

(4) The value f results from growth of existing voids and strain controlled nucleation of new voids:

f = $f_{growth} + f_{nucleation}$ =

$$= \left(1 - f_o\right)\dot{\varepsilon}^{pl}_{kk} + \frac{f_N}{S_N\sqrt{2\pi}} \exp\left[-\frac{1}{2}\left(\frac{\bar{\varepsilon}_{pl} - \varepsilon_N}{S_N}\right)^2\right]\dot{\bar{\varepsilon}}^{pl}$$

where
- f_o = initial void volume fraction
- f_N = volume fraction of newly nucleating voids at the characteristic equivalent plastic strain ε_N (measured by change of electric resistance)
- ε_N = characteristic equivalent plastic strain for new nucleation of voids
- $\dot{\varepsilon}^{pl}_{kk}$ = rate of plastic strain due to hydrostatic stresses
- $\bar{\varepsilon}^{pl}$ = equivalent plastic strain
- $\dot{\bar{\varepsilon}}^{pl}$ = rate of equivalent plastic strain
- S_N = 0.1 standard deviation of strain-controlled nucleation of secondary voids

(5) The input parameters that need to be determined for the particular case and cannot be put constant on the basis of sensitivity studies are then

- f_o = initial volume fraction of primary void initiated by constituents as non-metallic inclusions or hard micro structure constituents of sufficient size. The quantification is performed by scanning electron microscopy (SEM) and x-ray spectroscopy (EDX) of polished surfaces.
- f_N = volume fraction of secondary voids nucleating during primary void coalescence at smaller micro structure constituents to be quantified in a similar way as f_o, (more difficult due to their small size).
- ε_N = characteristic strain of secondary void nucleation, quantified by the direct current potential drop (DCPD) technique, i.e. by measuring the electric resistance of the cross-section which drops when cavities form.
- f_c = critical void volume fraction, determined e.g. by numerical cell model simulations or from tensile tests at the load drop point. As f_c depends on on the stress triaxiality, the test should comply with the triaxiality state expected in the structure considered.
- f_f = final void volume fraction which is in the range of 10% to 20%. Because of accuracy problems in measuring f_f, the κ-value is often given directly.

6.3.2 Examples for the determination of micro structures parameters

(1) For the determination of the micro structure parameters, a structural steel S355J2G3 and a pressure vessel steel P460Q are selected [7].

(2) Table 6-1 gives the chemical composition of the steels, fig. 6-4 gives the micrographs of the micro structure and fig. 6-5 gives the SEM-fracture surfaces [7].

Steel	C	Si	Mn	P	S	Cr	Mo
S355J2	0.15	0.36	1.35	0.020	0.009	0.073	<0.005
P460Q	0.13	0.32	1.38	0.007	<0.001	0.164	0.054
Steel	Ni	Al	Cu	Nb	Ti	V	Zn
S355J2	0.04	0.037	0.086	<0.001	0.001	0.006	0.002
P460Q	0.38	0.032	0.190	<0.001	0.004	0.032	0.002

Table 6-1: Chemical composition of the steels S355J2G3 and P460Q, mass contents in %

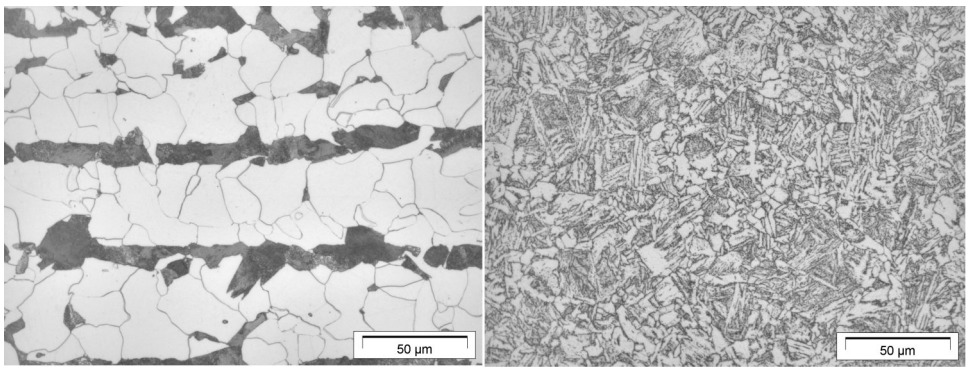


Fig. 6-4: Micrographs: left: ferritic-perlitic micro structure of steel S355J2G3; right: bainitic-ferritic micro structure of steel P460Q, both after HNO_3-etching

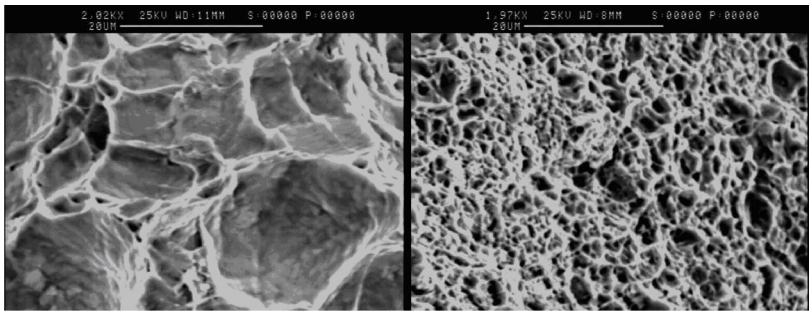


Fig 6-5: SEM-fracture surfaces: left ductile fracture surface of steel S355J2G3; right: ductile fracture surface of steel P460Q. Both fracture surfaces, with different sizes of dimples, result from fracture mechanics tests with CT-specimens carried out at room temperature

(3) Obviously the void size distribution differs a lot between the two materials:

- In steel S355J2G3 primary void nucleation at non-metallic inclusions is the major mechanism of ductile failure behaviour. Accordingly, $f_o = 0.20$ was chosen and the nucleation of secondary voids was neglected ($f_N = \varepsilon_N = S_N = 0$).

- In steel P460Q mainly secondary voids have nucleated and primary void growth was not considered ($f_o = 0$)

  The parameters for secondary void nucleation were

  $\varepsilon_N = 0.21$ from DCPD-technique
  $f_c = 0.04$ from cell model simulations
  $f_N = 0.3\%$ was selected,
  $\kappa = 6$ was selected.

(4) Table 6-2 gives the chemical composition of another pressure vessel steel P690Q, which gave the same GTN-model parameters as the steel P460Q except for $\varepsilon_N = 0.12$.

Steel	C	Si	Mn	P	S	Cr	Mo
P690Q	0.14	0.31	0.83	0.011	<0.001	0.61	0.42
	Ni	Al	Cu	Nb	Ti	V	Zn
	1.01	0.041	0.27	0.001	0.002	0.051	0.003

Table 6-2: Chemical composition of steel P690Q, mass contention [7].

6.3.3 Mesh sizes for FEM calculations

(1) In each finite element containing a void, the mesh sizes very much depend on the average spacing between non metallic inclusions.

(2) For steels with similar parameters

1. void size distribution
2. ductility
3. purity degree

the adequate mesh size is also similar.

(3) Fig. 6-6 gives element sizes in meshes determined from calibrations of test results, related to the 90% quantile value of void diameter; they are in the magnitude of grain sizes

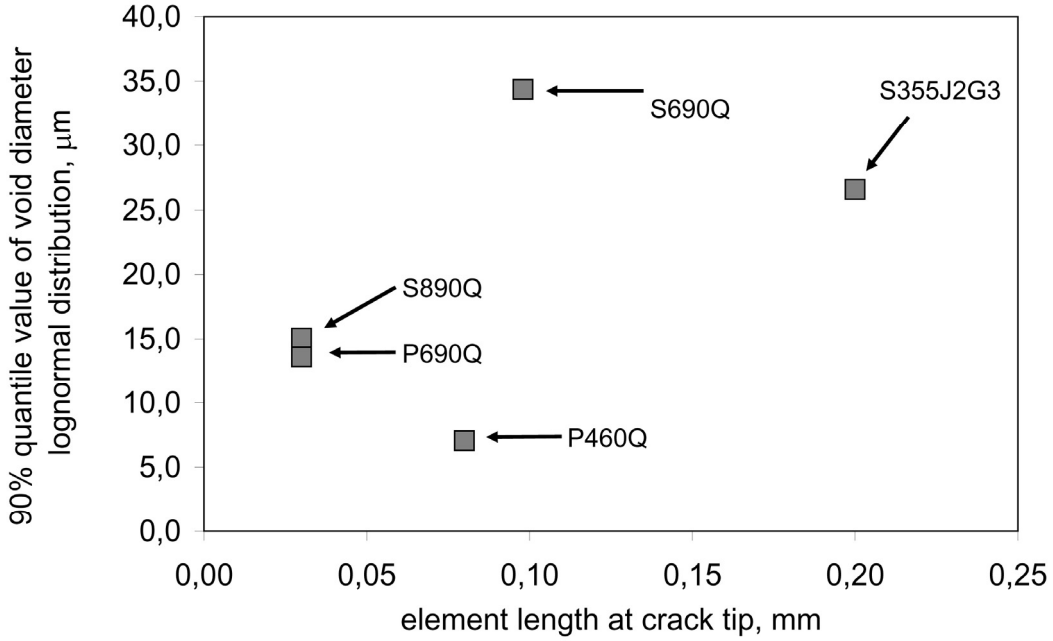


Fig. 6.6 Relations between FE-element size at a crack tip and size distributions of voids on ductile fracture surfaces for several pressure vessels and structural steels [7]

6.3.4 Calculation of J-integral values J_i

(1) Fig. 6-7 shows load-CTOD-curves from fracture mechanics tests with CT-specimens as well as the results of simulations with the GTN-damage model, resulting in J_i-values for crack initiation obtained from the ends of the curves.

(2) Obviously the experimental and numerical values coincide.

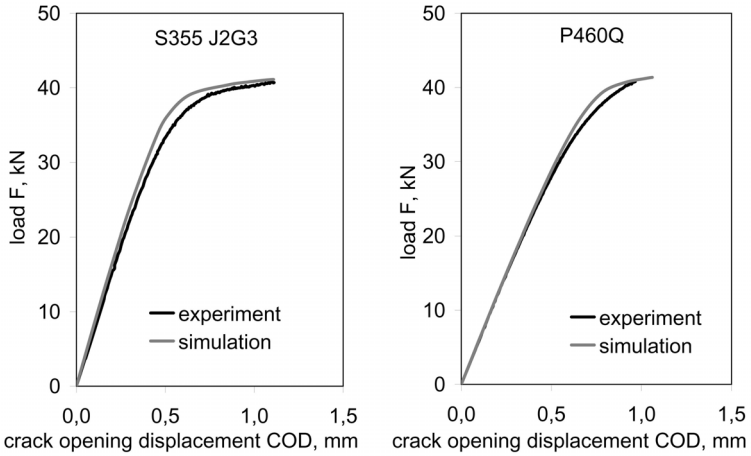


Fig. 6-7: Load crack tip opening displacement curves from experiment and simulation for steels S355J2G3 (left side) and P460Q (right side) [7]

6.3.5 Conclusions for practical FEM-calculations

(1) From tensile tests with cylindrical tension specimens with different notches or from calculations with the GTN damage model, the two parameters

- stress triaxiality h, which is calculated from

$$h = \frac{\sigma_1 + \sigma_2 + \sigma_3}{\sigma_V}$$

where σ_1, σ_2, σ_3 are the principle stresses

σ_V is the equivalent stress

- the equivalent plastic strain $\bar{\varepsilon}^{pl}$

have been identified as the leading parameters to characterize ductile crack initiation from the growth of voids and void coalescence.

(2) Hence a failure criterion for crack initiation could be developed as a function of these two parameters, see fig. 6-8.

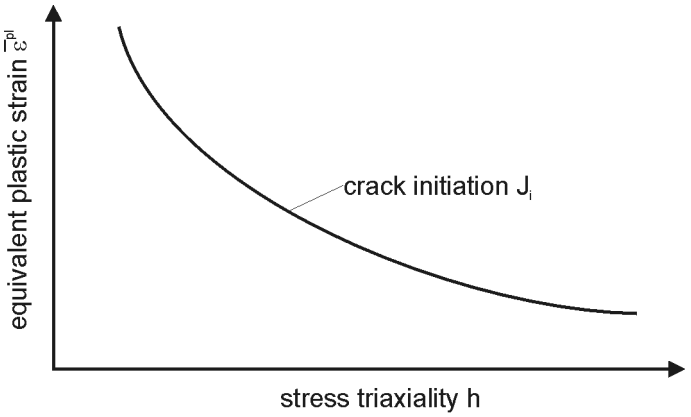


Fig. 6-8: Damage curve as ductile crack initiation criterion from void coalescence

(3) In general, such damage curves are determined by tests with variations of notch geometry accompanied by FEM-calculations to identify the stress triaxility and the equivalent plastic strain at the relevant spot. From a least square fit a mean curve satisfying the formula

$$\bar{\varepsilon}^{pl} = c_1 \cdot e^{c_2 h} + \bar{\varepsilon}_i^{pl}$$

can be derived, where

c_1, c_2 are fit parameters

$\bar{\varepsilon}_i^{pl}$ is the equivalent plastic strain necessary to provoke ductile failure at hydrostatic stress state

(4) Fig. 6-9 shows test specimens with different notch situations, which may lead to equivalent plastic strains as given in fig. 6-10.

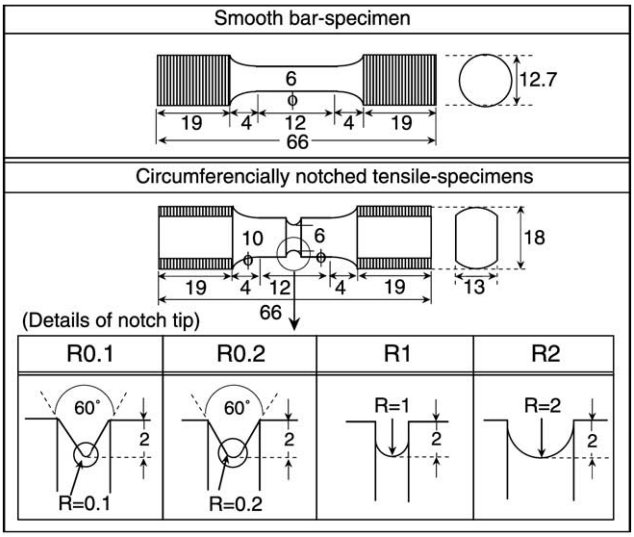


Fig. 6-9: Geometry and size of tensile specimens used to determine the damage curve

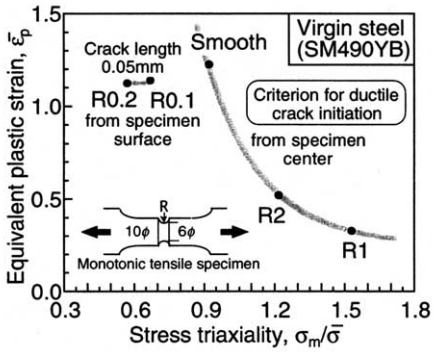


Fig. 6-10: Limits of equivalent plastic strain for different stress triaxialities

(5) Fig. 6-10 shows the exponential decrease of equivalent plastic strain for the smooth specimen and the notched specimens R_1 and R_2 on one hand and different plastic strain limits for the notch specimens $R_{0.1}$ and $R_{0.2}$ which are more or less independent of the stress triaxiality h on the other hand.

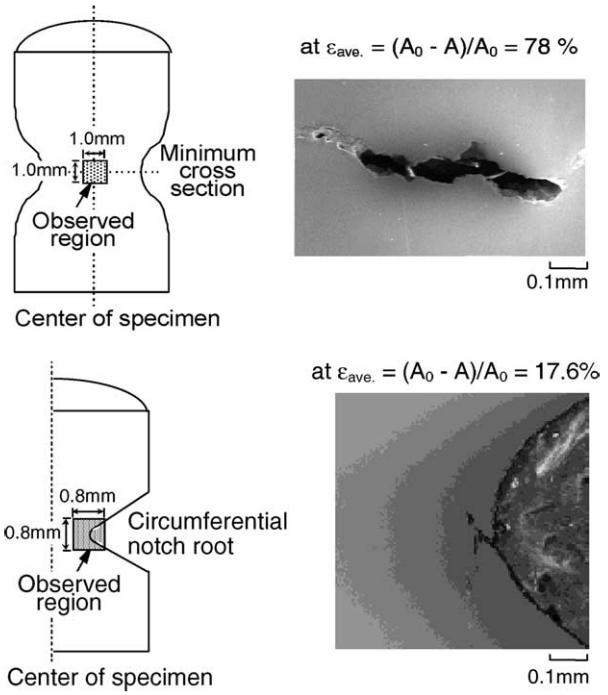


Fig. 6-11 Ductile crack initiation behaviour from specimen centre and notch root surface under single tension
a) R_2-specimen, b) $R_{0.1}$ specimen

(6) As fig. 6-11 demonstrates, the different results for $R_{0.1}$ and $R_{0.2}$ are caused by the fact that for those cases the relevant spot is not the centre of the cross-section with growth of voids controlled by triaxiality (equiaxed tensile mode of failure) but the surface, where the failure mode is controlled by the growths and coalescence of voids along a local shear band oriented at an angle of 45° to the tensile axes.

(7) In conclusion, the damage curve following the growth and coalescence of voids according to the triaxial stress state has a lower limit for h controlled by the shear type of failure at the surface, which is not covered by the GTN-model.

6.3.6 Example of practical application

(1) For a pressure vessel as given in fig. 6-12 made of steel P460Q, a FEM-calculation was carried out using the true stress-strain curve of the material from unaxial tensile tests and extrapolated according to the Hollomon approach to cover strains beyond the uniform elongation from tensile tests [8,9].

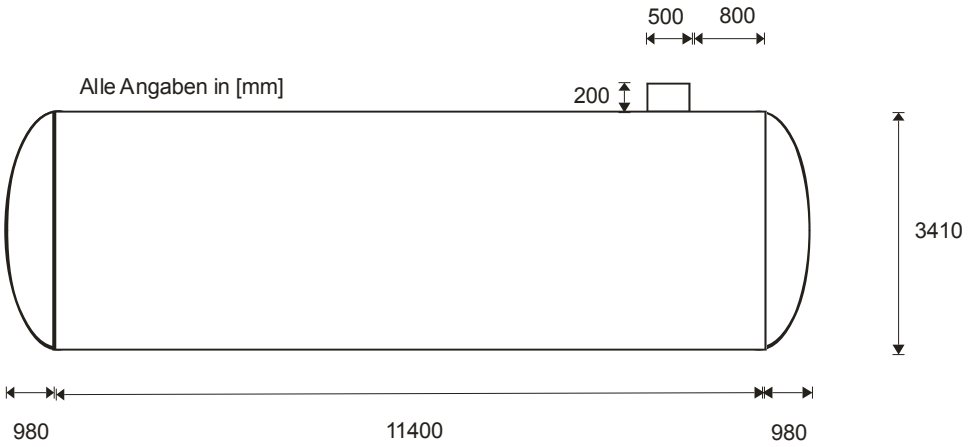


Fig. 6-12: Geometry of the pressure vessel

(2) The inner pressure was increased until it reached the critical level where for the first time an element in the model reached the damage curve for ductile crack initiation.

(3) The steel P460Q-damage curve has been identified by experimental and numerical investigations with cylindrical notched tensile samples as

$$\varepsilon^{pl} = 0{,}96\, e^{-0{,}6h} + 0{,}14$$

(4) Fig. 6-13 shows the position of ductile crack initiation from the distributions of plastic equivalent strain and stress triaxiality that are plotted.

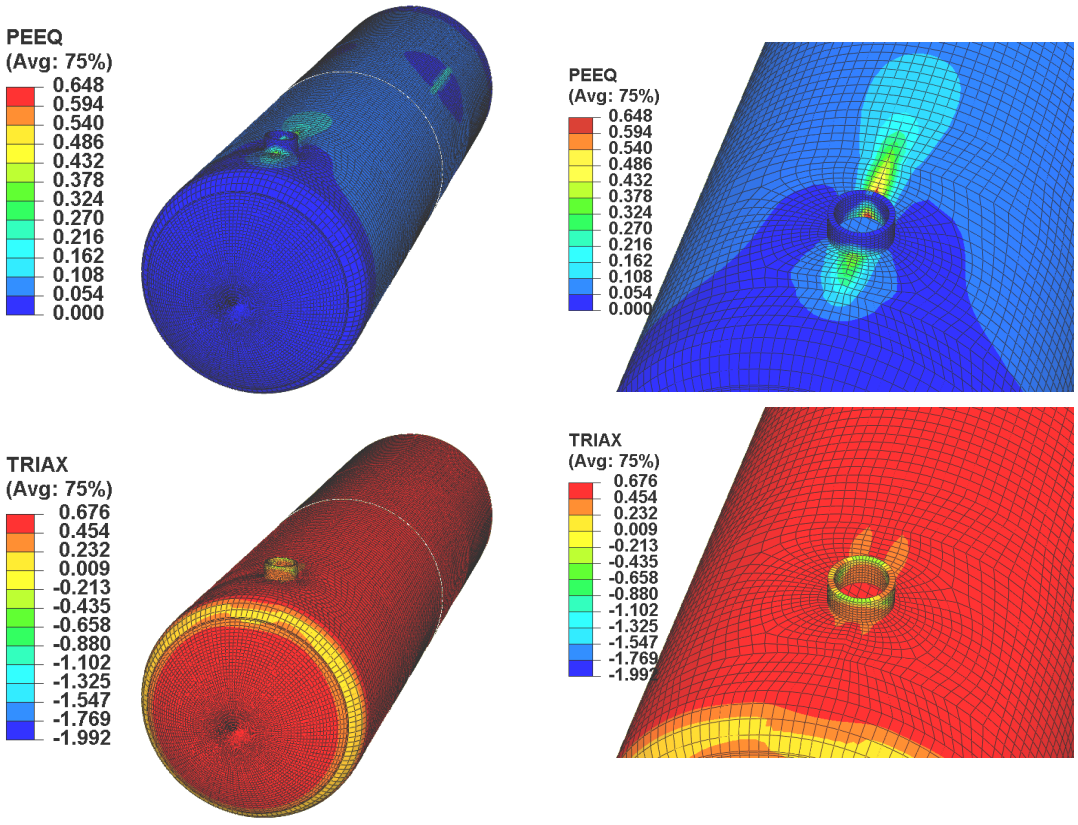


Fig. 6-13: Damage curve reached at a point near the nozzle

(5) The nozzle has been identified as the critical spot where a ductile crack could be initiated when the critical inner pressure is 16 MPa (expected value without safety elements).

6.4 The use of damage curves for crack initiation for cyclic straining

6.4.1 General

(1) According to Ohata and Toyoda [6] the damage curves according to fig. 6-10 determined for monotonic loading can also be used to determine the crack initiation with FEM for cyclic loading as relevant for seismic design.

(2) The assumptions made to obtain accurate results are the following:

1. For cyclic loading the Bauschinger effect is taken into account by a stress/strain field determined by a combined non-linear isotropic kinematic hardening model.

2. Strain accumulation only considers effective equivalent plastic strains $(\bar{\varepsilon}_p)_{eff}$, controlled by the loops of back stresses in the kinematic hardening component of the combined hardening model.

(3) In the following, the assumptions made and some results are described.

6.4.2 The combined isotropic-kinematic hardening model

(1) In the combined isotropic-kinematic hardening model, equivalent plastic strains and equivalent stresses of the true stress-strain curve are composed of two components:

1. the isotropic hardening component $\bar{\sigma}$
2. the kinematic hardening component $\bar{\alpha}$

see fig. 6-14.

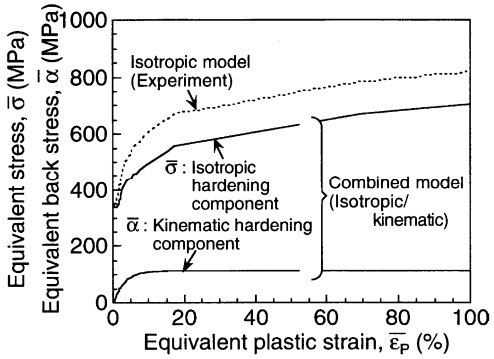


Fig. 6-14: Non-linear isotropic and kinematic hardening components used for the FE-analysis of cyclic loading

(2) The conclusions are hysteretic curves of true stress and true strain that are close to experiments as they consider the Bauschinger effect, see fig. 6-15.

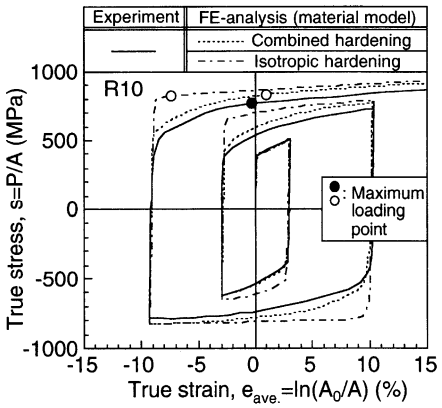


Fig. 6-15: Approximation of hysteretical true stress-strain curves by the combined hardening model

(3) The model also allows to follow the loops of the components of stresses $\bar{\sigma}$ and backstresses $\bar{\alpha}$ in all phases of the cycles, see fig. 6-16.

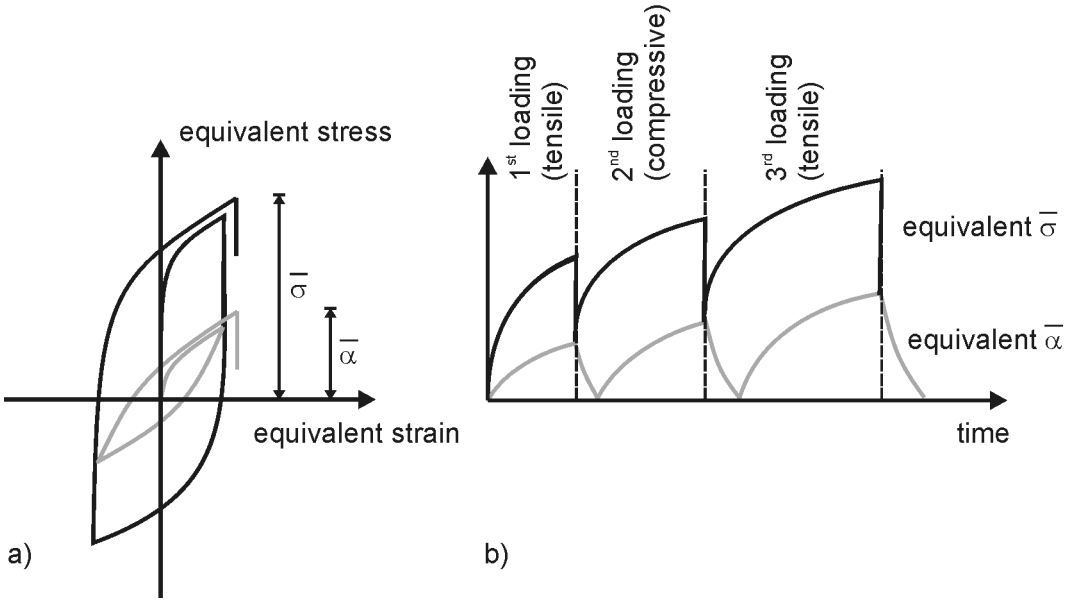


Fig. 6-16: Cyclic development of loops: a) Cyclic development of components $\bar{\sigma}$ and $\bar{\alpha}$; b) Time history of cycles $\bar{\sigma}$ and $\bar{\alpha}$

6.4.3 Accumulation of effective equivalent strains $\bar{\varepsilon}_{p,eff}$

(1) The basic assumption of the effective damage model [6] is that once the cyclic loops of equivalent stresses and strains are stabilized, there is no contribution from equivalent strains to damage.

(2) Hence contributions from equivalent plastic strains to damage are controlled by the cyclic development of back stresses such that only those portions of the equivalent plastic strains are damage-effective which belong to backstresses $\bar{\alpha}$ larger than the maximum $\bar{\alpha}$-values of the preceding loop, see fig. 6-17.

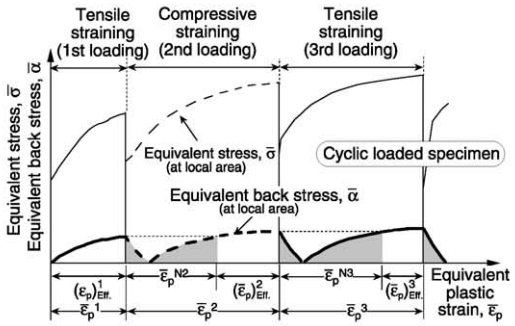


Fig. 6-17: Evolution of equivalent backstresses $\bar{\alpha}$ and determination of effective equivalent strains $(\varepsilon_{pl})_{eff}$.

(3) Fig. 6-18 shows on the left hand side the accumulation of the full equivalent plastic strains that would give very conservative results and on the right hand side the accumulation of effective equivalent plastic strains that gives accurate values.

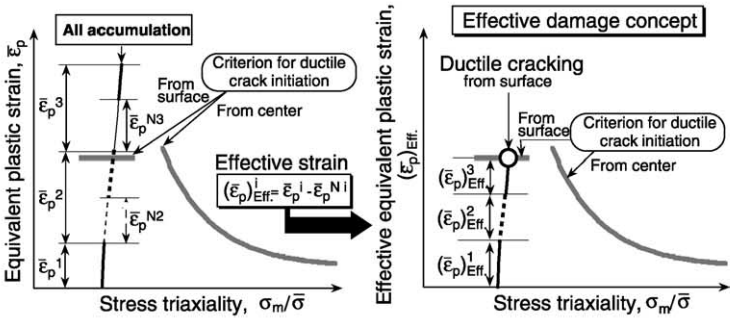


Fig. 6-18: Comparison of accumulation of a) all equivalent plastic strains; b) effective equivalent plastic strains

6.5 Numerical simulation of crack growth

(1) The GTN-model could be supplemented by a law for the stress transfer through damaged elements.

(2) One possibility is the use of cohesive elements in addition to the other continuum elements, which are positioned where crack initiation and growth is expected, see fig. 6-19.

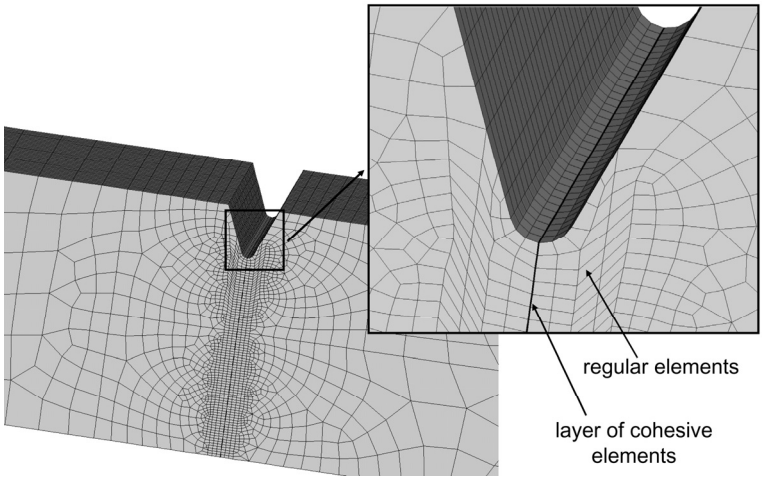


Fig. 6-19: FE-model of a Charpy specimen with a layer of cohesive elements

(3) The cohesive model is a traction separation law, that describes the transmittable stress T as a function of separation δ, see fig. 6-20, in which the maximum transmittable stress T_0 and the critical separation δ_0 leading to final failure are the input parameters.

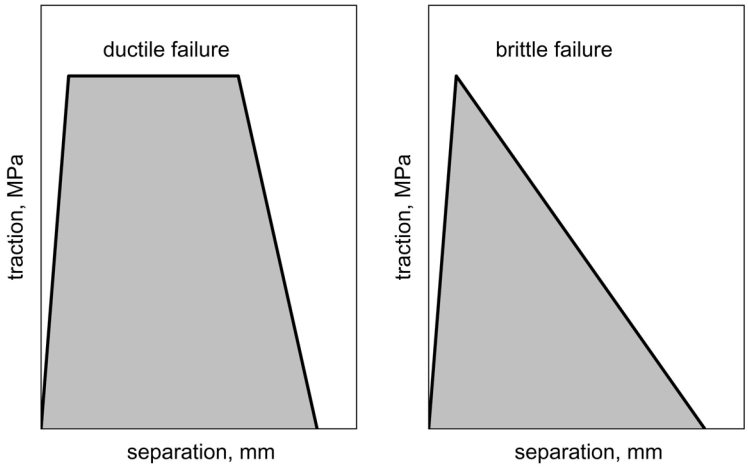


Fig. 6-20: Typical traction-separation laws for ductile and brittle behaviour in the cohesive zone model

(4) Also damage curves can be combined with a damage evolution law to consider the behaviour of damaged elements. Other than for cohesive zones the crack path needs not to be defined prior to the simulation start. The easiest way is the assumption of linear loss of strength which is final at a characteristic deformation of the element.

6.6 Bibliography

[1] Gurson, A. L., J. Engineering Material Technology, 99 (1977), 2.

[2] Tvergaard, V.: International J. Fract., 18 (1982), 237.

[3] Tvergaard, V.,Needlman, A.: Acta metall. 32 (1984) No. 1, 157.

[4] Needlman, A., Tvergaard, V.: J. Mech. Phy. Solids, 35 (1987), 151.

[5] Tvergaard, V., Needlman, A.: J. Mech. Phys. Solids, 40 (1992) No. 2, 447.

[6] Ohata, M., Toyoda, M.: Damage concept for evaluating ductile cracking of steel structures subjected to large-scale cyclic straining, Science and Technology of Advanced Materials 5 (2004) page 241-249.

[7] Münstermann, S.: Numerische Beschreibung des duktilen Versagensverhaltens von hochfesten Baustählen unter Berücksichtigung der Mikrostruktur, Berichte aus dem Institut für Eisenhüttenkunde IEHK – RWTH Aachen, Band 4/2006 Shaker Verlag.

[8] Münstermann, S., Prahl, U., Bleck, W.: Numerical modelling of toughness and failure processes in steel, Steel Research Int. 78 (2007) No. 3 page 224-235.

[9] Münstermann, S., Bleck, W., Langenberg, P.: New approaches for safety assessments of pressure vessels. 2nd International Seminar on Society and Materials, SAM 2, Nantes, 24-25 April 2008.

Section 7

7. Liquid metal embrittlement in hot dip zinc-coating

7.1 Introduction

(1) Liquid metal embrittlement (LME) or liquid metal assisted cracking (LMAC) are phenomena associated with the stress-corrosion attack of certain liquid metals on the surface of solid base metals.

(2) Examples of such phenomena are the attack of Gallium (melting temperature + 26°C) on aluminium alloys or of certain liquid zinc alloys (melting temperature ~ +419°C) on steel components in the zinc bath, see fig. 7-1.

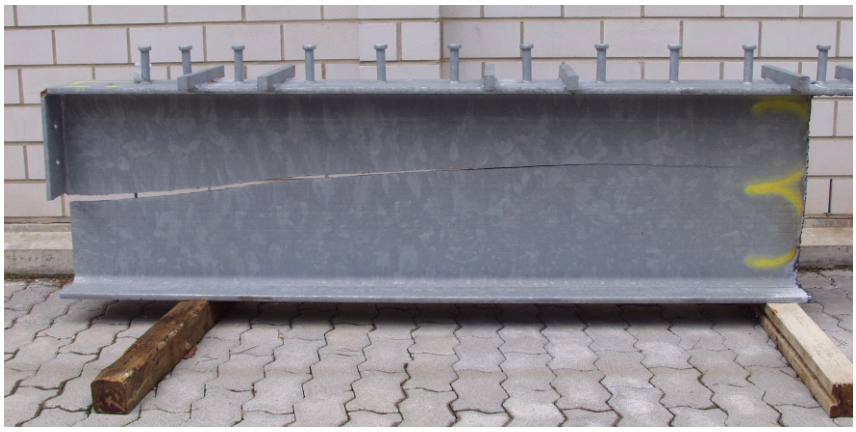


Fig. 7-1: Example of cracks from zinc coating by hot dip galvanizing

(3) The corrosion mechanism is such that the liquid metal attacks the grain boundaries of the solid metal and causes a reduction of surface tension so that the grains loose their coherence, in particular under tensile stresses. They separate in forming surface cracks in the zinc bath into which the liquid metal (the alloy or eutectica with lower melting temperatures) penetrate and allow initial cracks to grow, see fig. 7-2.

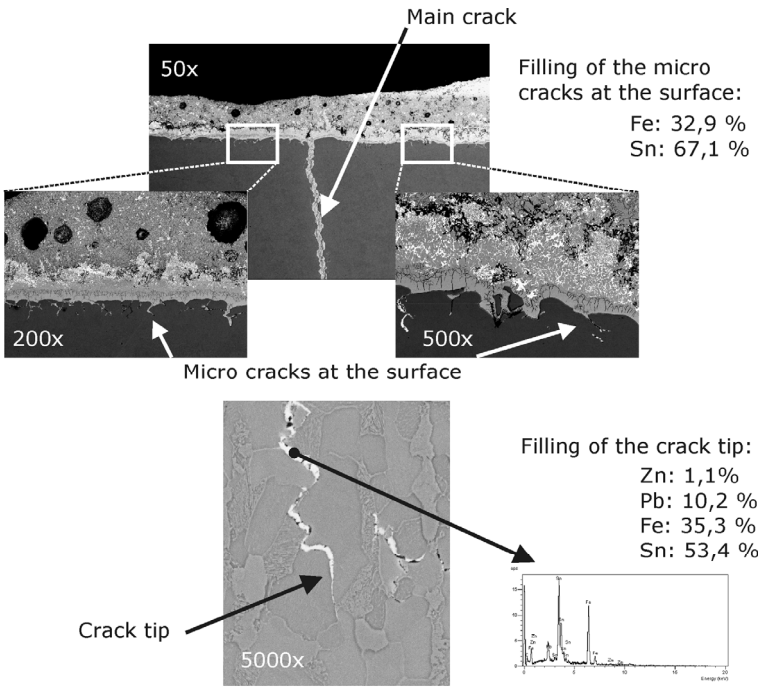


Fig. 7-2: Cracks filled with liquid metal in the zinc bath

(4) The main crack controlling parameters for the formation of such cracks in the zinc bath are

1. Surface conditions and microstructure of steel as well as aggressiveness of the zinc alloy, both measured in tests, that give the characteristic values of strain resistance versus the exposure time of the steel in the zinc bath and other parameters, like strain rate etc.

2. Time of exposure in the zinc bath reducing the strain resistance

3. Magnitude of residual strains in the steel component dependent on time, where a distinction is made between

   a) Residual strains arisen during fabrication of the steel component before dipping (stationary)
   b) Additional residual strains due to the dipping process until the steel component has attained a uniform temperature equal to the bath temperature (instationary)
   c) Residual stresses that remain in the steel component after it has attained the bath temperature in the zinc bath (stationary).

4. Other influences as a consequence of the treatment of the steel components before dipping, such as cleaning, application of flux agents, preheating etc.

(5) In the following paragraphs, an engineering model is presented that describes the limit state of crack initiation on the basis of equivalent plastic strains ε_{pl} in the steel material:

1. Equivalent strain requirements $\varepsilon_{pl,E}$ are derived from the steel fabrication and dipping process and exposure time

2. Equivalent strain resistances $\varepsilon_{pl,R}$ are determined from a standardized testing procedure, taking material properties and surface conditions of the steel and characteristics of the zinc alloy as well as the exposure time into account (modified LNT-test).

(6) The limit state equation reads:

$$\varepsilon_{pl,E} \leq \varepsilon_{pl,R} \tag{7-1}$$

(7) In this limit state equation, the role of strain resistance is dominant with regard to the sensitivity of all basic variables. It needs determination by refined methods, see section 7.2.

(8) The strain requirements are characterized by a mean level of residual stresses and strains expected in any structural component from fabrication, depending on the type of cross-section (see classification of column buckling curves in EN 1993-1-1 according to cross-section) and by variations from this mean value caused by the dipping process, depending in particular on the structural detailing (e.g. on the structural form and the thickness ratio of the welded plates connected). In general strain requirements can be categorized into groups on the basis of more refined numerical analysis with typical details, see section 7.3.2.4.

(9) For the time being, the limit state conditions presented in this report are assumed to give safe-sided solutions. So far, there is no possibility to define their reliability, because there are no sufficient statistics available yet.

(10) Therefore, in addition to the numerical verification of the limit state, inspections of the structural members after zinc coating are necessary. Inspection methods are specified that take account of the fact that a visual control of zinc coated surfaces is not sufficient, as cracks may be filled and covered by zinc, see section 7.4.

7.2 Equivalent plastic strain resistances of steels in the zinc bath

7.2.1 General

(1) During the dipping process in the liquid zinc bath, the zinc alloy causes a reduction of surface energy between the grains, which leads to a reduction of intercrystalline cohesion and hence to “liquid metal embrittlement“. A consequence of this embrittlement is a reduction of the equivalent strain resistance in the zinc bath, which is recovered after the zinc coating process.

(2) In order to obtain characteristic values of the equivalent plastic strain resistance that depends on the various process parameters, such as

- composition of zinc alloy and bath temperature
- steel-quality
- microstructure and surface condition of steel product or of machined surfaces
- strain rate

a standardized test with sufficiently small test specimens is needed. The results of this test are independent of the scale and the particular loading condition of this test specimen and can be transferred to any large scale structural component.

(3) Such a test has been developed from the fracture mechanics CT test specimen: the LNT-test specimen.

7.2.2 LNT-test specimen and test set up

(1) Fig. 7-3 gives details of the LNT-test-specimen with its dimensions that can be dipped into the liquid zinc bath and loaded horizontally by tensile forces, see fig. 7-4. The sharp crack tip of the CT test specimen (in general obtained by applying fatigue load cycles) is substituted by a drilled hole, the bottom of which is locally strained by the tension forces applied at the top of the specimen in such a way that after sufficient exposure time cracking can be expected.

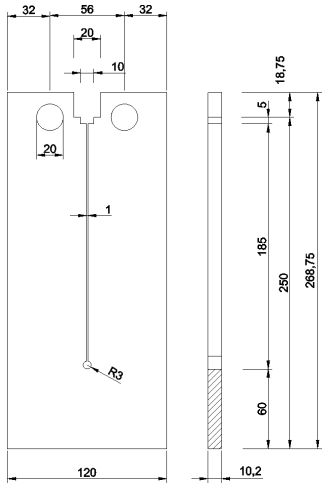


Fig. 7-3: LNT-test specimen

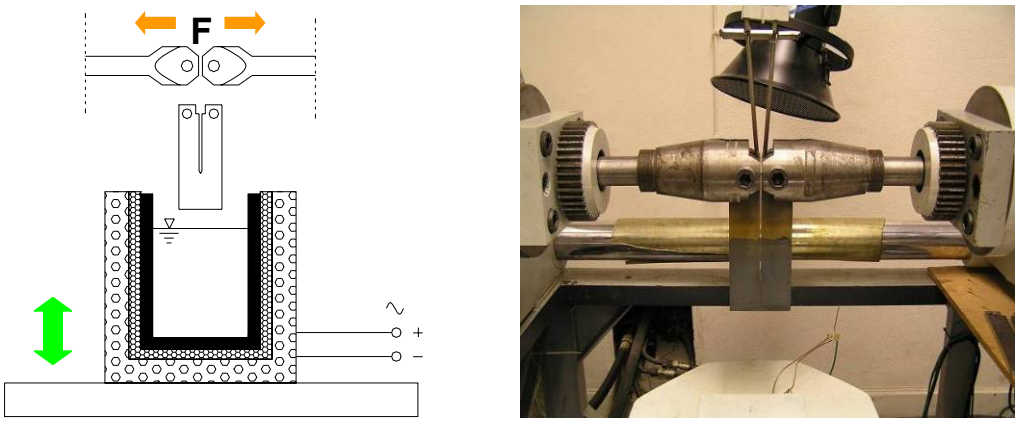


Fig. 7-4: Zinc bath, LNT-test specimen before dipping and application of tensile forces

(2) The local equivalent plastic strain at the bottom of the hole affected by the tensile forces can be determined by FEM-calculations:

$$\varepsilon_{pl,c} = \int \sqrt{\frac{2}{3}\dot{\varepsilon}_{pl}^2}\, dt \qquad (7\text{-}2)$$

(3) Fig. 7-5 gives an example of such calculations with the applied finite element mesh in fig. 7-5a) and the plot of equivalent plastic strains in fig. 7-5 b).

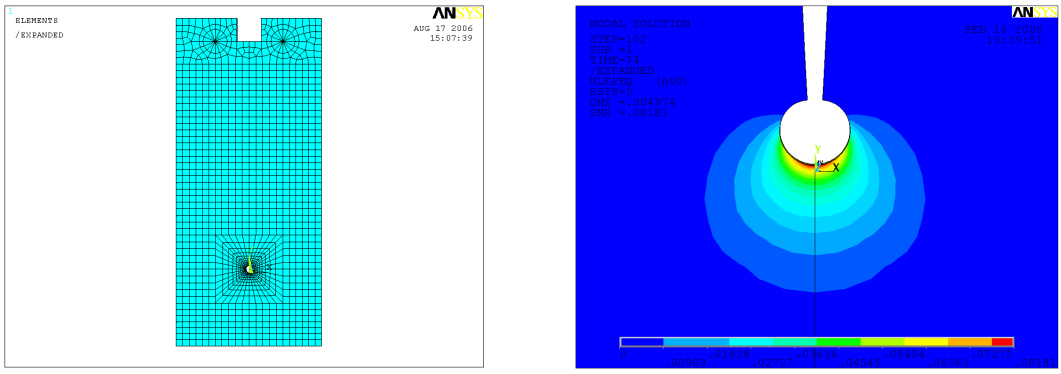


Fig. 7-5: FE-mesh and plot of equivalent plastic strains

7.2.3 Test results

(1) As indicated in fig. 7-6, the load displacement characteristic can be measured in a test. It exhibits a sudden drop when cracking starts.

(2) From FEM, the associated local equivalent strain at the bottom of the hole can be calculated.

(3) While the load-displacement curve in fig. 7-6 applies for a test specimen heated to 450°C without the corrosion effect of a liquid zinc bath (test specimen exposed to the air), giving a cracking strain of 27%, fig. 7-7 gives the values for a zinc alloy with a tin content Sn of 1.2%.

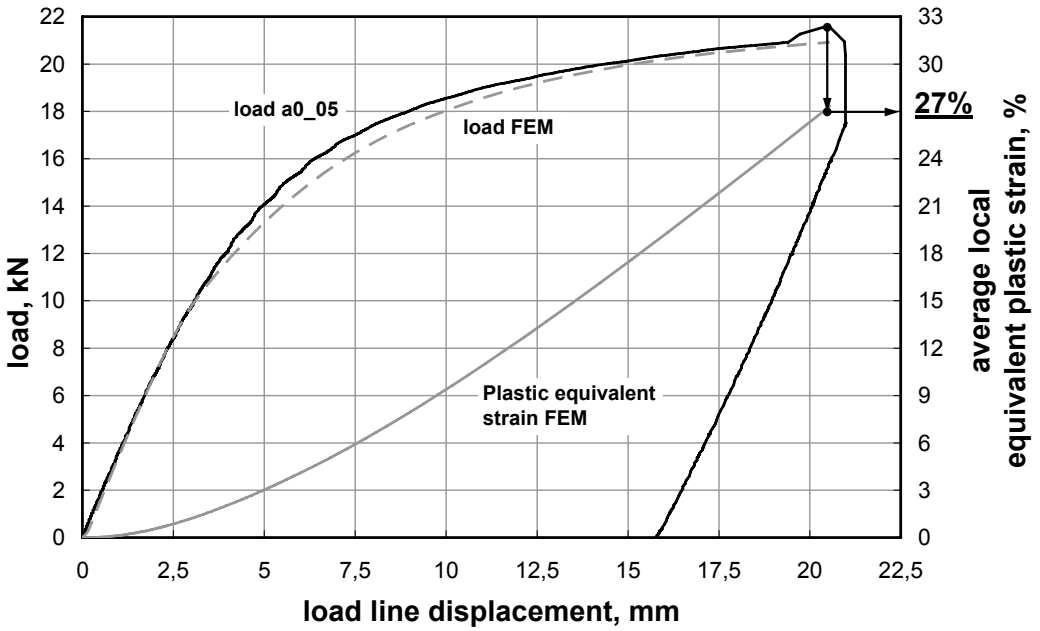


Fig. 7-6: Load displacement and equivalent plastic strain displacement curve for steel exposed to the air with a temperature of 450 °C

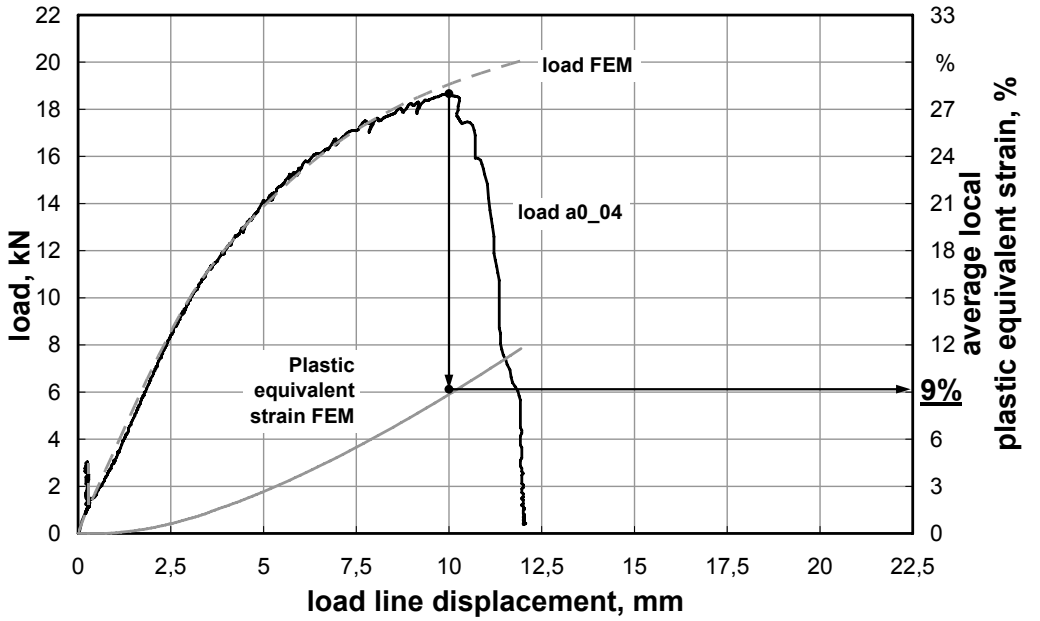


Fig. 7-7: Load displacement and equivalent plastic strain displacement curve in liquid zinc alloy with Sn 1.2%

(4) Fig. 7-8 gives a comparison of test results for zinc alloy a0, zinc alloy a1 and with exposure to the air at 450 °C, all related to steel S460N, see table 7-1.

alloy	Pb, M.-%	Sn, M.-%	Bi, M.-%	Al, M.-%	Ni, M.-%	Fe, M.-%
a0	---	1,20	0,11	0,0057	0,047	0,028
a1	0,70	---	---	0,005	---	0,03

Table 7-1: Chemical composition of zinc alloys

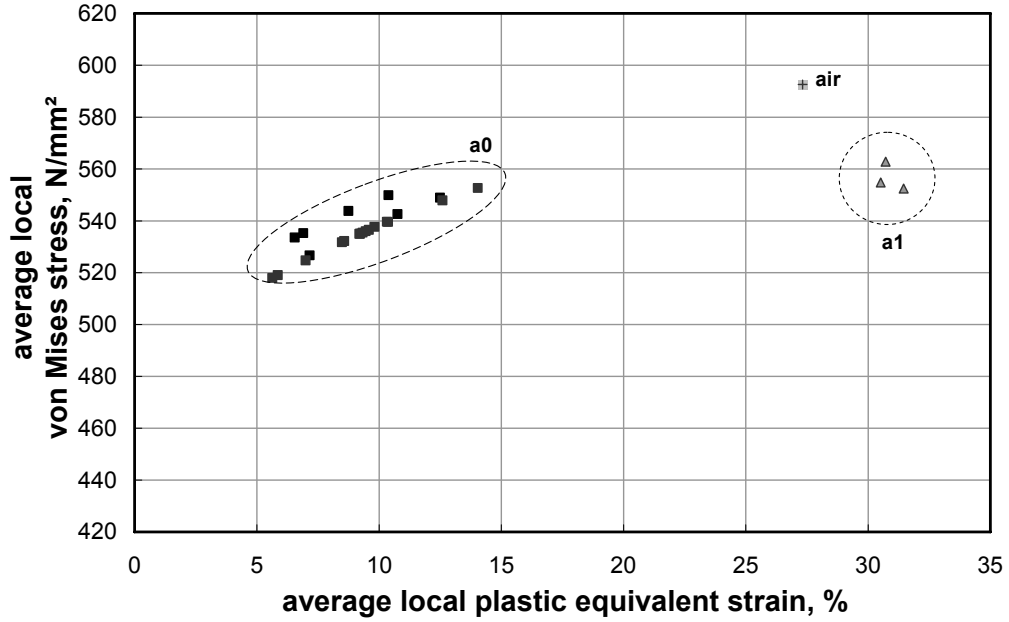


Fig. 7-8: Comparison of equivalent plastic strain resistances for different zinc alloys and for exposure to the air

(5) A systematic investigation of the influence of the components tin (Sn), lead (Pb) and bismuth (Bi) in the zinc alloy for steel S355J2 has lead to the equivalent plastic strains $\varepsilon_{pl,c}$ [%] as given in fig. 7-9. It demonstrates that:

1. Sn is the relevant constituent that gives the steepest gradient

2. classes of equal resistance can be established, e.g. for
   class 1 Sn < 0.1%
   class 2 0.1 % < Sn < 0.3%
   class 3 0.3 % < Sn

   with increasing aggressiveness.

3. the contents of Pb and Bi should be limited by Pb < 0.9%, Bi < 0.08% and Pb + 10 Bi < 1.2%.

(6) The dependency of exposure time is indicated in fig. 7-9.

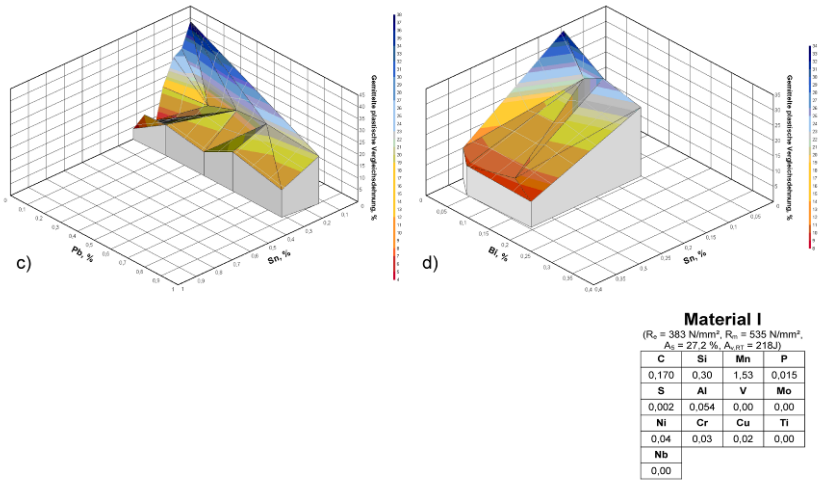


Fig. 7-9: Influence of interaction of Sn, Pb and Bi on equivalent plastic strain resistance

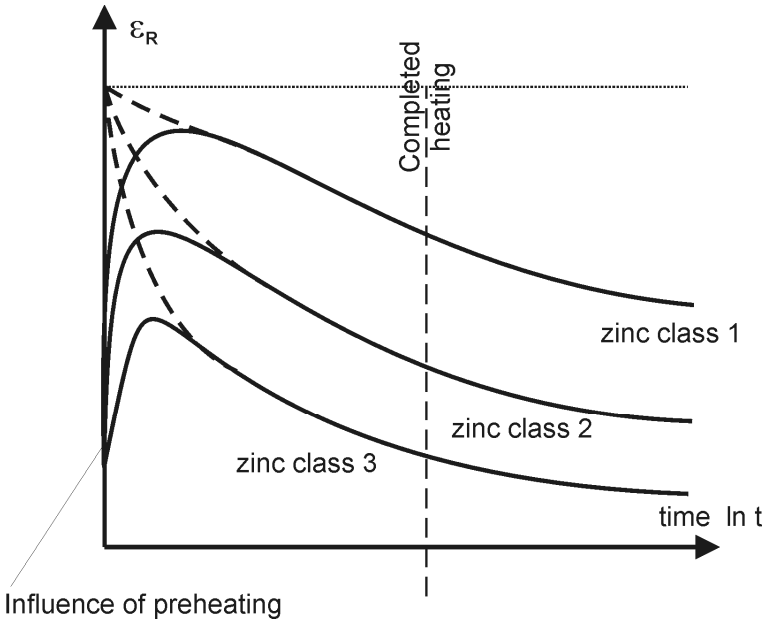


Fig. 7-10: Equivalent plastic strain resistance of different zinc alloys depending on exposure time

(7) A side effect of the testing procedure is that the coefficient α_t for the heat transfer from the zinc bath to the steel specimen required to calculate the heating time from the temperature of the steel component before dipping to the temperature of the zinc bath can also be experimentally determined.

(8) Fig. 7-11 gives a comparison of the temperature-time curve as measured during dipping and as calculated with a numerical model using α_t.

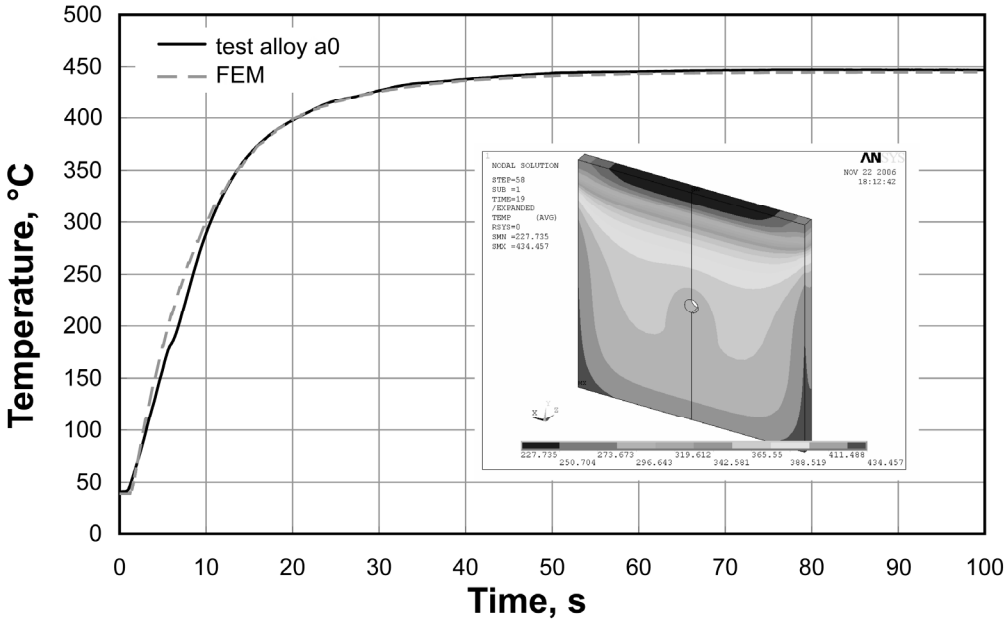


Fig. 7-11: Comparison of the time histories of temperature of a specimen as measured and as calculated

7.3 Equivalent plastic strain requirements from the steel components

7.3.1 General

(1) Equivalent plastic strain requirements result from an accumulation of strains due to

1. Time history of fabrication
2. Time history of heating process during dipping, if the heating process is relevant for cracking
3. Time history of the exposure in the zinc bath, if the time effect is relevant for cracking.

(2) Fig. 7-12 shows the dipping procedure versus time and fig. 7-13 gives an example of the temperature distributions over a selected cross-section resulting in residual strain distributions that are laid over the residual strain distribution of the component from fabrication.

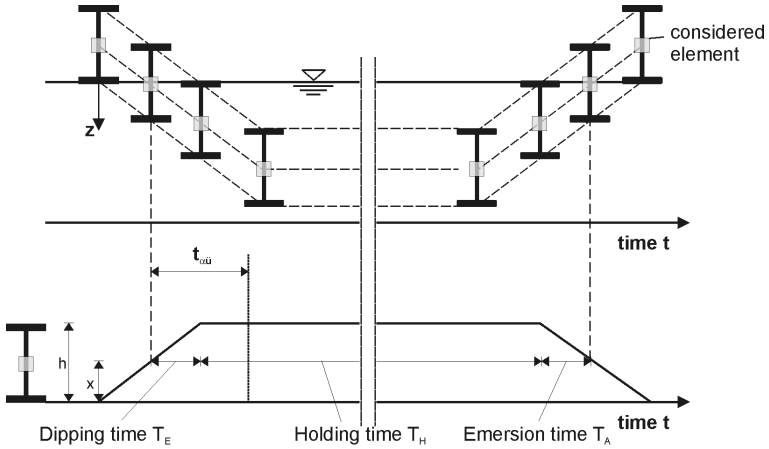


Fig. 7-12: Time history of dipping for a mass particle of the structural component

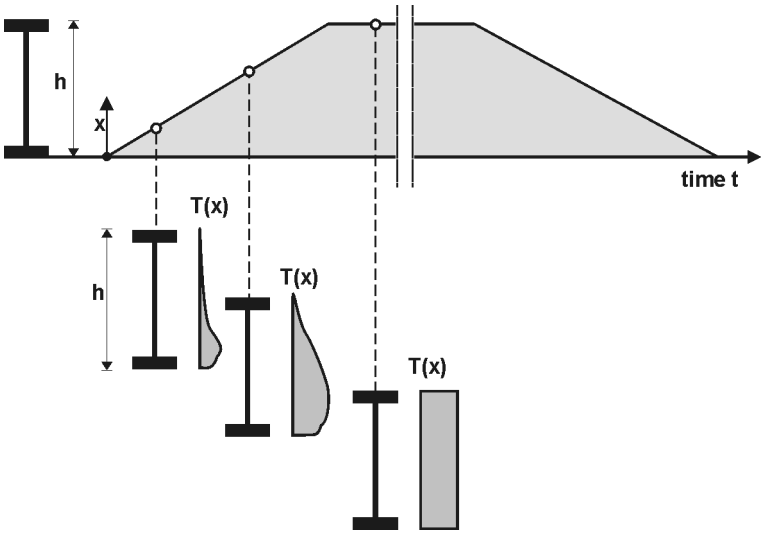


Fig. 7-13: Time history of temperature for a cross-section of a structural component

(3) The residual strains that arise from the temperature distribution are shown in fig. 7-14.

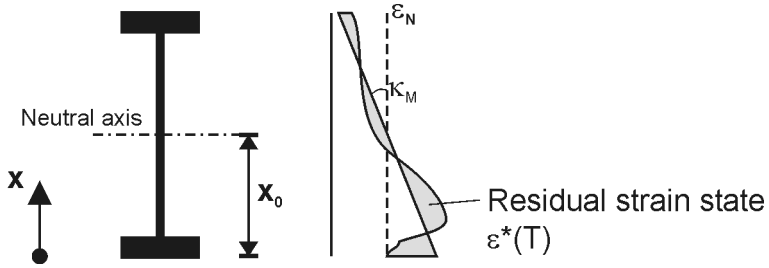


Fig. 7-14: Residual strain increments from temperature distributions

Fig. 7-15 demonstrates an example of the time history of equivalent plastic strain from fabrication (t = 0), superimposed with strains from the heating with time variant temperature distributions until full heating is achieved (without any temperature gradient). The full equivalent plastic strain accumulation process including stress relief by the exposure to the zinc bath heat is relevant for the strain requirement at a certain time.

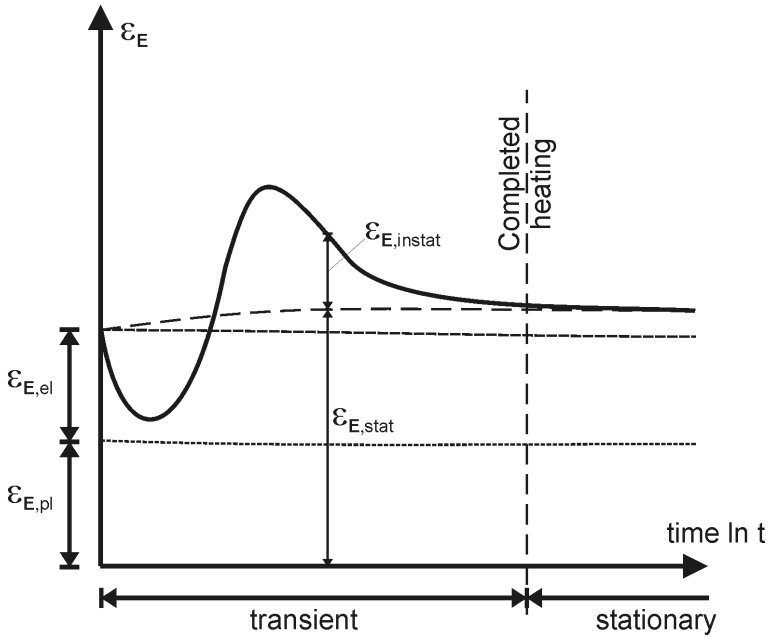


Fig. 7-15: Example of a time history of equivalent plastic strain requirements

(4) Fig. 7-16 gives an example for how various zinc alloys give different equivalent strain-time histories. This is due to the fact that the heat transition coefficient varies with the composition of the alloy. With increasing heat transition coefficient the maximum values of the occurring strain increases also.

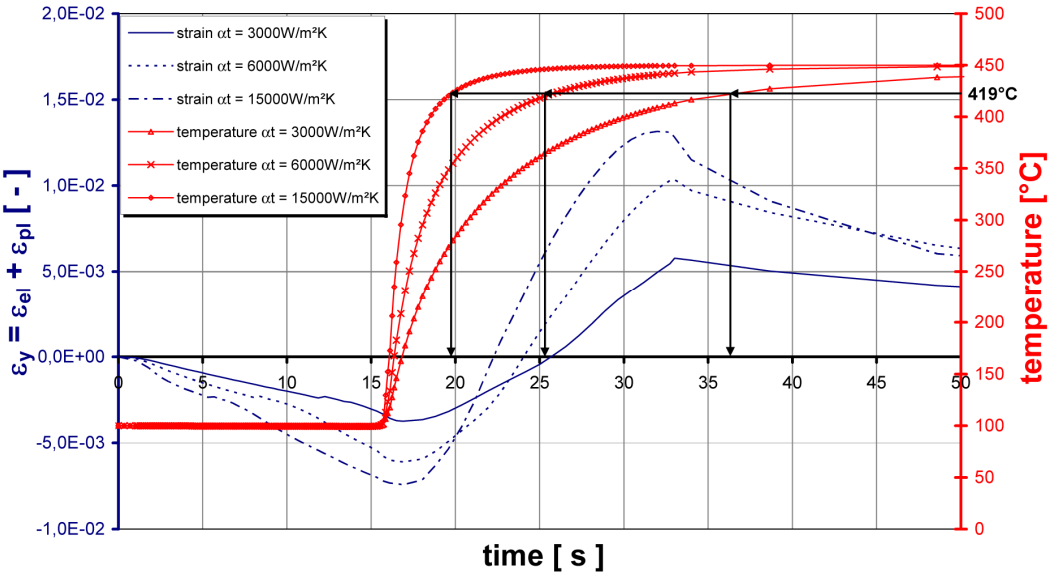


Fig. 7-16: Effect of different zinc-alloys with different heat-transition coefficients at on temperature- and equivalent strain-histories

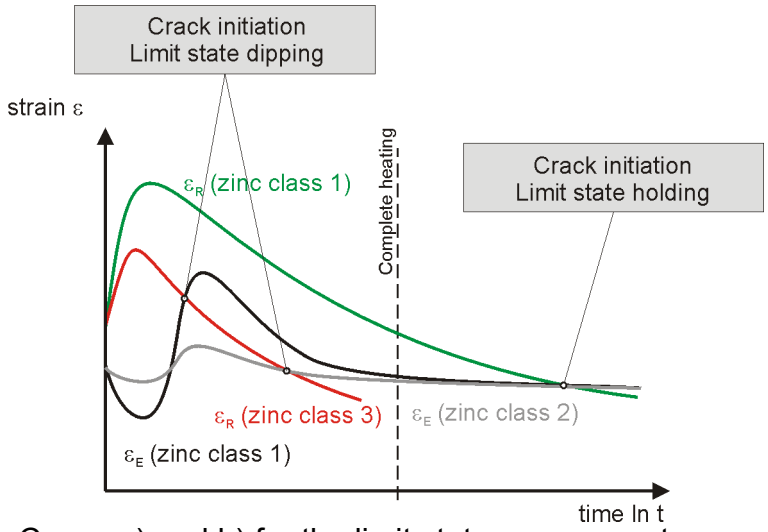


Fig. 7-17: Cases a) and b) for the limit state assessment

(5) Fig. 7-17 demonstrates the principle of the limit state assessment for two zinc alloys of different aggressiveness:

case a: For a highly aggressive zinc alloy (e.g. zinc class 3), the peak value of the time history of strain requirement reached during the dipping process is relevant for cracking. Cracks may occur during the submerging of the structural component into the zinc bath and appropriate measures to reduce the risk are related to reducing the peak value by preheating or reducing the required time for full submergence.

case b: For moderate or low aggressive zinc alloys (e.g. zinc class 1), the exposure time in the zinc bath leading to a reduction of strain resistance is relevant for cracking, and appropriate measures to reduce the risk are related to reducing the exposure time by reducing the thickness of plates and the differences in thicknesses of plates.

(6) In the following paragraphs, the basic characteristic for modelling the limit state case a) and the limit state case b) are explained.

7.3.2 Assessment for the limit state case a)

7.3.2.1 Reference model for the dipping process

(1) In order to obtain a simple reference model for the dipping process, a rectangular plate with the plate thickness s and the depth h is assumed to be dipped with the velocity v into the liquid zinc bath. The plate is supposed to be without residual stresses or strains, fig. 7-18.

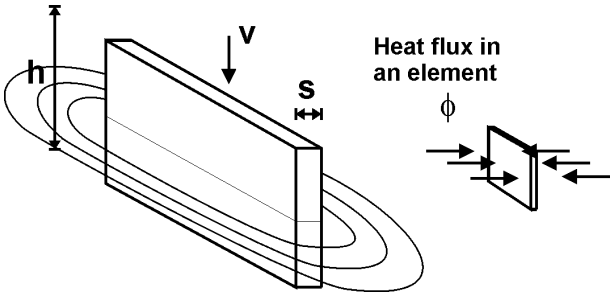


Fig. 7-18: Reference model for the dipping process

(2) The reference model is used for the following purposes:

1. to calculate the time $t_{\alpha t}$ of a particular plate element, see fig. 7-18, to heat up from the preheating temperature T_v to the melting temperature of pure zinc T_a = 419 °C.

   In this calculation, the heat conductivity in the plate is neglected. The heat transfer coefficient α_t is taken as the actual effective value for the zinc alloy in question, which may be determined according to 7.2.3 (7), see fig. 7-11.

2. to determine the time-history of instationary residual stresses and strains caused by strains ε^* from temperature differences from dipping with different velocities v to identify the time t_σ when the maximum of residual stresses and strains occurs.

3. to use the pseudo-limit state criterion based on the assumption that in the beginning of the heating up phase the zinc freezes at the "cold" surface of the steel component and hence reduces the corrosion effect of the zinc alloy until the steel component has adopted the temperature of the zinc bath (cracking of the frozen zinc layer is not considered).

   Based on this assumption, the limit state is defined by the requirement that the time interval t_σ for attaining the maximum of the time history of residual stresses should be longer than the heating up time $t_{\alpha t}$:

   $$t_\sigma - t_{\alpha t} \geq 0 \qquad (7\text{-}3)$$

   $$\frac{t_\sigma}{t_{\alpha t}} \geq 1 \qquad (7\text{-}4)$$

4. to link the simplified limit state equation (7-4) to the actual limit state as indicated as case a) in fig. 7-17 by adaption factors k_c that are used, as explained in section 7.3.2.3.

7.3.2.2 Determination of the reference time $t_{\alpha t}$

(1) The calculation of the reference time $t_{\alpha t}$ in fig. 7-18 is based on the following assumptions:

1. The heat-transfer between the zinc-bath and the steel plate is constant with time:

$$C\rho V \frac{dT}{dt} = \alpha_t A\left(T_a - T\right) \qquad (7\text{-}5)$$

where

C is the specific heat capacity of the plate
ρ is the specific mass
V is the volume of the plate
T is the temperature of the plate
t is the time
α_t is the effective heat transfer coefficient for the zinc alloy
A is the surface of the plate
T_a is the melting temperature of pure zinc (419 °C)
T_{Bath} is the melting temperature of the zinc alloy.

2. The first zinc coat freezes on the plate surface and prohibits further access of aggressive constituents of the zinc alloy to the steel surface, thus protecting the steel from cracking. Any cracking of the first zinc coat is not considered.

(2) Equation (7-5) leads to

$$dt = \frac{CV\rho}{A\alpha_t} \cdot \frac{dT}{T_a - T} \tag{7-6}$$

which gives

$$t_{\alpha t} = \frac{C \cdot s \cdot \rho}{2\alpha_t} \int_{T_v}^{T_a} \frac{dT}{T_a - T} = \frac{C \cdot s \cdot \rho}{2\alpha_t} \ell n \frac{T_v - T_{Bath}}{419 - T_{Bath}} \tag{7-7}$$

(3) For the example of a plate with

s = 0.01
T_{Bath} = 450 °C
T_v = 50 °C
α_t = 6000 W/m² K
C = 600 J/kg K
ρ = 7,800 kg/m²

the temperature-time curve is given in fig. 7-19.

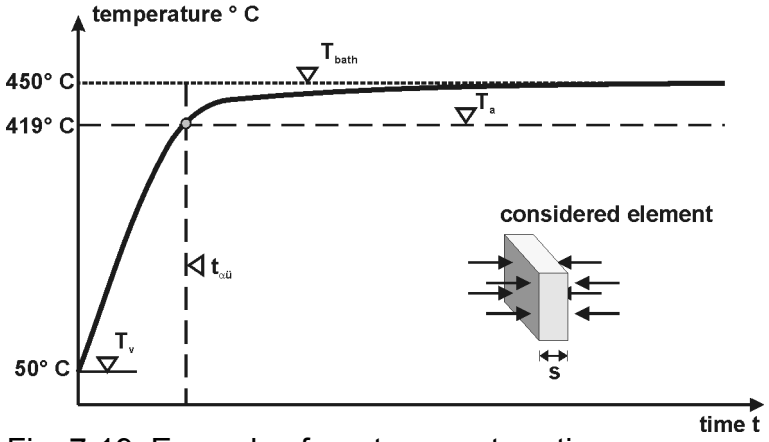


Fig. 7-19: Examples for a temperature-time curve

(4) Indicative values for effective coefficients of heat transfer are given in table 7-2 for zinc alloy classes as defined in 7.2.3(5).

Zinc alloy class	Weight proportion of zinc alloy					Effective heat transfer coefficient $\alpha_{t,eff}$
	Sn	Pb + 10 Bi	Ni	Al	Sum of other elements (without Zn)	
1	Sn ≤ 0,1%	1,5 %	< 0,1%	< 0,1%	< 0,1%	3000 W/m²K
2	0,1% < Sn ≤ 0,3%	1,5 %	< 0,1%	< 0,1%	< 0,1%	6000 W/m²K
3	Sn > 0,3%	1,3 %	< 0,1%	< 0,1%	< 0,1%	15000 W/m²K

Table 7-2: Effective coefficients of heat transfer

7.3.2.3 Pseudo-limit state equation for the reference model

(1) The pseudo-limit state equation for the reference model in fig. 7-18 reads:

$$\frac{h}{v} - \frac{C \cdot s \cdot \rho}{2\alpha_t} \ell n \frac{T_v - T_{Bath}}{419°C - T_{Bath}} \leq 0 \tag{7-8}$$

or

$$\frac{C \cdot s \cdot \rho \cdot V}{2\alpha_t \, h} \ell n \frac{T_v - T_{Bath}}{419°C - T_{Bath}} \leq 1 \tag{7-9}$$

(2) For the example of a plate with h = 0.50 m, s = 0.01 m without residual stresses and strains, the time histories of stresses during the submerging process are given in fig. 7-20 for various dipping velocities.

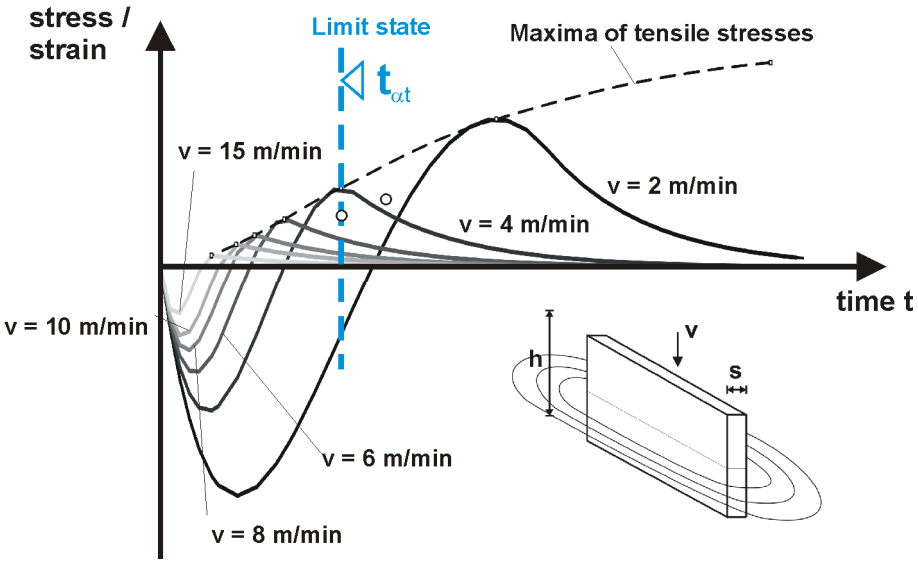
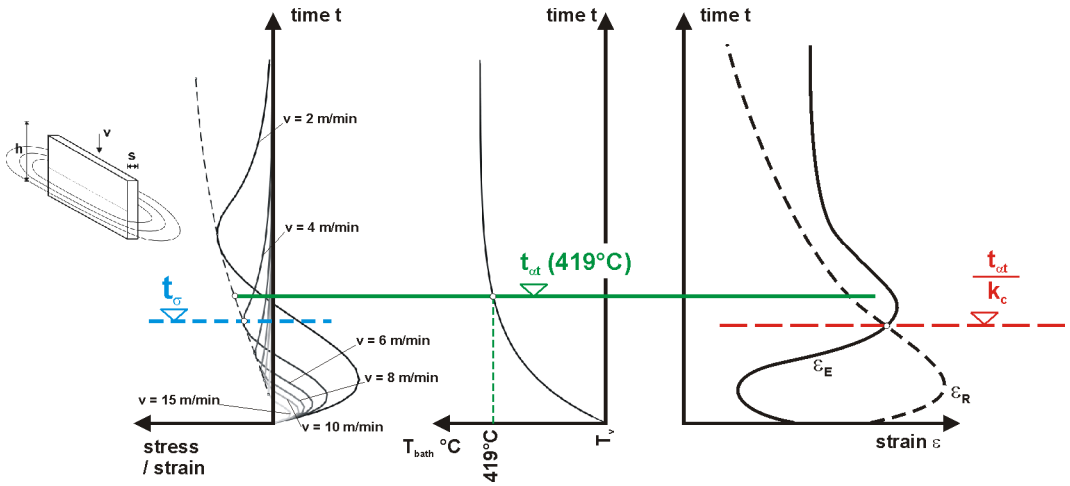


Fig. 7-20: Time histories of residual stresses for various dipping velocities

(3) In fig. 7-20 the pseudo-limit state is reached for a velocity v = 3.5 m/min.

(4) The conditions for the attainment of the pseudo-limit state are presented in fig. 7-21.



engineering model

$$\frac{t_\sigma}{t_{\alpha t}} = \frac{h \cdot 2\alpha_t}{C \cdot s \cdot \rho \cdot v} \cdot \frac{1}{\ln \frac{T_v - T_{bath}}{419° - T_{bath}}} \leq 1$$

verification model

$$k_c \cdot \frac{t_\sigma}{t_{\alpha t}} = k_c \cdot \frac{h \cdot 2\alpha_t}{C \cdot s \cdot \rho \cdot v} \cdot \frac{1}{\ln \frac{T_v - T_{bath}}{419° - T_{bath}}} \leq 1$$

Fig. 7-21: Conditions for the attainment of the pseudo-limit state

7.3.2.4 Adaption factor k_c

(1) To adapt the limit state equation (7-9) derived for the reference model to realistic limit state conditions, the definition of $t_{\alpha t}$ is modified, see fig. 7-21:

$$t_{\alpha t}^{real} = \frac{t_{\alpha t}}{k_c} \tag{7-10}$$

where k_c is the adaption factor.

(2) The factor k_c is composed of

$$k_c = k_{detail} \cdot k_{weld} \cdot k_{surface} \cdot k_{coldform} \cdot k_{preheat}$$

where

k_{detail}	represents the structural detailing
k_{weld}	represents the weld thickness
$k_{surface}$	represents the surface roughness
$k_{coldform}$	represents the effects of prestraining by cold forming
$k_{preheat}$	represents the effects of T_v in addition to its effect in the limit state formula.

(3) The factor k_{detail} has the most important effect. Fig. 7-22 demonstrates how the time interval for reaching the realistic limit state case a) in fig. 7-17 is correlated to the pseudo-limit state in fig. 7-21.

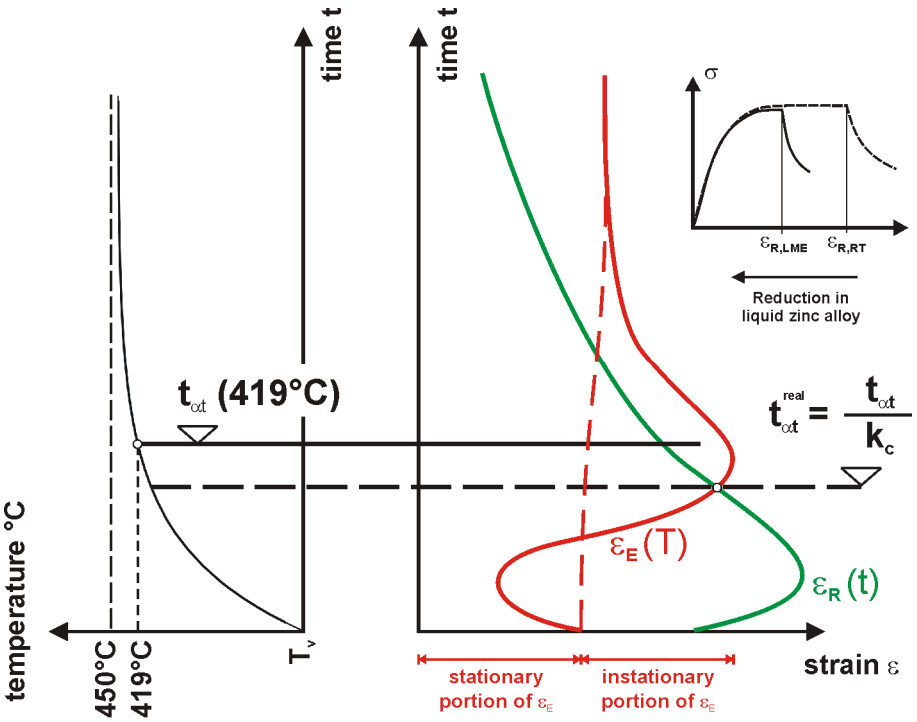


Fig. 7-22: Determination of $t_{\alpha t}^{real}$ and $t_{\alpha t}$ to determine k_c

(4) According to fig. 7-22, the determination of k_c needs to calculate the equivalent plastic strain requirements ε_E of structural components with different details and process conditions.

(5) In fig. 7-23, examples for equivalent plastic strain requirements ε_E are given for

v	=	0.25 m/min
α_t	=	15,000 W/m²
T_v	=	50 °C
T_{Bath}	=	450 °C

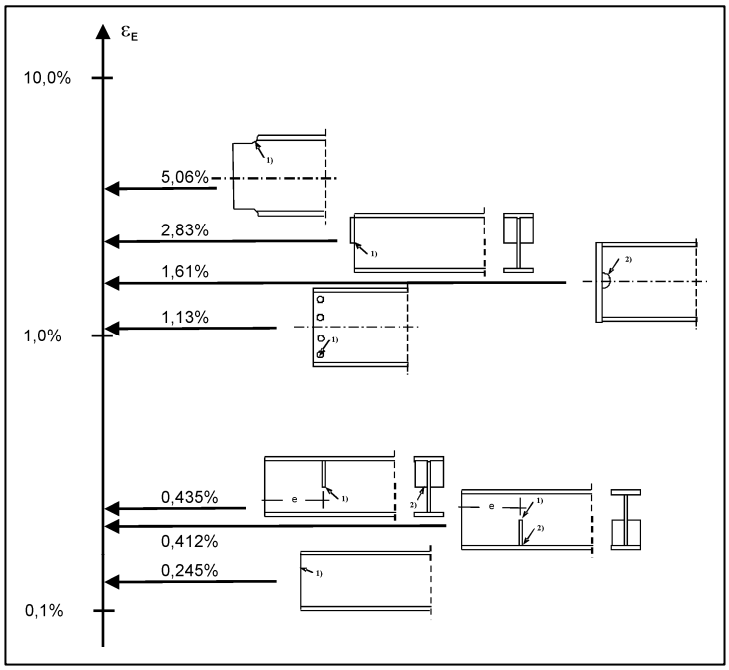


Fig. 7-23: Examples of equivalent plastic strain requirements for various details.

(6) The associated equivalent plastic strain resistances for the various zinc alloy classes are given in table 7-3.

Zinc alloy class	Weight proportion of zinc alloy					Plastic strain resistance $\varepsilon_{R,ref}$
	Sn	Pb + 10 Bi	Ni	Al	Sum of other elements (without Zn)	
1	Sn ≤ 0,1%	1,5 %	< 0,1%	< 0,1%	< 0,1%	12%
2	0,1% < Sn ≤ 0,3%	1,5 %	< 0,1%	< 0,1%	< 0,1%	6%
3	Sn > 0,3%	1,3 %	< 0,1%	< 0,1%	< 0,1%	2%

*) Pre-condition: salt content of flux ≥ 450 g/l and iron content in flux < 10g/l

Table 7-3: Equivalent plastic strain resistances

(7) A comparison of fig. 7-23 with table 7-3 shows that for zinc alloy class 3, many details frequently used in practice should not be used for zinc coating.

7.3.2.4 Conclusions for limit state assessment for case a)

(1) The limit state verification for case a) is based on the formula

$$k_c \cdot \frac{h \cdot 2\alpha_t}{C \cdot s \cdot \rho \cdot v} \frac{1}{\ell n \frac{T_v - T_{Bath}}{419° - T_{Bath}}} \le 1 \qquad (7\text{-}11)$$

where

$k_c = k_{detail} \cdot k_{weld} \cdot k_{surface} \cdot k_{coldform} \cdot k_{preheat}$.

(2) This formula is applicable to the following parameters:

1. α_t -values according to the zinc alloy classes in table 7-2
2. k_{detail}-classes according to table 7-4

class of structural detail	ε_E	Detail	k_{konst}
I	≤2%	Profiles without attachment parts, constant section, no constructive notches All rolled sections: I, IPE, HEA, HEB. HEM Welded sections taking into account the thickness ratio $t_{max} / t_{min} \leq 2,0$ Profiles with attachment parts, constant section, constructive notches in terms of attachments taking into account the thickness ratio $t_{max} / t_{min} \leq 2,0$	1,0
II	≤6%	Profiles with attachment parts, constant section, constructive notches in terms of attachments taking into account the thickness ratio $t_{max} / t_{min} > 2,0$ drillings nodes of lattice girders hollow sections with connection plates	2,0
III	≤12%	Profiles with constructive notches at the free end of a beam	5,0

Table 7-4: Classification of structural details and k_{detail}-values

3. Other k_i-values may be taken form table 7-5.

Adjustment coefficient		k
Weld thickness	a < 5mm 5mm < a ≤ 12mm 12mm < a	1,00 1,25 1,50
Surface roughness according to EN ISO 9013, table 5	Quality level 4 Quality level 1-3	1,00 1,20
Cold forming	ε_{pl} < 1% 1% < ε_{pl} < 5% 5% < ε_{pl} < 20%	1,00 1,10 1,25
Preheating effects on yield strenght	$T_V \leq 50$ °C 50 °C < < 200 °C	1,00 1,10 – T_v / 400

Table 7-5: Classification of weld, surface, cold forming- & preheating effects.

7.3.3 Assessment for the limit state case b)

7.3.3.1 General

(1) Case b) of limit states according to fig. 7-17 leads to the critical time t_s, when the degradation of strain resistance in the zinc bath has attained the residual strain requirement, see fig. 7-24.

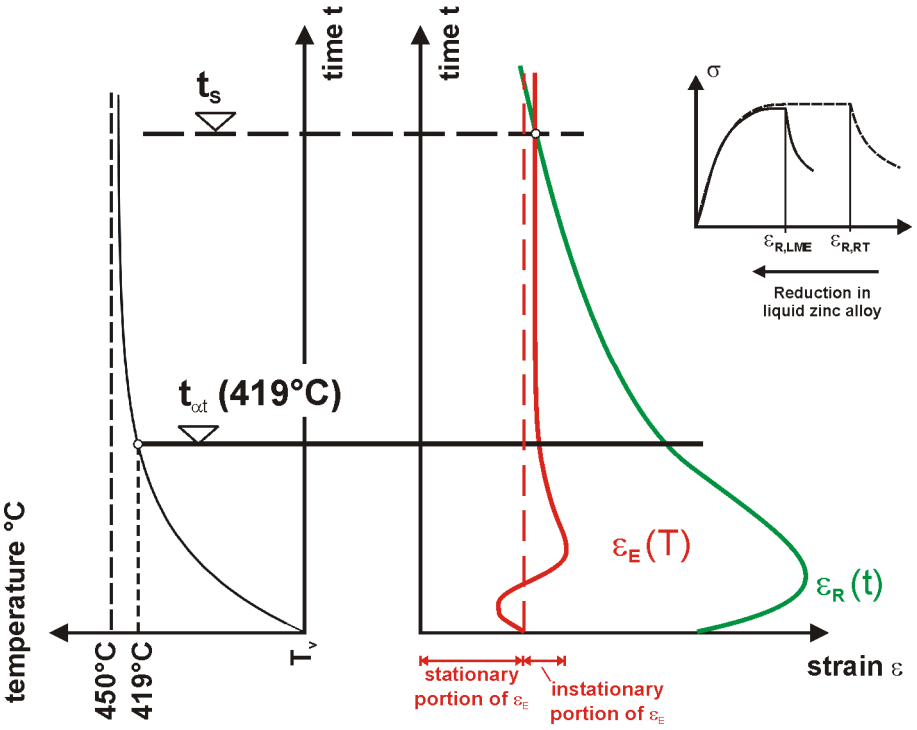


Fig. 7-24: Determination of t_s for the limit state case b)

(2) The verification is carried out in terms of equivalent plastic strains

$$\varepsilon_{Es} \leq \varepsilon_{Rs} \tag{7-12}$$

7.3.3.2 Equivalent plastic strain requirements ε_{Es}

(1) The main cause of equivalent plastic strain requirements ε_{Es} is fabrication, e.g. by rolling, cold forming and welding and the liquid zinc bath.

(2) The values of these equivalent plastic strains are correlated with the thickness s of steel products and give a function for ε_{Es} depending on plate thickness s and the process time of the steel material in the liquid zinc bath as indicated in fig. 7-25.

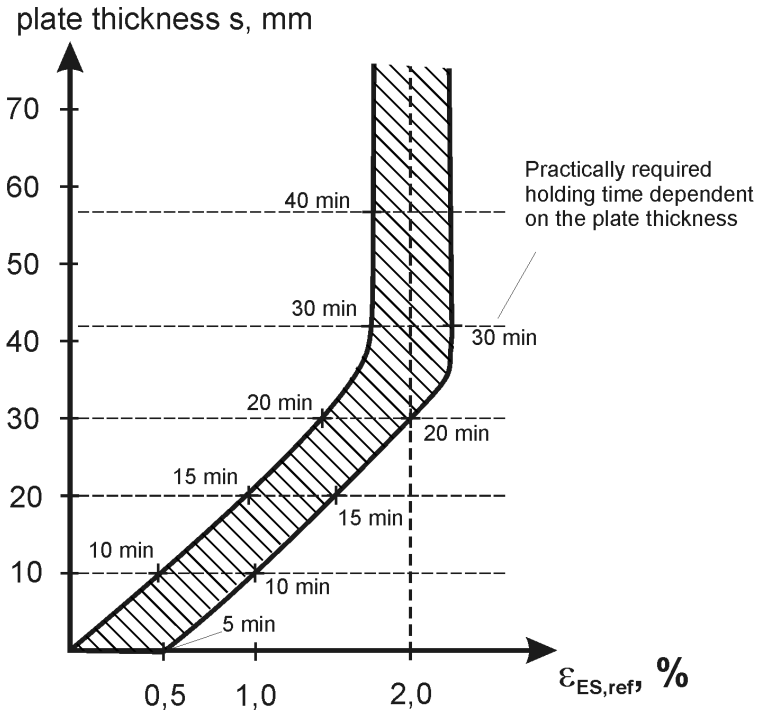


Fig. 7-25: Relationship between ε_{Es} and s and dipping time t_s.

7.3.3.3 Equivalent plastic strain resistance ε_{Rs}

(1) For the decrease of equivalent plastic strain resistance with the time, the function given in fig. 7-26 can be used.

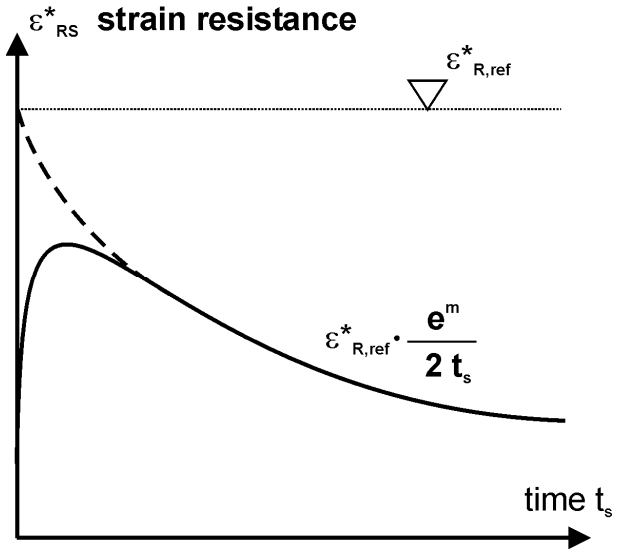


Fig. 7-26: Decrease of strain resistance of steel in the zinc bath

(2) The parameters have been determined from deformation-controlled LNT-tests, where the strain ε is proportional to the load-line displacement δ, see fig. 7-27 using different strain rates $\dot{\varepsilon} = \frac{\partial \varepsilon}{\partial t}$.

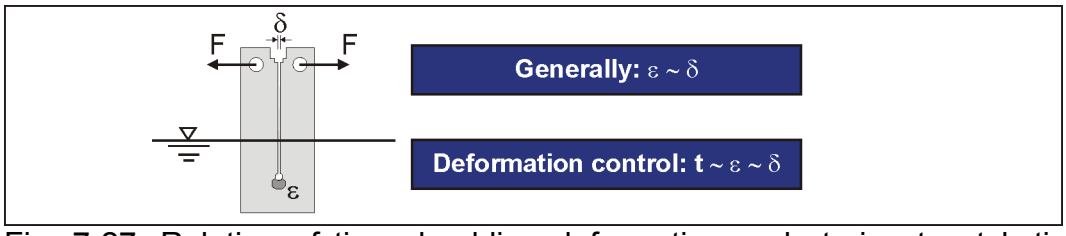


Fig. 7-27: Relation of time, load-line deformation and strain at notch tip for deformation controlled LNT-tests

(3) Fig. 7-28 shows a matrix with variation of the composition of the zinc-alloy on the vertical axis and the applied strain rate $\dot{\varepsilon}$ on the horizontal axis.

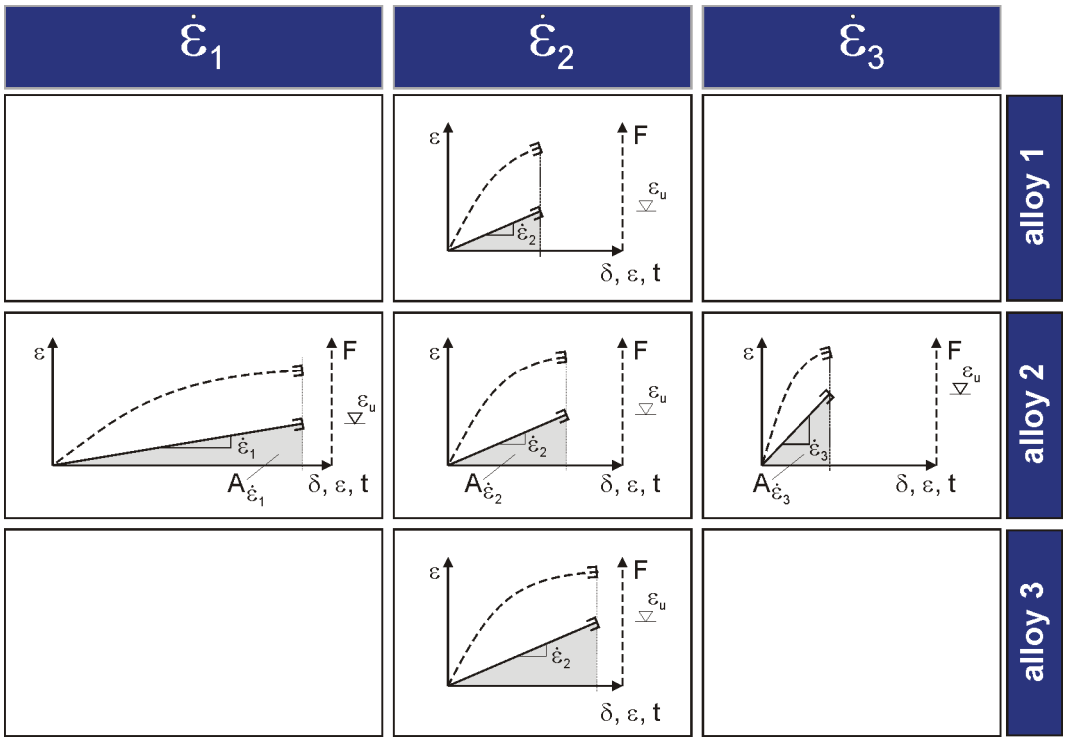


Fig. 7-28: Dependence of the LNT-test results on the zinc alloy and the strain rate

From test results it can be seen that, while holding the composition of the zinc alloy constant, a decrease of the strain rate from test to test leads to lower strain resistances. For constant strain rates the strain resistance decreases with increasing content of low melting alloying elements (e.g. tin).

(4) Some results of the variation of the composition of the zinc-melt for $\dot{\varepsilon}$ = const and of the variation of the strain rate $\dot{\varepsilon}$ in case of constant composition of the zinc-melt are given in fig. 7-29.

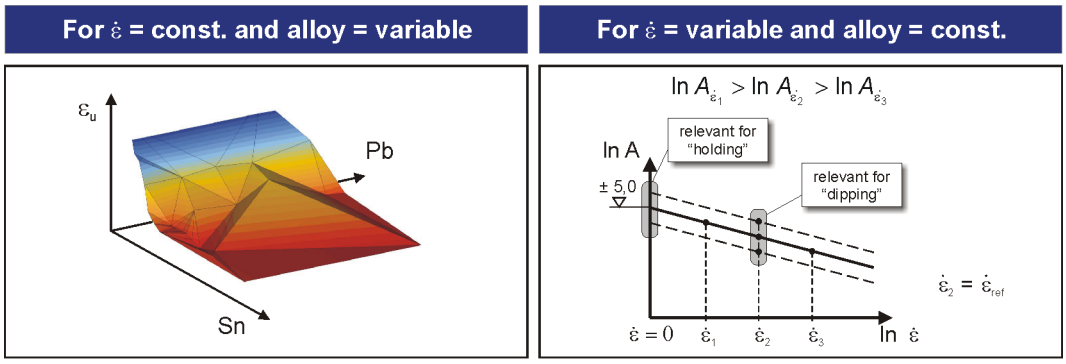


Fig. 7-29: Decrease of strain resistance of steel in the zinc bath

(5) The function in fig. 7-26 is based on the following assumptions:

1. The reference value $\varepsilon_{Rs,ref}$ is the value, determined with the LNT-test according to section 7.2 with the typical strain rate

$$\dot{\varepsilon} = 5 \cdot 10^{-4} \left[\frac{1}{s}\right] \tag{7-13}$$

2. To transfer the results of the LNT-test to the case $\dot{\varepsilon} = 0 \left[\frac{1}{s}\right]$ a relationship between the integral

$$\ell n \left[\int \frac{\varepsilon_{Rs}(t)}{\varepsilon^{*}_{Rs,ref}} dt \right] \tag{7-14}$$

where $\varepsilon^{*}_{Rs,ref}$ is

$$\varepsilon^{*}_{Rs,ref} = 60 \cdot \varepsilon_{R,ref} \tag{7-15}$$

and the strain rate $\dot{\varepsilon}$ according to fig. 7-30, which has been determined from evaluations of tests, see fig. 7-6 and fig. 7-7, is used

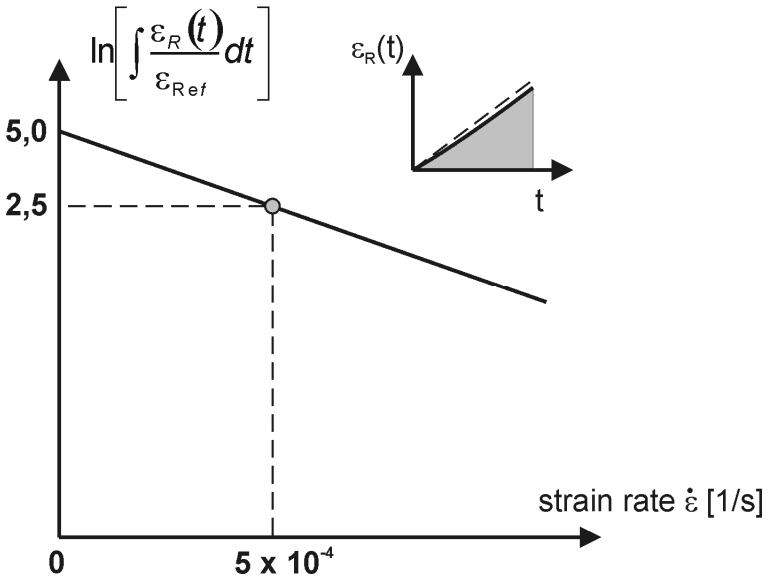


Fig. 7-30: Correlation related to $\dot{\varepsilon}$

3. From fig. 7-30 the pairs of values

$$\ell n\left[\int \frac{\varepsilon_{Rs}(t)}{\overset{*}{\varepsilon}_{Rs,ref}}\,dt\right] = 2{,}5 \;and\; \dot{\varepsilon} = 5\cdot 10^{-4}$$

and

$$\ell n\left[\int \frac{\varepsilon_{Rs}(t)}{\overset{*}{\varepsilon}_{Rs,ref}}\,dt\right] = 5{,}0 \;and\; \dot{\varepsilon} = 0 \qquad (7\text{-}16)$$

can be determined.

4. From (7-16) follows

$$\int_0^{\varepsilon_{R(t_s)}} \frac{\varepsilon(t)dt}{\overset{*}{\varepsilon}_{R,ref}} = e^5 \qquad (7\text{-}17)$$

And from fig. 7-27 with assumption of a linear function follows

$$\int_0^{\varepsilon_{R(t_s)}} \frac{\varepsilon(t)}{\overset{*}{\varepsilon}_{R,ref}}\,dt \approx 0{,}5\,\frac{\varepsilon_R(t_s)}{\overset{*}{\varepsilon}_{R,ref}}\cdot t_s \qquad (7\text{-}18)$$

so that in conclusion the dipping time t_s reads:

$$t_s = 2\cdot 148\cdot \frac{\overset{*}{\varepsilon}_{R,ref}}{\varepsilon_R(t_s)}[s] = \frac{5\cdot \overset{*}{\varepsilon}_{R,ref}}{\varepsilon_R(t_s)}[\text{min}] \qquad (7\text{-}19)$$

7.3.3.4 Limit state assessment for case b)

(1) In the ultimate limit state of cracking the requirement ε_E according to fig. 7-25 and the resistance $\varepsilon_R(t_s)$ according to equation (7-19) are equal, and the critical dipping time t_s for various zinc alloy classes and equivalent plastic strains can be determined, as given in fig. 7-31.

Strain requirement ε_{ES}	Zinc class		
	1	2	3
	$\varepsilon_{R,ref}$ = 12 %	$\varepsilon_{R,ref}$ = 6 %	$\varepsilon_{R,ref}$ = 2 %
0,5 %	120 min.	60 min.	20 min.
1,0 %	60 min.	30 min.	10 min.
1,5 %	40 min.	20 min.	6,7 min.
2,0 %	30 min.	15 min.	5 min.

Fig. 7-31: Critical dipping time t_s for various zinc alloy classes and strain requirements ($\varepsilon_{Ref} = \varepsilon^*/60$)

(2) It is evident from fig. 7-31 that for zinc alloy class 1 all time values for dipping are within safe limits, whereas zinc alloy classes 2 and 3 require restrictions of dipping time and hence of plate thicknesses.

7.3.4 Conclusions for standardisation

(1) The limit state procedure to avoid cracking from liquid metal embrittlement requires cooperation between the designer and the zinc coating expert, as both structural detailing and the zinc coating-process influence the limit state.

(2) The flow chart giving the influence of structural detailing and of the zinc coating process is given in fig. 7-32.

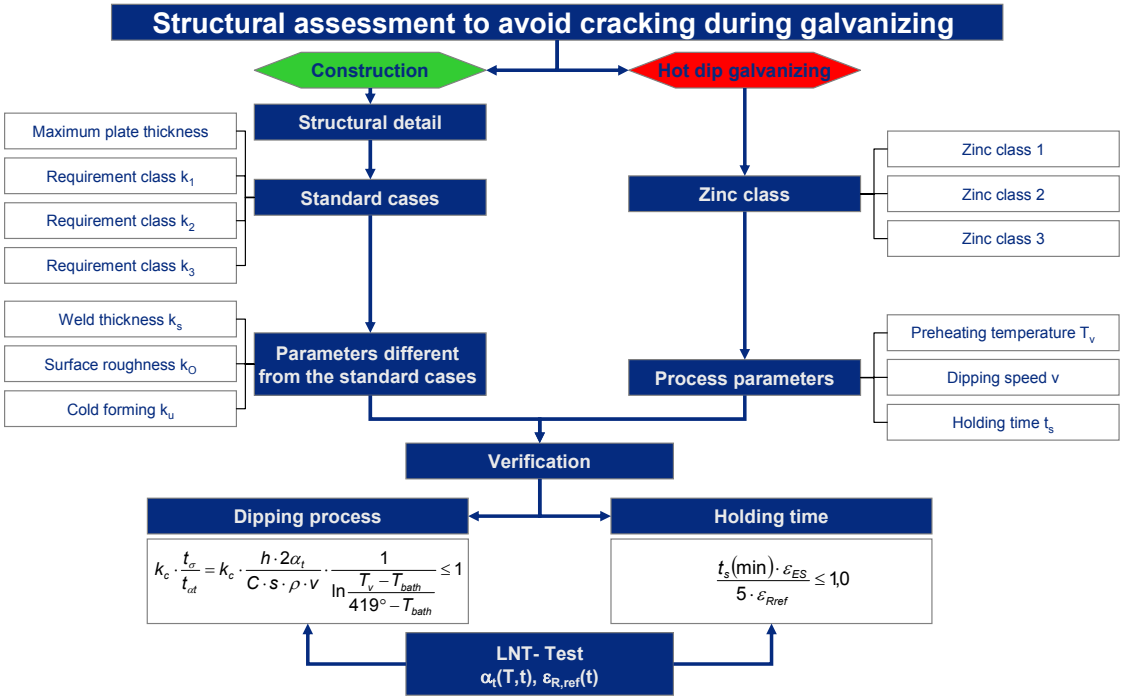


Fig. 7-32: Flow chart for the structural assessment to avoid cracking from liquid metal embrittlement

(3) As the assessment procedure so far cannot be controlled in view of its actual reliability, structural members after zinc coating should be checked anyway in view of cracks.

7.4 Testing of structural elements that are zinc coated for cracks

(1) Non Destructive Testing should be performed with the MT-procedure, taking into account:

1. The reduced sensitivity for coating thicknesses $t_z \geq 50$ µm (see EN 1290, Annex 1)

2. The reduced accessibility at the corners of web, flange and plates.

(2) Therefore, the procedure should be modified with regard to the magnetic specific flow and magnetic field potential, the testing system and the powder suspension.

7.5 Bibliography

[1] Feldmann M., Pinger T., Tschickardt D.: Cracking in large steel structures during hot dip galvanizing. Intergalva 2006, Neapel (Engels: Naples) 2006.

[2] Katzung W., Schulz W.-D.: Beitrag zum Feuerverzinken von Stahlkonstruktionen - Ursachen und Lösungsvorschläge zum Problem der Rissbildung. Stahlbau 74 (2005), S. 258-273.

[3] Sedlacek, G. et al.: Zur sicheren Anwendung feuerverzinkter Träger. Stahlbau 73 (2004), S. 427 – 437.

[4] Bleck W., Mansfeld A., Dilthey U., Gräb T., Sedlacek G., Feldmann M., Stangenberg H., Grotmann D., Langenberg P.: Pilotstudie zum sicheren Einsatz des hochfesten Stahls S460 in stückverzinktem Zustand in geschweißten Konstruktionen; P 504, Studiengesellschaft für Stahlanwendung e.V., Düsseldorf 2002, nicht veröffentlicht.

[5] Forschungsvorhaben „Vermeidung von Rissen beim Feuerverzinken von großen Stahlkonstruktionen mit hochfesten Stählen“. AiF-Forschungsvorhaben 14545 N71 gefördert von dem Gemeinschaftsausschuss Verzinken e.V. (GAV) im Rahmen der Arbeitsgemeinschaft industrieller Forschungsvereinigungen „Otto von Guericke“ e.V. (AiF). Forschungsstellen: Lehrstuhl für Stahlbau und Leichtmetallbau und Institut für Eisenhüttenkunde, RWTH Aachen.

[6] Herbsleb, G; Schwenk, W.: Untersuchungen zur Lötbrüchigkeit von hochlegierten Stählen. Werkstoffe und Korrosion 28 (1977), S. 145-153.

[7] Poag, G.; Zervoudis, J.: Influence of various parameters on steel cracking during galvanizing. AGA Tech Forum, Kansas City, 2003.

[8] Pankert, R., Dhaussy, D., Beguin, P. and Gilles, M.: Drei Jahre industrielle Erfahung mit GALVECO® Legierung. GAV Forschungskolloquium Feuerverzinken, Wiesbaden, 2003.

[9] Kikuchi, M.: Liquid metal embrittlement of steels by molten zinc, Koyoto, Japan: Proceedings of the 23rd Japanese Congress on Material Research, 1980.

[10] Kikuchi, M.: Study on fracture mechanisms of liquid metal embrittlement cracking of steels in molten zinc, Proceedings of the 24th Japanese Congress on Material Research, 1981.

[11] Klemens, D., Kaszàs, S.: Untersuchung der Spannungsrisskorrosion von Baustählen in flüssigem Zink. Werkstoffe und Korrosion 43(1992), 561-564.

[12] Klemens, D.: Inbetriebnahme von Verzinkungskesseln, Spannungen im Kesselmaterial und Rissgefährdung durch unterschiedliche Zinkschmelzen. Gemeinschaftsausschuss Verzinken e.V. Düsseldorf, Vortrags- und Diskussionsveranstaltung GAV 1983.

[13] Schulz, W.-D., Schubert, P.: Zum Einfluss der Topographie der Stahloberfläche auf Fehler beim Stückgut-Feuerverzinken, Mat.-wiss. Und Werkstofftechnik 22 (2002), 128-131.

[14] Richter, F.: Die wichtigsten physikalischen Eigenschaften von 52 Eisenwerkstoffen. Stahleisen-Sonderberichte, Heft 8, Verlag Stahleisen mbH, Düsseldorf, 1973.

[15] Richter, F.: Physikalische Eigenschaften von Stählen und ihre Temperaturabhängigkeit, polynome und graphische Darstellungen. Stahleisen-Sonderberichte, Heft 10, Verlag Stahleisen mbH, 1983.

[16] Nürnberger, U.; Menzel, K.: „Rissbildung beim Feuerverzinken von Feinkornbaustählen“, Abschlussbericht in der Forschungs- und Materialprüfungsanstalt Baden-Württemberg, 1998

[17] Pargeter, R.: Liquid metal penetration during hot dip galvanizing, http://www.twi.co.uk/j32k/unprotected/pdfs/ksrjp003.pdf (2003)

[18] Abe, H. et al.: Study of HAZ Cracking of Hot-Dip Galvanizing Steel Bridges (IIW-Doc. IX-1795-94). International Institute of Welding, Paris, 1994.

[19] Feldmann M., Bleck W., Langenberg P., Pinger T., Tschickardt D., Völling A., Ermittlung der Rissanfälligkeit beim Stückverzinken, MP Materials Testing 49 – 5 2007

[20] Feldmann M., Pinger T., Tschickardt D., Bleck W., Völling A., Langenberg P.: Analyse der Einflüsse auf die Rissbildung infolge Flüssigmetallversprödung beim Feuerverzinken, Stahlbau 77 (2008)

[21] Feldmann M., Pinger T., Tschickardt D. Langenberg P., v. Richthofen A. Karduck P., Rissbildung durch Flüssigmetallversprödung beim Feuerverzinken, Stahlbaukalender 2008

[22] Pinger, T.: Zur Vermeidung von Flüssigmetallversprödung beim Feuerverzinken von Stahlkonstruktionen, Diss. RWTH Aachen 2008.

European Commission

EUR 23510 EN – Joint Research Centre

Title: Commentary and Worked Examples to EN 1993-1-10 "Material Toughness and Through Thickness Properties" and Other Toughness Oriented Rules in EN 1993

Author(s): G. Sedlacek, M. Feldmann, B. Kühn, D. Tschickardt, S. Höhler, C. Müller, W. Hensen, N. Stranghöner, W. Dahl, P. Langenberg, S. Münstermann, J. Brozetti, J. Raoul, R. Pope, F. Bijlaard

Editors: M. Géradin, A. Pinto and S. Dimova

Luxembourg: Office for Official Publications of the European Communities
2008 – 247 pp. – 21x 29.7 cm
EUR – Scientific and Technical Research series – ISSN 1018-5593

Abstract
This commentary gives explanations and worked examples to the design rules in Eurocode 3 that are influenced by the strength and toughness properties of the structural steels used. It is a commentary and background document to EN 1993-1-10 "Material toughness and through thickness properties" and its extension in EN 1993-1-12 "Design rules for high-strength steels", where toughness properties are explicitly addressed.
It however provides also background to other parts of EN 1993, e.g. to EN 1993-1-1 "Design of steel structures – Basic rules and rules for buildings", where the design rules are related only to strength properties as the yield strength and the tensile strength without explicitly mentioning the role of toughness that is hidden behind the resistance formulae. Finally it gives some comments to chapter 6 of EN 1998-1: "Design of structures for earthquake resistance – Part 1: General rules, seismic actions and rules for buildings".

The mission of the JRC is to provide customer-driven scientific and technical support for the conception, development, implementation and monitoring of EU policies. As a service of the European Commission, the JRC functions as a reference centre of science and technology for the Union. Close to the policy-making process, it serves the common interest of the Member States, while being independent of special interests, whether private or national.

JRC
EUROPEAN COMMISSION

The European Convention for Constructional Steelwork (ECCS) is the federation of the National Associations of Steelwork industries and covers a worldwide network of Industrial Companies, Universities and Research Institutes.

ECCS
CECM
E K S

Publications Office
Publications.eu.int